UNIVERSITY OF SOUTHAMPTON

FACULTY OF ENGINEERING AND THE ENVIRONMENT

SHIP SCIENCE

Residual Life Assessment of Composite Structures

With application to all weather lifeboats

Roberton D.M.V.

Thesis for the degree of Doctor of Engineering

April 2015

UNIVERSITY OF SOUTHAMPTON

ABSTRACT

FACULTY OF ENGINEERING AND THE ENVIRONMENT

Fluid Structure Interactions Research Group

Doctor of Engineering

Title: Residual Life Assessment of Composite Structures: With Application to All Weather Lifeboats

With world shipping and other maritime based industries tending to operate assets requiring a large capital investment representing over half the total operating cost of the vessel, considering life extension at the end of a structure's design life can postpone further capital investment and reduce the yearly operating costs of a particular asset for the owner. Despite this experience the concept of asset life extension for continued use once design life is exceeded is one which has been covered in very limited detail in the academic community. In more recent years the concept of asset life extension has become important to a growing number of maritime industries and as such has become an industry lead area for investigation, with the lead being taken by the Health and Safety Executive in the UK and other regultory bodies abroad.

The work presented here describes the investigations into life extension assessment of assets, with a special focus on the Severn class lifeboat fleet owned by the RNLI, who wish to assess the potential for life extension of this fleet to enable the continued use of a successful asset and offset a £120 million replacement program. The vessels themselves are a monolithic stiffened composite construction with a design life of 25 years.

A methodology is devised which uses material static and fatigue data, environmental conditions and structural response data to determine the expected useful life of a composite structure. This methodology is then applied to the Severn class fleet by conducting experiments to determine the fatigue life of the materials through coupon tests, understanding the environmental conditions and the errors involved in predicting them and carrying out measurements of the structural response of a Severn class lifeboat whilst in service. Combining these variables using Monte Carlo simulations and the Miner's rule allows an estimate of the useful life of the asset to be made.

Table of Contents

Intentionally left blank

Table Of Figures

Intentionally left blank

List of Tables

Declaration of Authorship

I, ……, [please print name]

declare that the thesis entitled [enter title]

……

……

and the work presented in the thesis are both my own, and have been generated by me as the result of my own original research. I confirm that:

- this work was done wholly or mainly while in candidature for a research degree at this University;
- where any part of this thesis has previously been submitted for a degree or any other qualification at this University or any other institution, this has been clearly stated;
- where I have consulted the published work of others, this is always clearly attributed;
- where I have quoted from the work of others, the source is always given. With the exception of such quotations, this thesis is entirely my own work;
- I have acknowledged all main sources of help;
- where the thesis is based on work done by myself jointly with others, I have made clear exactly what was done by others and what I have contributed myself;
- none of this work has been published before submission, **or** [delete as appropriate] parts of this work have been published as: [please list references]

Signed: ……

Date:……

Intentionally left blank

Acknowledgements

I would like to express my thanks to my academic supervisors Professor Shenoi and Dr Boyd as well as my industrial supervisor Steve Austen for their help along the way, it's been a long hard road!

I would also like to thank the RNLI for the unending support given to me throughout this doctorate and to the many donors who enable this amazing charity to continue their work and enabled me to be a part of saving lives at sea. There will always be a special place in my heart for those I have met both in the head offices in Poole and the crews at the various stations I spent time with and on the passages I was able to be a part of. I would also like to thank Dr Blake, Dr Sobey and Jodie Walshe for their hints, tips and help along the way, it was very much appreciated.

I have made many new friends during this process and every single one of them has impacted this thesis in some way or another, I am truly thankful to everyone who has made a positive contribution to my life during this process.

I would like to thank my family who have been wonderful in supporting me in various different ways throughout the last few years, I don't think I would have done it without you. Finally I would like to thank Silvia who helped me escape during the final year.

Intentionally left blank

1 Introduction

The continued use of assets is not a new idea, there have been many examples in history of items which were designed and built in one era being used continuously well into another, where the original technology has been surpassed and become obsolete. A general web search using terms such as “classic vehicles” reveals a veritable medley of experience, advice or services focused around motor vehicles with technology either revolutionary or evolutionary at any time from the beginning of the automobile revolution but since superseded. This analysis is not limited to automotive or indeed transport methods and is easily extended to any type of asset which may hold an interest to any individual. There are collectors who purchase assets purely for interest and whole nations, such as Cuba, who are forced to use and maintain assets considered vintage elsewhere in the world as a matter of course (Enoch et al., 2004) as well as specific industries such as power generation (Reinertsen, 1996) or defence (Prescott, 1995) who have assets decades old still going strong.

Despite this experience the concept of asset life extension for continued use in its initially intended or new role is one which has been covered in very limited detail in the academic community as discussed in section 2.1. In more recent years the concept of asset life extension is one that has become important to a growing number of maritime industries and as such has become an industry lead area for investigation. The most prevalent of these is the Offshore Oil and Gas industry, which resulted in the instigation of the Health and Safety Executives KP4 program (Stacey, 2011) and, as the focus of this thesis, search and rescue services offered by the Royal National Lifeboat Institution (RNLI).

With world shipping tending to operate assets requiring a large capital investment that can represent over half the total operating cost of the vessel (Fan and Luo, 2013) careful consideration of what to do when the total service life has been reached may result in the option for life extension. This may allow postponing further capital investment and reducing the total operating cost per year for the asset owner. Current life extension methodologies for large marine structures determined by organisations such as the American Bureau of Shipping (ABS) (2004;2010) rely on the application of spectral analysis to computational models of assets where the size of the vessel make fatigue related issues due to global bending moments the most dominant cause for structural failure through fatigue. However these methods are not applicable to smaller assets, typically less than 20m in length but still representing a large capital expenditure, as operated by the RNLI where failures caused by transient local loads are more likely.

In the specific case of the Royal National Lifeboat Institution (RNLI), lifeboat classes have typically been replaced after 25 years. However in more recent times the use of advanced composite materials have led to lifeboat structures which have proven exceptional in service. The Severn Class Lifeboat, shown in Figure 1-1, was originally brought into service in 1995 and as such could be expected to be retired in 2020. However operational experience has been so positive that there is interest in life extending the Severn class well beyond 25 years, to up to 50 years. This class of vessel will provide the case study for the remaining investigation.

Figure 1-1: RNLI Severn Class Lifeboat

1.1 Research Challenges and Scope

The scope of this research is limited to generating and implementing a method which will provide enough information to determine an expected value of operational fatigue life for an asset under investigation as well as providing validation information for numerical models which may follow after.

The challenges within this area are as follows: determining the appropriate variables to investigate; identifying and implementing an appropriate test methodology; and finally analysis and interpretation of results to achieve an expected life prediction.

1.2 Research Aims and Objectives

The aim of this project is to provide and implement a methodology which will allow a rigorous analysis of the Severn Class lifeboats' suitability for life extension.

Key research objectives to meet the challenge set out above are outlined below.

1. Identify the state of the art for life extension and the supporting investigations.
2. Generate a methodology for assessing the structural life of an asset.
3. Determine a method for identifying the fatigue properties of materials and conduct fatigue tests on materials of a specific case study.
4. Develop a fatigue spectrum which can be applied to high performance marine vehicles operating in known sea state conditions.

1.3 Research Contributions

As a result of meeting the objectives in section 1.2 the novel contributions provided by this research are:

1. **Identification of structural life assessment method using limited data for initial assessment**

Approaching the issue of fatigue is fraught with difficulties. As a minimum, a range of loads and some characteristic material data is required. However for marine applications the loading conditions are very poorly understood; additionally the fatigue life of composite materials is extremely difficult to predict without conducting expensive material tests. This makes it very difficult to conduct a cheap first pass life prediction with a high level of confidence in the result. A method to overcome this is developed and implemented throughout this thesis.

2. **Characterisation of complex materials as used in some extreme marine applications**

A method using data pooling from fatigue tests of other complex composites is developed and then physical fatigue experiments are conducted to determine the applicability of the former analysis in this case and provide detailed fatigue information to be used in further analysis.

3. **Application of structural monitoring techniques to a new vessel type.**

In the past structural monitoring techniques have been implemented on a small range of vessels. The vast majority of these investigations were carried out early in the 20th Century or have been applied to vessels with a completely different end use such as yachts. In this work an operational vessel operated by the RNLI was instrumented with strain gauges in 32 separate locations to determine structural strains. This data base of applied strain histories can be used to support structural analysis work carried out in the design phase by validating the results generated.

4. **Development of a complex fatigue spectrum for vessels used in extreme environments**

Current methods for producing a fatigue spectrum for vessels rely on the application of advanced modelling techniques; whilst this is a sensible approach in making a prediction for a new asset the ideal is for detailed knowledge of the assets' usage to be obtained. By taking the results of research contribution 3, applying an appropriate counting algorithm to each data set and then grouping them according to the operating environments distributions can be developed which together can form a fatigue spectrum.

5. **Development of life prediction model**

To make best use of the data captured in research contributions 2 and 4 an appropriate model needs to be developed which can account for the uncertainty in the data as well as the unique profile for the different vessels. Therefore a model is developed which uses a Monte Carlo technique to simulate results in areas where there are gaps in the data and thus generate an estimate of used and remaining life for vessels with variable operational profiles.

1.4 Published articles that support this work are:

1. Roberton D.M.V, Shenoi R.A., Boyd S.W., Austen S.A., "A Plausible Method For Fatigue Life Prediction Of Boats In A Data Scarce Environment," in *Proceedings of the 17th International Conference on Composite Materials (ICCM17)*, 2009, Paper 14

1.5 Thesis Structure

This thesis contains ten chapters and an appendix. Chapter 2 reviews the current state of the art as published. The review covers Rescue Boats, The RNLI and the Severn lifeboat class in particular, Fluid Structure Interactions and their application to high performance marine vehicles, composite materials and the application of experimental and modelling techniques for their assessment, the life extension process for a range of industries, and fatigue spectra including their use, generation current examples.

Following this is the Methodology which highlights and provides outline justification for the approach that will be taken through the thesis as well as defining some of the important variables and language which will be used throughout the rest of the thesis.

Chapter 4 contains information about the static and fatigue characteristics of the materials used within the construction of the Severn class lifeboat. This includes information determined from standard modelling methods for the static material properties as well as a novel approach for determining expected fatigue characteristics from pooled data. The results of these approaches are also compared to material test data for validation and provision of more robust information.

The next chapter discusses the influence of the operating environment on the expected life of a marine structure, firstly by defining exactly what the operating environment is for the Severn class lifeboat, assessing the duration of time spent in the environment and then using this information to make predictions for the future. Due to the way the operating environment influences marine vessels, combined with the typical reporting methods used, it became clear that the assessment methods used to determine the operating environment should be investigated and potential errors accounted for. This is also completed in chapter 5.

Chapter 6 contains the approach taken to and results of monitoring an exemplar Severn class lifeboat. The test methodology is introduced as well as the system used to collect strain data. The installation approach is explained as is the data post processing method. The experimental results are then introduced and processed according to the methods outlined and then discussed, as is the use of data grouping where variations between monitored locations were minimal and finally a brief discussion on the effect of mass variation between lifeboats within the same class.

Having understood the material static and fatigue characteristics, assessed the operating environment and highlighted the uncertainty in the declaration of particular environments, and then measuring the response of the structure within the different environments, a method needs to be developed to use all this information. This is developed in chapter 7 where structural life assessment modelling approaches are defined for different stages of the assets existence including at the design stage and in service, additionally an analysis of the confidence that can be had in the approach based on the errors within the data sets is conducted.

This is followed by a discussion which summarises the previous sections, reiterating the links between them and how they fit in the overall structural life assessment model. Then the work is concluded and a future work section highlights the areas where further work would benefit the overall approach to asset life assessment and ultimately extension.

2 Literature Review

In this chapter an assessment is made of a selection of the previous work conducted relevant to the research contributions identified in section 1.3.

2.1 Rescue Boats

Rescue boats, the case study of this thesis, are subjected to some of the most extreme operating requirements of any marine vehicle, with the expectation that they are able to survive storm force seas, collision with other vehicles brought on by close operation and complete capsize without endangering the life of the operators. Lifeboats like the RNLI's All Weather Lifeboats (ALBs) are expected to maintain a mean speed of up to 17 knots in beaufort wind force 7 and safe operation in wave heights up to 15 metres (Hudson et al., 1993). At the top end of this operational envelope the operating environment is extreme and confused. Although there has been work conducted in this area, there are still significant unknowns when considering marine loading conditions which have led to further research projects and the requirement of more focused reference data (Rosén, 2004).

Advancements in composite materials, such as use of long rather than short fibres, woven mats and the introduction of carbon and aramid fibres, since their first introduction to the marine industry in the 1940s (Smith, 1989), has allowed the construction of structures which meet these extreme operational requirements whilst also being lighter and more durable than structures constructed from typical materials such as aluminium (Hudson et al., 1993). The use of composite materials in the marine industry does bring its own set of unique problems and challenges which include but are not limited to: load transfer methods and joining mechanisms, variability in loads, material properties and manufacturing methods (Shenoi et al., 2011).

The durability of composite materials has been tested through both academically and industry led research investigations such as that carried out by Sandia National Laboratories resulting in an in-depth database of composite material fatigue data (Mandell, 2009). The results of such programs and operational experience have led some asset owners to seek out opportunities for the extension of operating life beyond the original design intent. Although asset life extension is fairly common place within various industries, it has taken regulatory involvement through the Health and Safety Executive KP4 program for formal identification of life extension as a specific engineering activity which has specific needs and requirements (Stacey et al., 2008).

The major point for nearly all investigations into asset life extension, whether marine, automotive or civil structures is developing an understanding of the historical and potential future loading

regimes; this is achieved through fatigue spectra (Sunder et al., 1984). There has been limited investigation into developing a fatigue regime appropriate for general application to marine assets, however there are methods available for determining an expected fatigue profile using measured structural responses from life limiting structure (BS ISO 12110-2, 2012).

In this chapter the case study for investigation is introduced and state of the art of investigations conducted in marine structural loading, composite materials, life extension processes and fatigue spectra are reviewed. From this the direction of research will be defined and appropriate research areas acknowledged with the current state of knowledge for each critiqued, providing justification for the investigations carried out in this work.

2.2 The Royal National Lifeboat Institution (RNLI)

The RNLI has a long and rich tradition of being on the forefront of sea based rescues, having been founded in 1824 through a bill to parliament. In the early years oar and sail power were used to reach floundering vessels which were generally in sight and sound of shore. In the following years numerous different boat types were tried with significant changes coming with the introduction of the inshore life boats in the 1960's, which had faster response times although weather limited service windows, and the introduction of fast ALB with the Waveney followed by the Arun, Tyne and Mersey lifeboats. Following the success of these vessels, in the early 1990s the speed requirement was increased to 25 knots and the mandate that all ALB classes be self-righting was introduced. This led to the development of the geometrically similar Severn and Trent class lifeboats. Both of the vessels were constructed from fibre reinforced polymer materials with the Trent being of sandwich construction and the Severn being a monolithic stiffened structure. Extensive fatigue evaluation was conducted on representative materials of the Trent lifeboat whilst limited work was carried out concerning the Severn lifeboat (Hudson et al., 1993), the case study used within this thesis.

2.2.1 The Severn Lifeboat

The fleet of Severn lifeboats are operated all around the coast of the United Kingdom and Ireland, and are wholly owned and operated by the RNLI. The Severn lifeboat is 17.3m from bow to stern with a beam of 5.92m and a draught of 1.78m. Nominally the vessel weight is 42.3 tonnes in the load condition and 35.96 tonnes in the light weight condition. A lines plan can be found in Hudson and Hicks (1993). The Severn is operated by a crew of six, helmsman, coxswain, navigator, mechanic and two deckhands as well as an option to carry a doctor if required. There is room for 10 seated survivors in the survivors cabin which also contains provision for hot food and drinks. Maintaining the self-righting stability criteria the Severn can hold up to 40 survivors

and crew, although not all will be secure in the vessel, and it will carry over 140 survivors and crew whilst adhering to the Maritime Coastguard Agency's adequate stability requirements. As with all modern ALBs the Severn has an enclosed wheel house which provides a significant buoyant volume and contributes greatly to the boat's self-righting ability. Additionally there is an upper steering position which provides the helmsman with an excellent view of the lifeboat exterior when in use, which is primarily during close manoeuvring and whilst on station during rescues. The Severn lifeboat is powered by two MTU 20 litre engines generating 1600 horsepower each driving 1of 2, 5 bladed props which allows the Severn to reach speeds of 25 knots in calm sea state at 80 to 85% load, 20 knots achievable up to a sea state 6 ensuring rough weather operating requirements are successfully met. Electrical systems are powered by a 24 volt power supply and includes radar, GPS, autopilot, VHF and MF radios and assorted warning bells and buzzers in case of emergency. There is also an on-board CCTV which can be used for monitoring the various compartments.

The Severn lifeboats are the largest in the RNLI fleet and are expected to perform in the toughest of conditions the seas and oceans surrounding the UK can throw at them, therefore understanding how these conditions will likely interact with the Severn lifeboat during a service is a sensible next step to take.

2.3 Fluid Structure Interactions of High Performance Marine Craft

As identified in section 2.1 the interaction conditions for boats are varied and complex with rescue boats taking this to the extreme. The research reviewed covering this topic is split into the following; understanding the environment (the seas and oceans), understanding hydrodynamic influences, understanding the loading conditions resulting from the hydrodynamics and how the structure reacts to the loading conditions.

2.3.1 The Environment of the Seas and Oceans

Addressing the first of these research areas, for marine assets understanding the operating environment means understanding how the seas and oceans behave. In the case of marine vehicles the operating environment can vary quite dramatically due to the influence of weather systems and large scale natural events both locally and globally. In the case of rescue boats the design case must include operation within the most extreme of these variations (Hudson et al., 1993).

There have been various investigations into the sea way and several representations have been generated as discussed by Bishop and Price (Bishop and Price, 2005). The most basic representation of the sea conditions are the well-known Douglas Sea State Scale (DSSS) (Rawson

and Tupper, 2001) and Beaufort Wind Force Scale (BWFS) (Huler, 2004). The main difference between the two scales is the number of categories used, the BWFS runs to 12 and the DSSS to 9, the BWFS is shown in Table 2-1. The distribution of wave heights varies between zero and more than 14m in both scales and they both use descriptive terms to understand the state of the sea, making both applicable by sea farers whilst at sea.

Table 2-1: Beufort Wind Force scale in terms of sea state description

	Beaufort Scale	
Code	Description of Sea state	Significant Wave Height
0	Flat	0
1	Ripples Without Crests	0 – 0.2
2	Small Wavelets, not breaking	0.2 – 0.5
3	Large Wavelets beginning to break, Scattered Caps	0.5 - 1
4	Small waves with breaking crests, fairly frequent whitecaps	1 – 2
5	Moderate waves of some length. Many white caps. Small amounts of spray	2 - 3
6	Long waves form, frequent foamy white crests, some airborne spray.	3 – 4
7	Sea heaps up. Some foam from breaking waves blown into streaks along wind direction. Moderate amount of airborne spray	4 – 5.5
8	Moderately high waves with breaking crests forming spindrift. Well marked streaks of foam are blown along wind direction. Considerable airborne spray.	5.5 – 7.5
9	High waves with crest that sometimes roll over. Dense foam blowing in wind direction. Large amounts of airborne spray reducing visibility.	7 – 10
10	Very high waves with overhanging crests. Large patches of foam from wave crests give the sea a white appearance. Considerable tumbling of waves with heavy impact. Large amounts of spray reduces visibility.	9 – 12.5
11	Exceptionally high waves. Very large patches of foam, driven before the wind, cover much of the sea surface. Very large amounts of airborne spray severely reduces visibility.	11.5 – 16
12	Huge waves. Sea is completely white with foam and spray. Air is filled with driving spray, greatly reducing visibility.	> 14

Guedes Soares (1986) carried out investigations assessing the uncertainty of visual observation of wave height by comparing the observations from ships undergoing passage against hindcast predictions. The author combined a large quantity of data from various different studies to refine previous regression equations which related the visually observed wave height to an expected wave height. This analysis showed that the following relationships could be used to define the relationship between the measured wave height and the visually recorded wave height. This is extremely useful if the operators oboard a boat use wave height as an indication of the sea state, however for a significant majority of sea farers the seaway is defined in terms of the BWFS or DSSS as described above, if this is the case when using these reports the analyst is faced with a variety of potential observed wave heights for each sea state. In this case the above analysis is useful in as much as identifying that there is a difference between the reported conditions and the actual conditions.

It has long been recognised that there are numerous influences to the sea's behaviour at various points around the world, which has led to the development of various empirically derived wave spectrum definitions. Bishop and Price (Bishop and Price, 2005) carried out a comparison of some of these definitions showing that the JONSWAP (Hasselman et al., 1973), Bretschneider (1961) and Mean Famita Storm (Seatre, 1961) spectra are all similar with significantly more peakiness than the Neumann (1954), Darbyshire (1955) or Pierson Moskowitz (1964) spectra which are comparable.

The American Bureau of Shipping (ABS, 2010, 2004) suggest the use of the Bretschneider or two parameter Pierson-Moskowitz spectrum for ocean applications and the JONSWAP spectrum in areas of limited fetch to generate a representation of the operating environment for use within fatigue life prediction of structures. For the application of all of these spectra, information about the significant wave height and the average period of the waves is required. Where there are weather ships available this information can easily collated, however where there aren't, the crews observations from transiting ships are relied upon.

Additionally even though the JONSWAP spectrum is advised by ABS for waters with limited fetch, it is still representative of a deep water developed sea state. In the case of lifeboats a significant proportion of the time spent at sea is in close proximity to land and can be considered littoral waters, in these waters local topology may be such that the sea state is modified compared to the general state, but not enough to cause breaking waves in anything other than the most severe sea states, therefore the spectrums discussed here are not immediately relevant to the situation lifeboats often find themselves in as shown in Table 2-2.

Table 2-2: General water body from which observations were made to determine the sea state spectrum defined.

Source	Ocean	Sea	Littoral Waters	Unknown	First Principles
(Neumann, 1954)				√	
(Darbyshire, 1955)	√				
(Bretschneider, 1961)					√
(Seatre, 1961)	√				
(Pierson and Moskowitz, 1964)	√				
(Hasselman et al., 1973)		√			

2.3.2 Hydrodynamics of Marine Vessels

There are three distinct hydrodynamic conditions a marine vessel can attain; hydrostatic where the vessel's mass is supported by the reaction of the fluid, displacement condition where the speed of advance is slow enough for buoyancy forces to dominate and planning where the speed of advance is fast enough that hydrodynamic forces provide the vast majority of mass support. Each of these conditions requires a different hull form to achieve optimum performance (Rosén, 2004; Savitsky, 2003).

The choice of hull form type is directly related to a form of the Froude number defined in Savitsky (2003) as $F_{fps} = V_{fps}/\sqrt{gL}$, Where V_{fps} is the speed of the vessel in feet per second and L is the water line length of the vessel in feet. There are considered to be three different hull form types, displacement, semi displacement and planing hull forms. One problem with planing vessels is that as the hydrodynamic forces increase, the water line length often changes as the vessel rises further out of the water. To overcome this Savitsky and Brown (1976) noted that the breadth of the waterline rarely changes with speed and proposed a modification of the Froude number replacing the water line length with gB where g is the acceleration due to gravity and B is the breadth of the vessel. For this parameter the semi planing regime is defined as $0.5 < V_k/\sqrt{gB} < 1.5$ with the planing regime greater than 1.5. For the Severn lifeboat at full speed the two Froude numbers are: $F_{n,L_{WL}} > 6$ and $F_{n,L_B} > 3$ placing the boat clearly in the planing regime. With the lifeboat operating in higher sea states at 17 knots the two Froude numbers are: $F_{n,L_{WL}} > 4$ and $F_{n,L_B} > 2$ placing the vessel firmly in the planing craft regime.

The above assessment is applicable to smooth water operations, however as the sea state increases this ideal becomes less and less applicable and hydrodynamic loading events falling outside of these assessments become increasingly likely. These events are highly transient and

can cause significant crew discomfort or potentially even structural failure in the worst cases. Fridsma (1971) conducted research into the behaviour of planing hulls in rough weather. The work involved a number of constant deadrise angle hulls with variable length, load and centre of gravity. The important result for this work is that as the sea state increased all performance indicators reduced and in the fully planing condition smaller waves were passed without incident whilst comparitavely large waves resulted in extreme motions.

Research efforts on vessels in rough weather beyond the work by Fridsma (1971) and Savitsky and Brown (1976) is limited, with the focus generally being on seakeeping characteristics as found in Garme et al (2012). In this work the authors compared the seakeeping characteristics of an existing fast patrol vessel utilising aluminium structure with a theoretical craft nominally identical but utilising carbon fibre sandwich as an alternative and, as a result, lighter structure. Despite the economic advantages of a vessel with a significant weight reduction there is the potential for reduced rough weather controllability and therefore reduced performance envelope. This is a significant problem for some vessel types such as patrol vessels which are expected to be both fast and operate in potentially extreme conditions for long periods of time, a trait in common with all lifeboats. The authors showed the expected involuntary speed reduction due to increasing wave height is the same for both vessels whilst the onset of voluntary speed reduction occurred much earlier at a wave height of 0.7m for the composite vessel compared to 1.1m for the aluminium boat.

They also showed that by applying a ballast condition representing an increase of 4% mass exclusively in the bow area the vertical accelerations were reduced by a factor of roughly 1/3 compared to the un-ballasted condition and a reduction of nearly 1/4 when compared to the acceleration of the heavier aluminium vessel. The authors do point out that the studies conducted are examples of approaches to future designs for lightweight vessels however they stress that further study is required to further investigate other impacts and validate the models generated for the lightweight structures.

The studies identified in this section have shown that there is still a lot of work to be conducted when it comes to understanding the performance of high speed vessels in confused sea states as is the case for many lifeboat operations.

2.3.3 Loading and Structural Response

Loading and structural response are discussed together as the two are inextricably linked, there is no reason to try to develop load cases if there are no structures to load. The first investigations into fluid structure interactions and the applied loads were conducted by von Karman (1929). In

this work sea plane floats, simplified as wedges, impinging a fluid were investigated to determine the expected loading pressures based on conservation of momentum. Limited experiments conducted showed good correlation with the predicted peak pressure value, however the author indicated that significant further investigation was required. With the demise of sea planes as a mode of transport the majority of work in this area has been conducted on behalf of the marine industry with the majority of experimental investigations focused on the 2D wedge drop problem (Aquelet et al., 2006; Bisplinghoff and Doherty, 1952; Payne, 1981; von Karman, 1929; Wang and Soares, 2013).

However a real marine structure does not contain only wedge shapes and some, such as the RNLI's Severn class lifeboat, contain complex geometry which is not directly comparable to simple wedge drop tests. Therefore full scale testing is likely to provide better insights into structural loads, despite this there has been relatively little reported investigation into full scale boat loading. Those that have been conducted have tried to either develop further understanding or validate design predictions through experiments for particular cases (Faltinsen, 2000; Jasper, 1949; Kenney, 1969; Lankester S.G., 1964; Rosén, 2004).

The earliest of these was conducted by Jasper on a motor torpedo boat (YP110 Ex PT 8) (Jasper, 1949), where a dynamic load factor was developed. This factor takes into account the rise and fall times, t_0 and t_1 respectively, from an initial pressure value P_0, the fraction of critical damping the system is subjected to, the un-damped circular frequency of the system and the system mass.

During sea trials at speeds of between 25 and 35 knots hull bottom pressures, hull strain and accelerations were measured for comparison to the dynamic load factors and general characterisation of loading conditions. As discussed in the paper by Heller and Jasper (1960) the resulting information can be combined to produce an acceptable prediction of the maximum design loads expected for a particular vessel. However, there is still a significant amount of uncertainty in the methods suggested as the vessel used to validate and develop the methodology is of a very particular type and not necessarily comparable to other vessels in use, as can be seen from Table 2-3.

The RNLI commissioned a report on hull stress analysis based on a 40 foot all weather lifeboat (Kenney, 1969). Vessel details are shown in Table 2-3. The results of the experiments showed that for moderate and low seas the magnitude of the stresses was low irrespective of the direction of the craft relative to the sea. This was different in rough sea conditions where head seas gave greater slamming conditions. The report also states that for this vessel peak stress was applied over a reasonable period of time, 3/10ths of a second and that the peak stresses were

found in roughly the forward 3rd of the boat during a slamming event, supporting the evidence presented in Jasper (1949). Since the focus of this report was to analyse and test design methods for lifeboats, the report highlights the panel analysis for the slamming condition and hull girder bending moment theory along with a dynamic "G loading" just prior to this as the significant design points.

To further simplify design methods Allen and Jones (1978) defined a design limit pressure, this is based on the assumption that there will be a uniform equivalent static pressure which will result in deformations equivalent to those found in transient responses (Allen and Jones, 1978). The completeness of the methods described in this work is quite exceptional providing the designer with a number of tools which can be applied in a manageable way with confidence. This is further backed up by the method being the basis for the vast majority of the classification societies rules and regulations for high performance craft design.

However the extreme nature of the expected operations for rescue boats means that some organisations prefer to be more conservative and rely on their own loading estimations from data available within the organisation. This is the case with the RNLI where a standard design panel pressure relationship has been developed and is in regular use (Hudson et al., 1993). This linear relationship between the design weight multiplied by the vessel speed and the expected panel pressure, was proposed as a practical solution for the RNLI to encompass the unknown transient forces that were expected to be present on lifeboats when in the concept design stage. The design pressures proposed were confirmed using the Lloyd's Register hull pressure prediction program (Bottomley, 1983).

The assertion that panel analysis is of importance for considering slamming events is also confirmed by Faltinsen (Faltinsen, 2000). In this work a catamaran, detail outlined in Table 2-3, wet deck was instrumented to determine the structural loads that were applied during fluid structure interaction events. The purpose of this test was to compare the structural response as measured on a structure, to that measured in beam tests and compared to a theory developed by the author. Considering only the data presented from measurements recorded on the catamaran the authors present a recorded strain time history showing structurally significant strain oscillations (up to just over 800 microstrain) occurring over a time period of less than 0.05 seconds. From the point of view of structural modelling for development of a fatigue spectrum, the conclusion to be drawn is that the rate of data capture needs to be seriously considered as recording at a data rate which won't capture these high speed structural oscillations will mean that a significant proportion of fatigue inducing events could well be missed.

Table 2-3: Particulars for vessels undergoing structural measurement

	(Heller Jr and Jasper, 1960; Jasper, 1949)	(Lankester S.G., 1964)	(Kenney, 1969)	(Faltinsen, 2000)	(Miller, 2001)	(Rosén, 2005)
Data Source	Reference	http://en.wikipedia.org/wiki/Brave-class_fast_patrol_boat	Reference	Reference	http://jboats.com/j24-tech-specs	Reference
Boat Type	Motor Torpedo Boat	Fast Attack Craft	Rescue Launch	Catamaran	J/24 sailing yacht	
∇ (Tonnes)	49.4	90	11.7	100	1.4	6.5
Load Waterline (m)	22.86	27	12.19	35	6.1	10
Beam (m)	4.75	7.7	Un-known	9.4	2.7	
Draft (m)	0.97	2.1	Un-known	1.25	1.22	
Max Operating Speed (Knots)	35	52	Un-known	Un-known	Un-known	40
Hull Material	Aluminium	Mahogany over aluminium	GRP	Aluminium	GRP Sandwich with Balsa core	Carbon fibre / Foam cored sandwich panels

One of the most recent attempts to extend the analysis of experimental data as conducted by Jasper (1949) has been conducted by Rosén (2005). In this work a method for reconstructing a pressure pulse in both the time and space domains was presented. The key difference between the work of Rosén and that of Jasper is the treatment of the pressure pulse front. As is described at the beginning of this section, as a wedge shape impacts the water surface the wetted area increases with time, associated with this increase in wetted area is a movement of peak pressure transversely from the keel line to the hull chine. This movement of pressure peak can be identified with the use of pressure gauges placed at points across the transverse section of a plate which has been achieved by various authors but firstly by Jasper and latterly by Rosén. Rosén produced a method of Pulse Distribution Reconstruction (PDR) which takes a 3 dimensional rather than 2 dimensional approach to the problem using an array of pressure sensors which cover both longitudinal and transverse variations on a plate, recording data at a time interval of Δt with the output being a number of 3D maps of the pressure distribution at any point in time where there is pressure transducer data.

2.3.4 Summary

Table 2-4 identifies the work discussed in this chapter and identifies whether it is theoretically based or practically based, the vast majority of work in this area contains elements of both with practical experiments used to test the theoretical findings.

The environment plays a commanding role in the application of loads to a boat, in terms of environmental prediction a lot of work has gone into creating accurate sea state predictions which is useful for designers trying to understand the likely loading conditions in fully developed sea states in the oceans and seas. However for retrospective analysis, such as a life extension assessment a measured history of the experienced sea conditions needs to be obtained to provide an accurate time versus load history. This data can come from wave buoys or the observations of sea farers on vessels, however further investigation into the accuracy of prediction of environmental conditions should be made for the case study under investigation to identify the reliability of historical data which is often determined by the crew's observations. Additionally the operating environment of the lifeboats discussed in this thesis tends to focus on the close shore and littoral waters around the UK where local topology can change the response of the seas from the wave spectra identified.

The hydrodynamic loading of vessels is fairly well understood in the hydrostatic regime, as can be seen from the many millenia old references to man's travels across the sea to distant lands. This understanding has been formalized through Archimedes' principle. Hydrodynamic load cases have been investigated with some success using wedge drop tests, with and without forward speed, however add a confused surface to this picture and these forces become less fathomable. The forces are seen to be significantly different to those expected due to simplifying assumptions, with the source of the increase in force being the different angles of impingement on the surface as well as the increasingly violent motions due to increasingly confused sea states. The result of these variables is that a designer only can only claim to have a vague understanding of the magnitude of forces to design to and thus the design values used are more a description of the designers' attitude towards risk rather than understanding of the system designed for. This is shown well with the RNLI's design line from Hudson et al (1993).

Whilst this may be acceptable for designers, with the most risk averse using a larger design pressure, for those investigating fatigue it can become problematic as overdesigned structures result in unnecessary weight which then increases fuel consumption as one example. For any fatigue investigation the expected pressures must at least vary according to some known value, the obvious answer would be to scale the design pressure used according to an appropriate factor.

However since the maximum loads experienced in reality can vary hugely from the loads designed to, depending on the degree of conservatism of the original designer, the level of conservatism is difficult to determine. Additionally whilst focusing on the worst case scenario in any particular sea state, it may be that a large number of smaller loads may be missed.

The combination of the methods discussed would provide some sense of statistical accuracy for a design case, but is less likely to be correct for a specific case with a known history. Thus they may be applicable at the design stage where the future cannot be predicted, only estimated, but for assets in service the best way for determining the loads, if they can't be directly measured, and structural responses developed is by monitoring the structure of interest.

Table 2-4: Summary of the work discussed in this section. The section highlighted green is of most interest to this study.

	Theoretical	Practical
Littoral Waters		(Guedes Soares, 1986)
Hydrodynamics	(Fridsma, 1971; Rosén, 2004; Savitsky, 2003; Savitsky and Ward Brown P., 1976)	(Fridsma, 1971; Rosén, 2004; Savitsky, 2003; Savitsky and Ward Brown P., 1976)
Loading and Structure – Displacement craft		(Miller, 2001))
Loading and Structure – Semi Planing craft		
Loading and structure – Planing craft (Homogenous materials)	(Heller Jr and Jasper, 1960; von Karman, 1929)	(Jasper, 1949)
Loading and structure – Planing craft (Composite materials)		(Kenney, 1969; Lankester S.G., 1964; Rosén, 2005)
Loading and Structure – Catamaran wet deck	(Faltinsen, 2000)	

For the case of the Severn class lifeboat fleet the importance of the variables identified are magnified as there are 45 lifeboats, operating in environments which vary hugely both in terms of the expected generalised weather and sea conditions. In addition to this the impact of the weather conditions around the UK varies drastically from the Western coast of Scotland, Ireland and the South West of England which experience large Atlantic swells, the East of the UK, Ireland and South coast of England which experience shorter seas and therefore. Finally the local topography also varies considerably; the North West tip of Scotland to the South Eastern corner

of Kent in England are vastly different and creates significant variations in the length, and profile of the waves the Severn lifeboat is likely to encounter. This has a dramatic impact on the loading one particular Severn class lifeboat, serving one part of the country may see over its lifetime compared to any other. If the loading profiles differ, then it is reasonable to expect that for identical vessels the structural response will differ accordingly. However, the vessels are not all identical therefore some variation in response from one vessel to the next may be expected and with the structure being a composite construction an understanding of composite material response is required.

2.4 Composite Materials

Composite materials are defined as those consisting of two or more components with clear interfaces and distinct phases; these are generally one of fibrous or discontinuous form and the other a homogenous continuous form. In the final composite, each material retains its physical and chemical identity and contributes to the final properties. The continuous phase, termed as the matrix, is reinforced by the discontinuous phase, known as the reinforcement. Polymer thermosets and thermoplastics are most commonly used as matrices and are characterised by weak mechanical properties, but they do maintain the direction of the discontinuous phase which is often characterised as having very high directional strength (Daniel, 2006). The resultant structural material often has a high strength to weight ratio and as such is finding more and more usage in high performance areas, such as rescue boats (Hudson et al., 1993).

This section looks at how the understanding of failure of composites materials, as used in the structure of the case study, has progressed. The focus is on tensile and flexural loading conditions and the experimental techniques which are available for determining the ultimate strength and fatigue characteristics of composite materials under these loading conditions. These conditions were chosen as it was felt they best represented the potential loads experienced in service.

2.4.1 Fatigue Performance of Composite Materials

In the early 1970s research into composite fatigue concluded that components designed using these materials would have superior fatigue properties to other materials in use at the time, superior to the point that composite fatigue was not considered a limiting factor (Talreja, 2008).

There have been many investigations into the fatigue of composite materials with early investigations mostly driven by the aerospace industry, as a result the majority of material testing has been conducted on carbon fibre materials, however more recent use of GFRP composites in wind energy applications has led to a large investigation into GFRP fatigue (Mandell, 2009). It has been reported that composite fatigue strengths are heavily influenced by the constituent

materials which are used in its construction, even within composites using the same matrix there are differences in fatigue performance depending on the fibres used (Papakonstantinou and Balaguru, 2007).

Tensile fatigue failure of composites is well described by Talreja (1981) with 3 different fatigue modes identified as shown in Figure 2-1. The first involves the fracture of fibres resulting from the applied stresses exceeding the strength of the individual fibre and is generally due to high fatigue loads. With lower applied load values fatigue is expected to initiate within the matrix material according to typical homogenous material fracture processes, crack initiation and propagation normal to the tensile stresses. However when the cracks have propagated to an interface between the fibre and matrix constituents it is possible that the crack will either be arrested by the increased fracture resistance of the fibre under low strains, or the crack will propagate through the fibre at high strains continuing to propagate until the next interface, where the crack will either continue or possibly cause debonds along the length of the fibre.

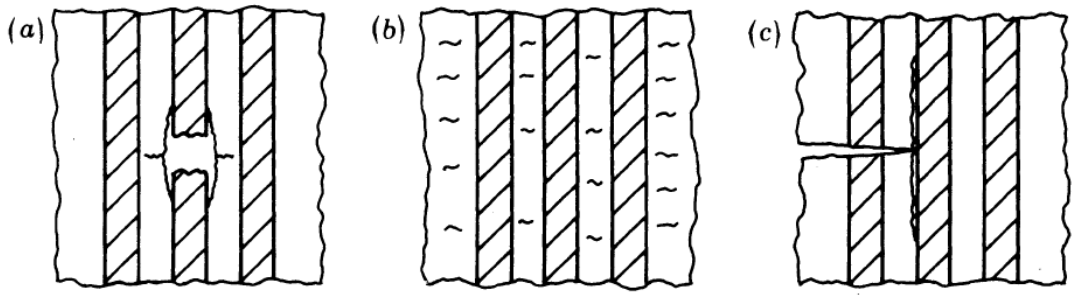

Figure 2-1: Fatigue damage mechanisms in unidirectional composites. (a) fibre breakage and interfacial debonding; (b) matrix cracking; (c) interfacial shear failure.

Kim and Ebert (1981) investigated the flexural fatigue of uni-directional E-Glass laminates using epoxy, vinyl ester and polyester matrix materials under load, strain and stroke control. Four distinct failure steps were found to occur during the fatigue tests, they are outlined in Table 2-5. This analysis showed that although there are difference between matrix materials and their fatigue response, the general process is consistent between matrix materials for this loading regime.

Read and Shenoi (1995) reviewed fatigue damage mechanisms and modelling characteristics for marine composites ranging from chop strand mat to multidirectional composites as used in mine hunter construction. In general it was found that damage initiation occurred at fibres aligned perpendicular to the load direction. In the case of chopped strand mat the damage was found to take the form of cracking which then went on to form delaminations around fibres aligned with

the loading direction. For complex laminates a characteristic damage state is formed within the matrix material which is independent of load history, but dependent on the material. Once the material has reached this state the local stresses have been relieved sufficiently that the applied local stress does not exceed the local fracture toughness of the matrix material. However the interlamina shear and normal stresses take on nonzero values which then lead to delaminations in the fibre direction leading to a further reduction in laminate stiffness. Woven composites introduce stress raisers due to the kink introduced by the undulation of the fibres. This leads to expected sites for crack initiation which then developed in the transverse direction along the fibre. Additionally longitudinal cracks develop along the fibres and where there is a coincidence of longitudinal and transverse cracking delaminations begin leading to stiffness reduction and final failure.

Salvia et al (1997) conducted a comprehensive investigation into composite fatigue under three point bending, their findings compliment the findings of Kim and Ebert but add fibre debonding as a further initial response to fatigue loads along with matrix cracking and fibre failure rather than being a result of matrix cracking or fibre debonding as described by Talreja. Reis conducted 3 point bending fatigue tests, post fatigue test inspection of the laminates identified two different and distinct failure modes for the glass fibre laminates (Reis et al., 2007): Fibre rupture at high stress levels; delamination failure at lower stress levels.

Whilst the hybrid laminates expressed a failure mode equivalent to that seen in the static load tests. Cavatorta (2007) described the fatigue process at constant displacement as being limited to matrix degradation, leading to a sharp drop off in stiffness initially, as cycling progresses the stiffness change reduces until the change is minimal compared to the initial change. The authors also found that for loads of 10% and 20% ultimate strength there was no discernible stiffness degradation within the run out period (10^6 cycles). At levels over this the stiffness degradation becomes obvious and increasing as the applied stress increases.

From the investigations discussed here some key points can be identified. Firstly it is clear that composite fatigue failure is due to a number of different but interacting failure modes, trying to model each of these and their interactions in microscopic detail could be computationally extremely expensive, therefore a macroscopic approach to fatigue analysis may be the most efficient.

The subtlety of different fatigue failure modes can also be extended to different reinforcement types and layup direction where differences can cause bias towards one mode. This is also true of

different types of load application, therefore to fully understand a particular material type testing should be conducted to determine the fatigue life and the expected failure mode of the material.

There is some limited evidence for a fatigue limit at very low loads, however to supplement these investigations fatigue tests at very low loads would need to be conducted, additionally often the run out definition for this type of test is 10^6 cycles. It is conceivable that stresses applied in service within the expected life time could easily exceed this number, however reaching 10^6 cycles is time consuming and therefore expensive, so exceeding this level of cycles will only increase the costs of a testing program. A safer, although potentially flawed, assumption is to dismiss the idea of an endurance limit and work to a finite life at no load.

There has been very little work carried out into the fatigue performance of multi-reinforcement composites of the type used in marine composites and specifically used in the Severn class life boat. Without knowing the expected ratio between the design and actual loads experienced standard fatigue test methods should be used to allow comparison of data sets for other materials.

Table 2-5: The 4 stages of composite fatigue as identified in Kim and Ebert (1981) for the three different material systems, these are summarised in Table 2-7. Similar stages were also reported in Salvia et al (1997)

Step	Epoxy	Vinyl ester	Polyester
1	Fibre surface cracking and interface failure.	Embedded glass fibre above and below mid plane crack as in tensile fatigue conditions	Fibre surface flaw propagation, fibre surface cracking and interface failure.
2	Shear crack propagation outside midspan and simultaneous preferential fibre failure and transverse matrix cracking on both surfaces	Shear crack initiation and propagation. Bending fatigue Failure	Preferential fibre failure and transverse matrix cracking occurred on both surfaces
3	Flexural surface crack and shear crack coalescence causing through delamination outside the mid-span	Fibre breakage through shear crack propagation and coalescence	Coalescence of surface cracks to cause flexural surface crack.
4	Through delamination propagated into mid span while flexural surface crack propagated to longitudinal direction causing final failure	Through delamination to complete shear failure.	Through thickness and longitudinal crack propagation until final failure.

2.4.2 Experimental Techniques

Experimental methods have been used for centuries to determine the properties of some physical phenomena. For material testing, standards (BS EN ISO 527, 1997; BS EN ISO 14125, 2011; BS ISO 13003, 2003) have been developed to cover both static and fatigue tests allowing the comparison of materials from different sources.

In static tests the properties to be found are the ultimate load carrying properties, maximum stresses to failure, generally for tensile, flexural, and compressive or shear stress. There are

numerous ways to load a specimen in order to determine a particular property each method having its own advantages and disadvantages. This section seeks to review previous work on composite bending testing both in static and fatigue environments, summarising the advantages and disadvantages and identifying references for each testing method.

In one comparison Reis et al (2007) performed static tests under 3 point bending at a constant rate of 5mm/s, 5 specimens were tested for a new material for comparison to others conducted by the following authors; (Agarwal and Dally, 1975; Ferreira et al., 1999; Mandell, 2003). Salvia et al (1997) conducted fatigue tests on various materials under 3 point bending. Under this type of loading Salvia et al found that damage began on the compressive side of the sample near the mid-loading point and spread very quickly through the thickness of the sample. Salvia et al felt that due to the unique nature of the loading condition, part lifetime predictions could not be made from this type of test. The following authors have conducted fatigue tests under 3 point bending conditions (Chambers et al., 2006; El Mahi and Bezazi, 2009; Matsubara et al., 2006; Miyano et al., 2006; O'Brien et al., 2002; Salvia et al., 1997). A more comprehensive review of the different test methods used by different authors can be found in Table 2-6.

During their experimental investigations Kim and Ebert (Kim and Ebert, 1981) found that as the support span to specimen thickness ratio increased, the failure mode of the specimens changed from shear failure to flexural failure. They also identified that there was an influence of test frequency on the number of cycles to failure through the comparison of specimens cycled at 1Hz and 10Hz, the 1Hz specimens were found to last roughly 3 times longer under stroke control, although the failure modes did not seem to be affected by the cyclic rate. The 10Hz specimens were found to have a temperature on the surface of the specimen of around 100^{o}C, above the glass transition temperature of the vinyl ester matrix used, it was postulated that the internal temperature would be higher still, although this was not measured.

Finally they identified that under the shear failure mode the different loading regimes had a significant effect on the material life with load control being the most damaging, strain control less damaging and the stroke control least damaging of all of the different testing regimes. The difference between constant strain and constant stress tests should be considered in comparison to the loading environment where as the structure ages, assuming there is no intervention, the applied loads are unlikely to change. Therefore constant stress tests producing applied stress versus number of cycles to failure graphs are more realistic. Composites are often designed with a constant strain in mind, this does not account for the effects of repeated loading on the structure.

Since this early work 4 point bend tests have been used in the following papers (Cavatorta, 2007; O'Brien et al., 2002).

Cavatorta (Cavatorta, 2007) describes the stress redistribution which occurs as structures degrade at specific locations and links this to his use of constant displacement tests to understand the stiffness degradation. However to achieve this constant displacement, the force required reduces through time. A phenomenon which is very unlikely as the force applied locally to a structure is likely to remain similar throughout that structures life.

A significant amount of work has been conducted by the Montana State University looking into fatigue of materials for the renewable wind energy sector (Mandell, 2009). The experiments were wide ranging including various loading conditions as well as glass and carbon fibre reinforcements. This suggests that no one test is applicable to completely characterise the fatigue of a structure, however there are also well defined fatigue problems within this sector including huge variations in loading types due to the complex nature of the environment and operational limits within it, issues around specific structural detailing and the large variation in materials used in the construction of wind farms (ten Have, 1993).

2.4.3 Composite Fatigue Representation

There have been many investigations into the fatigue of composite materials mostly driven by the aerospace industry; as a result the majority of material testing has been conducted on carbon fibre materials. It has been reported that composite fatigue strengths are heavily influenced by the constituent materials which are used in its construction, as well as differences due to matrix material, shown in Table 2-5, composites using the same matrix there are differences in fatigue performance depending on the fibres used (Papakonstantinou and Balaguru, 2007). The most commonly used fatigue representation method is the S - N graph (Chen and Hwang, 2006; Demers, 1998; Post et al., 2008) which can represent data for either constant applied strain or constant applied stress versus number of cycles to failure. Of these two options the most commonly used is the constant stress variation.

The general philosophy behind generating the S-N curve is discussed by Bond and Ansell (1998) in which statistical intervals are discussed and the implications of their use (the generation of 95% probability of survival boundaries) are identified. Read (1995) discussed the generation and use of applied stress divided by ultimate stress versus Log(N) (S-N) graphs and found that for glass fabric/polyester resin layup the log-linear straight line theory was the best overall fit, although at the extreme ends of the graph, extremely low and high cycle fatigue, an alternative fit was more applicable. O'Brien et al (2002) investigated the possibility of improving the S - N curve through

investigating the influence on various parameters including specimen preparation, thickness and type of fatigue test undertaken using a weibull scaling law to predict 4 point bending from 3 point bend tests and vice versa, the author found that the resulting scaled S - N curves were not adequate to generate accurate predictions. Chen and Hwang (2006) investigated the use of an alternative sigmoid curve to the standard linear model using carbon tensile data, it was found that this curve provided a better fit to the S-N data than a linear curve by using parameters based on the stress ratio R and the test frequency. Although this curve does potentially represent a significant step in the representation of fatigue data, a significant amount of testing needs to be conducted at various R ratios and frequencies to determine the defining properties for the curve. As yet this has not been conducted on a wide range of materials, so the curve fitting cannot be expanded beyond the investigation conducted by Hwang et al. Qiao and Yang (2006) present equations for S-N curves for 4 different materials.

Talreja (1981) suggested an alternative fatigue failure diagram for design based on the first applied strain and the number of applied cycles. Strain was chosen over stress as the applied variable since throughout the entire material the strain will remain constant whereas the internal stresses will vary depending on the constituent part investigated. The fatigue life diagram developed identifies three distinct features. The first, bounded between strain values $0 \leq \varepsilon_{max} < \varepsilon_m$, where ε_m is the fatigue limit strain, the second $\varepsilon_m \leq \varepsilon_{max} < \varepsilon_{c,lower\ bound}$ where $\varepsilon_{c,lower\ bound}$ is the lower bound of the scatter band around the value ε_c, the critical strain. For applied strains that are below the fatigue limit of the composite, Talreja suggests there is no cracking or non-propagating cracks appear and thus the material can be considered resistant to fatigue at this loading condition. In the second feature it was suggested that matrix cracking and interfacial shear mechanisms cause the material to degrade. In this fatigue regime the damage is dependent on the number of cycles applied and the rate of change of damage is dependent on the strain applied. The scatter band around ε_c, is due to the fibre breakage and interfacial debonding being a random process due to the random distribution of fibre strength variation within the fibre constituent of the matrix. Comparing the proposed fatigue life diagram with material data found from various papers, numerous interesting findings were observed, of all of the observations the clearest is that the nature of composite materials means that extensive testing should be carried out to identify the two strains of interest, the critical strain ε_c, and the strain fatigue limit, ε_m. The biggest drawback with this work is that the vertical axis represents the maximum strain reached during the first load cycle, not the maximum stress achieved, nor the maximum strain in a strain controlled test (Talreja, 2008). Therefore, although it can be a powerful tool for design fatigue resistant structures, it cannot be used in the application of fatigue

life prediction methods. Salvia et al offers an extension to this for life prediction by suggesting that the Strain v Number of cycles to failure curve can be generated by using a 10% loss of stiffness as the failure criteria (Salvia et al., 1997) then using a linear regression analysis to create the line, one significant finding was that under constant strain conditions the various materials all tended towards a common fatigue life value in the high cycle fatigue region, although Bond and Ansell warn against using constant strain data for fatigue due to the reduction of applied load through time (Bond and Ansell, 1998)

When considering constant life diagrams it is clear that there is a significant difference between materials and that a significant amount of irregularity is present suggesting that further information is required, hence the generation of large sets of S - N data as in the DOE Fatigue Database (Mandell, 2009). However from this work it is clear that for low stress high cycles to failure regimes there are some similarities. This suggests that in the absence of any other data these diagrams can be used to determine S - N curves at a particular 'R' ratio if an ultimate failure stress can be estimated. However the amount of data required to determine whether the chosen parameters are correct means there is potentially a large amount of uncertainty which needs to be quantified.

Having reviewed work looking at particular fatigue representations it is clear that there is limited commonality between the different fatigue diagrams. The most used is the stress life graph, the reason for this is that it best uses data that can be estimated at the design stage and collected from structures at a later date. The downside to this method is that it does not take into account the changing structure of the material as it fatigues which may lead to decreased Young's modulus values over time. However fatigue damage models may be able to overcome this problem. Some evidence has been presented that high cycle fatigue leads to a common fatigue life between materials, however a large amount of further testing is required to confirm this for specific materials before it can be implemented with confidence.

2.4.4 Composite Fatigue Modelling

This section reviews some of the work completed on predicting the lifetime of composites under fatigue loading. It is fair to say that the modelling of composite fatigue has evolved in tandem with the investigations discussed in sections 2.4.2 and 2.4.3. The earliest fatigue model was developed by Miner (1945) for application to metallic composites, using a simple damage accumulation rule. When the accumulated damage is equal to 1, the model predicts failure. This is common to all damage accumulation and residual strength models. Within homogenous materials the Pamlgren-Miner's damage accumulation methodology has been used successfully.

Post and other authors have found that a Miner's rule approach can be un-conservative in some instances (Post et al., 2008; Sarkani et al., 2001); despite this it is still often used as the standard to test against and it is also an extremely easy model to implement with knowledge of the ultimate failure strength and a rudimentary S-N graph. An excellent review of the numerous investigations into composite fatigue modelling that have been undertaken since the 1970s is found in Post (2008).

Kim and Ebert (1981) identified that hysteresis loop energy measurement can be used to detect the onset of permanent fatigue damage in composites since they were able to identify energy spikes associated with 4 different failure steps. This was identified by comparing the hysteresis loop energy variation of a pre cycled specimen versus an undisturbed specimen. Although this does represent a potential improvement over other methods, the main downside is that for it to be implemented in practice the material requires constant monitoring from the moment it is created to ensure the different hysteresis events described are captured. Although this may be implementable for structures that are newly built, when a structure has already been in service for a period of time and is undergoing a life extension review, a number of these hysteresis spikes may well have been missed and therefore knowledge of the current state of the structure is limited.

Of the damage accumulation models, the extensions over the Miner's rule include the addition of extra parameters obtained through experiments or in the case of the Hashin and Rotem model the inclusion of a residual life parameter based on the previously applied stress state which is used iteratively. With the exception of the Broutman and Sahu approach the residual strength laws all required the generation of several parameters beyond the number of cycles to failure. After application of the fatigue spectra to the various models and despite significant scatter within the experimental results Post (2008) was able to show that the models had mixed success in predicting the fatigue failure of the materials. Overall it was considered that the Broutman and Sahu residual strength model could viably be used as a replacement for the Miner's rule due to its consistency and simplicity in application.

Micromechanics models, which mimic the approaches proven successful in metallic materials, have been applied to fibre reinforced plastics. The major drawback to these methods is the required material testing to apply the various models. Results have been mixed for those models that do not require a large amount of experimental data; although working for their specific case, either no further cases have been explored or results have been questionable (Post et al., 2008).

Based on this review there are a number of fatigue life models available for use however due to the nature of material testing and the apparent quantity required to provide enough information for the effective application of some of these methods, those requiring more information than can be obtained from a basic S - N curve will not be used in this investigation.

2.4.5 Summary

In this section the static and fatigue failure mechanisms of composite materials have been identified from various papers. 3 different experimental approaches have been reviewed. These were chosen due to the nature of the case study investigation to be carried out (Figure 1-1) where it is considered tensile and bending loads are of significance. It was found that there is a significant difference between the failure characteristics of composites with different reinforcements and under different loading types and with the loads applied to different fibre orientations.

A number of well-defined techniques that can be used to determine the life of composite materials at varying applied stress level is presented in Table 2-6. A summary of these investigations is presented in Table 2-7 and Table 2-8 the boxes highlighted green show the areas of interest for this case study. The following key points were identified.

1. Composite fatigue failure is due to a number of different but interacting failure modes.
2. The subtlety of different fatigue failure modes can also be extended to different reinforcement types and layup direction where differences can cause bias towards one mode. This is also true of different types of load application.
3. There is some limited evidence for a fatigue limit at very low loads.
4. There has been very little work carried out into the reinforcement of multi-reinforcement composites of the type used in marine composites and none that can be found looking at unbalanced laminates.
5. The most used life diagram is the stress life graph graph.
6. Damage accumulation models limited to those using data easily accessible from the basic S - N curve will be used in this study.

Having an expectation of how the materials might behave according to repeated loading provides the opportunity to generate an expected fatigue life of the asset. However properly accounting for all the variables that can influence the fatigue life is important. In the case of the Severn lifeboat these variables are material and load based as discussed in the previous section. To determine how best to use the tools and techniques identified in these last sections, existing methods and processes for life extension should be investigated to identify best practice

Table 2-6: Range of methods used for the characterisation of the static loads and the fatigue evaluation parameters found in literature.

Reference	Standard Static	Standard Fatigue	Control Method	Fatigue Method	Failure Criteria	Test Frequency (Hz)	Applied Load Ratio (R)	Applied Stress Range (MPa or $\sigma_{app}/\sigma_{ult}$)
(Kim and Ebert, 1981)	N/A – Early Work		load and displacement	4 Point bend	Total Failure of sample			
(El Mahi and Bezazi, 2009)	ASTM Standard D 790		load and displacement	3 Point Bend	Total Failure of sample	10	0	0.4-0.98
(Reis et al., 2007) (GHFRP)	ASTM D 2344		Load	3 Point Bend	Stiffness reaches 80% of initial value	10	0.25	210 – 270
(Chambers et al., 2006)	ASTM Standard D 790		Load	3 Point Bend	Total Failure of sample	4	0.1	0.7 – 0.9
(Cavatorta , 2007)	ASTM D3039	N / A (Schenk type)	Displacement	4 Point Bend	Run out (10^6) cycles)	10	0.1	0.1 – 0.6
(Chen and Hwang, 2009)	Not Mentioned		Load	Tensile	Not Mentioned	3, 5, 8, 10, 12	0, 0.1, 0.3, 0.5	0.5, 0.6, 0.7, 0.75, 0.8, 0.9, 0.95
(Salvia et al., 1997)	N / A Early Work		Deflection	3 Point Bend / compression bending	10% Stiffness Loss	25	0.1	N / A
(Philippidis and Vassilopoulos, 2002)	N/A		Load and Displacement	Tensile / Compressive / Fully reversed	Ultimate Failure	10	0.1, 0.5, -1, 10	0.9 to 0.26
(Clark, 1997)	ASTM 1990		N/A	Tensile	Ultimate Failure	4	0	0.85 – 0.6
(O'Brien et al., 2002)	N/A		Load Control	3 and 4 point bend	N/A	10	0.1	0.65 – 0.575
(Qiao and Yang, 2006)	ASTM (Unknown)		Displacement Control	Tensile	Ultimate Failure	1, 3, 5	0.05, 0.1, 0.5	0.8-0.2

Table 2-7: Static Properties of material found in literature (All properties are average preoperties as found in the literature) *Where 'Available in referenced paper' the author of this thesis was unable to obtain a copy of the original work.

Data Source	Fibre	Matrix	Layup	Construction Method	V_f (%)	Tensile σ_{max} MPa	E_{tens} GPa	Flex σ_{max} MPa	E_{flex} GPa	τ_{max} (MPa)
(Kim and Ebert, 1981)	E-Glass (system 1)	Epoxy	$[0]_?$	Wet Filament Winding	57.4	N/A	N/A	1240	47	73
(Kim and Ebert, 1981)	E-Glass (system 2)	Vinyl Ester	$[0]_?$	Dry Filament Winding	58.6	N/A	N/A	1140	40	57
(Kim and Ebert, 1981)	E-Glass (System 3)	Polyester	$[0]_?$	Pultrusion	47.6	N/A	N/A	700	32	43
(Salvia et al., 1997)	Glass	Epoxy	$[0]_?$	Pultrusion Press Moulding Filament Winding	50 - 60	N/A	N/A	N/A	34.2 – 38.2	N/A
(Ferreira et al., 1999)	E-Glass	Polypropylene	$[0]_?$	Available in referenced paper	0.338	438	15.9	N/A	N/A	N/A
(Philippidis and Vassilopoulos, 2002)	E Glass	Polyester	$[0/(\pm 45)_2/0]_T$	According to ASTM 3039-76	N/A	245 (On Axis) / 140 (45^o) / 85 (Off Axis)			N/A	
(Sang wook and Tsai, 2005)	E-Glass	Available in referenced paper *	$[0/90/+45/-45]_S$ $[0/+45/90/-45]_{2S}$	Available in referenced paper						
(Reis et al., 2007)	Glass/ Hemp	Polypropylene	$[0/90]_7$	Moulded	N/A	N/A	3.4	366	11.3	N/A

Table 2 7 continued: Static Properties of material found in literature (All properties are average preoperties as found in the literature) *Where 'Available in referenced paper' the author of this thesis was unable to obtain a copy of the original work.

Data Source	Fibre	Matrix	Layup	Construction Method	V_f (%)	Tensile σ_{max} MPa	E_{tens} GPa	Flex σ_{max} MPa	E_{flex} GPa	τ_{max} (MPa)
(Reis et al., 2007)	Glass	Polypropylene	$[0/90]_9$	Moulded	33.4	N/A	17.3	381	11.8	N/A
(Chambers et al., 2006)	Carbon	Epoxy	$[0]_?$	Vacuum Bag	N/A	N/A	N/A	850 - 1050	1.75 - 3	N/A
(Matsubara et al., 2006)	Glass	Epoxy		N/A	N/A	N/A	55.4	N/A	N/A	N/A
(Qiao and Yang, 2006)	E-Glass	Polyurethane	[CSM / 0 / 90 / 0 / 90 / 0 / CSM]							
(Cavatorta, 2007)	Carbon / Glass	Epoxy	$[0/90]_{10}$	Hand Layup	55	96 (45^0) / 509 (On Axis)	8.3/ 36.4	145 / 516	8.9 / 43.5	N/A
(Cavatorta, 2007)	Carbon / Glass	Epoxy	$[0/90]_{10}$	Resin Transfer Moulding	42	107 (Off Axis) / 464 (On Axis	8.7 / 27.7	150 / 455	9.8 / 33.8	N/A
(Chen and Hwang, 2009)	Carbon	Epoxy	$[0]_8$ and $[0]_{16}$	Bag Moulding Process	66	2,302	141	N/A	N/A	N/A
(El Mahi and Bezazi, 2009)	Glass/ Aramid	Epoxy		Vacuum Bag	N/A	N/A	N/A	300	-	N/A
(El Mahi and Bezazi, 2009)	Glass	Epoxy		Vacuum Bag	N/A	N/A	N/A	320	-	N/A
(Clark, 1997)	Glass / Aramid	Epoxy	[0/90/ ±45]	Vacuum Bag	N/A	289	18.0	N/A	N/A	N/A

Table 2-8: Current experimental fatigue data found within open literature sources. The cells shaded green mark the areas of interest for this study.

		Glass		
		Uni-directional (UD)	Balanced Multi-directional (BM)	Unbalanced Multi-directional (UM)
Tension Tension (0<R<1)	On Axis	(Mandell, 2009; Qiao and Yang, 2006; Sangwook and Tsai, 2005)	(Al-Assaf and El Kadi, 2001; Clark, 1997; Mandell, 2009; Philippidis and Vassilopoulos, 2002)	
	Off Axis	(Mandell, 2009; Sangwook and Tsai, 2005)	(Al-Assaf and El Kadi, 2001; Mandell, 2009; Philippidis and Vassilopoulos, 2002)	
Compression Compression (R>1)	On Axis	(Mandell, 2009)	(Mandell, 2009; Philippidis and Vassilopoulos, 2002; Post et al., 2008)	
	Off Axis	(Mandell, 2009)	(Mandell, 2009; Philippidis and Vassilopoulos, 2002)	
Fully Reversed (R=-1)	On Axis	(Mandell, 2009; Sangwook and Tsai, 2005)	(Mandell, 2009; Philippidis and Vassilopoulos, 2002; Post et al., 2008)	
	Off Axis	(Mandell, 2009; Sangwook and Tsai, 2005)	(Mandell, 2009; Philippidis and Vassilopoulos, 2002; Sangwook and Tsai, 2005)	
Flexural	On Axis	(Kim and Ebert, 1981; Matsubara et al., 2006; O'Brien et al., 2002; Salvia et al., 1997)	(El Mahi and Bezazi, 2009; Matsubara et al., 2006; Reis et al., 2007)	
	Off Axis	(Kim and Ebert, 1981; O'Brien et al., 2002)	(El Mahi and Bezazi, 2009)	
Double Cantilever Beam			(Huanchun et al., 2008)	
Torsion			(Kassapoglou, 2007)	
Fatigue Spectrum (Varied but generally 0<R<1, R<1)			(Bond, 1999; Bond and Farrow, 2000)	

Table 2-8 Continued: Current experimental fatigue data found within open literature sources. The cells shaded green mark the areas of interest for this study.

		Glass / Aramid		
		Uni-directional	Balanced Multi-directional	Unbalanced Multi-directional
Tension Tension (0<R<1)	On Axis			
	Off Axis			
Compression Compression (R>1)	On Axis			
	Off Axis			
Fully Reversed (R=-1)	On Axis			
	Off Axis			
Flexural	On Axis		(El Mahi and Bezazi, 2009)	
	Off Axis		(El Mahi and Bezazi, 2009)	
Double Cantilever Beam				
Torsion				
Fatigue Spectrum (Varied but generally 0<R<1, R<1)				

2.5 Life Extension Process

Operating and maintaining engineering assets beyond their design life is a concept which has seen support in many industries for many years. There are numerous examples of assets which have far exceeded their design life all around us, from motorcars designed in the early 20th century which are lovingly cared for by enthusiastic owners (Nieuwenhuis, 2008) to military aircraft (Baker et al., 2004). However despite there being a number of consultancy firms who include the life extension process within their core business, there has been very little development within open literature, in fact the majority of research which is returned when searching for life extension methodologies or variations on the theme are actually investigations into material performance under cyclic fatigue loading or using short term material tests to predict long term material properties.

2.5.1 Marine

Specifically within the marine industry this area has become of interest in the oil and gas sector as a large number of existing installations have reached or are coming close to reaching their nominal installation life. With the economic drivers behind maintaining a current asset beyond its original design life superficially obvious (no decommissioning costs for the original asset and no installation costs for a replacement) the practice of operation beyond design life is becoming more and more common (Stacey et al., 2008). However, as is evident from the location of literature, the development and approaches to life extension of assets for the marine industry has been driven by regulatory bodies such as the Health and Safety Executive, specifically in the UK with the KP4 program discussed later.

Stacey et al also discussed the age of assets at the time of publishing and the identification of uncertainty in structural performance as a major issue for any life extended facility was raised. These uncertainties were identified as being from the following sources:

- Loss of corporate knowledge.
- Increasing relevance of small defects.
- Structure condition and associated responses.

The paper also identifies the regulatory requirements at the time, which are focused on the creation and review of appropriate safety cases for structures undergoing life extension, 4 triggers are identified for the review of any safety case of which life extension is one. Supporting documentation from a range of providers is also identified; where available the most recent articles from these providers are discussed later in this section. Stacey also identifies that *"The design life is the assumed period for which a structure is to be used for its intended purpose with*

anticipated maintenance but without substantial repair from ageing processes being necessary", which is set by regulators as a 20-year minimum period and is assumed at the time of the design. A significant description is then presented of different investigation requirements and resourcing requirements for producing a life extension assessment of a structure, but in essence this boils down to reassessing the original design assumptions based on updated data collected over years of operation against modern requirements.

After the previously discussed investigation was completed, the UK Health and Safety Executive instigated "The Ageing and Life Extension Program (KP4)", with the aim of promoting awareness and management of the risks associated with ageing plant in the offshore oil and gas industry. There were many outcomes of this work the most significant of which are summarised in (*KP4 Technical Policy - Ageing and Life Extension of Offshore Installations*, 2012) including:

- The adoption of a previous definition of ageing for the case of life extension.
- The identification of key hazard areas.
- Identification of key issues for ageing installations.
- The development of a an Asset Integrity Management System.
- The re-iteration of requirements for review of any Safety Cases developed.

The paper by Stacey and the Health & Safety Executives investigations supporting the KP4 program have primarily focused on the assessment of structures used in the Offshore Oil and Gas industry. A number of methods have been investigated to help these asset owners incorporate the recommendations into their life extension assessments which range from information gathering methods to management techniques (Horrocks et al., n.d.). However the assets of interest in the KP4 investigation are primarily steel structures and as such the presented methods not necessarily relevant to the subject of this thesis, relevant methods are discussed in later sections. The broader management topics are applicable but are focused on maintaining a minimum standard within the industry, on the assumption the decision to life extend has been made. The subject of this thesis is to help provide the asset owner with a more holistic understanding of the potential implications of a decision to life extend an asset before a decision is reached.

The American Bureau of Shipping (ABS) provides guides for the fatigue analysis of steel vessels (ABS, 2004) and floating production, storage and offloading (FPSO) installations (ABS, 2010). Det Norse Veritas (DNV) provides similar rules (DNV, 2010).

In the documentation provided by ABS a fairly detailed schematic procedure for the application of spectral based fatigue analysis is shown, the process is based on stochastic modelling methods with only a limited reference to validation for a specific case. The approach consists of 8 separate modelling phases for determining a "fatigue demand" and three further stages to determine the fatigue damage. Although this procedure does not cover the entirety of the life extension process as defined in other references, it does provide a tool for the specific analysis of structures undergoing fatigue loading by providing environmental data and relying on simulation methods to make the prediction. The biggest criticism of these documents is lack of reference to any validation work or other documentation within the ABS rules about verifying the assumptions made. This is a big risk as the implications are that a life extension assessment is a one off event with an easily obtained answer, when the reality may be different. In this approach a stochastic method is used to make a prediction however any stochastic approach is only as good as the data which is input into the model, therefore it is surely imperative that empirical work be carried out to verify the statistical data set used and further refine and thus improve the confidence in the outputs used to make a decision for life extension.

The rules and methodology provided by DNV are broadly the same with some increase in detail on how the methods work and should be applied (DNV, 2010). However this does not address the issues raised in reference to the rules set by ABS in the previous paragraph. Vassilopoulos (2010) outlines a clear series of steps which should be undertaken in order to achieve a life prediction of a composite structure, these are

1. Derive the load – time series.
2. Derive the material fatigue properties
3. Develop models and prediction methodologies for the fatigue data.
4. Select a cycle counting algorithm to summarise load v time histories
5. Produce a fatigue life prediction.

This method is broadly similar to those presented by ABS and DNV and as such supports the idea that the general approach to structural life extension is similar irrelevant of the materials or construction used.

The investigations into life extension for marine industries discussed in the previous paragraph are comparatively new compared to other industries. The most consistent investigations in the area of life extension which are available in literature tend to refer to the life extension of power stations, a selection of which are discussed here (de Witte, 1989; Erve and Bartholomé, 1991; Stumpf, 1994). Work in other areas has been conducted on a fairly isolated basis with no other

industries generating the consistent interest in this area until the KP4 program. Other isolated investigations include those by Reinertsen (1996) considering application to North Sea installations, Blech (2000) concerning the Tornado aircraft and (Foster and Monkman, 2004) working in the telecoms industry.

2.5.2 Energy Generation

In 1989 de Witte (1989) introduced a general approach for life assessment which includes considering the following parameters:

- Technical and Safety
    - Component operation, overhaul repair and replacement
    - Design rules and requirements
    - Component features
    - In service conditions
    - Use of Non Destructive Testing (NDT)
- Time
- Cost

This list is extended by Erve and Bartholomé (1991) who introduced an analysis concept and four main items for life extension:

- Knowledge of life limiting mechanisms
- Knowledge of potential failure mechanisms
- Evaluation of potentially critical components
- Monitoring activities

The life assessment approach defined in de Witte was then applied to 5 different components within a fossil fuel fired power station with individual assessments made for the different components, the author concludes that for different components the use of NDT and destructive testing carry varying importance, with the entire process carrying many uncertainties which reduce the confidence in any long term view significantly. De Witte argues however that these areas of uncertainty can be reduced through the implementation of measurements in critical areas and improving understanding of material behaviour. This argument is backed up by Erve and Bartholomé who used an array of thermo couple and strain gauge sensors to monitor the responses in specified locations, during this analysis they found that there was a significant number of components subjected to unexpected thermal loads and unexpected physical loads which were caused by both correct and incorrectly functioning equipment. Both of the references discussed here represent early developments of life extension thinking which focus on the state of

the structure as the main focus for determining the life of an asset, whilst there is little argument with the importance of understanding the structural requirements of a life extension assessment, it will be argued in this study that there are other areas which are also important and should be identified as such.

In 1994 Stumpf (1994) delivered a keynote address on the ageing of materials and life extension strategies of engineering plant which, although focused on economic and environmental impacts on life extension strategies for power stations, identified several fundamental points for life extension activities. The first is that the decision to conduct a life extension activity is a high level strategic management decision which should be recognised as an explicit technology strategy within the investigating organisation. The second is that there is such a broad range of investigations required, it is extremely important that there are knowledgeable specialists who are committed to organised investigation to develop a deep understanding of the technological issues confronting them. The third is that although these specialist investigations are required, ultimately it is the ends-objectives of the organisation which define the decision making parameters. Although this address was given to an audience whose interests lay in the power industry the concepts easily carry through to any organisation which is planning on investigating an asset life extension.

2.5.3 Military

As an example in 1995 Prescott (1995) identified that in the case of the United Kingdom's Armed Forces military equipment far outlasts its predetermined life and that as long as the equipment allows continued effective performance in modern theatres around the world there is no reason to discontinue the practice. Two types of equipment life are defined, that of useful life which is relevant to the basic design and is determined by political, tactical or technological factors and durable life which is defined by the physical degradation of the equipment and the cost of ownership. Prescott has identified the three ends-objectives important to the Ministry of Defence of the United Kingdom: Continued Effective Performance; Useful Life; and Durable Life.

At this stage it is worth reiterating that the majority of research into life extension methodologies up until this point was focused on a very specific sector, power generation, as pointed out by Reinertsen (1996), with little or no expansion to the general case. Reinertsen's investigation focuses on the maintenance aspects which need to be considered in a life extension assessment focusing on understanding the technical health of an asset as it passes through stages in its life.

One of the best examples of the development of a generalised life extension assessment method is that developed for the Tornado aircraft as operated by air forces around the world (Blech,

2000). In this paper Blech describes a four part model which was applied by the organisations operating the aircraft. The work discusses structural fatigue issues in common with de Witte; there is also a concerted effort to assess the impact of subsystems and the subsequent impact on any maintenance policies already in place. The four part process presented consists of the following phases:

A. Identification of safety relevant equipment and attachment structures.
B. Nations(operational working group) review of previous phase recommendations and selection of items which should be subject of further life extension work.
C. Equipment extended certification activities.
D. Aircraft extended certification and preparation of a new lifed items list.

Phase A took into account both the original safety relevant systems as identified by the original equipment manufacturer as well as those which have been added as a result of in service experience of the operators. 3 categories ranging from category 1, safety relevant, through category 2, item safety relevant but qualification life limitations unlikely to be critical, to category 3, items where failure can be tolerated were then identified. In Phase B the different items which made up the sub systems were considered by experts from the participating nations and placed into one of the 3 sub categories. In phase C the individual operating nations then begin work packages in conjunction with the original equipment manufacturers to requalify the category 1 and 2 items for continued airworthiness to the extended lifetime. The final phase, D, deals with those items which have not achieved the required air worthiness standard and therefore need alternative arrangements to be made to achieve an aircraft level life extended certification.

This approach complements the assertion by Stumpf that the decisions to be made are strategic but adds the element of review based on evidence gathered. Blech makes the point that although the aging process can be slowed, it can never be stopped. The preventative actions presented to achieve this improvement must include but are not limited to:

- Identifying critical areas and components where ageing could have serious consequences.
- Reviewing the current ageing process of subsystem components in high aged aircraft or of high aged components.
- Reviewing the current maintenance procedures and policy regarding the aging problem.
- Improving preventative maintenance actions in order to address aging in an early stage.
-

It is also mentioned that to carry out these analyses an obvious requirement is that of specific system specialists with the correct training and experience with the systems. The point is also made in this paper that although a significant amount of re-qualification testing is required at some significant cost, if the original qualifications requirements had been expanded to include the investigation of possible life limiting criteria at the design and prototype stage, rather than testing focused on achieving a predetermined number of flying hours, the current process could have been far simpler, quicker and cheaper to investigate. The main criticism with the work presented is that it seems to be a very linear process with little opportunity for review. The problem with this method of working is that as new simulation or investigation methods are developed, the opportunities to apply them and learn more about the asset are missed.

Also the process developed is driven by the question, "can the asset perform beyond the original lifetime?" Whilst there is no argument that the assets can indeed achieve this target; a better question would be "how long can the assets last?". This would focus the attention of the investigations into understanding the different criteria in as much depth as possible, revisiting areas of investigation as improved methodologies become available refining the expected life with each iteration. The outcomes of the project which was this subject of this article were expected in 2002, however efforts to find the reports have drawn a blank.

2.5.4 Other

Foster and Monkmann (2004) produced an asset management plan for Telecom New Zealand to help ensure the minimisation of short term investments during the upgrade and replacement of the infrastructure to support network upgrades. The method considered aspects specific to the industry as well as presenting a general asset management philosophy with examples to illustrate its use. Its main focus being the integration of risk into asset management. Although the subject of this investigation was a life extended asset the discussion was very narrowly focused on the risk aspects of investigations.

Other examples of life extension investigations in literature include Thirumeni (2005) who described the specific work undertaken in the process of extending the life of the SEWA Layyah unit 4-5 desalination plant in the Middle East, presenting the problems faced and methods used to overcome them. Suzuki et al (2006) have outlined the benefits of a retrofit programme to steam turbine power generators, describing the technology improvements utilised and gains achieved through specific case studies. Picard et al (2007) provide a financial model that compares future costs for use-up, retrofit, reconditioning and full replacement of switch gears throughout western Europe, the author identifies minimum long term cost of ownership as the

main driver behind any final decision in the asset management. Harper and Thurston (2008) proposed using utility analysis to assess the environmental impacts in engineering system designs and redesigns. Using this method the author was able to identify the best decision route for dealing with fossil fuel power stations. However none of these investigations add any real improvement over those already identified.

2.5.5 Summary

In summary life extension of assets is an area where the application by industry has out stripped the investment in knowledge in open literature. Table 2-9 represents a significant proportion of the discussion that has been developed over time and shows the dispersed nature of investigations carried out. Specifically within the marine industry ABS, LR and DNV are currently applying technology and solutions in this area which relying heavily on the use of statistical environmental data and the use of modelling tools to generate the data required to help asset owners instigate recommendations made by the Health & Safety Executive in the KP4 program. There are very few investigations which consider the holistic aspects of application of a life extension assessment on an asset with those that do keeping the investigations very high level and showing little understanding of interdependencies between areas.

In all instances discussed above there are a number of key investigations that are identified as required for the successful life extension of an asset. These are

- An understanding of the operating environment that the asset is subjected to.
- Understanding how the assets structure responds to that environment.
- Capturing a representative sample of the likely conditions and responses the asset is likely to be subjected too during operation.
- Understanding the asset's previous operational history and projecting an expected future operational requirement.
- Understanding the fatigue parameters of the materials being loaded.
- Determining an appropriate fatigue model for use in calculating the useful fatigue life of the asset.
- Pulling all of these things together to give a useful fatigue life prediction. One which can ideally be updated at will.

However for a full life extension assessment to be carried out prior to a strategic decision being made other investigations need to be tackled before and a method of assessing the impact of each investigation on the lifetime of the asset is needed, these include but are not limited to:

1. Maintenance issues

2. Economic issues
3. Systems
4. Management methods

As highlighted in Table 2-9 none of the investigations reviewed cover the broad range of problems holistically. This is important for the RNLI as being a charity they are responsible to their donors to ensure a significant benefit can be realised by life extending their assets compared to providing a completely new class of lifeboat as has been the case in the past. The development of a model which is able to incorporate all of the investigations identified will allow the RNLI to ensure a complete view of the costs and benefits to the RNLI as well as the technical challenges which are faced during a life extension exercise.

However to determine the expected fatigue life of the Severn class lifeboat it is clear that defining a way to take into account all of the parameters discussed in the bullet pointed list above is required, typically this is done through a fatigue spectrum and variations are discussed in the following chapter.

Table 2-9: Summary of the reviewed investigations into life extension analysis. The tick systems works as follows, 3 = in depth, 2 = some discussion, 1 = mentioned.

Source	Structure	Economic	Maintenance	Systems	Management
(Stacey et al., 2008)	√√√	√			√
(*KP4 Technical Policy - Ageing and Life Extension of Offshore Installations*, 2012)	√√√				√√
(Horrocks et al., n.d.)	√√√				
(ABS, 2010, 2004)	√√√				
(DNV, 2010)	√√√				
(de Witte, 1989)	√√	√	√		
(Erve and Bartholomé, 1991)	√√			√√	√
(Stumpf, 1994)					√√
(Prescott, 1995)					√√
(Blech, 2000)	√√		√	√	√√
(Thirumeni, 2005)		√		√	
(Suzuki et al., 2006)		√			
(Picard et al., 2007)		√√√			

2.6 Fatigue Spectra

Examples of fatigue spectra found in literature often consist of random sequences of measures which are deemed representative of the service an asset can be expected to undertake, in its most basic form this data is taken from local stresses and strains of a structural member which is considered life limiting (Socie, 1977). These measures are generally in the form of applied loads or strain responses, examples of fatigue spectra can be seen for combat aircraft (Sunder et al., 1984) and for wind turbines (ten Have, 1993). This section discusses the options available for generating and representing a fatigue spectrum which can then be used in conjunction with material fatigue data and a material fatigue model to provide a life prediction for an asset. The historical research can generally be summarised into two separate parts; the different methods of representing the measurement history and the methods used to record the appropriate measures.

Ten Have (1993) identified 3 different conditions that should be met for the successful generation of a loading standard, number 1 in Vassilopoulos' list of requirements for a life extension assessment (Vassilopoulos, 2010), these are

1. The loading must exhibit a spectrum shape that is characteristic for the type of structure under consideration.
2. The loading must contain interaction properties that are, at least, understood and means must be found to incorporate this interaction in the final standard.
3. The standard must comply with certain applicability requirements, e.g. simple structure, clear generation procedure and finally, it must be fully documented.

In terms relevant to the RNLI lifeboat, the conditions above will come from:

1. Understanding the loads and response of the vessel.
2. The interactions can be developed through the combination of advanced computational analysis which will provide in depth detail into the structures behaviour in key areas and measured data which will provide quantitated evidence of the magnitude of the response.
3. The final requirements can be achieved by defining the dominant factors for fatigue in the case of the Severn and using those to define the structure evidenced through appropriate documents.

Sunder (1984) considered fatigue spectra from the point of view of crack propagation for a homogenous material and identified the idea of bounding typical operational cycles, this allowed

the development of a spectrum which has distinct parts identified by each of these operational cycles. The subsequent loading sequence is defined by:

- Blocks – A sequence of peaks and troughs repeated over a given interval of crack extension.
- Steps – A set of identical load cycles.
- Segments – One or more sets of unique combination of peaks and troughs.
- Interruptions – A peak - trough / trough - peak excursion introduced as part of a larger load excursion.

By defining these phases fatigue characteristics within the fatigued material structure could be correlated with particular cycles. For homologous materials such as those investigated by Sunder this makes perfect sense, especially when comparing different materials for use within a particular environment. This approach can be used on occasions where there are a large number of nominally identical assets for which limited operational data is available (such as a fleet of airliners or boats), but where one has significant data capture on board. By identifying the different operational cycles in the characterised vessel and attributing particular data to each of these cycles, the data can then be exported to the other assets based on their known operational cycles and thus produce a fatigue life estimate for their usage profile.

2.6.1 Current fatigue spectra

There are various fatigue spectra available for use in various industries for evaluating the fatigue life of assets. Within the renewable energy industry there is the WISPER (Wind turbine reference SPEctRum) and WISPERX (a shorter version of WISPER) spectra for wind turbines (ten Have, 1993), within the aerospace industry there is the FALSTAFF (Fighter Aircraft Loading STAndard For Fatigue) which was developed for a variety of European fighter aircraft and represents load intensity at the wing root (Bond and Farrow, 2000). Both of these spectra are fixed length spectra with a variation of loads. An example of a fatigue spectra for marine craft can be found in Smith(1989).

The WISPER spectrum was developed from load measurements on a range of different wind turbines made of several different material types in numerous different locations around northern Europe (ten Have, 1993). This spectrum was developed for the fatigue testing of different materials under what could be considered a realistic fatigue loading sequence for the purpose of material characterisation. As such the organising working group took the decision to omit any cycles which had a load magnitude smaller than 0.6 of the once-per-1000-rev level (a level which ranges from 0 to 2.9). This decision was taken as a result of engineering judgement

within the working group and considered to be a good compromise between cycle resolution and overall sequence length (ten Have, 1993). This approach is perfectly satisfactory for comparing material choices, however for determining asset life these low magnitude events are the most likely to be encountered and could possibly cause a significant amount of cumulative damage and should therefore be captured where possible.

The FALSTAFF fatigue spectrum block contains a total of 17,983 cycles, which is the equivalent of 200 flights of recorded data. The cycles are distributed into peaks and troughs with a range from 1 to 32 with 7.5269 representing 0. In order to apply the spectrum a scale factor is required to attain the appropriate stress levels to be applied (Bond and Farrow, 2000). The scale factor approach is very useful when comparing assets of nominally identical structural design, but variable operational outfit which may affect variables that might influence loading conditions. Other fatigue spectra for the aerospace sector identified by ten Have (1993) which have had no further investigation as they are very specific to particular applications but are broadly similar in practical approach and makeup to those identified above.

Smith (1989) presents a histogram of hull bending moments estimated for a 60m minesweeper. The bending moments are split into 7 different bins, with each bin representing a particular bending moment range at a particular number of cycles and is presented as a histogram. This histogram shows that the maximum number of cycles expected in any one load condition is somewhere between 10^7 and 10^8 cycles. Although this spectra is specifically marine focused, the focus vessel and the associated fatigue location is significantly different to the case study in this thesis, a small high performance craft, and as such not relevant, although this does provide reference for comparison when considering the number of cycles to be expected for any particular condition.

A fatigue spectrum for lifeboats has been previously used in an investigation into sandwich structures for use in RNLI lifeboats (Clark and Shenoi, 1998). This spectrum was applied to Trent class lifeboats during their introduction to the RNLI to confirm whether the lifeboats could be expected to last a 20 year service life. This can provide a starting point for the fatigue investigations for this project; however the way it is presented makes it difficult to break down according to other parameters such as sea state. The assumption that each of the 11 different load blocks can be representative of a different sea state (assuming sea state 0 does not produce any fatigue events) does not hold as the largest applied load only occurs once. Therefore the spectrum must be an amalgamation of data from different sea states. Unfortunately there is no information published to either confirm or deny this speculation therefore the spectrum can only

be used in its current form making it difficult to apply to different vessels with varying service histories.

Not all fatigue spectra are in the form of applied fatigue constants, ABS (ABS, 2010) presents a wave scatter diagram from which fatigue stresses can be developed. Within this procedure the fatigue damage is calculated from a combination of structural analysis using modelling methods, the assumption that a stress transfer function can be used to relate wave data to a particular stress within the structure and finite element modelling to determine this function.

The biggest downfall for this procedure is that nowhere is it mentioned that the predictions should be validated in some way by collecting appropriate data from the asset under investigation. This is unfortunate as it could lead to a false confidence in the model outputs as well as instilling a belief that this type of analysis is a one off event, whereas (as argued by the HSE (*KP4 Technical Policy - Ageing and Life Extension of Offshore Installations*, 2012)) any analysis supporting a safety case for life extension should be reviewed and updated at regular intervals with the inclusion of knowledge and methods developed in the intervening time period.

Having identified different fatigue spectra currently available in literature and through classification societies it is clear that a specific spectrum needs be developed for the case study in this thesis. In order to ensure the best understanding of the structural fatigue a mixture of advanced modelling methods and structural testing is to be used. Considering the time frames available priority has been placed on the physical testing of the structure as this can not only provide historical data on the use of the asset, but can also provide important validation information for when a detailed modelling investigation does take place.

2.6.2 Fatigue Histories

In general, fatigue histories are derived from the long term measurement of structures undergoing particular operations; a large amount of the work discussed section in 2.1 could easily have been extended to determine a fatigue history for a particular vessel if the instrumentation had been able to run continuously. It is an obvious step from recording pertinent data for development of design loads to recording the appropriate variables for fatigue histories by implementing similar systems over a longer period of time to catch a greater range of data for analysis. As it is, the investigations could be used to extrapolate out from the conditions experienced, however often these conditions were artificially created as in Kenney (1969). The trials conducted artificially focused the operation of the lifeboat into particular engine speeds and particular headings to the seaway. This does not represent completely how the vessel would be handled by an experienced operator. Therefore any data that could have been obtained would

have been unrealistically high due to the occasions when the vessel was heading into seas at a significant speed. On these occasions an experienced operator would manoeuvre around the sea to avoid discomfort and would therefore stress the hull less. Nevertheless the experimental set up here could be recreated and develop into a long term measurement system used to develop a fatigue record. A system used in this way is commonly considered a structural health monitoring (SHM) system.

Farrar and Worden (2007) discuss the challenges associated with implementing an SHM system. In this work the authors identify conditional maintenance of rotating machinery as being the most effective implementation of SHM technology which use pattern recognition applied to particular spectra measured at a single point in the system to identify fatigue failure. The key reasons for success for this application are highlighted as minimal variation in operational use and environmental conditions, very well defined damage types, large databases of examples of damage and clear and quantifiable economic benefits that the technology can provide. The authors identify a "*statistical pattern recognition paradigm*" containing the following 4 steps: operational evaluation; data acquisition, normalisation and cleansing; feature selection and information condensation; statistical model development for feature discrimination. This approach is a good first start in addressing the uncertainties surrounding SHM, however there is still a very long way to go in developing methods to address these steps outside rotating machinery. The successful application of SHM to rotating machinery could well be down to the very rapid growth in data sets for statistical analysis associated with monitoring a piece of machinery that goes through one operational cycle in a fraction of a second. For industries or structures where the duration of an operational cycle can be measured in hours or days, or where the environment changes so significantly that every operational cycle needs to be experienced a significant number of times, may not be palatable for some operators. However operators who have very long term goals should not shy away from such applications as the potential economic and life-safety benefits through successful implementation of SHM are expected to be significant (Cross et al., 2013), especially when trying to understand fatigue histories. The following investigations all seek to address the development of fatigue histories experimentally through the use of SHM methods of one sort or another.

Socie et al (1979) proposed a system for recording field usage with the application to fatigue analysis. Although the focus of the paper was providing information for the development concepts in the design and early implementation of a product, the measures used to provide this information are the same as that required for a fatigue life extension. The two measures discussed in this work were strain and load. Strain measurement is used to directly measure the

structural response of an asset whilst load measurement is made at the interface between the environment and the structure. The argument is made that load histories are generally more useful as they are less likely to change with structural modification, whereas a strain history will become useless once structural modification has been made in the area of interest. Although this may be true for design and development process, for the life extension process clever selection of monitoring locations, which are unlikely to be modified, can mitigate this issue. These measured strains can then be used to back calculate loads where required using the advances in simulation tools since Socie's paper. These same tools can be used to model any modifications made as a result of in depth analysis of the asset.

Erve and Bartholome (1991) investigated fatigue within a nuclear power plant. The argument made is that in this case the margins of safety developed in the as-built condition should be maintained throughout the asset lifetime. These margins of safety can be maintained in various different ways, but in all of them information on the current state is required to determine whether the remaining margin of safety is adequate. The authors used an online calculation of fatigue usage factors to take into account transient history when predicting the fatigue usage of the materials of interest which is achievable in an asset with large amounts of real estate to house significant computing power, however in some applications there may not be the space to house a simple PC, therefore methods which process the data offline must be used in these cases.

In 2001 full scale experiments supporting an investigation into the fatigue of fibreglass hulls was carried out in San Francisco Bay (Miller, 2001). Investigations into material characterisation, understanding the service histories and full scale testing of the asset in question was carried out. The full scale testing element consisted of sailing 2 separate J class vessels, class details are outlined in Table 2-3, on particular courses whilst measuring strain and acceleration data on a laptop computer. Conceptually the methods proposed within the paper are perfectly valid however there are a number of limitations with respect to the subject of this thesis. The major drawback is that the vessel type is a sailing yacht with a significantly different structural make-up to the case study used here so of the conclusions drawn only the general concepts can be extrapolated.

A final example of structural monitoring on ships reviewed was carried out on the Visby class corvette (Burman et al., 2010), see Table 2-3, core shear readings taken from an area roughly one third the length of the vessel from the bow. The original trials were performed in rough seas in the Baltic and were initially for the purpose of validating design assumptions and calculations, with data taken from a number of positions allowing the recording of structural and hull girder

responses. The focus of the discussed work was to take the previously recorded data and produce a useful time history trace which could be used to predict fatigue within the Visby class hull. The authors stopped short of developing a fatigue spectrum.

Based on the evidence above it is clear that the use of strain gauges, pressure transducers and accelerometers is a well-defined method for investigating structural response. However the focus of most of this work was verification of design loads or structural detailing and as such only specific instances were investigated and compared to results found at the design stage. Of the investigations which did look at fatigue, the data gathered was of a fairly short duration and used for the development of the applied fatigue spectrum (Burman et al., 2010; Miller, 2001). Although this is not a great surprise due to the potential expense and quantity of data produced in conducting long term tests, it is the suggestion here that to understand the fatigue history of a vessel with the least uncertainty, long term tests on the vessel of interest is crucial. On top of reduced uncertainty, the other benefit of long term testing is that every operational use of the vessel can be considered a trial therefore actual operational use is captured producing an operationally correct time history of fatigue events. This is more important for fatigue than specifically understanding what is causing the structure to behave the way it is which are important design considerations. Once the asset has been designed then the mechanisms causing a structural response to occur are less important than the historical record of the stress responses which lead to fatigue within a structure.

2.6.3 Cycle Counting

Having generated a relevant history, a method for counting the different individual relevant occurrences needs to be employed. There are 4 different counting techniques identified in general use in British Standards (BS ISO 12110-2, 2012). These are Level-Crossing counting, Peak counting, Simple Range Pair counting and Rainflow counting. Of these, although limitations have been identified, Rainflow counting (Sunder et al., 1984) has been considered the superior counting method for fatigue spectrum generation for some time (Socie, 1977; Tovo, 2002).

The Rainflow counting and Simple Range Pair counting algorithms were developed to count fully closed hysteresis loops in the notch root stress strain history for metallic structures, making the assumption that crack growth rate only occurs in the rising portion of the hysteresis cycle. This basis was validated by Sunder et al (Sunder et al., 1984). Although developed for metallic fatigue, this method has also been used for developing a fatigue spectrum for composite materials (ten Have, 1993).

Okamara et al (1979) found that both Rainflow and Simple Range Pair counting, did not provide satisfactory results in some cases. To remedy this they proposed a variation on the range pair counting method called the hysteresis loop counting method (not in (BS ISO 12110-2, 2012)). The major difference between the methods is that the initial value is held to be the starting point of unclosed hysteresis loops during data acquisition, and a closed loop is determined as soon as the compared ranges are equal or the later range is greater than the former. Once this condition has been reached the mean and the range values of the closed loop are returned.

Yigang et al (Yigang et al., 1993) introduced a modification to the Rainflow analysis which allowed the load sequence to be maintained, this was to allow evaluation of the effect of sequencing of fatigue life which traditional Rainflow analysis does not allow. This method was applied to crack tip growth for metallic materials where it is suggested load application sequence is a significant concern, however the description merely refers to damage, therefore any method of computing damage can be used allowing the method to be employed in a variety of areas where sequencing is of interest as it is with composite materials (see section 2.2).

An alternative to the Rainflow and range pair counting methods is to use the simpler peak counting method to compute damage then reduce this using a statistical analysis (Tovo, 2002). To achieve this Tovo points out that since fatigue damage is caused by amplitudes and mean values of loading cycles, and that these cycles are random events with a probability distribution and rate of occurrence associated with them, it is the evaluation of these parameters that are the usual target of fatigue load investigations. Tovo described the properties of a complete cycle counting method as thus:

"a counting method in which every peak is paired with a lower or equal valley so that, in complete countings, the number of counted cycles is equal to the number of peaks."

And defined a second property of a complete counting method where:

"In a set of cycles obtained by means of a complete counting method, the number of cycles having peaks higher than or equal to a level u and lower valleys is equal to the number of peaks minus the number of valleys higher than or equal to u: i.e., the number of level crossings of level u"

This property was defined as the crossing consistency. According to this definition Peak counting methods are not considered complete or consistent, the Level crossing method is complete and Range counting and Rain flow counting methods are both complete and consistent. The relationship between the different damage estimations for the mentioned counting methods is:

Range Counting < Rainflow Counting < Level Crossing Counting < Peak Counting

On the face of it this suggests that for the most conservative estimate of life, peak counting should be used to represent the estimated damage used. There are some drawbacks to this though, firstly at the design stage this could easily lead to an artificial inflation of safety factors which may in turn lead to unnecessary weight gain in structural elements. Secondly it may lead to the unnecessary scrapping of assets which still have significant life left in them levying the owner an unnecessary economic cost.

2.6.4 Summary

This section of the literature review has identified different fatigue spectra currently available in literature, since there is not a directly relevant spectrum available it is clear that a specific spectrum need be developed for Severn class lifeboat fleet. Considering the time frames available priority has been placed on the physical testing of the structure as this can provide not only historical data on the use of the asset, but can also provide important validation information for when a detailed modelling investigation does take place.

Strain gauges, pressure transducers and accelerometers are well-used sensing methods for investigating structural response. However the focus of most of this work was verification of design loads or structural detailing and as such only specific instances were investigated and compared to results found at the design stage. Although this is not a great surprise due to the potential expense and quantity of data produced in conducting long term tests, it is the suggestion here that to understand the fatigue history of a vessel with the least uncertainty, long term tests on the vessel of interest is essential in producing time history sequences and fatigue spectral densities. This is important for fatigue as once the asset has been designed the mechanisms causing a structural response to occur are less important than the historical record of the stress responses which lead to fatigue within a structure.

In order to generate a fatigue spectrum there are a number of methods that can be applied the most common of which are the Rainflow counting method, the Range counting method and Peak counting methods. For this investigation Rainflow counting will is the selected cycle counting method as it allows the capture of the complete hysteresis loop of all applicable strains as well as dealing with half cycles. Finally it has been the cycle counting method of choice for the majority of fatigue spectra discussed within section 2.6.1 and the capability to implement a solutions is available within the resources of this doctorate.

Table 2-10: Summary of fatigue spectra available in literature and from classification rules. Green colour highlights area of interest.

	Marine: Hull Girder Bending	Marine: Local Panel Loading	Other
Structural Spectrum – Design application	(Smith, 1989)	(Clark and Shenoi, 1998; Miller, 2001)	(Bond and Farrow, 2000; Erve and Bartholomé, 1991; Socie et al., 1979; Sunder et al., 1984; ten Have, 1993)
Structural Spectrum – retrospective application		(Burman et al., 2010)	
Environmental Spectrum	(ABS, 2010, 2004)	(ABS, 2010, 2004)	

2.7 State of the Art Summary

Drawing all of the conclusions from this review together it is clear that the following areas are ripe for further investigation within the context of the RNLI's Severn class lifeboat:

1. Understanding the fatigue of complex hybrid composite materials.

A fundamental step in understanding the possible life of an asset requires knowledge of the material fatigue characteristics. To achieve this, appropriate materials need to be selected and tested according to appropriate test standards.

2. Understanding the operational envelope of the lifeboats.

The general environment of operation for the Severn class lifeboat can be easily defined as any coastal area within 100 miles of the UK's coastline. However within this bracket the services can be conducted anywhere from at the base of a cliff to the 100 mile limit. This will produce localised variations and therefore the operational envelop which is best able to account for these differences should be identified.

3. The reliability of sea farers in determining their local environment.

In the case of the RNLI it is the on board crew that declare the operating environment experienced for any service, therefore understanding the likely accuracy of these declarations is important as they ultimately decide the operational envelope applied in any particular instance.

This can be achieved through statistical analysis of available declarations compared declarations from other sources.

4. Generation of appropriate fatigue spectra from structural monitoring.

To produce a life prediction for any structure a historical knowledge of the fatigue forces the boat has been subjected to is a must, therefore an approach based on structural measurement is developed to determine the fatigue spectrum for the Severn class lifeboat, allowing for any variation in operational envelope.

5. Development of a structural life assessment method to generate a lifetime prediction.

A way of drawing all of the information together to determine the expected service life of the asset needs to be developed. This method needs to be able to use all the data generated in support of the life extension, to determine the expected life of any lifeboat within the Severn class fleet.

6. The structural loading of semi planing craft for application to fatigue load prediction.

Further developing computer aided engineering programs to a point where the interaction between a random and confused environment and a structure to identify load sets for dynamic conditions will help improve a designers understanding of fatiguing loads and therefore initial life prediction of a structure.

7. Understanding the structural response for application to fatigue life prediction.

The use of computer aided engineering in understanding the response to both static and dynamic loads is well researched. However when considering fatigue many variations occur over the lifetime and a way which enables the combination of these into an expected damage coefficient without being extremely computationally expensive should be developed.

8. The description of the waters around the coastal regions of the UK which are affected by significant changes in local topology.

As the local topography of the sea bed changes in, either through shelves or gentle undulation, the response of the sea will change accordingly. In very deep water this is not necessarily a problem. However in shallow water, where a significant number of lifeboat services are carried out, the effects can be considerable. Finding a way to account for these effects for individual assets will allow a better prediction to be made for each individual asset.

9. The development of a methodology to address the holistic aspects of life extension such as maintenance, economics, systems and management methods.

Although a fundamental part, the structural assessment is still only a single part of the life extension story. As identified there are a number of other factors which need to be accounted for

and developing a holistic analysis approach will allow a complete analysis of the potential costs and benefits prior to a decision on life extension to be made.

The list above is ordered based on the ease of investigation, ease of validation and expected impact of each investigation on the accuracy of the conclusions drawn on the expected life of the lifeboat. Of these 9 possible areas for investigation the first 5 are chosen based on their potential impact on solving what has been identified in this chapter as the fundamental problem; whether the structure will last an extended amount of time. In addressing these issues it is expected that some areas of the remaining investigations will be touched upon although due to time and scope constraints no further investigations are carried out.

It is worth noting that investigations 4, 6 and 7 are different sides to the same coin. Where investigations into the loads and responses using computer aided engineering is becoming the norm, significant extra information can be provided to designers for consideration. However where assets have been in use or are already designed the gap between the realities of the life a vessel has led and that which can be accurately simulated is still poorly understood. Additionally the time taken to develop an accurate set of models which are able to trace the loads and responses from the global structure, through the local detail and into the macroscopic material response can be expected to be considerable. Thus it was felt that the best option would be to monitor the structure and therefore detail directly providing a direct evaluation with a significant degree of certainty, which can then be used for validation of simulation models which come in the future.

3 Methodology

As identified in the literature review, for the life extension of any asset to be successful the fundamental structure, which forms the primary structure of the vessel, needs to be investigated and a remaining life predicted. The primary/fundamental structure can be considered as 'one piece' which will require some form of destructive work to remove and replace any part. The chassis of a car or the hull of a ship are good examples of fundamental structure. This definition allows the method to be applied to any system, irrelevant of its size or complexity, this aspect of a life extension is the major focus of this thesis.

The ultimate outcome of this research is a structural life assessment, how this assessment is carried out depends on the materials used in the structure, the operating environment and the dominant loads and responses expected within the structure. One of the biggest areas of concern for any long life structure is fatigue or time dominated degradation which can lead to failure (Clark and Shenoi, 1998; Harral, 1987). In this thesis the degradation due to fatigue through repetitive use is considered dominant with any issues caused by other time based degradation reserved for future work.

Although fatigue has been a well investigated subject since the early work of Miner (1945), designers use safety factors to build in margins which they hope account for "knowns" and "unknown" structural degradation influences, one "known" influence is fatigue. Due to the ill-defined understanding of aspects such as the accumulation of damage from fatigue or extreme events, these safety factors are often found by allowing for multiples of the maximum design load to be experienced before ultimate failure can be expected. This is the reason that life extension can be considered. In order to account for the fatigue life at the initial design, an understanding of three main questions which describe how the structure is likely to be affected during service needs to be gained, these are;

1. What events cause fatigue response within the structure (a collection of these events is defined as a fatigue spectrum).
2. What aspects will cause modifications to these events?
3. How much damage is likely to be imparted by the different events?

These same three variables need to be accounted for in this work. The following 3 packages of work provide the route to understanding the variables used in this thesis:

1. Material Characterisation

2. Load and Response Measurement
3. Structural Life Assessment

Working backwards from the end goal specific to this case study, a structural life assessment for a composite life boat, will allow the links between chapters to be easily identified. Thus the methods and approaches within each section will be shown to complement one another and answer the three questions previously identified.

Prior to obtaining a remaining life an expected life for the asset structure needs to be identified. To achieve this, a spectrum of structural responses, the expected fatigue characteristics of the material used and a method of combining these two inputs to achieve a structural life prediction is required. For composite materials the literature review identified that material testing is the most reliable method of obtaining fatigue characteristics for individual materials.

To generate a spectrum of structural responses either modelling or measurement techniques can be used. For this thesis, the opportunity to directly measure the structural response was available. The benefit of measurement over modelling is that intrinsically the measured values are truly representative of the total load case on the vessel at the time of the measurement. This removes the complication present within modelling methods of generating appropriate and realistic load cases.

However there does need to be some way of relating the measured values to a particular set of instances which can be reasonably expected to repeat throughout the life of the vessel. Without this link no forward prediction would be possible and only an estimate of the total damage experienced based on measured events could be created. With the case study being a Severn lifeboat operating up to 100 miles off shore, the different Beaufort force numbers are used as the unique set of instances and their use is discussed in chapter 5.

These three distinct inputs are pulled together in the structural life assessment model shown Figure 3-1. In this model the structural responses, discussed in chapter 6 are separated according to the different operating environments encountered, modified by the mass of the asset investigated and then applied according to operational environment distributions discussed in chapter 45. These are then combined with the material fatigue information found in chapter 4 to generate an understanding of the current state of fatigue life and predicted life to failure of the structure in question, discussed in more detail in chapter 7.

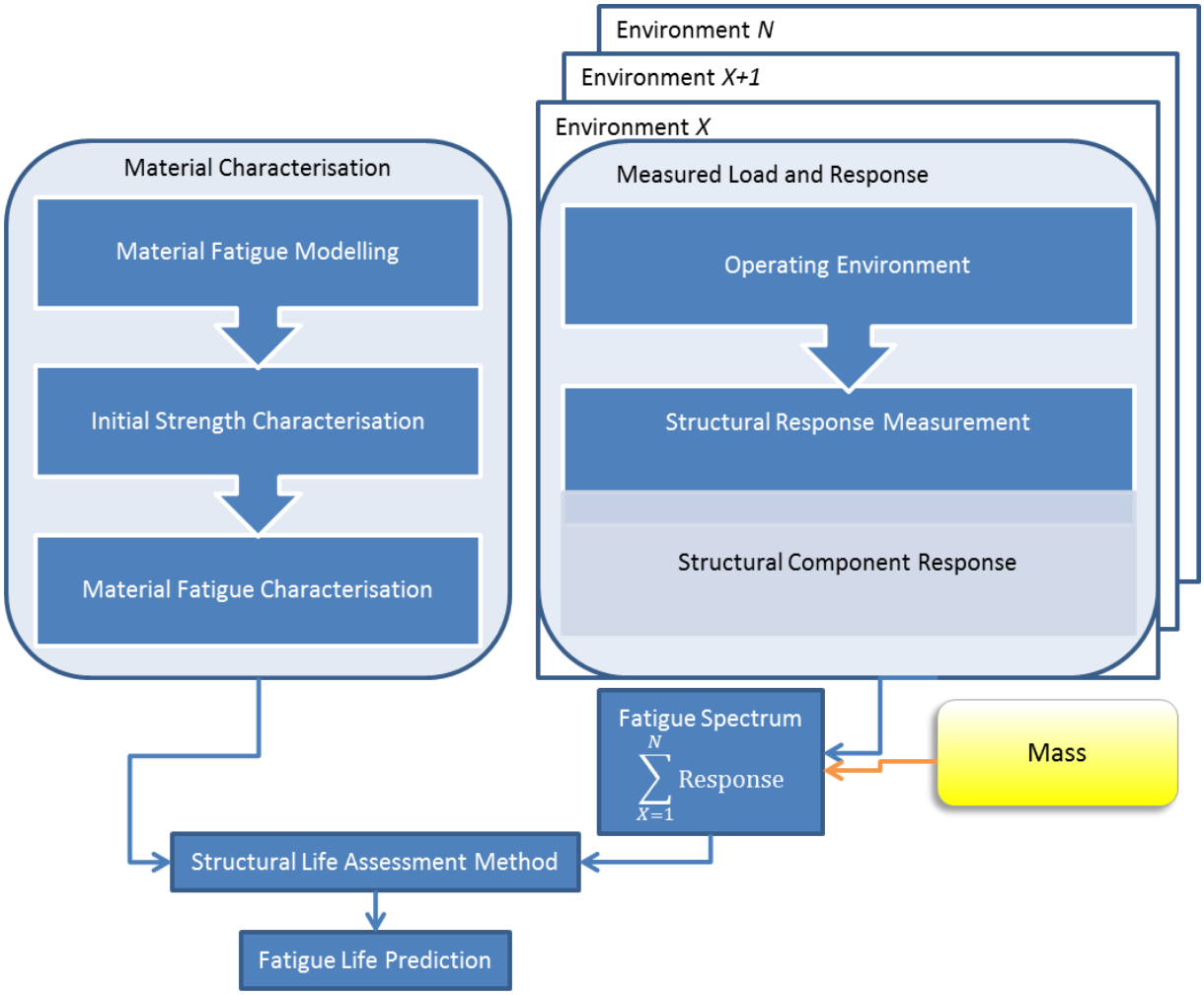

Figure 3-1: General methodology which is used to conduct a Structural Assessment and represent the method applied in this thesis.

To understand how these distinct investigations can be combined the relationships between them need to be defined. The relationship between the measured responses and the operating environment is made through the observations of the crew on board the lifeboat whilst underway. The crew on board the lifeboat declare a particular Beaufort number on service returns, giving them a possible 12 options according to Table 2-1. Since the date of the service is known and the measured structural responses can be time and date stamped, it can be stated that for a particular Beaufort number a particular range of responses are expected. This approach is useful as it can very quickly build up a picture of average structural responses in a particular Beaufort number, whilst becoming ever more accurate as the vessel is used and data gathered. This is to some extent limited by the accuracy of the crew on board the vessel at the time; this is also investigated in chapter 5.

The relationship between the material characterisation and the structural response is determined through the materials used in the construction of the structure and the geometry of the structure where measured. The materials should be the same or directly comparable to those used in the structure of the lifeboat, this is especially important with composites where the material is created at the same time as the structure. There are numerous different tests that are available to determine different material properties. It is important that the tests chosen closely represent the physical responses that can be expected on the structure.

Small marine craft, as the Severn class lifeboat is, are subject to loads which produce a mixture of global and localised responses. As is seen in the literature review typically panel responses are measured when trying to understand these responses experimentally. Engineering judgement was used to specify measuring panel response at the centre of a number of different panels longitudinally and transversely in this work. Figure 3-2 shows the reference directions used within this thesis when referring to the global vessel and local panel directions.

Figure 3-2: References to longitudinal and transverse directions are specific to the panels within the lifeboat. The long edge of the panel is coincident with the longitudinal direction and the short edge with the transverse.

When considering structural response at a panel level, the individual panels can be considered flat plates of differing sizes. The local loading of the flat plates in this scenario can be considered a distributed load over the entire plate. However the exact distribution and application of that load is outside the scope of this thesis to investigate and is therefore reserved for further work.

The response of a flat plate to the load case identified results in the centre point of the plate deflecting by some amount depending on the load and the boundary conditions; with reduced deflections radiating from this point towards the edges, with the boundary conditions having

more of an effect as you get closer. The result of this deflection is that the loaded face of the plate will be in compression whilst the opposite face will be in tension which results in shear stresses acting through the thickness of the plate. In many instances it is acceptable to simplify this problem to assume the shear stresses are negligible and therefore the plate acts like a shell with membrane stresses either side of the neutral axis (Timoshenko and Woinowsky-Krieger, 1987). Under this assumption material tests conducted in pure tension will represent the problem well enough to generate representative material properties.

However for composite materials the through thickness shear stresses caused by bending are more important than for homogenous materials. As well as the through thickness shear stresses that are induced through bending there is also likely to be stress discontinuities through variations in lamina properties within the laminate material. There is a strong possibility that the combination of these shear stresses may invalidate the assumption of membrane stresses in this instance. Therefore engineering judgement was exercised and tests under bending conditions were also specified.

Since the easiest way to conduct material characterisation tests are through beam tests, the best representation of the actual conditions is required. Ideally this would be a beam under uniform load, as shown in Figure 3-3 [1]. This is not an easy loading regime to represent experimentally and as discussed in the literature review two standard options for conducting bending tests are available, four and three point bend tests. Considering the shear force and bending moment diagrams under the different regimes, shown in Figure 3-3 [2] and [3] respectively, will identify the best representation achievable.

As can be seen from this figure a four point bend results in a constant bending moment and zero shear force between the applied loads whereas a three point bend results in a constant shear force and an increasing bending moment between the support points and the load application point. Comparing this to the uniform load which shows a linear reduction in shear force and a parabolic increase in bending moment between the supports and the centre of the beam, in terms of shear force the 4 point bend is more comparable. In addition if the length of the beam l is significantly less than the length or width of the plate, a or b, then considering that only a small portion of the central part of the plate is being measured in the load response measurement work, a constant bending moment can be assumed.

Therefore considering both shear force and bending moments 4 point bends are more representative of the measured problem and will therefore be used alongside tensile tests when characterising the materials. Finally when considering composite plates material orientation must

be taken into account and as such material tests in both the longitudinal and transverse directions are carried out.

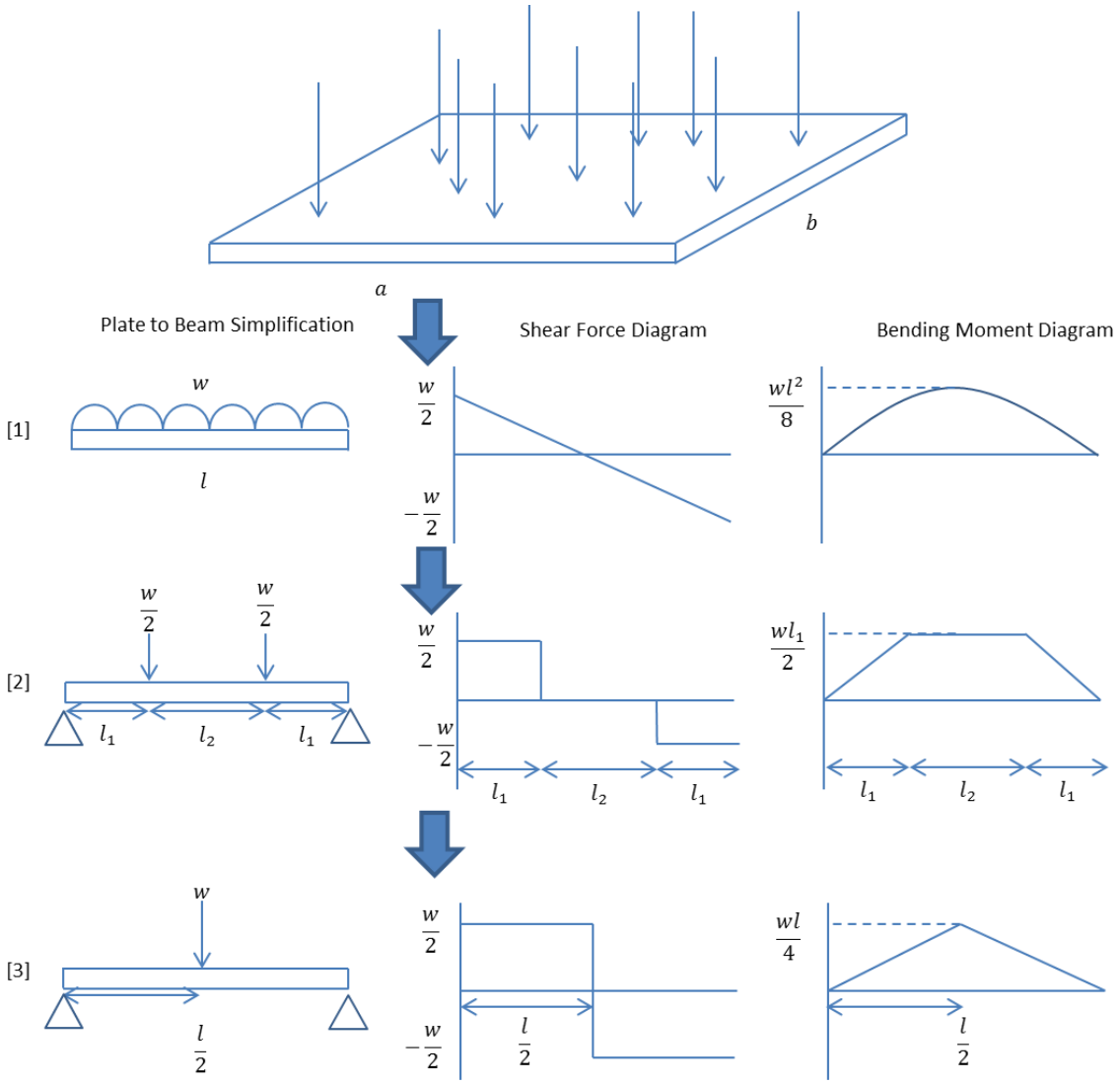

Figure 3-3: Simplification of panel with constant load to different possible test regimes with associated shear force and bending moment diagrams. [1] beam with uniform load, [2] beam with two point loads, 4 point bend and [3] beam with a single point load, 3 point bend.

Referring to the plate schematic at the top of Figure 3-3, side a will be considered coincident with the longitudinal direction in Figure 3-2 and side b with the transverse direction. Typically composite materials have a principle material direction which is the strongest direction and normal to that is the weakest direction. In this work the principle material direction is coincident with the transverse direction and is referred to in the material characterisation chapter as the [90] direction and normal to this with the longitudinal direction and is referred to as the [0] direction. The references are in terms of the boat principle and normal directions not the material principle and normal directions, this is summarised in Figure 3-4

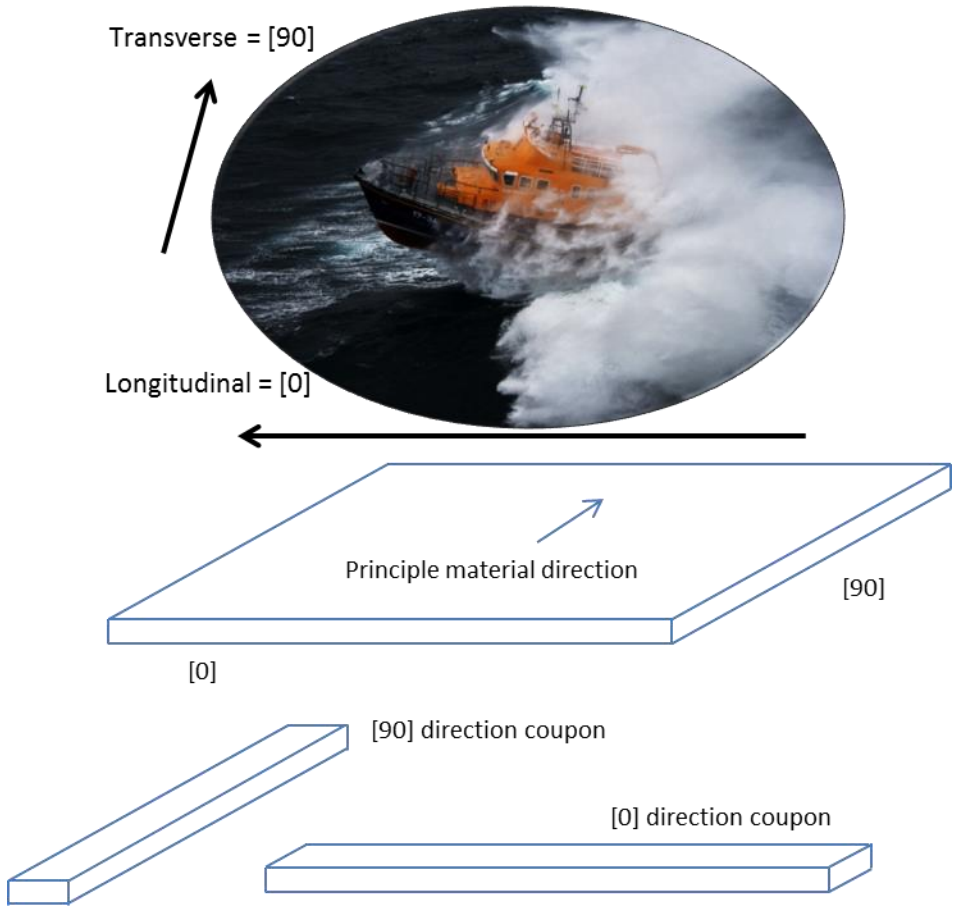

Figure 3-4: Summary of the references used within this thesis when moving between boat, plate, coupon and material directions.

Intentionally left blank

4 Material Characterisation

Figure 3-1 highlighted that understanding how the materials within the structure will last during operations, understanding how the structural materials fatigue, is key to deciding whether to life extend an asset or not. This chapter introduces a method to generate that understanding, providing an extension to current knowledge of fatigue of complex hybrid glass and aramid materials as used in the Severn class lifeboat.

Material characterisation is in this case defined in terms of the fatigue properties of materials, specifically the derivation of S-N data. There are numerous different ways to represent fatigue data of materials as discussed in section 2.4. Ideally an understanding of all the different types of structural features is required for a full and complete analysis, however this type of complete characterisation is outside the scope of work of this thesis and therefore only the hull shell is analysed for fatigue properties.

4.1 General Approach to Material Characterisation

Figure 4-1 shows the general model for understanding the materials; initially material fatigue modelling should take place, the methodology used here is easily applied to any feature on an asset, assuming appropriate test samples and test regimes developed. This is achieved through an appropriate theory to determine the expected strength and developing an appropriate S-N curve for the material under investigation, an example of this is shown in Roberton et al (Roberton D.M.V et al., 2009). This work is expected to have taken place during the initial design phase for an asset. However, within the marine industry often the initial analysis relies on the assumption that building a structure with a large enough factor of safety will account for any fatigue issues within the design life of the asset. Therefore fatigue studies are often not conducted on the specific materials used on marine assets.

Once the modelling of the engineering constants has been completed the resulting S-N curves should be used as the one material variable in a structural life extension assessment, which combined with an understanding of the structural response, discussed in Chapter 6, should be able to provide an initial structural life assessment. Once this has been completed a decision can be made as to whether further material characterisation through experiment is necessary.

If it is determined that further characterisation is necessary then appropriate testing needs to be conducted. This testing begins by finding the ultimate strength (σ_{ult}) values for the material then setting these as the initial material properties for the structure. Following this appropriate fatigue tests at various values of applied stress normalised by the ultimate strength $\left(\sigma_{app}/\sigma_{ult}\right)$ need to

be conducted thus producing an S-N curve. Once the appropriate fatigue tests have been conducted, a comparison between the modelled S-N curve and that derived through testing should be made to understand the variation between the two and therefore the potential margins of safety generated at this stage.

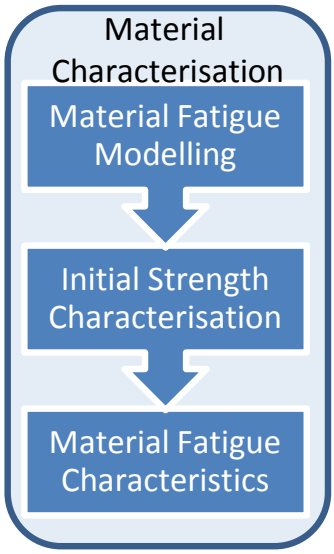

Figure 4-1: General approach to determining the fatigue characteristics of the materials used in the structure under investigation.

4.2 Materials

For the Severn Class Lifeboat all the materials used in the construction of the original hull lamina cloths and resin system (Ampreg 75 pre yr. 2000 and ST 94 post yr. 2000) was provided by SP Systems between 1995 and 2004, material details are shown in Table 4-1 and the original hull layup is shown here:

$$[(2xYE)_{90}, (4xQEA), (2xYE)_{90}]$$

Table 4-1: Details of original hull laminate construction materials, *data taken from the ST 94 data sheet

Ply Name	Reinforcement Detail	Matrix Detail	Manufacture Method
YE 1597	Glass (90,±45)	Pre Yr 2000 Ampreg 75 Post Yr 2000 ST94	Dry Layup, Oven Cured
QEA 1201	Glass / Aramid (0, 90, ±45)		

The original materials were not available, and in addition the ST 94 has been modified by the manufacturer significantly since its first use by the RNLI. Information regarding the material properties of the QEA1201 and the Ampreg 75 layup were taken from a material mechanical properties document provided to the RNLI in 1995 (Belgrano, 1995). Material properties for the

ST 94 was taken from the ST 94 data sheet (Gurit, 2007) which also contains material data using this resin system for QEA1201 and YE1597.

To overcome the missing YE1597 a combination of Uni directional and bidirectional lamina were used, the comparable weight of fibres in each direction are shown in table Table 4-2. The difference between the resulting lamina and the original YE1597 was a reduction of 134 g/m^2 in the longitudinal direction and the fact they are not stitched together, which accounts for the difference in weight.

Table 4-2: Details of the final construction materials chosen to replicate the original YE1597 lamina no longer available.

Ply Name	Glass in 0^o (g/m^2)	Glass in 45^o (g/m^2)	Glass in 90^o (g/m^2)	Glass in -45^o (g/m^2)
YE 1597	0	225	1134	225
UE 500 (x2)	0	0	1000	0
XE 450	0	225	0	225
Difference	0	0	134	0

The QEA 1201 was replaced with QEA1204, the difference being that the (0/90) core of the 1201 was woven whereas for the 1204 it was stitched. This was not expected to have a significant impact on the ultimate strength values, but may have an impact on the fatigue characteristics of the material due to the stress concentrations caused by the kinking of the fibres. The final ply layup chosen for the tests is shown below:

$$[(2x((2xUE500)_{90}, XE450)), (4xQEA1204), [(2x((2xUE500)_{90}, XE450))]$$

The resin system used was Ampreg 26 a wet laminate epoxy resin with material properties which are considered comparable to those of ST94, this resin system is regularly used to perform repairs on Severn Class Lifeboats and has been proven to be compatible in service. Table 4-3 shows the weight of the constituent in the lamina in the four different directions [0/90/±45] for all the lamina used in both the construction of the original structure and the test coupons.

Table 4-3: Fibre content for each of the individual lamina discussed in this section.

Ply Name	Glass / Aramid in 0^o (g/m^2)	Glass / Aramid in 45^o (g/m^2)	Glass / Aramid in 90^o (g/m^2)	Glass / Aramid in -45^o (g/m^2)
YE 1597	0 / 0	225 / 0	1134 / 0	225 / 0
QEA 1201	283 / 51	236 / 51	267 / 54	267 / 54
UE 500	500 / 0	0 / 0	0 / 0	0 / 0
XE 450	0	225 / 0	0	225 / 0

4.2.1 Expected Effects due to Material Inconsistencies

The original Ampreg 75 was a pre-preg system and the replacement, ST94, is a proprietary dry fabric backed with resin which is cured under pressure and temperature, a form of resin transfer moulding (RTM). The representative material was constructed using a resin infusion process. This also presents the possibility for differences between the representative and actual laminates due to the manufacturing processes. This is discussed by Cavatorta (Cavatorta, 2007) who found that in a comparison between hand layup HL and RTM methods the HL coupons had superior fatigue lives to those created using the RTM method. In this case, although the differences in manufacturing method are not as significant it can still be expected that the material fatigue properties may change.

4.2.2 Material Test Procedure

The coupon test panel was made in the RNLI's own construction facility using a resin infusion technique on a panel table according to the layup specification on the previous page. The resin used for the coupons was Ampreg 26 wet laminating system provided by Gurit. Two types of samples were then cut from this panel using a diamond band saw, type 2 specimens as specified in (BS EN ISO 527, 1997) and type III specimens as specified in (BS EN ISO 14125, 2011).

The details of the coupons used for tensile and flexural tests are shown in Table 4-4. Due to the thickness of the samples using end tabs for the tensile tests would have resulted in samples to wide for the machine grips available at the time. Additionally advice in the standard suggests testing without tabs first, then if there are grip induced failures tabs should be added. No premature failure due to the machine grips was found therefore there was no reason to apply end tabs.

The tensile tests were carried out by TWI according to Parts 1 and 4 of BS EN ISO 527 (1997), with 5 in the [0] direction and 5 in the [90] direction. The strain was measured by strain gauges on both sides of the coupons as well as optical strain measurement on one side, with longitudinal and transverse strain being measured. The use of both optical and foil gauge recording techniques was to mitigate against failed foil gauges. The standard DIC speckle pattern application method proved difficult to achieve due to the surface finish of the specimens, so a manmade speckle effect was used to provide the DIC referencing points. Due to the nature of the setup the opportunity to use a trigger line to start the optical strain reading at the same time as the load application was not possible. However it was expected that the strain gauge applied to the transverse direction to the coupon would not fail therefore the initial transverse strain values

could be used to match the strain traces developed from the strain gauges and the optical strain measurement.

22 4 point bend tests according to BS EN ISO 14125 (2011), initially 10 tests at a support span of 221mm were carried out at TWI. Due to issues identified during fatigue testing with achieving actuation frequency of 5mm, further tests at a lower support span of 159mm were carried out. 10 tests were carried out at high actuation speeds and 2 at low actuation speeds as shown in Table 4-4.

Table 4-4: Test coupon details

Tensile Test Coupon Numbers	L x b (mm)	Load Application Speed (mm/min)
T[0]-01 to 05 and 11 to 35, T[90]-06 to 10	250 x 25	2
Coupon Numbers (Test House)	**Support / Load Span (mm)**	**Load Application Speed (mm/min)**
F[0] – 01 to 05 and F[90] – 06 to 10 (TWI)	221 / 74	5
F[0]-11 to 29, F[0]-32 to 35 and F[0]-61, 62 (NPL)	159 / 53	30
F[0]-30 (NPL)	159 / 53	5
F[90]-36 to 60 (NPL)	159 / 53	50
F[90]-55 (NPL)	159 / 53	5

4.3 Static Properties

Initially the static material properties were modelled through rule of mixture and elastic equivalent property calculations, which were then compared to tensile and flexural test results. Tensile and flexural tests were carried out as it is expected that in this application both tensile loads due to membrane stresses and bending loads due to localised loading will be experienced. Four point bend tests were carried out over 3 point bends to isolate the loaded region from shear forces, subjecting the samples to bending moments, therefore bending stresses only and thus better represent the area of strain measurement discussed in the Structural Response Monitoring chapter.

4.3.1 Modelling Engineering Constants

The material data for the UE 500 was estimated from a simple rule of mixtures calculation, shown in equation 4-1, with an assumed fibre volume fraction of 0.47 and the material data for the QEA1201 and XE450 systems were taken from the RNLI's own material data base.

$$E_c = E_f v_f + E_m(1 - v_f) \qquad \textbf{4-1}$$

Some of the material information for the YE 1597 lamina used in the original layup can be found in the data sheets for the ST94 laminating system, the missing information such as the shear modulus, G_{12} and poisons ratio ν, were estimated from material values for similar woven glass/epoxy fabrics found in the RNLI's material data base. The cast tensile modulus for the Ampreg 26 Epoxy resin was taken from the Ampreg 26 data sheet (Gurit, 2008), G_{12} and ν values were taken from Epoxy (977-3) in Table A.3 in Daniel (Daniel, 2006).

Table 4-5: Material properties for the individual lamina used in the original build and in this investigation.

Ply Name	Fibre Volume Fraction (%)*	E_x (GPa)*	E_y (Gpa)	G_{xy} (Gpa)	Poissons Ratio ν
YE 1597 (ST 94 Data Sheet)	49.1	31.2	12.9	5.2	0.15
QEA 1201 (ST94 Data sheet)	47.5	17.8	17.8	5.7	0.28
QEA 1201 (Ampreg 75 Data shet)	Unspecified	21.3	21.3	Unspecified	Unspecified
UE 500 (calculated, Ampreg 26)	47	36.0	8.0	3.5	0.29
XE450	42	18.6	18.6	2.8	0.09

A classical laminate theory tool was used to generate the elastic equivalent properties for both the original laminate specification and the test coupon specification. The predicted constants are shown in Table 4-6.

The thickness of the original laminate was found to be 9.28mm, the thickness of the resultant representative laminate was predicted to be 14.72mm an increase in thickness of nearly 60%. However this is due to the fact that in the original laminate there are 2 layers of YE1597 with a thickness of 1.25mm each, whereas the representative laminate contains 6 glass layers of 2 different constructions (XE450 and UE500) to replicate the YE1597 with a total thickness of 4.84mm rather than 2.5mm, an increase of nearly 90% over the original laminate. This increase in thickness can be managed during the manufacture of the coupons through increased consolidation of these layers, although this may have detrimental effects on the fatigue life by causing dryness in the samples. There are also significant differences between the predicted values of the structural material and the representative layup, for some constants a reduction of up to 37% is seen.

Table 4-6: Laminate constants for analysis.

Laminate	In Plane Properties			Flexural Properties		
	E_x (MPa)	E_y (MPa)	G_{xy} (MPa)	E_{xj} (MPa)	E_{yj} (MPa)	G_j (MPa)
Original	17095	26701	6044	13829	30262	5380
Replicate	13228	27243	4131	10852	31492	3408
Difference (%)	22	-2	32	22	-4	37

4.3.2 Static Tests

The full set of images of failed coupons can be found in the Appendix, section 11.1. A select summary are used to support the following discussions. The coupons are referred to as **T/F[0/90]-##** where **T** indicates tensile and **F** indicates flexural, **[0/90]** the direction in relation to the lifeboat structure as defined in Figure 3-4 and **##** is the coupon number.

The machine used for the tensile tests was an Instron servo-hydraulic machine with an 8800 controller and 100kN capacity. For all tensile tests equation 4-2 was used to calculate the stress at failure, σ_f, (BS EN ISO 527, 1997).

$$\sigma_f = \frac{F}{A} \qquad \textbf{4-2}$$

Where F is the applied force and A is the cross sectional area of the specimen.

The modulus values $E_{[0,90]}$ were calculated using using equation 4-3 and calculated stress values at 500με and 2500με, except in the case of the optically recorded analysis where the closest values were chosen

$$E_t = \frac{\sigma_{2500_{\mu\varepsilon}} - \sigma_{500_{\mu\varepsilon}}}{\varepsilon_{2500_{\mu\varepsilon}} - \varepsilon_{500_{\mu\varepsilon}}} \qquad \textbf{4-3}$$

Where E_t is the tensile modulus in either the [0] or [90]direction

The poisons ratio,μ_b, was calculated using the longitudinal strain value of 2500με and the corresponding measured transverse strain value using equation 4-4.

$$\mu_b = \frac{\varepsilon_{\text{long}}}{\varepsilon_{\text{trans}}} \qquad \textbf{4-4}$$

The first batch of flexural tests were conducted on an Instron servo-hydraulic machine with an 8500 controller with a 500kN capacity, using a 50kN load cell. The machine used for the second batch of tests was an Instron 1250 servo-hydraulic machine with a 10kN load cell controlled using Instron series IX software. For all the flexural tests the procedures found in BS EN ISO 14125

(2011) where used to calculate the failure stress, where equation 4-5 was used for the short span tests and equation 4-6 for the wide support span tests where the deflection was found to exceed 0.1 x L.

$$\sigma_f = \frac{FL}{bh^2} \quad \textbf{4-5}$$

Where F is the applied force, L is the support span, b the specimen width and h the specimen thickness.

$$\sigma_f = \frac{FL}{bh^2}\left\{1 + 8.78\left(\frac{s}{L}\right)^2 - 7.04\left(\frac{sh}{L^2}\right)\right\} \quad \textbf{4-6}$$

Where F is the applied force, L is the support span, b the specimen width, s the displacement and h the specimen thickness.

The expected strains were calculated using 4-7 in the small deflection case and 4-8 in the large deflection case.

$$\sigma_f = \frac{FL}{bh^2} \quad \textbf{4-7}$$

Where F is the applied force, L is the support span, b the specimen width and h the specimen thickness.

$$\varepsilon = \frac{h}{L}\left\{4.7\frac{s}{L} + 14.39\left(\frac{s}{L}\right)^3 - 27.70\left(\frac{s}{L}\right)^5\right\} \quad \textbf{4-8}$$

Where F is the applied force, L is the support span, b the specimen width, s the displacement and h the specimen thickness.

The flexural modulus was calculated by first calculating the displacements which would give a flexural strain of 500με and 2500με from equation 4-9:

$$s_\varepsilon = \frac{\varepsilon^f L^2}{4.7h} \quad \textbf{4-9}$$

Where s_ε is the resultant displacement, L is the support span, h the specimen thickness and ε^f the flexural strain, either 500με or 2500με

The resultant displacements are then used to calculate the modulus from equation 4-10

$$E_f = \frac{0.21L^3}{bh^3}\left(\frac{\Delta F}{\Delta s}\right) \quad \textbf{4-10}$$

Where E_f is the flexural modulus in either the [0] or [90] direction, ΔF is the change in applied force and Δs is the change in displacement.

The resultant strain on the outer surface was then calculated using equation 4-11 for the shorter span tests and equation 4-12 for the longer support span tests due to the deflection exceeding 0.1 x L.

$$\varepsilon = \frac{4.7sh}{L^2} \quad \textbf{4-11}$$

$$\varepsilon = \frac{h}{L}\left\{4.7\frac{s}{L} - 14.39\left(\frac{s}{L}\right)^3 + 27.7\left(\frac{s}{L}\right)^5\right\} \quad \textbf{4-12}$$

Having calculated the failure stress and modulus values for each of the samples within each group the standard deviation, SD, was calculated using the procedure in (BS 2846-2: 1981, 1981), according to equation 4-13 where μ is the variance, $\bar{x}$ is the average and N is the total number of samples taken.

$$\mathrm{SD} = \sqrt{\frac{1}{N-1}\sum_{i=1}^{N}(x_i - \bar{x})^2} \quad \textbf{4-13}$$

The 95% confidence limit, which determines the expected range of values either side of the mean which is expected to contain 95% of the total population, based on this sample is calculated from 4-14

$$95\%\ \text{Confidence Level} = \pm t_{0.95}\frac{\mathrm{SD}}{\sqrt{N}} \quad \textbf{4-14}$$

Where $t_{0.95}$ is the value selected from students table of t values for two sided distribution, in this case taken from (BS 2846-2: 1981, 1981, p. 4).

4.3.2.1 Coupons T[0]-01 to 05

A Typical image for the coupon failure in the [0] direction are shown in Figure 4-2. All coupons failed in a consistent manner, typically failing in the centre portion of the material. Failure

occurred well away from the grip locations in the region being monitored by both the strain gauges and the optical strain measurements. The failure of the coupons can be split into two distinct parts, failure in the e-glass outer layers and failure in the inner E-glass / Aramid hybrid layers. With a single crack across the coupon width occurring in the E-glass layers associated with the unidirectional and ±45 direction plies. The crack generally occurred in different locations on the two different sides with localised delamination's occurring at the interface between the outer glass plies and the inner hybrid lamina. In the hybrid layers the failure comprised of cracking across lamina and delamination's between layers.

Figure 4-2: Typical post failure images for tensile tests in the [0] direction.

Figure 4-3 shows a typical graph of the applied stress verses resultant strain for these coupons, graphs for the rest of the tests are found in Appendix 1.1. Table 4-7 shows the variables recorded and the results of the derivation of the failure stress, moduli and poisons ratio information from the tests as dictated in the standard (BS EN ISO 527, 1997).

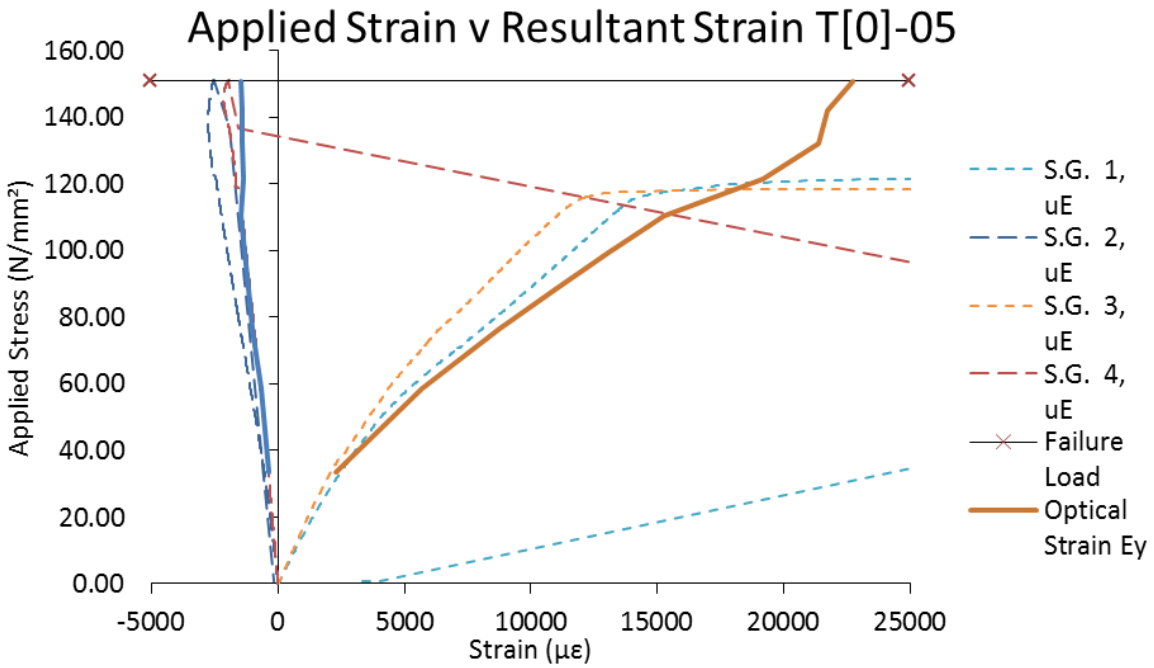

Figure 4-3: Strain gauge and optical strain measurement values for tensile test conducted on sample T[0]-05. This result is typical of the Applied Stress v Strain curves for all the [0] tests. The full sets of graphs are shown in Appendix 1.

Table 4-7: Selected data from the ultimate tensile strength test results for the individual test coupons

Coupon Number	Strength (N/mm^2)	Poissons Ratio, μ_b			Modulus ($E_{[0]}$)		
		SG2 / SG1	SG4 / SG3	Trans / Long	SG1 (Gpa)	SG3 (Gpa)	Opt Long
T[0]-01	157.1	0.20	0.17	0.20	16.0	15.3	9.07
T[0]-02	158.1	0.21	0.17	0.13	13.9	16.4	5.96
T[0]-03	164.1	0.20	0.17	0.17	12.8	16.8	6.35
T[0]-04	132.9	0.22	0.18	0.13	19.7	13.4	7.94
T[0]-05	151.0	0.22	0.18	0.17	12.9	15.3	7.44
Average	152.6	0.21	0.17	0.16	15.1	15.4	7
Standard Deviation	12.0	0.01	0.01	0.03	2.90	1.31	1.25
Confidence Interval (95%)	±14.86	±0.01	±0.01	±0.04	±3.59	±1.64	±1.55

4.3.2.2 Coupons T[90]-06 to 10

A Typical image for the coupon failure in the [90] direction are shown in Figure 4-4. The failure could also be split into 2 distinct failure areas 1 either side of the coupon, characterised by clear signs of fibre breakage in the E-glass plies (with the fibre direction longitudinal to the coupon). The failure did not occur as close to the central monitored location as hoped, however all coupons failed in excess of 10mm from the location of the grips. The failure still showed a transverse crack across the E-glass layers, however the crack site was significantly less well defined and on one test, T[90]-06, two separate possible initiation sites were observed on one face. Failure in the hybrid layers was typically due to delamination between layers in several locations followed by fibre breakage.

Figure 4-4: Typical post failure images for tensile tests in the [0] direction (a) and the [90] direction (b)

Figure 4-5 shows a typical graph of the applied stress verses resultant strain for these coupons, graphs for the rest of the tests are found in Appendix 1.1. Table 4-8 shows the variables recorded and the results of the derivation of the failure stress, moduli and poisons ratio information from the tests conducted in [90] directions.

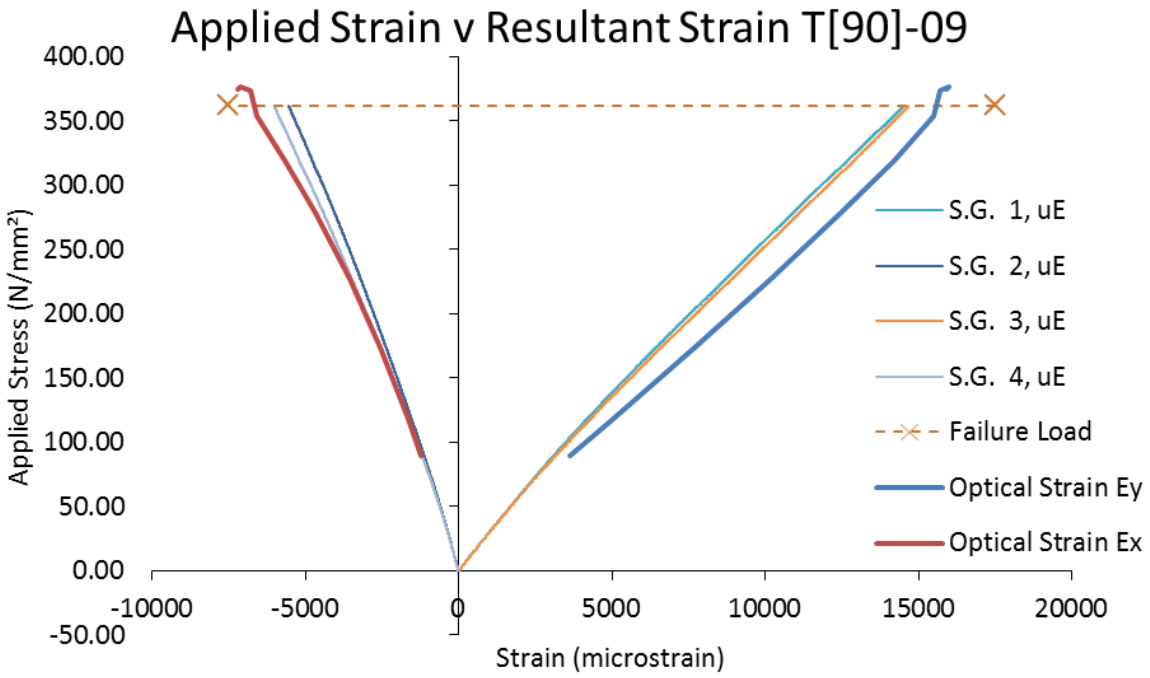

Figure 4-5: Strain gauge and optical strain measurement values for tensile test conducted on sample T[90]-09. This result is typical of the Applied Stress v Strain curves for all the [90] tests. The full sets of graphs are shown in Appendix 1.

Table 4-8: Data from the ultimate tensile strength test results for the individual test coupons, full data is found in Appendix 1.2. *The maximum load and calculated strength values were not used to calculate the Standard Deviation or Coefficient due to known issues with the test resulting in premature test ending.

Coupon Number	Strength (N/mm^2)	Poissons Ratio, μ_b			Modulus ($E_{[90]}$)		
		SG2 / SG1	SG4 / SG3	Trans / Long	SG1 (Gpa)	SG3 (Gpa)	Opt Long
T[90]-06	353.8	-0.35	-0.41	-0.28	27.84	29.8	31.06
T[90]-07	353.5	-0.42	-0.41	-0.30	29.44	29.1	20.13
T[90]-08*	342.4	-0.36	-0.41	-0.27	29.18	29.8	17.15
T[90]-09	361.7	-0.38	-0.41	-0.34	29.75	29.4	20.10
T[90]-10	359.3	-0.41	-0.40	-0.29	29.09	29.2	17.76
Average	357.1	-0.38	-0.4	-0.3	29.06	29.4	21.2
Standard Deviation	7.45	0.03	0.00	0.03	0.73	0.32	5.65
Confidence Interval (95%)	±9.25	±0.04	±0.00	±0.03	±0.64	±0.28	±4.95

4.3.2.3 Coupons F[0]-01 to 05

As can be seen in Figure 4-6 for the coupons F[0]-01 to 05 there was limited significant permanent set shown after the completion of the tests. In all cases failed samples were found to have indications of buckling on the upper surface as well as through thickness cracks in this layer leading to delamination which runs along the interface between the outer glass layers and the inner aramid glass layers. In two coupons (F[0]-02, 04) there was also evidence of delamination at the interface between the aramid / glass and glass only layers and in the case of coupon F[0]-01 within the glass only layers associated with the tensile surface.

Figure 4-6: Typical post failure sample for static tests F[0]-01 to 05.

Figure 4-7 shows a typical graph of the flexural stress verses strain for these coupons, both measured and calculated. Graphs for the rest of the tests are found in Appendix 1.1. Figure 4-8 shows the measured displacement against applied flexural stress for all the F[0] flexural tests. Focusing on the results for F[0]-01 to 05 it is seen that there is very close correlation in the coupon response to flexural stress across all five specimens. Table 4-9 shows the variables recorded and the results of the derivation of the failure stress, moduli and poisons ratio information from the tests conducted in [0] directions.

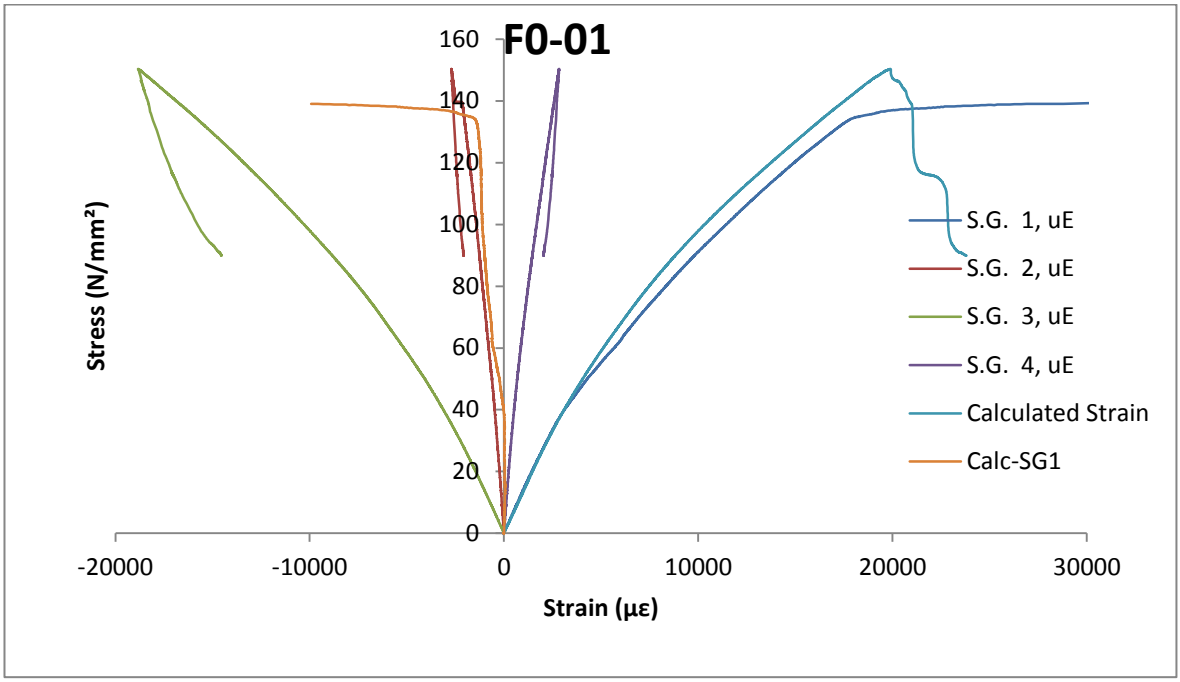

Figure 4-7: Stress strain plot for sample F[0]-01 which is representative of plots for F[0]-01 to 05.

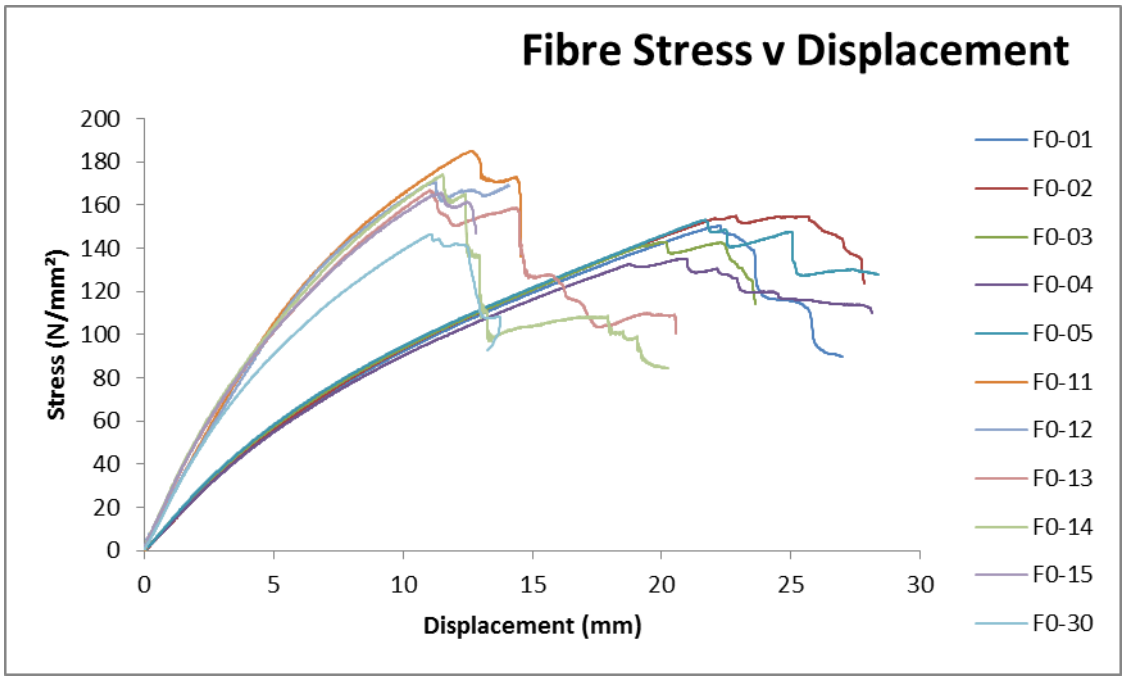

Figure 4-8: Comparison of Stress versus displacement plots for samples F[0]-01 to 05, F[0]-10 to 15 and F[0]-30.

Table 4-9: Material properties determined from F[0]-01 to 05 test coupons. For these coupons all of the strain gauges failed prior to material failure; however enough information was gathered to calculate the flexural modulus from the measured strains.

Specimen Number	Failure Stress (N/mm^2)	Failure Strain Calculated (με)	Failure Strain Measured (με)	Flexural Modulus Calculated Strain (kN/mm^2)	Flexural Modulus Measured Strain (kN/mm^2)
F[0]-01	150.38	1990	-	13.0	13.0
F[0]-02	154.98	2030	-	13.3	13.2
F[0]-03	142.88	1790	-	13.9	12.7
F[0]-04	134.95	1860	-	13.1	13.0
F[0]-05	153.15	1920	-	14.1	13.1
Average	147.27	1910	N/A	13.47	13.00
Standard deviation	8.29	97	N/A	0.49	0.19
Confidence Interval (95%)	10.29	120	N/A	0.61	0.23

4.3.2.4 Coupons F[0]-11 to 15 and F[0]-30

Coupons F[0]-11 to 15 were all left with a considerable degree of permanent set as seen in shown in Figure 4-9. There were also clear signs of buckling in the compressive surface which lead to fracture in this layer and the first layer of the glass / aramid material, associated with this is an intra-lamina delamination in the first hybrid layer. This can be seen through the presence of fibres on both sides of the delamination face. In all samples there are also delaminations on the tensile side of the coupon within the glass only material which appear to be at the interfaces between the longitudinal material and the [±45] material.

For coupon F[0]-30 also shown in Figure 4-9 there showed signs of compressive failure within the glass layers along with through thickness cracking in this layer and limited delamination between layers.

Figure 4-9: Typical post failure sample for static tests F[0]-011 to 15 and F[0]-30.

Figure 4-10 shows a typical graph of the flexural stress verses strain for these coupons, both measured and calculated. Graphs for the rest of the tests are found in Appendix 1.1. Table 4-10 shows the variables recorded and the results of the derivation of the failure stress, moduli and poisons ratio information from the tests conducted.

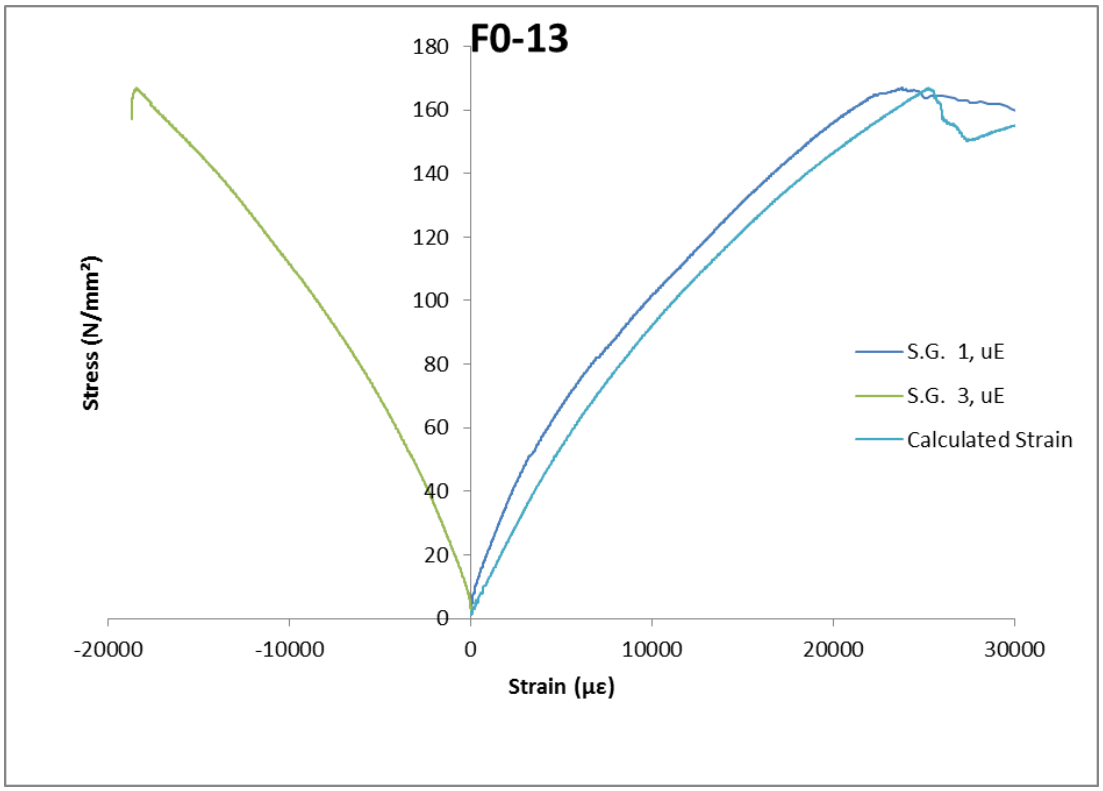

Figure 4-10: Stress strain plot for sample F[0]-13 which is representative of plots for F[0]-11 to 15.

Table 4-10: Material properties determined from F[0]-11 to15 test coupons. For these coupons 4 out of 5 strain gauges failed prior to material failure; however enough information was gathered to calculate the flexural modulus from the measured strains. *Values not used to calculate the average, standard deviation or confidence interval of the flexural modulus as measured due to strain gauge errors.

Specimen Number	Failure Stress (N/mm2)	Failure Strain Calculated (με)	Failure Strain Measured (με)	Flexural Modulus Calculated Strain (kN/mm2)	Flexural Modulus Measured Strain (kN/mm2)
F[0]-11*	201.70	2200	-	13.0	10.1
F[0]-12*	183.24	1970	-	12.0	6.4
F[0]-13	178.92	1950	2380	14.1	14.0
F[0]-14	187.52	2030	-	14.5	13.9
F[0]-15	178.66	2040	-	13.9	13.6
Average	186.01	2038	N/A	13.50	13.85
Standard deviation	9.49	98.34	N/A	1.00	0.21
Confidence Interval (95%)	11.78	122.08	N/A	1.24	0.4
F[0]-30	146.56	1980	-	17.8	19.4

Referring back to Figure 4-8, focusing on the results for F[0]-11 to 15 it is seen that, as with the previous set there is very close correlation in the coupon response to flexural stress across all five specimens. The trace of the F[0]-30 specimen shows a comparable failure stress as the F[0]-01 to 05 samples helps to confirm that the increase in failure stress for F[0]-11 to 15 coupons is caused by the increase in load application speed, rather than the reduction in span.

4.3.2.5 Coupons F[90]-06 to 10

A typical image of post failure samples for F[90]-06 to 10 coupons is shown in Figure 4-11, indications of buckling of the upper surface were found in some cases, though there was no evidence of through thickness cracking in these layers. There was also evidence of inter lamina delamination within the glass only layers as well intra-lamina delamination in the hybrid layer, which interfaces with the glass only lamina on the compressive side. In the case of F[90]-06 the tensile side also showed delamination of the aramid layers, although this was not present in all coupons.

Figure 4-11: Typical post failure sample for static tests F[90]-06 to 10.

Figure 4-12 shows the measured displacement against applied flexural stress for all the F[90] flexural tests. Focusing on the results for F[90]-06 to 10 it is seen that there is very close correlation in the coupon response to flexural stress across all five specimens.

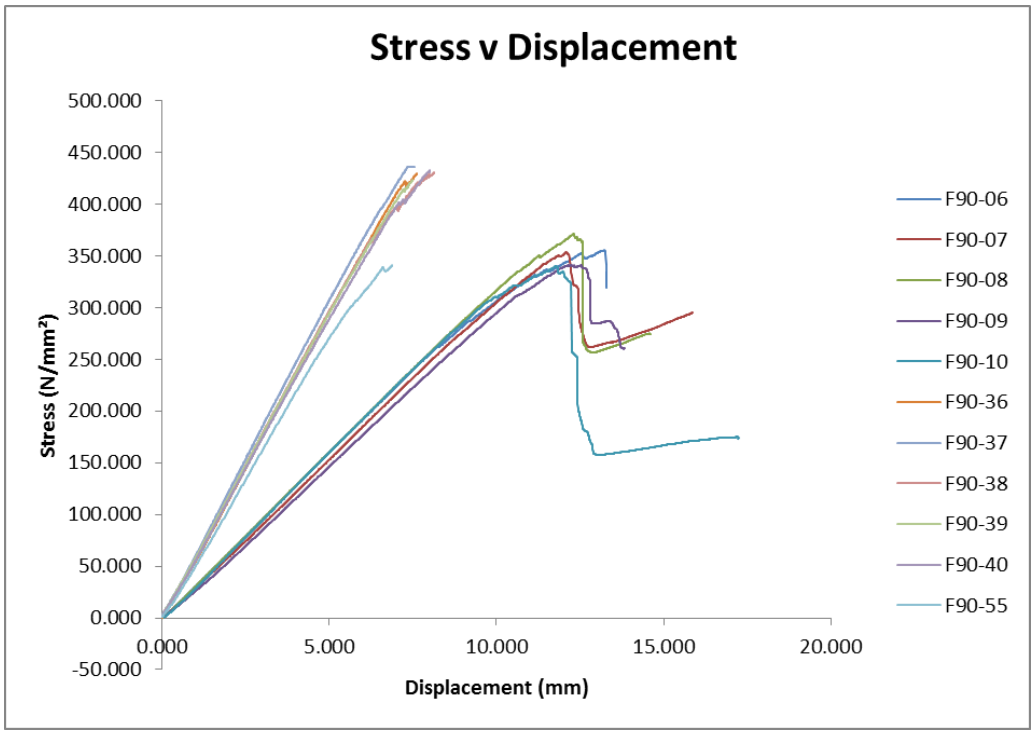

Figure 4-12: Comparison of Stress versus displacement plots for samples F[90]-06 to 10, F[90]-36 to 40 and F[90]-55.

Figure 4-13 shows a typical graph of the flexural stress verses strain for these coupons, both measured and calculated. Graphs for the rest of the tests are found in Appendix 1.1. Table 4-11 shows the variables recorded and the results of the derivation of the failure stress, moduli and poisons ratio information from the tests conducted.

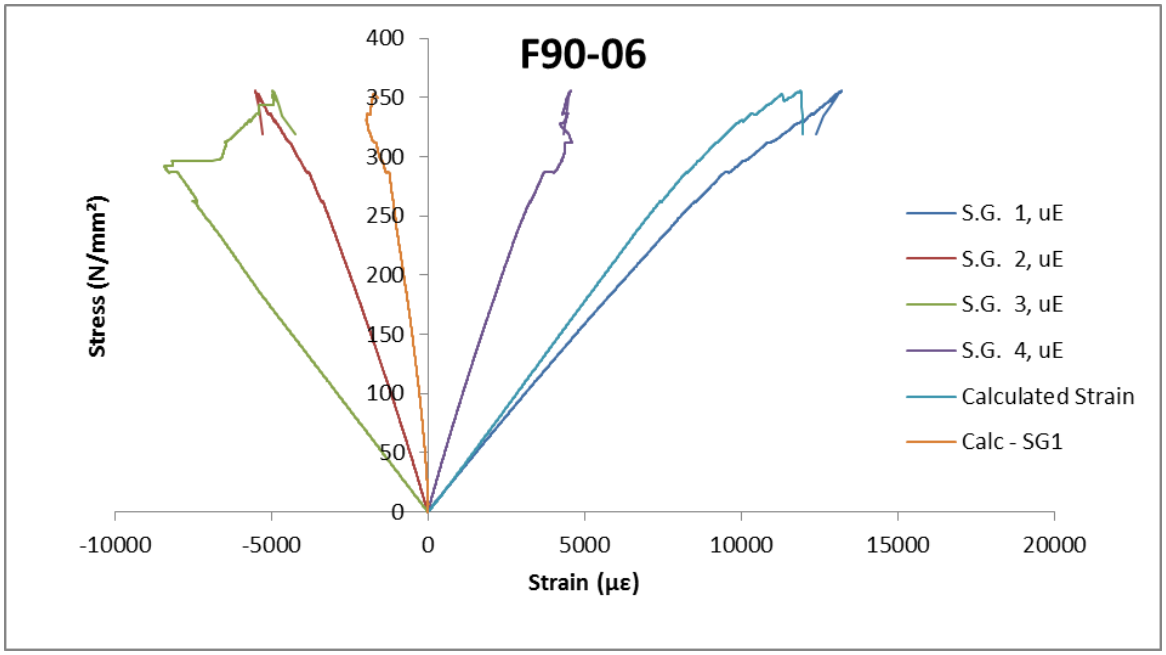

Figure 4-13: Stress strain plot for sample F[0]-13 which is representative of plots for F[0]-11 to 15.

Table 4-11: Material properties determined from F[90]-06 to10 test coupons.

Specimen Number	Failure Stress (N/mm^2)	Failure Strain Calculated %	Failure Strain Measured %	Flexural Modulus Calculated Strain (kN/mm^2)	Flexural Modulus Measured Strain (kN/mm^2)
F[90]-06	360.48	1180	1320	35.2	31.8
F[90]-07	357.35	1080	1200	33.4	31.2
F[90]-08	375.42	1080	1140	36.4	33.9
F[90]-09	345.04	1090	1270	31.4	29.8
F[90]-10	343.57	1070	1270	35.0	31.0
Average	356.37	1100	1240	34.27	31.53
Standard deviation	12.97	45	70	1.93	1.51
Confidence Interval (95%)	3.64	56	87	2.40	1.87

4.3.2.6 Coupons F[90]-36 to 40 and F[90]-55

A typical post failure image For F[90]-36 to 40 coupons shown in Figure 4-14. The coupons were found to have permanent set after the tests, although it is much less than for F[0]-11 to 15 samples. All coupons displayed significant indication of buckling within the upper layers and delamination between layers within the glass only material. In 3 of the 5 samples (F[90]-36, 37 and 39) there is also associated through thickness cracking in the very outer delaminated layers. 2 coupons (F[90]-37 and 38) also displayed significant intra-lamina delamination in the hybrid layer interfacing with the glass only lamina on the tensile side of the specimen. Coupon F[90]-40, also

shown in Figure 4-14, displayed significant delamination, however in this case it was at an interface within the aramid / glass layers.

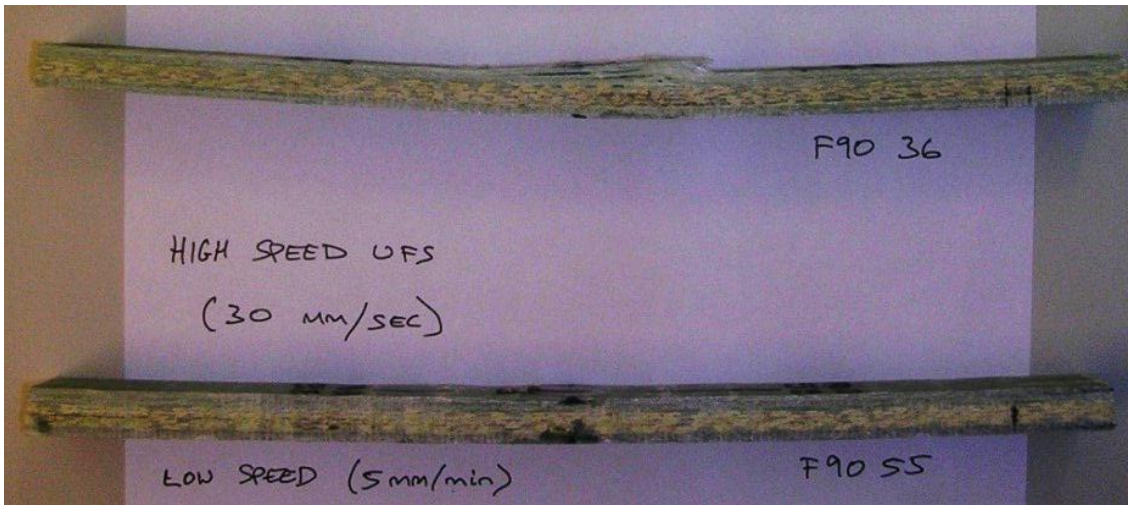

Figure 4-14: Typical post failure sample for static tests F[90]-06 to 10.

Figure 4-15 shows a typical graph of the flexural stress verses strain for these coupons, both measured and calculated. Graphs for the rest of the tests are found in Appendix 1.1. Table 4-12 shows the variables recorded and the results of the derivation of the failure stress, moduli and poisons ratio information from the tests conducted.

Referring back to Figure 4-12, focusing on the results for F[90]-36 to 40 it is seen that, as with the previous set there is very close correlation in the coupon response to flexural stress across all five specimens. The trace of the F[90]-55 specimen shows a comparable failure stress as the F[90]-06 to 10 samples which, as with the [0] direction coupons shows some evidence that the increase in failure stress for F[90]-36 to 40 coupons is caused by the increase in load application speed, rather than the reduction in span.

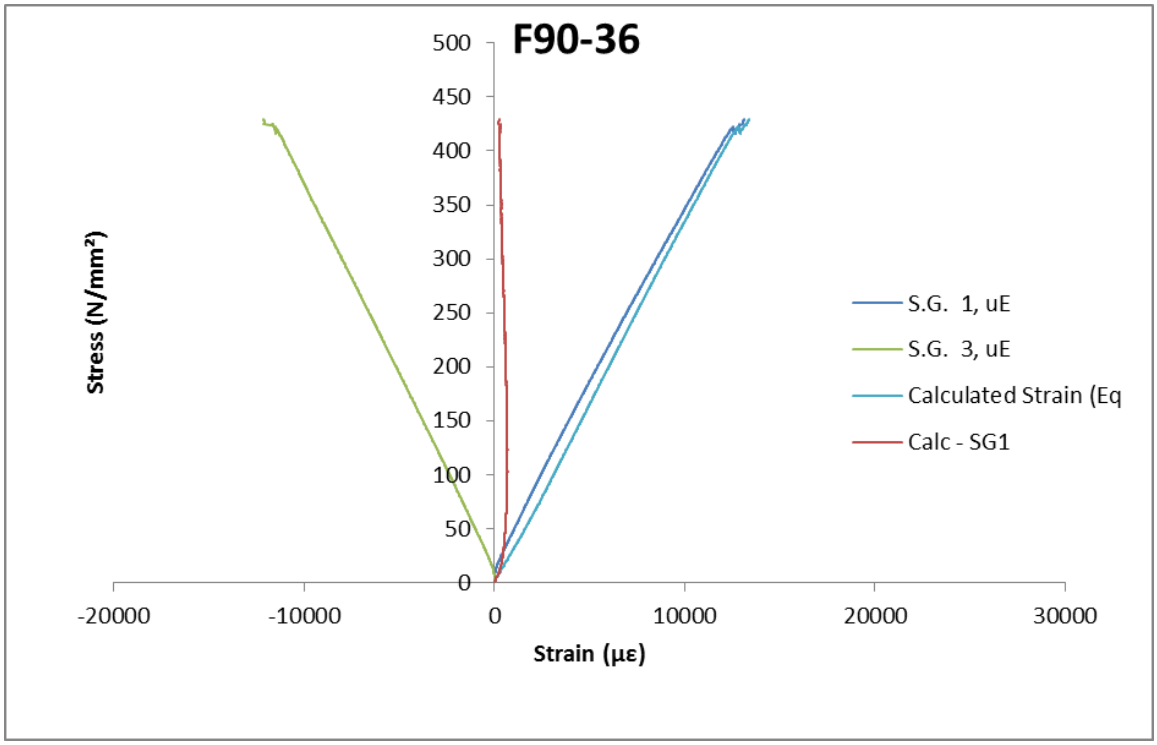

Figure 4-15: Stress strain plot for sample F[90]-36 which is also representative of plots for F[90]-37 to 40 and 55.

Table 4-12: Material properties determined from F[90]-36 to 40 and 55 test coupons.

Specimen Number	Failure Stress (N/mm^2)	Failure Strain Calculated %	Failure Strain Measured %	Flexural Modulus Calculated Strain (kN/mm^2)	Flexural Modulus Measured Strain (kN/mm^2)
F[90]-36	446.80	1330	1310	31.1	35.3
F[90]-37	452.21	1300	1280	33.1	34.3
F[90]-38	450.33	1440	1480	30.9	32.8
F[90]-39	440.25	1330	1340	32.5	32.4
F[90]-40	451.84	1420	1370	32.1	34.6
Average	448.29	1340	1364	31.94	33.88
Standard deviation	4.97	62	77	0.93	1.23
95% Confidence interval	1.11	77	96	1.16	1.53
F[90]-55	340.82	1.27%	1.18%	37.0	43.8

4.3.3 Comparison of Static Properties

Comparing the results of the static tests to the predicted values there is some difference between the material properties, these are shown in Table 4-13. The greatest difference between the predicted values is in the flexural modulus in the [0] direction where the replicate properties were predicted to be 19% lower than measured. In the [90] direction the modulus was directly comparable suggesting the prediction method is more accurate in the fibre dominated direction

than off axis, this is backed up when looking at the in plane properties, where the [0] direction modulus is underpredicted by 15% whereas the [90] direction modulus is under predicted by 7%.

For the rest of this thesis the tested material properties will be used where appropriate.

Table 4-13: Static properties as per Table 4-6 compared with average properties from the static test results presented in the previous section. The lower value is used in this comparison where multiple values were calculated from different strain gauge data to maintain conservatism. The optically derived values are not used due to issues with the testing.

Laminate	In Plane Properties			Flexural Properties		
	$E_{[0]}$ (GPa)	$E_{[90]}$ (GPa)	G_{xy} (GPa)	$E_{[0]_f}$ (GPa)	$E_{[90]_f}$ (GPa)	G_f (GPa)
Original	17.1	26.7	6.0	13.8	30.3	5.4
Replicate	13.2	27.2	4.1	10.9	31.5	3.4
Tested	15.1	29.1	Not Tested	13.0	31.5	Not Tested
Difference Original (%)	-12%	9%	N/A	6%	4%	N/A
Difference Replicate (%)	15%	7%	N/A	19%	0%	N/A

4.4 Fatigue Properties

As mentioned in the previous section modelled engineering constants should be used along with an assumed S-N curve equation for the initial analysis. For homogenous materials this information is often readily available within literature or other sources such as MATWEB (www.matweb.com, n.d.). However the flexibility of composite materials requires the engineering constants to be calculated for each individual material under investigation. There are well defined methods which allow the basic material properties to be calculated to a reasonable accuracy (Daniel, 2006).

Roberton et al (Roberton D.M.V et al., 2009) showed that for an initial life prediction estimate a general fatigue model can be built using generic data, however this introduces a certain amount of uncertainty for composite materials which cannot be quantified because of their complex mechanical properties therefore this can only be applied as a first pass investigation. This sort of investigation is best suited to and would generally be expected to be carried out during the design phase of an asset, with supporting testing used to verify the assumptions made.

4.4.1 Modelling Fatigue Properties

Having modelled the engineering constants for the material under investigation, the next step is to select appropriate data to create this graph. Due to the complex nature of composite laminates the likelihood of obtaining results which are a match for any laminate system investigated from literature is unlikely. For this reason as much fatigue data as possible should be obtained. By obtaining a large quantity of fatigue data it is expected that the spread of data which will be generated by the resulting S-N curve will be conservative in all cases allowing designers to make an assessment of the expected life of the structure based only on predicted values of the applied stress ratio, R_{app}, and the number of expected applications, n. Further refinement can then be made once the materials and laminate construction have been finalised, using only the fatigue data from materials which have a close match to the material being used ie glass or carbon, multi or unidirectional, stitched or woven etc.

For the investigation of the Severn class lifeboat there is a significant difference in the method of application of this process, however some of the problems faced are the same. The physical structure is already built and has been in service in various locations for between 8 and 15 years. However although the static material properties for the structural laminate were predicted prior to the build of the Severn, there was no investigation into the fatigue properties of the laminate.

Table 4-14 shows the extent of fatigue data collected for the present research, this is a simplified version of table 2-9 found in the Literature Review. The data varies in the application of load, the

frequency of loading, the R ratio used and material type. It has been grouped into areas according to fibre type and construction Uni-Directional (UD) and Multi Directional (MD) testing and angle of application, Table 4-14 shows this grouping in more detail. Of major interest to this study is the flexural fatigue, which can be representative of plates under bending stresses and tensile fatigue, which can be representative of plates experiencing membrane stresses of glass fibre and aramid reinforced epoxy composites with multi directional layups.

Table 4-14: Current experimental data found reviewed in this thesis, (√ = 1-2 papers reviewed, √√ = 3 – 5 papers reviewed)

Fibre type		Glass Fibres		Glass / Aramid
Tension-Tension	On Axis	√√	√√	
	Off Axis	√	√√	√
Compression-Compression	On Axis	√	√√	
	Off Axis	√	√	
Fully Reversed	On Axis	√	√√	
	Off Axis	√	√√	
Flexural	On Axis	√√	√√	√
	Off Axis	√	√	√
WISPER/WISPERX			√	
Double Cantilever Beam			√	
Torsion			√	

As is discussed in the Literature Review there are several different equations which can be used to describe an S-N curve. However all of the methods available require some form of S-N test data, either for validation or tuning of the shape of the curve. Due to this and considering that at this stage the data used is not specific to the material under investigation, there is likely to be a significantly increased uncertainty within the resulting graph. For this reason a simple linear regression analysis is used to define the S-N curve equation.

The linear mean regression line was found from the following equations (James et al., 2001):

$$y = a + bx \text{ ,where } a = \bar{y} - b\bar{x},\ b = \frac{S_{xy}}{S_{xx}},\ S_{xy} = \sum(x - \bar{x})(y - \bar{y}) \text{ and } S_{xx} = \sum(x - \bar{x})^2 \quad \textbf{4-15}$$

Where $\bar{x}$ is the mean value of *x* and $\bar{y}$ is the mean value of *y*

The $(100 - 2P)\%$ confidence limit for the mean value of y at $x = x_0$ is given by:

$$y = a + bx_0 \pm t_c S\sqrt{\frac{1}{n} + \frac{(x_0 - \bar{x})^2}{S_{xx}}},\ \text{where } S = \sqrt{\frac{\sum(y - a - bx)^2}{n-2}} \quad \textbf{4-16}$$

The $(100 - 2P)\%$ confidence limits for a predicted value of an individual y-observation when $x = x_0$ is given by:

$$y = a + bx_0 \pm t_c S \sqrt{1 + \frac{1}{n} + \frac{(x_0 - \bar{x})^2}{S_{xx}}} \quad \textbf{4-17}$$

S-N curves have been created by collecting as much data from literature as possible and plotting a common S-N graph followed by graphs of tension and compression and flexural fatigue separately. This approach allowed a direct comparison of simple parameters such as mean line equation and y-axis intercept to help draw any similarities or differences.

The data was obtained from identified sources using *Get Data Graph Digitizer* version *2.25.0.25,* where the discrete numbers were not available. The resulting S-N curve is shown in Figure 4-16. As expected there is a large amount of scatter in the data gathered. The equation of the resulting S-N curve mean line from the linear regression analysis is:

$$\frac{\sigma_{app}}{\sigma_{ult}} = 0.8534 - 0.0779 \log_{10} N \quad 4\text{-}18$$

It is possible to see instantly that there is some degree of conservatism in this curve in the high stress, low fatigue cycle region due to the $\sigma_{app}/\sigma_{ult}$ axis crossing point of 0.8534 being well below the expected value of 1. The 95% confidence prediction boundaries are extremely widely spread, the lower bound which would be used to make a conservative estimate of any life time crosses the high stress, low fatigue cycle region axis at just above 0.5.

Figure 4-17 shows S-N information for the tensile tests identified (Clark, 1997; Philippidis and Vassilopoulos, 2002; Post et al., 2008; Qiao and Yang, 2006; Sangwook and Tsai, 2005). Similarly to Figure 4-16 there was a large amount of scatter found within the data, with the removal of the flexural fatigue data serving producing apparent gaps in the scatter graph, changing the slope of the mean line and therefore the y-axis intercept value. This shows how important the choice of data when estimating fatigue can be as the equation has drastically changed. The equation of the resulting S-N curve mean line is:

$$\frac{\sigma_{app}}{\sigma_{ult}} = 0.9567 - 0.1021 \log_{10} N \quad 4\text{-}19$$

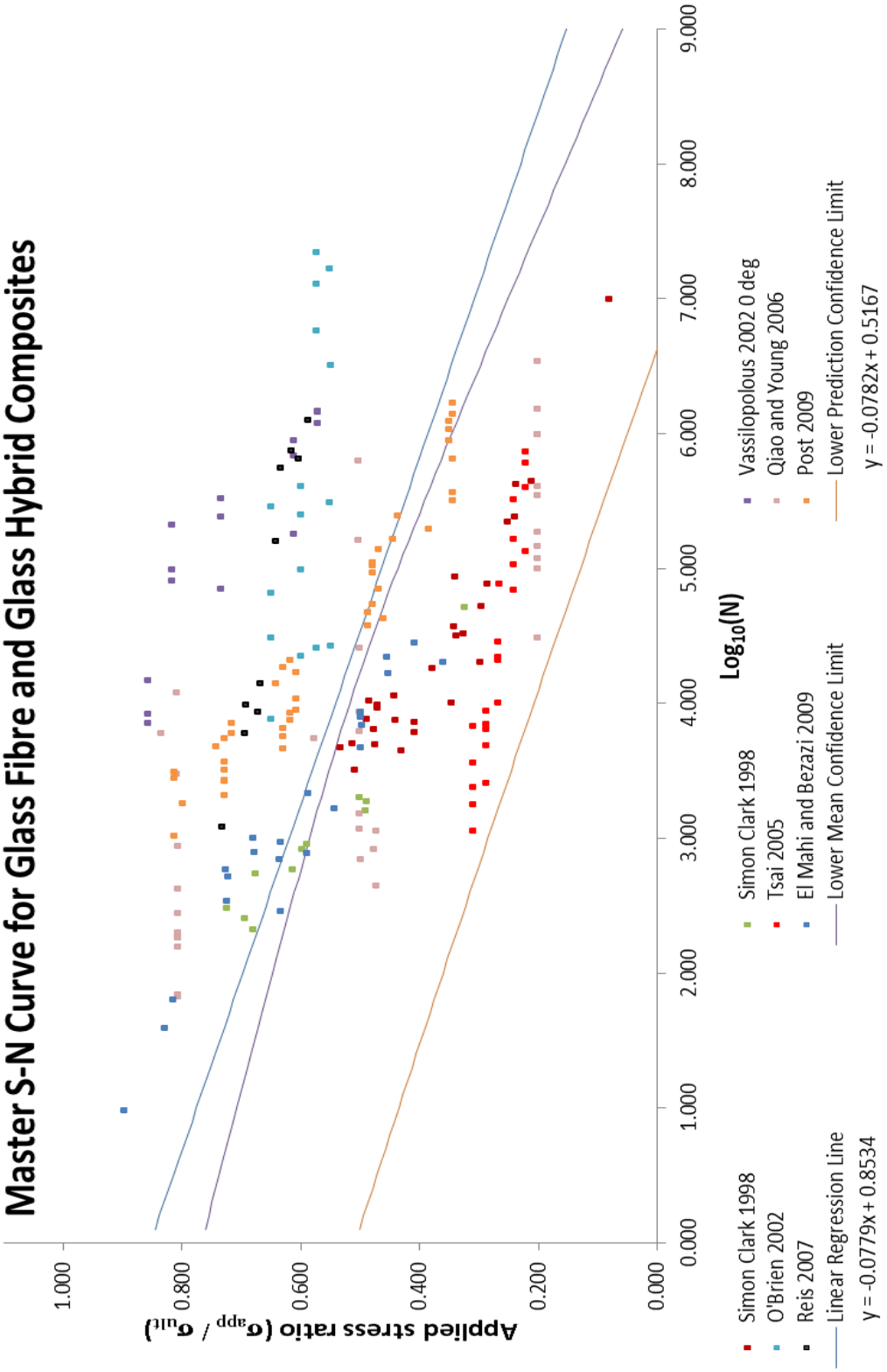

Figure 4-16: Master S-N curve based on data from a variety of different sources which include Uni-directional, Woven Multidirectional and stitched Multi-Directional composite materials with Glass Fibre as the main or sole reinforcement

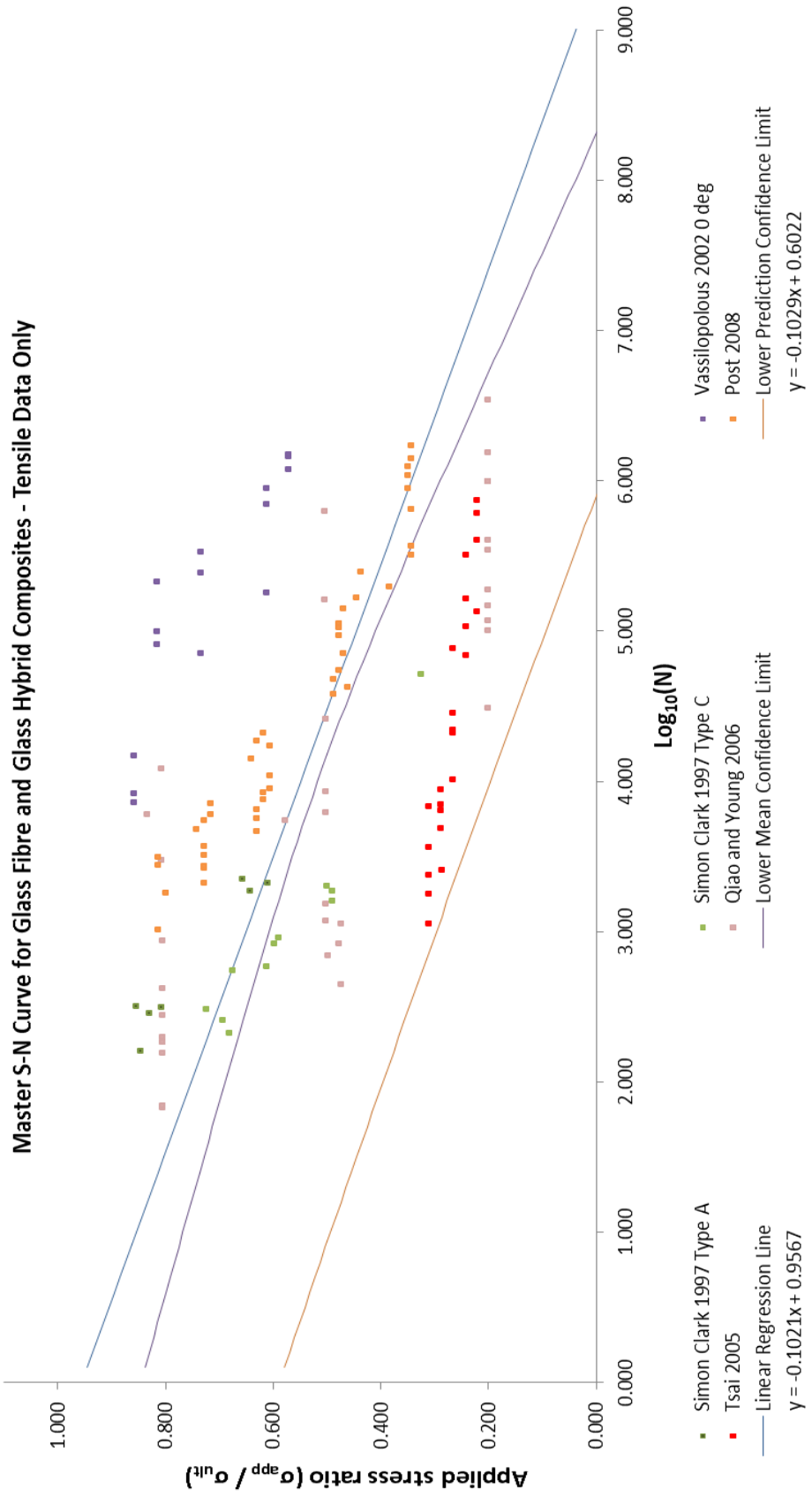

Figure 4-17: S-N data taken from fatigue investigations concerned with tensile fatigue only.

Compared to the previous S-N curve there has been a reduction in the level of conservatism in the high stress, low fatigue cycle region due to the $\sigma_{app}/\sigma_{ult}$ axis crossing point of 0.9567 being much closer to the expected value of 1. The conservatism, although slightly reduced, does remain in the lower mean prediction boundary however which crosses the $\sigma_{app}/\sigma_{ult}$ axis just over 0.6 compared to nearer 0.5, which suggests there is less conservatism in the high stress, low fatigue cycle region. However in the high cycle, low fatigue region the level of conservatism increases due to a reduction in the crossing point on the $\log_{10} N$ axis from a value between 6.5 and 7 to a value below 6. Therefore using the lower prediction boundary from this graph as the basis for any fatigue life predictions would provide a significant level of conservatism in all cases.

Figure 4-18 shows the S-N information for the flexural fatigue investigations identified (El Mahi and Bezazi, 2009; O'Brien et al., 2002; Reis et al., 2007), additionally in this graph applied strain v number of cycles to failure data from (Salvia et al., 1997) is also included. The spread of the data was significantly reduced in comparison to both previous figures, the equation of the mean line is:

$$\frac{\sigma_{app}}{\sigma_{ult}} = 0.745 - 0.0196\log_{10} N \qquad 4\text{-}20$$

As can be seen the resultant mean line shows an increased conservatism in the low cycle, high load region over the previous figures, crossing the $\sigma_{app}/\sigma_{ult}$ axis at a value of 0.745, well below the expected value of 1. However the slope of the mean line is significantly shallower in comparison to the previous graphs, this results in a mean line crossing point on the $\log_{10} N$ just in excess of 38. Although the lower prediction boundary is likely to be significantly lower than this due to the lack of high cycle, low load data used in this analysis, without further investigation of flexural fatigue in this area it is still likely to remain extremely un-conservative. Inclusion of the strain data, which represents the maximum applied strain in the first cycle, shows that for one of the material systems used (M1/EP) the fatigue life is generally improved, whilst for the other (M1/MP) the results are comparable to using constant applied stress data.

The final graph in this series, Figure 4-19, shows the same data as Figure 4-18, but with the removal of the strain data from (Salvia et al., 1997). The removal of this data does not cause any significant changes over Figure 4-18 other than a slight increase in gradient to 0.0334, this does not change the conclusions drawn from Figure 4-18.

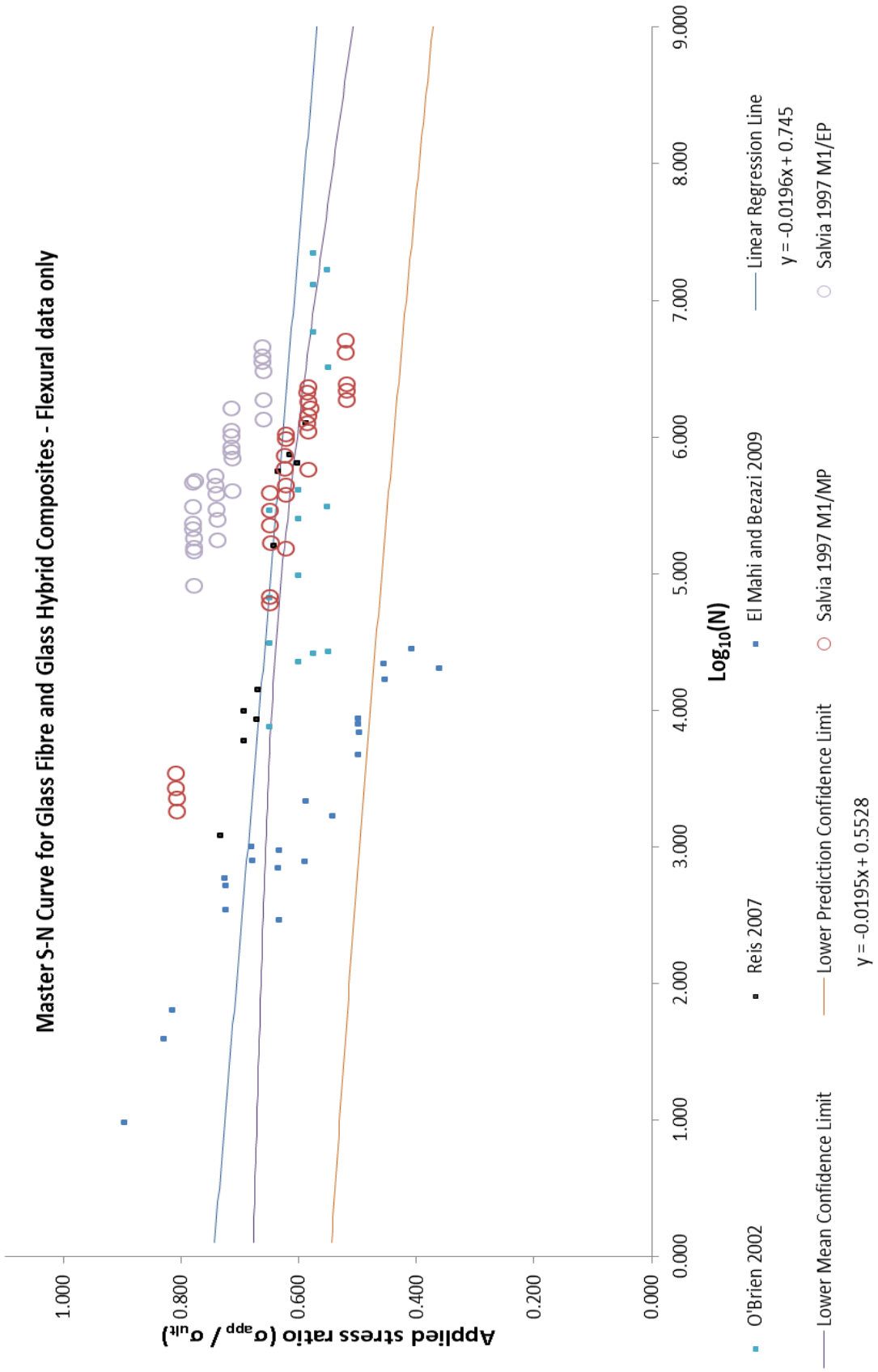

Figure 4-18: S-N Curve for flexural fatigue investigations only, including strain data from Salvia

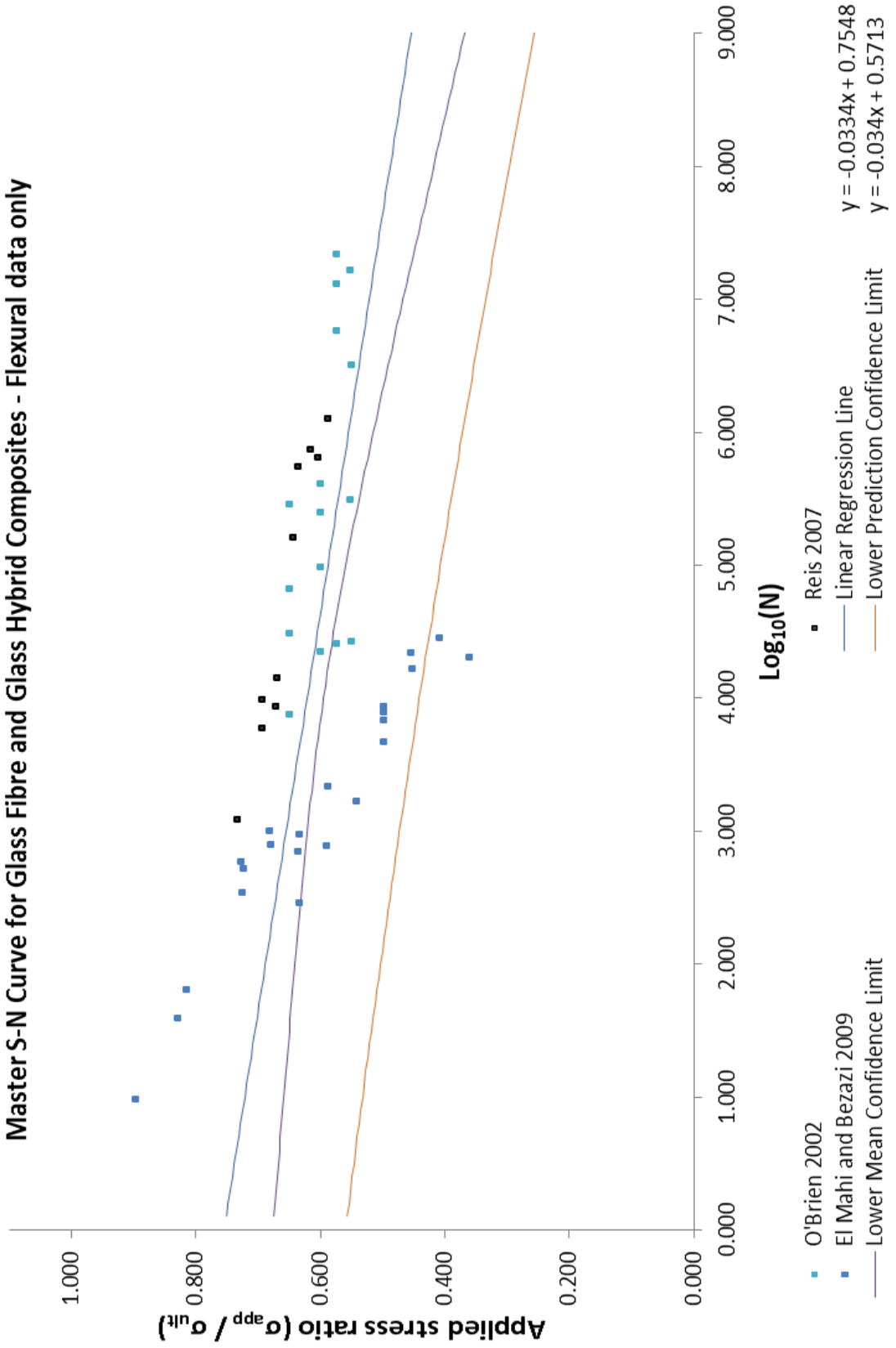

Figure 4-19: S-N curve generated from flexural fatigue data only without strain based data from Salvia

A similar analysis was conducted by Demers et al (Demers, 1998) to produce a fatigue prediction line for use at the design stage of civil engineering structures. Although the literature does not produce a mean regression line, a 95% confidence limit is generated from the data selected. The equation of the 95% confidence line is given as:

$$\frac{\sigma_{app}}{\sigma_{ult}} = 0.79 - 0.08\log_{10} N \qquad 4\text{-}21$$

This is less conservative than the equivalent lines generated through this analysis with a higher $\sigma_{app}/\sigma_{ult}$ axis crossing point and a shallower gradient. There is no obvious reason for the reduced spread of the data which increases the confidence, since the variation within the data sources was as wide as in this study with the exception of the load type, which was tension – tension fatigue so all sources were of this test method.

4.4.2 Fatigue Tests

The full set of images of failed coupons can be found in the appendix section 11.1. A select summary are used to support the following discussions. The coupons references are as used for the static testing.

Both the tensile and flexural fatigue tests were carried out according to (BS ISO 13003, 2003) with reference to the appropriate static standard where appropriate. The fatigue tests were carried out according to the parameters in Table 4-15.

Table 4-15: Fatigue testing parameters

	Tensile	Flexural
$\boldsymbol{R}$	0.1	0.1
$\boldsymbol{R_{app}}$	0.9, 0.8, 0.7, 0.6, 0.5	0.8, 0.65, 0.55, 0.4
Load Application	Monotonic sinusoidal	Monotonic sinusoidal
Frequency	5Hz	5Hz

The fatigue tests were split into 2 different parts, tensile [0] degree tests and flexural [90] and [0] degree tests. Tests were only conducted one direction for the tensile tests as flexural tests were deemed more important and there was limited availability of material, the [0] direction was chosen for both sets of tests as this represents the weakest direction for the laminate. Strain gauges were used on both sides of the tensile material and only on the lower face of the four point bend coupons. By recording the changing strain values under constant amplitude loading the modulus change can be observed, providing a further insight to the fatigue behaviour of the material under investigation.

4.4.2.1 Coupon Failure

For all coupons failure was consistent with the static tests occurring well away from the grips in the area monitored for compliance change in the case of the tensile tests, examples of failed tensile coupons are shown in Figure 4-20. In general the failure of the flexural fatigue samples were consistent with high speed static tests, examples of failed samples can be found in Figure 4-21 for the F[0] samples and Figure 4-22 for the F[90] samples. There were occurrences of roller indentation and roller "burning" on the face of F[0]-32 to 35 and 61 due to roller movement on the material. An attempt to reduce this through the use of shims was made, however due to the material surface it was found the shims would not stay in place. (Shaw and Pilkington, 2012).

Figure 4-20: Examples of post fatigue failure modes of selected samples for each of the applied load ratios, (a) $R_{app} = 0.9$, (b) $R_{app} = 0.8$, (c) $R_{app} = 0.7$, (d)$R_{app} = 0.6$, (e) $R_{app} = 0.5$.

(a)

(b)

(c)

(d)

Figure 4-21: Examples of post fatigue failure modes of selected samples for each of the applied load ratios, (a) $R_{app} = 0.8$, (b) $R_{app} = 0.65$, (c) $R_{app} = 0.55$, (d)$R_{app} = 0.4$.

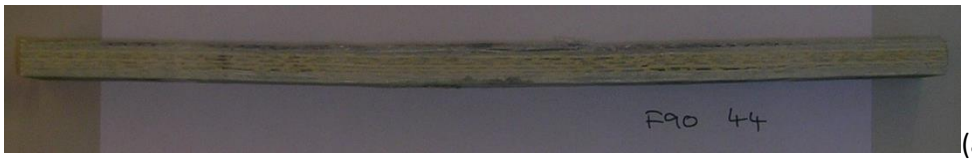

(a)

(b)

(c)

(d)

Figure 4-22: Examples of post fatigue failure modes of selected samples for each of the applied load ratios, (a) $R_{app} = 0.8$, (b) $R_{app} = 0.65$, (c) $R_{app} = 0.55$, (d)$R_{app} = 0.4$.

4.4.2.2 Compliance Change

The compliance change of T[0]-11 to 15, tested at $R_{app} = 0.9$, is comparable to coupons tested at $R_{app} = 0.8$. With both having some coupons remaining generally linear for a large proportion of the coupon life before an exponential growth in compliance until failure as seen in Figure 4-23.

Figure 4-24 shows the response of coupons tested at $R_{app} = 0.7$, T[0]-21 and 23 displayed a fairly variable rate of change of compliance over the life of the specimen with, in the case of T[0]-23, the compliance seeming to increase just prior to failure. Coupons T[0]-24 and 25 displayed a linear change in compliance through life until failure. Coupon T[0]-22 displayed very unusual behaviour with an apparent increase in modulus over the initial cycles followed by a sudden and sharp increase in compliance before displaying similar traits to T[0]-23 just before final failure.

The coupons tested at 60% ultimate tensile strength T[0]-26 to 30 displayed two distinct compliance changes, shown in Figure 4-25. Coupons T[0]-27, 28 and 30 all displayed an exponential increase in compliance throughout the life of the coupons whilst T[0]-26 and 29 displayed a small linear compliance change towards the end of the life of the coupon.

For the 50% tests there were a number of problems, which meant only limited confidence can be had in the results. Due to strain gauge failure the strain v cycle result for T[0]-33 was not captured and due to software errors the grip displacement results (shown in the appendix) for T[0]-32 to 34 were not recorded. Figure 4-26 shows the compliance change based on the measured strain. The results are very erratic but show a trend of increasing compliance with increasing cycles which is as expected.

Figure 4-27 shows the change in compliance of the F[90] coupons tested at 55% of the ultimate failure stress this response is representative of all F[90]. For F[0] fatigue tests, the initial slope is not always flat, but rather has a steeper initial slope as seen in Figure 4-28.

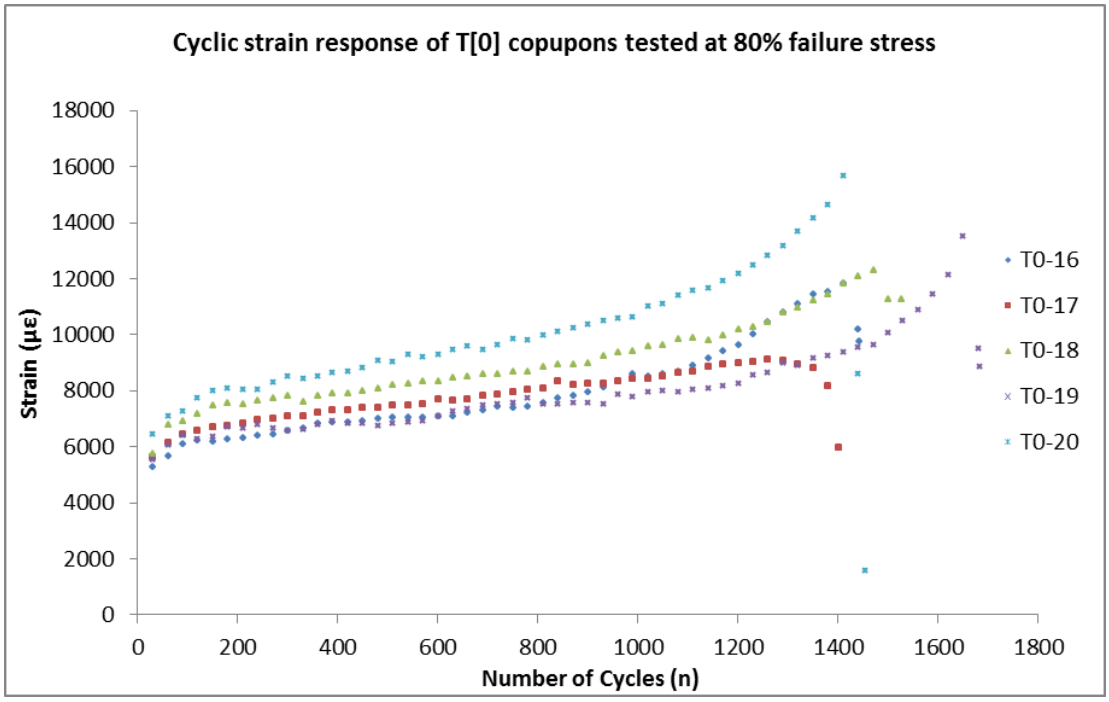

Figure 4-23: Increase in strain response of the coupons as the applied cycles increase for the coupons fatigued at 80% of Ultimate Tensile Strength.

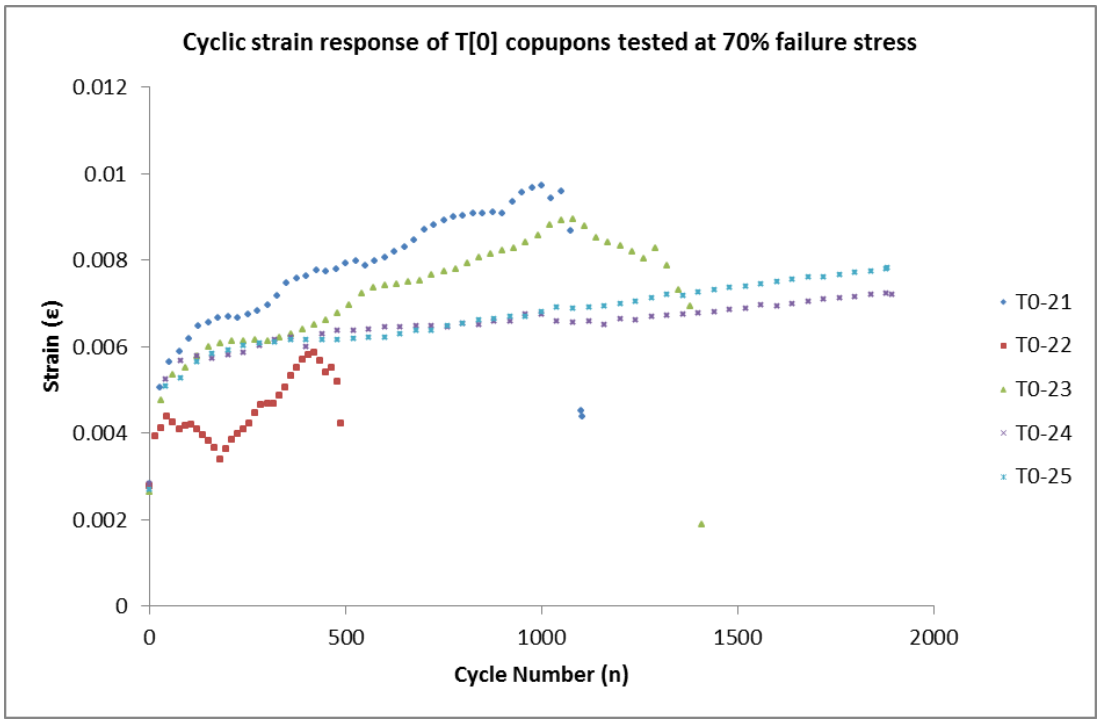

Figure 4-24: Increase in strain response of the coupons as the applied cycles increase for the coupons fatigued at 70% of Ultimate Tensile Strength.

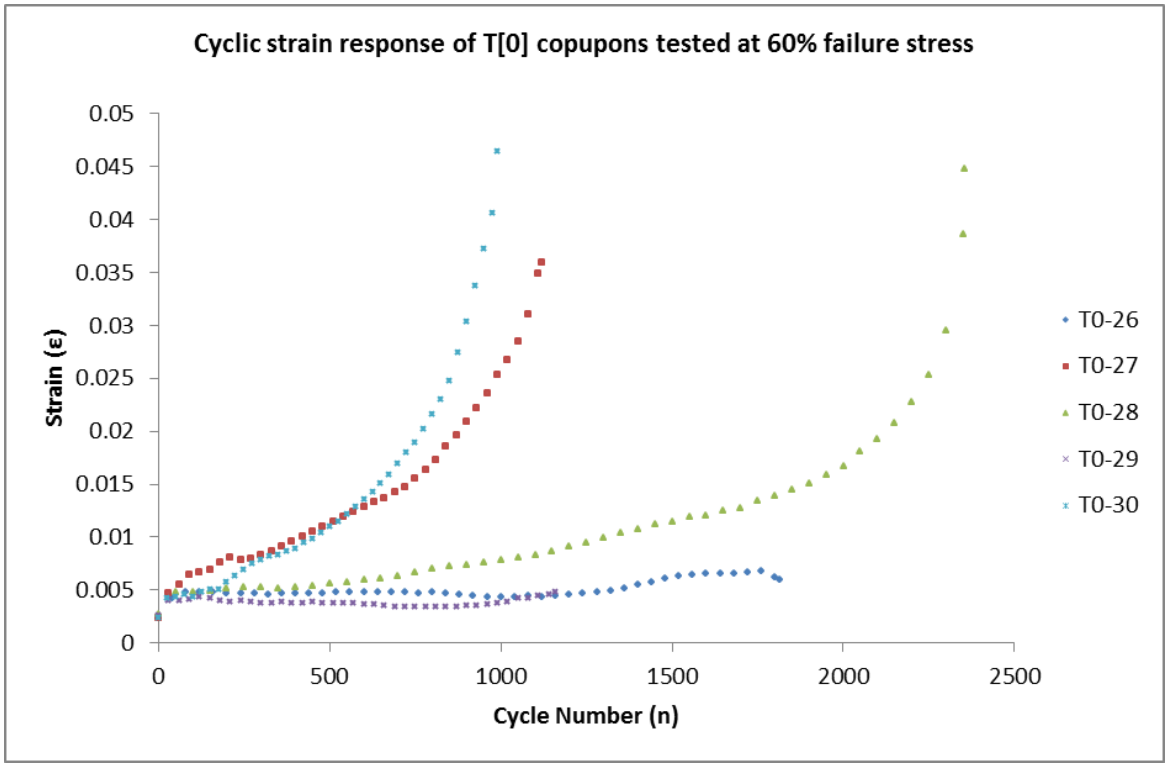

Figure 4-25: Increase in strain response of the coupons as the applied cycles increase for the coupons fatigued at 60% of Ultimate Tensile Strength.

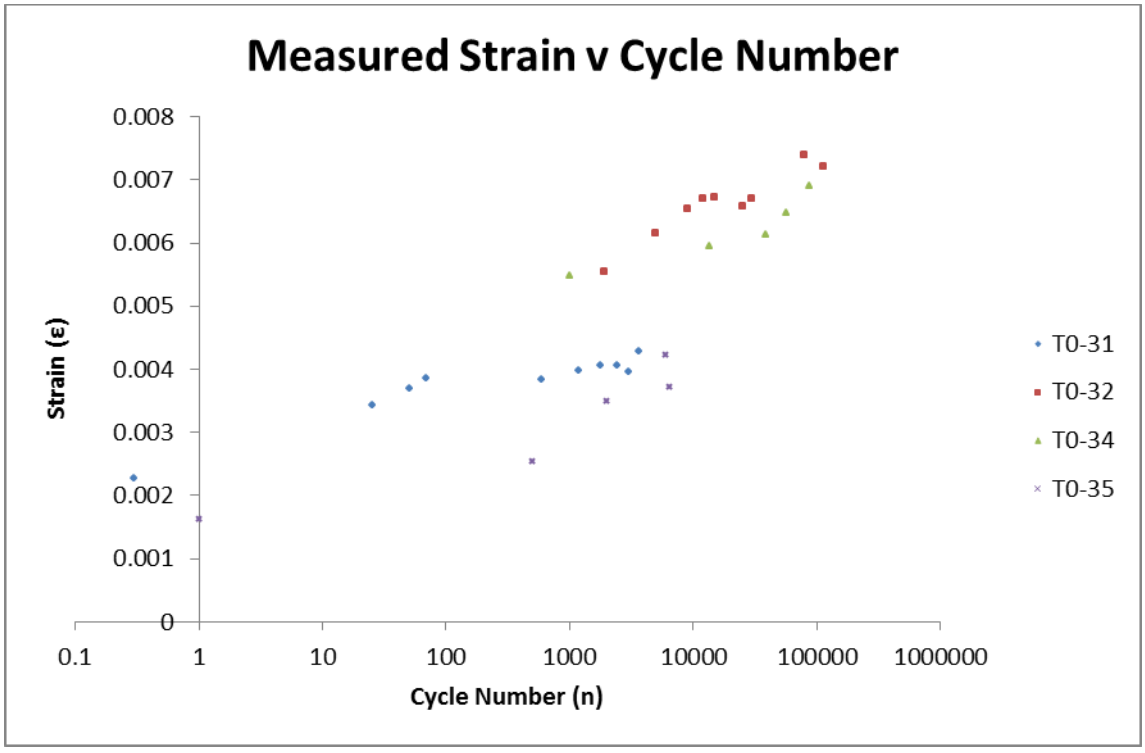

Figure 4-26: Increase in strain response of the coupons as the applied cycles increase for the coupons fatigued at 50% of Ultimate Tensile Strength.

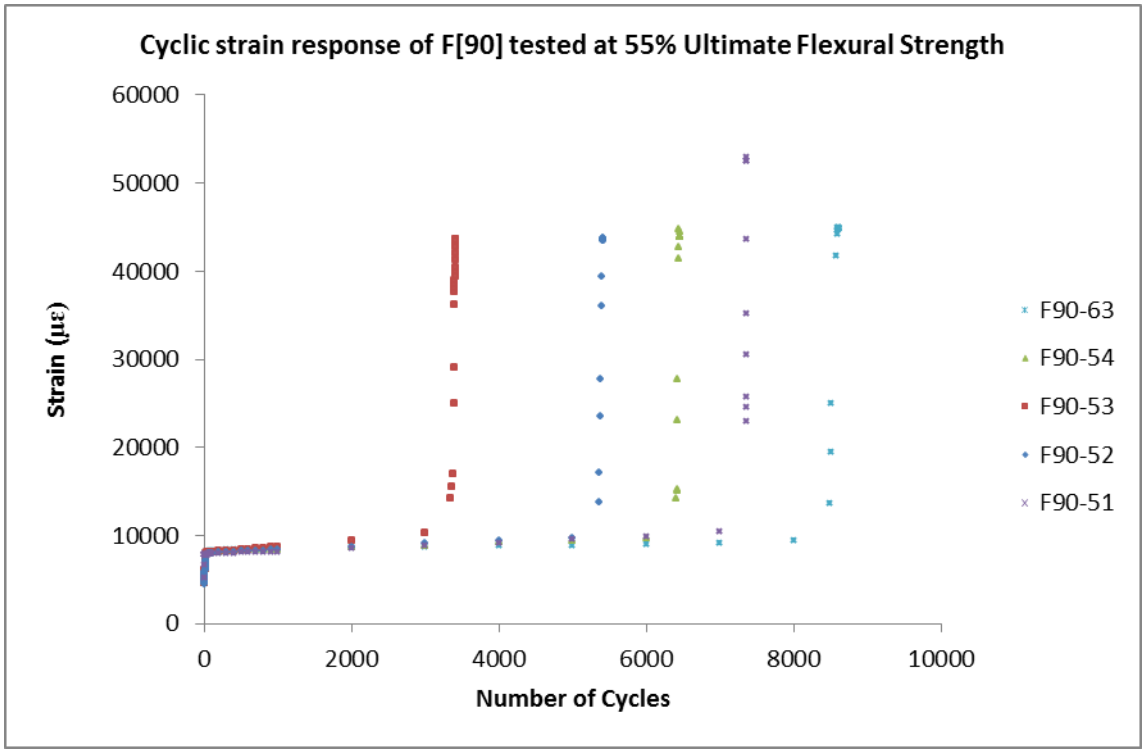

Figure 4-27: Calculated strain v number of cycles applied until failure for F[90] samples tested at 55% of ultimate flexural strength.

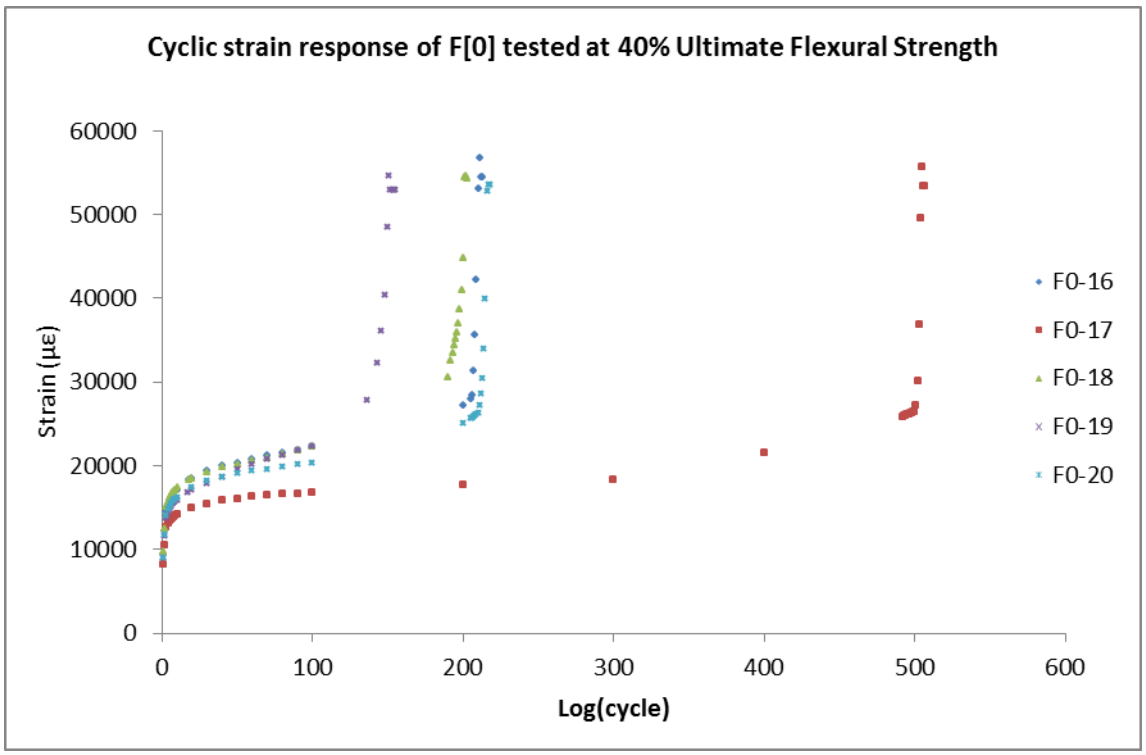

Figure 4-28: Calculated strain v number of cycles applied until failure for F[0] samples tested at 40% of ultimate flexural strength.

4.4.2.3 Cycles to Failure

Table 4-16 shows the number of cycles to failure for the T[0] tests. Investigating the coefficient of variation using all the available data found that in general it was high, with the exception of coupons T[0]-16 to 20 where the results were extremely consistent. For coupons T[0]-11 to 15 and T[0]-26 to 30 the coefficient of variation was 33% and 29% respectively, for T[0]-21 to 25 it was 69% and for T[0]-31 to 35 it was found to be 93%. Further investigation into the results for T[0]-21 to 25 found that there were no particularly erroneous results with a fairly even spread between the maximum and minimum values. Further investigation of coupons T[0]-31 to 35 found that the two outlying results were T[0]-31 and 35 which have been previously identified as being incorrectly tested. Removing these results from the data set changed the coefficient of variation to 37% which is more comparable to other tests.

For all the tabulated data the same linear regression analysis was applied to the data shown in Table 4-16 as used in section 4.3.1. The resulting equation of the linear regression line for the T[0] fatigue data is shown in equation 4-22.

$$\frac{\sigma_{app}}{\sigma_{ult}} = 1.0556 - 0.1075\log_{10} N \qquad \textbf{4-22}$$

As shown in Figure 4-29 the mean line crosses the applied stress ratio axis within the boundary of the tested ultimate values, although at the very highest value, the Lower Mean Confidence Limit also crosses the axis within this boundary, at the very lower end. This suggests that there is limited conservatism associated with the mean line; however it does increase confidence in the use of a linear regression line to represent the data. The lower prediction confidence limit crosses the applied stress ratio axis at a value just over 0.8 and successfully bounds all the data generated from this testing.

Table 4-17 shows cycles to failure for the F[90] coupons, in all cases the coefficient of variation was very high, although generally lower than for the [0] direction results, with the lowest value being 30% for 46 – 50 and the largest being 75% for 56 – 60. The coefficient of Variation for group 41 to 45 is 45% and for 51 to 55 is 31%. The resulting equation of the linear regression line is shown below.

$$\frac{\sigma_{app}}{\sigma_{ult}} = 0.9493 - 0.0993\log_{10} N \qquad \textbf{4-23}$$

Table 4-16: Table of test results for T[0] test specimens. *significant differences between the number of cycles at failure as counted and as identified by the optical strain analysis. +Outlying results due to problems with testing removed from S-N curve.

Coupon Number	Applied Load (kN)	Applied Load Ratio (App / $UTS_{(ave)}$)	Cycles to Failure (N)			
			As Counted	Optical Strain	Difference	From Grip Amplitude Measurement
T[0]-11	34.8	0.90	63	62	2%	N/A
T[0]-12*			115	37	68%	N/A
T[0]-13*			145	76	48%	N/A
T[0]-14			68	67	1%	N/A
T[0]-15			84	83	1%	N/A
Average			95	65		
CoV			33%	24%		
T[0]-16	30.56	0.80	1496	1443	4%	1496
T[0]-17			1405	1402	0%	1405
T[0]-18			1528	1527	0%	1528
T[0]-19			1693	1684	1%	1693
T[0]-20			1457	1455	0%	1457
Average			1516	1502		
CoV			6%	7%		
T[0]-21	26.74	0.70	1107	1105	0%	1107
T[0]-22			492	488	1%	492
T[0]-23			1412	1411	0%	1412
T[0]-24*			4346	1894	56%	4346
T[0]-25			3562	1881	47%	1562
Average			2184	1356		
CoV			69%	39%		
T[0]-26	22.92	0.60	1846	1815	2%	1846
T[0]-27			1223	1120	8%	N/A
T[0]-28			2368	2355	1%	2368
T[0]-29*			1700	1159	32%	1700
T[0]-30			1056	990	6%	1056
Average			1639	1488		
CoV			29%	35%		
T[0]-31*+	19.10	0.50	10471	3596	66%	10471
T[0]-32*			367128	114000	69%	N/A
T[0]-33*			459381	N/A	N/A	N/A
T[0]-34*			849629	87000	90%	N/A
T[0]-35+			6708	6501	3%	6708
Average			558713	100500		
CoV			37%	13%		

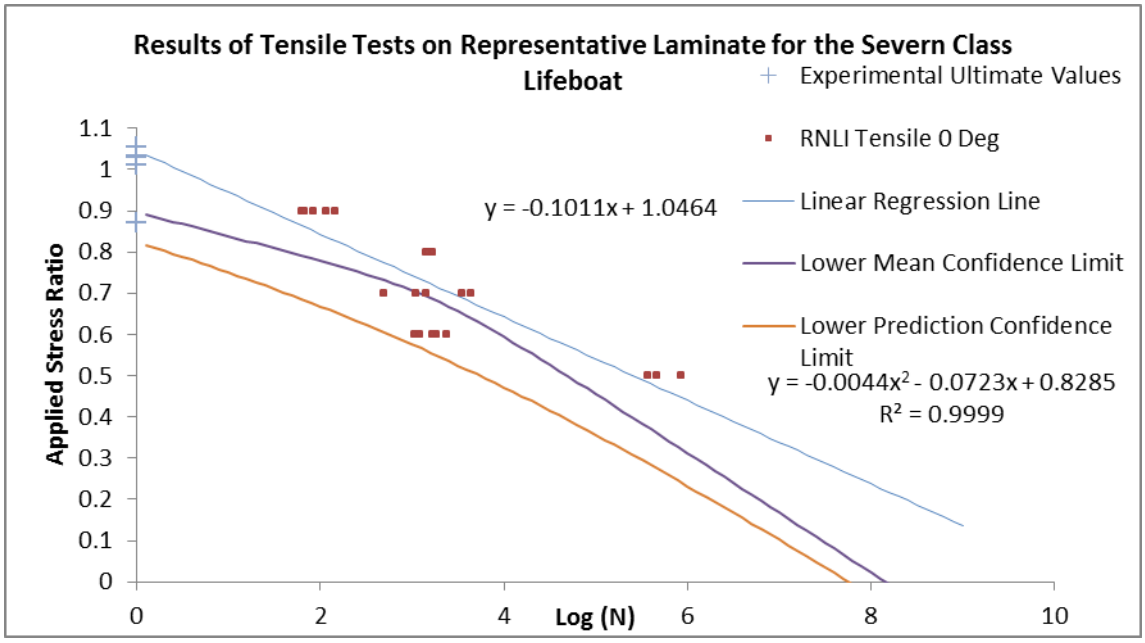

Figure 4-29: S-N curve for T[0] coupons

Table 4-17: Test results for F[90] test specimens.

Specimen Number	Applied Stress (N/mm^2)	Applied Load Ratio (App / $UTS_{(ave)}$)	Cycles to Failure (N)	Notes
F[90]-41	346.98	80.00*	40	
F[90]-42			32	
F[90]-43			80	
F[90]-44			30	
F[90]-45			43	
Average			45	
CoV			45%	
F[90]-46	281.92	65.00	1339	
F[90]-47			1607	
F[90]-48			1221	
F[90]-49			622	
F[90]-50			1365	
Average			1230.8	
CoV			30%	
F[90]-51	238.55	55.00	7357	
F[90]-52			5359	
F[90]-53			3410	
F[90]-54			6418	
F[90]-55			8503	
Average			6209.4	
CoV			31%	
F[90]-56	173.49	40.00	144516	
F[90]-57			263685	
F[90]-58			888802	
F[90]-59			311435	
F[90]-60			1000000	Run out
Average			521687.6	
CoV			75%	

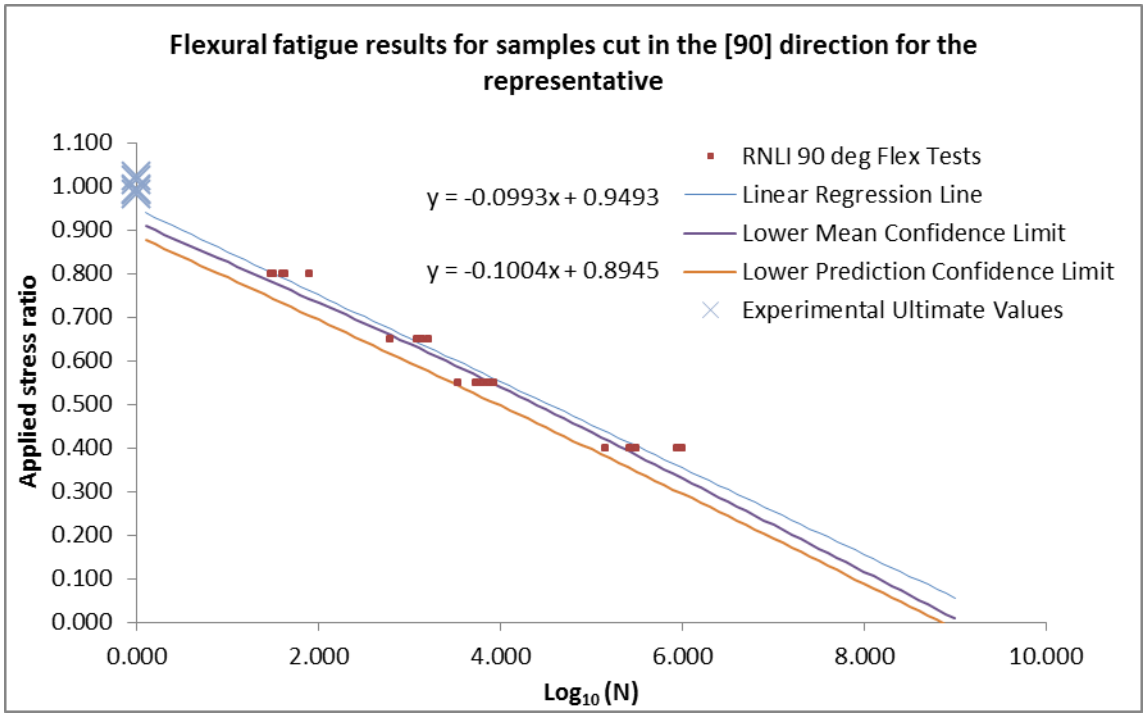

Figure 4-30: S-N curve for F[90] direction coupons.

As seen in Figure 4-30 the mean line crosses the applied stress ratio axis well below the boundary of the tested ultimate values, although at the very highest value, the Lower Mean Confidence Limit crosses the axis below this boundary, this suggests that there is further increased conservatism associated with the mean line in this case.

The lower prediction confidence limit crosses the applied stress ratio axis at a value just over 0.8 and successfully bounds all the data generated from this testing. In comparison to the F[0], discussed next, and T[0] fatigue tests the confidence limits associated with the F[90] fatigue tests are much closer together.

Table 4-18 shows the cycles to failure for the F[0] coupons, in all cases the coefficient of variation was very high with the lowest value being 34% for 21 – 25 and the largest being 105% for 26-29 and 62. Unfortunately there is no ready explanation for the large spread of data, with F[0]-26 achieving 15394 cycles at the top end. Removing it from the analysis reduces the CoV to 38%, however without some physical explanation such as the test being set up incorrectly there is no reason to remove the result from the analysis. Removing F[0]-32 from the analysis due to premature test stopping reduces the CoV for the 32 to 35 and 62 from 78% to 69%. CoV for group 16 to 20 is 56%.

Figure 4-31 shows the S-N graph for the F[0] tests, the mean line crosses the applied stress ratio axis within the boundary of the tested ultimate values, the Lower Mean Confidence Limit crosses

the axis below this boundary suggesting there is adequate conservatism within the resulting data as with the previous graph. Although not as close as the scatter in the F[90] curve, the F[0] results are much tighter to the mean line than those of the T[0] tests.

Table 4-18: Test results for F[0] test specimens. *significant differences between the number of cycles at failure as counted and as identified by the optical strain analysis. +Outlying results due to problems with testing removed from S-N curve.

Specimen Number	Applied Stress (N/mm^2)	Applied Load Ratio (App / $UTS_{(ave)}$)	Cycles to Failure (N)	Notes
F[0]-16			207	
F[0]-17			501	
F[0]-18	138.77	80.00	198	
F[0]-19			146	
F[0]-20			213	
Average			253	
CoV			56%	
F[0]-21			775	
F[0]-22			929	
F[0]-23	112.75	65.00	1402	
F[0]-24			940	
F[0]-25			561	
Average			921.4	
CoV			34%	
F[0]-26			15394	
F[0]-27			4355	
F[0]-28	95.40	55.00	2304	
F[0]-29			1807	
F[0]-62			3126	
Average			5397.2	
CoV			105%	
F[0]-32*			207408	Premature Test Stop
F[0]-33			1000000	Run out
F[0]-34	69.38	40.00	479417	
F[0]-35			1000000	Run out
F[0]-61			83851	
Average			640817	
CoV			69%	

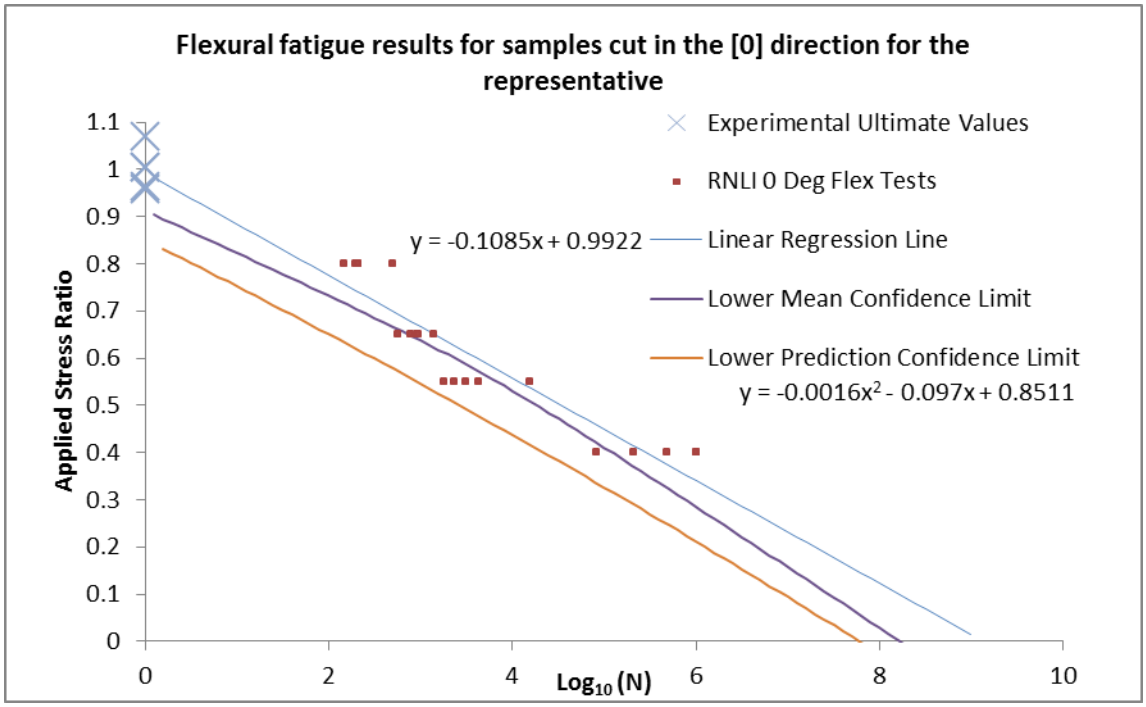

Figure 4-31: S-N results for F[0] direction coupons.

4.4.3 S-N graph Comparison

Table 4-19 shows the equations for the linear regression analysis mean line and 95% prediction limit for each of the graphs presented in this work and (Demers, 1998). Comparing the resulting S-N curve parameters between the different tests conducted in this work there is a significant amount of similarity. The slope of both the linear regression line and the 95% prediction line is comparable across all three tests, the only major difference is with the $\sigma_{app}/\sigma_{ult}$ axis crossing point which varies between a value of 0.95 and 1.05. The coefficients for the 95% prediction line are more similar still with comparable slope and $\sigma_{app}/\sigma_{ult}$ axis crossing point values. Using these lines to predict the life of a composite, using Figure 4-30 will result in the longest fatigue life due to the shallower slope, followed by Figure 4-29 and then Figure 4-31 due to the lower $\sigma_{app}/\sigma_{ult}$ axis crossing point.

Comparing the results from these graphs to those generated in section 4.4.1 in all cases the $\sigma_{app}/\sigma_{ult}$ axis crossing point is significantly higher for both the linear regression lines and the 95% prediction line in the case of the tested data. This is not a surprise as the data collected for Modelling Fatigue Properties was from numerous different sources covering various different material layups as discussed previously.

Table 4-19: Comparison of the S-N curve equations developed in this work and that of Demers (Demers, 1998)

Data Source	95% prediction line	Linear Regression line
Figure 4-29 Tension [0]	$\frac{\sigma_{app}}{\sigma_{ult}} = 0.89 - 0.11\log_{10} N$	$\frac{\sigma_{app}}{\sigma_{ult}} = 1.05 - 0.10\log_{10} N$
Figure 4-31 Flexure [0]	$\frac{\sigma_{app}}{\sigma_{ult}} = 0.84 - 0.11\log_{10} N$	$\frac{\sigma_{app}}{\sigma_{ult}} = 0.99 - 0.11\log_{10} N$
Figure 4-30 Flexure [90]	$\frac{\sigma_{app}}{\sigma_{ult}} = 0.89 - 0.10\log_{10} N$	$\frac{\sigma_{app}}{\sigma_{ult}} = 0.95 - 0.10\log_{10} N$
All RNLI Data	$\frac{\sigma_{app}}{\sigma_{ult}} = 0.87 - 0.11\log_{10} N$	$\frac{\sigma_{app}}{\sigma_{ult}} = 1.01 - 0.11\log_{10} N$
(Demers, 1998)	$\frac{\sigma_{app}}{\sigma_{ult}} = 0.79 - 0.08\log_{10} N$	N/A
Figure 4-16	$\frac{\sigma_{app}}{\sigma_{ult}} = 0.52 - 0.08\log_{10} N$	$\frac{\sigma_{app}}{\sigma_{ult}} = 0.85 - 0.08\log_{10} N$
Figure 4-17	$\frac{\sigma_{app}}{\sigma_{ult}} = 0.6 - 0.10\log_{10} N$	$\frac{\sigma_{app}}{\sigma_{ult}} = 0.96 - 0.10\log_{10} N$
Figure 4-18	$\frac{\sigma_{app}}{\sigma_{ult}} = 0.55 - 0.02\log_{10} N$	$\frac{\sigma_{app}}{\sigma_{ult}} = 0.75 - 0.02\log_{10} N$
Figure 4-19	$\frac{\sigma_{app}}{\sigma_{ult}} = 0.57 - 0.03\log_{10} N$	$\frac{\sigma_{app}}{\sigma_{ult}} = 0.75 - 0.03\log_{10} N$
All RNLI Data + Figure 4-17 Data	$\frac{\sigma_{app}}{\sigma_{ult}} = 0.62 - 0.09\log_{10} N$	$\frac{\sigma_{app}}{\sigma_{ult}} = 0.92 - 0.09\log_{10} N$

Combining the data from this work with the data from Figure 4-17 produced a slight change in the resultant linear regression and 95% prediction lines. The addition of the data reduces the axis $\sigma_{app}/\sigma_{ult}$ crossing point of linear regression line by 0.04 but decreases the gradient, suggesting a slight increase in conservatism at the lower cycle / higher stress ranges but increased at longer cycle / lower stress ranges. The 95% prediction limit modification resulted in an increased $\sigma_{app}/\sigma_{ult}$ crossing point and reduced gradient suggesting a general decrease in conservatism for this line, this reduction in conservatism is easily explained due to the increased number of data points and their relatively tight location to the mean line of the original data presented in Figure 4-17. These findings are shown graphically in Figure 4-32 and provide confidence in the use of

Figure 4-17 for the initial lifetime prediction to be applied at the design stage, or for an initial life prediction prior to further information becoming available.

Figure 4-32 shows a comparison between the data collected in this testing and the different linear regression mean and 95% confidence prediction lines. The first observation to make is that both the linear regression line and the 95% confidence limit found from the information presented in Figure 4-18 do not accurately fit with the data generated within this exercise. The linear regression mean lines generated in Figure 4-16 and Figure 4-17 do fit the data fairly well with the mean line shown in Figure 4-17 fitting the data best. Both of the 95% confidence lines from the same graphs are well below the spread of the data tested, showing that a life prediction from the graphs would be extremely conservative in comparison to the actual data tested. Most interesting is that the 95% confidence limit generated by the data in Demers (Demers, 1998) fits closest to the data recorded in this analysis whilst still being below the spread of the data suggesting that in this instance the analysis conducted by Demers et al would have been sufficient to conduct an initial fatigue life assessment.

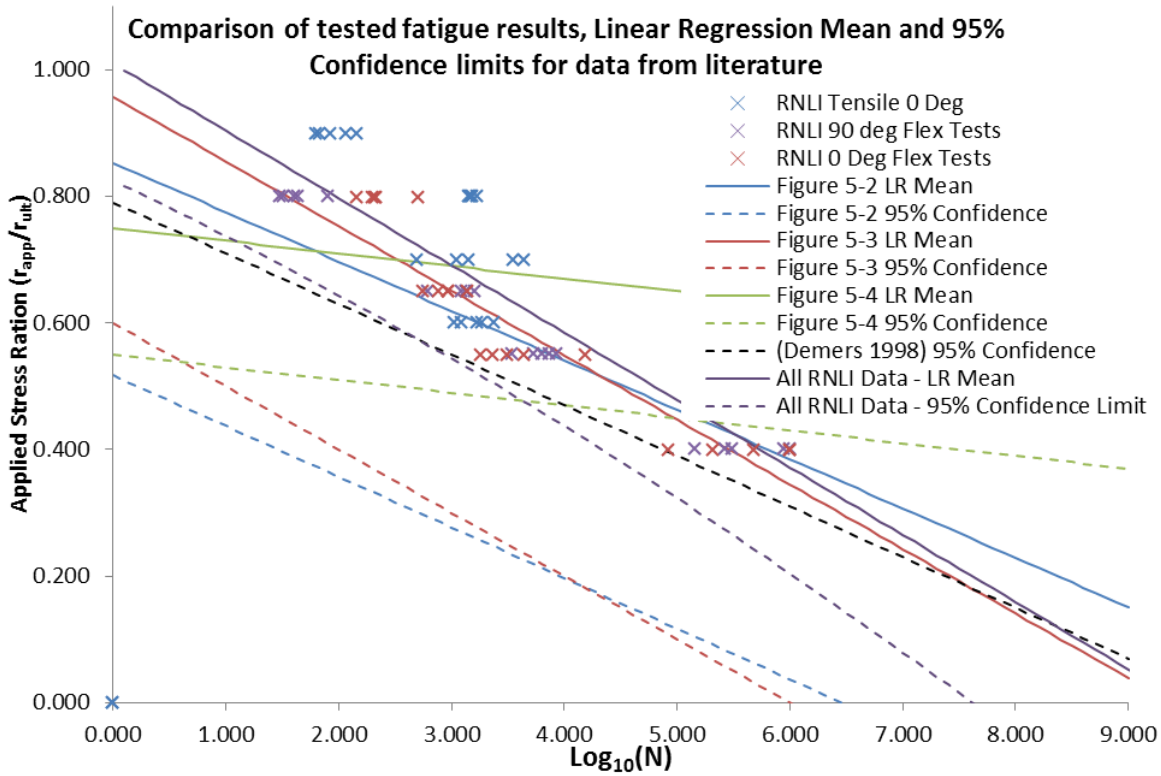

Figure 4-32: Comparison between the test results and the different linear regression mean and 95% confidence limits as well as the 95% confidence limit taken from Demers (Demers, 1998).

4.5 Discussion

This chapter has tested one of the fundamental variables identified by the life extension model, the material performance. Initially a fatigue life diagram was generated from data within the literature and compared to a similar task undertaken within the civil engineering industry by Demers et al (Demers, 1998) for the purposes of fatigue life prediction at the design stage. The 95% confidence limit for that work was found to be significantly less conservative than that found in this work.

This was followed by static and then fatigue tests for material which is considered representative of that used in the case study, the Severn class lifeboat under tensile and flexural loading conditions. The tests found that for in all cases the failure modes were consistent with the literature reviewed.

Comparing the tested S-N data gathered through these experiments against the S-N curves developed in the earlier analysis found that the linear regression mean line from Figure 4-17, equation 4-19, was the best fit for the data and the 95% limit line from Demers et al (Demers, 1998) provided an acceptable boundary for the data, although it was significantly less conservative than the equivalent line in Figure 4-17. No obvious reason was identified for the reduced scatter when compared to the current investigation.

Using the graphs presented in Figure 4-16 to Figure 4-18 for initial fatigue life prediction at the design stage could be acceptable, provided all simulated $\sigma_{app}/\sigma_{ult}$ values and their associated $\log_{10} N$ values applied fall within the envelope bounded by the axis and the 95% confidence line.

Having completed this analysis the next stage is to combine the identified fatigue life prediction graphs with known applied stress histories to determine a fatigue life from an appropriate fatigue life prediction model. The following chapters will explore this analysis with the results culminating in a life prediction for the Severn class lifeboat in the Structural Life Assessment Model or SLAM as shown in Figure 4-33 which highlights where the analysis within this chapter is used within the methodology highlighted in Figure 3-1.

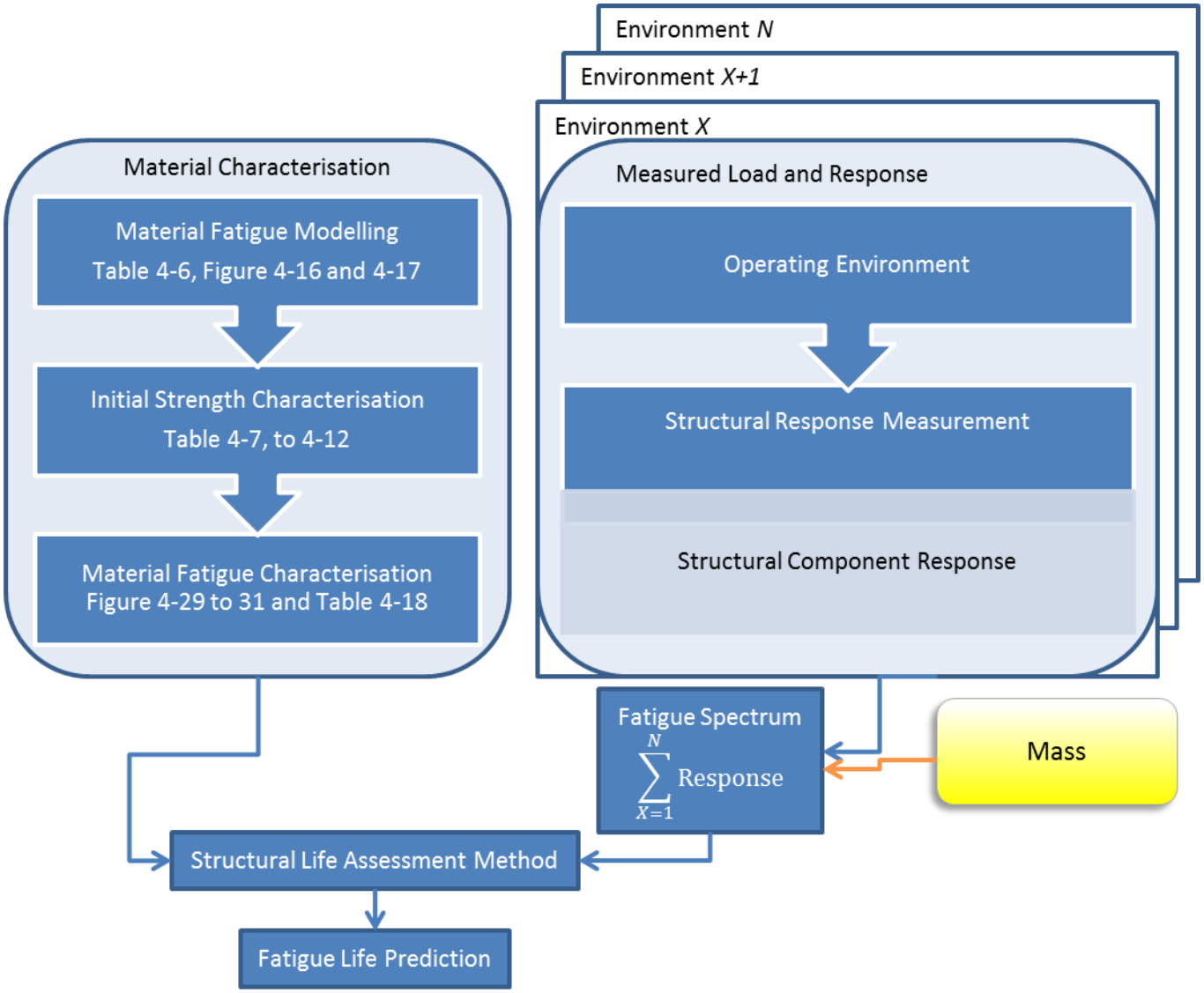

Figure 4-33: The areas identified within the methodology that are addressed so far chapter. With table 4-6 and Figures 4-16 and 17 providing expected values of initial strength and fatigue parameters which are then confirmed through materials tests to obtain the ultimate strength values, found in tables 4-7 to 4-12 and to develop specific fatigue curves for the material in use, figure 4-32.

5 Defining the Operating Environment

Having carried out the material characterisation in chapter 4, this chapter describes and demonstrates how environmental monitoring can be used to define the appropriate environmental conditions which, as shown in Figure 3-1, control the structural response variables required (discussed in chapter 6) as inputs for a fatigue life analysis. The focus of this chapter is gathering an understanding of the operating environment and the errors associated with trying to determine which of the variations the appropriate choice is at any particular time, which were highlighted as areas in need of investigation in the literature review.

The assumption here is that whilst moored there is negligible structural loading and therefore negligible impact on the life of the structure. For the vast majority of Severn lifeboats this is an acceptable assumption as the moorings are sheltered. Additionally for those that are moored at exposed moorings, due to the fact that the lifeboats have to be accessible 24 hours a day 365 days a year, if the weather becomes extreme enough that it may become an issue, the crew will move the boat from its exposed mooring and moor at a more sheltered location to ensure the crew can board the boat in the event of an emergency at sea.

The environment that each of the lifeboats has been subjected to can be derived from the RNLI's service returns for the different classes of lifeboats and is discussed in section 5.1, however there is some uncertainty in the data which is addressed in section 5.2. From this an understanding of the applied loads in each of the environments is required.

5.1 Operating Environment for Severn Class Lifeboats

For the Severn class lifeboat the operating environment is the littoral waters around the UK and Ireland as identified in the literature review; the different spectra identified to represent the seas and oceans are not applicable so close to the shoreline due to local topological effects. The variation within this environment is best captured by the Douglas and Beaufort scales (Huler, 2004; Rawson and Tupper, 2001) as it relies solely on the information presented to the crews on board the vessel. In the RNLI the Beaufort scale along with an estimation of wave height is used to define the sea states, this leaves us with 12 different operating environments which can be identified by expected wave heights and direct observation of the sea. In this case the operating environment parameters are the wave height and the direct observations, with the output parameter being the sea state, numbered 1 to 12.

The next decision to make is defining the monitoring techniques, there is currently a large UK government sponsored investigation underway, which involves observing and modelling the

marine environment (DEFRA, 2012). During their research a number of wave buoys and wave stations have been stationed around the coast of the United Kingdom and Ireland, amongst the data that is collected is the wave height of passing waves. This data can then be used where possible to define the sea state at the time of a service through the relationship mentioned previously.

However these wave buoys do not offer complete coverage of the UK's coastal waters, and certainly not in every location attended by a lifeboat. To address this issue, a monitoring system which is capable of interpreting the descriptive terms used in the Beaufort scale needs to be developed. Luckily evolution has defined such a machine, the human being, although there is evidence of inconsistencies between one human's interpretation of a description and the environment presented to them and another human's interpretation (Guedes Soares, 1986).

One way to mitigate against this is to develop a "whole use spectrum", whereby all the event data generated is input into a single spectrum which defines the whole life of the lifeboat, as used in Clark and Shenoi (1998) and Smith (1989). However by taking this approach a level of fidelity in the data is lost, making it difficult to corroborate previous predictions with measured data. It also has the problem of masking areas of poor or missing data unless the whole use spectrum is developed in a way to allow the areas lacking in data to be highlighted. If it was assumed that the lifeboat was continuously monitored throughout its life then eventually the "whole use spectrum" could be generated. This spectrum would include all the structural responses seen in all of the different operating environments throughout its life making the investigation into operating environment meaningless as it would be captured in the full data set.

There are two distinct parts to understanding the operating environment, the first is to understand the historical operating environment and define the necessary detail required to allow a retrospective analysis of the fatigue life used. The second is to use the historical records to develop appropriate averages which can be used to understand the potential remaining life of the structure assuming the data collected can accurately represent the future service demands on the individual lifeboats.

5.1.1 Historical Operating Environments

The RNLI keeps records of all of the services conducted throughout the life of a lifeboat, these records are generated from the crews on the lifeboat at the time and their assessment of the conditions they encounter, the assumption for this analysis is that the crews are accurate with their assessments. This assumption will be investigated in the following section. The data was sorted according to the amount of time the lifeboat has been at sea in the various different

conditions specified by the Beaufort scale in any particular year. Figure 5-1 shows the total duration of service time of the fleet of Severn class lifeboats in any one year. This figure shows that for the first ten years from 1995 to 2005 there was a steady climb in the total time on service before becoming relatively level from 2005 until the latest data set from 2012. Figure 5-1 also breaks down the total duration for each year by Beaufort number through shaded bars within the total duration bar. The deeper the shade of red the lower the Beaufort number. This gives us an initial estimation on the distribution of total lifeboat services by the Severn lifeboat within any Beaufort number. It can be seen that generally the lifeboats spend more time in the sea states 2 to 8 than 0 or 9 to 12.

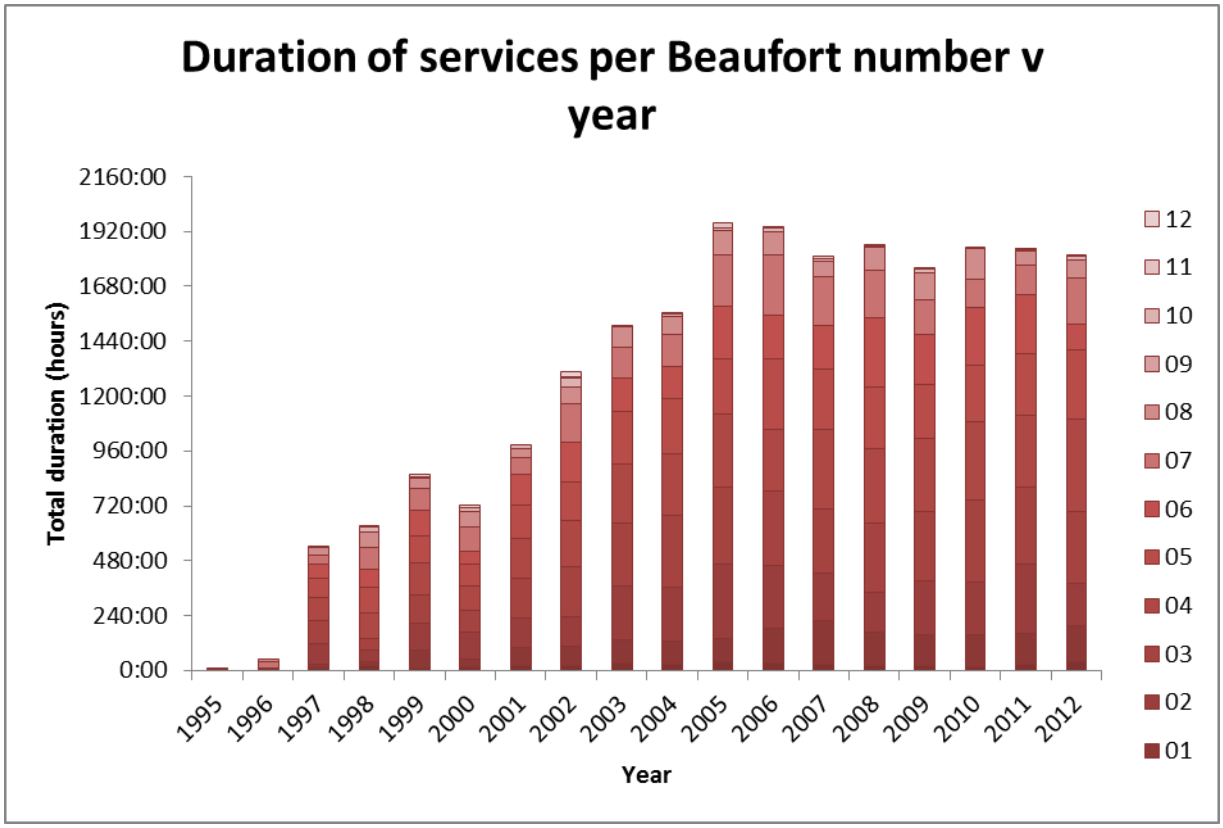

Figure 5-1: The duration of lifeboat services by year as calculated from service return data for all lifeboats in the fleet.

The change in total duration of services is explained by Figure 5-2 which shows the cumulative number of lifeboats in the Severn fleet per year as well as the number of lifeboats built per year from 1995 up until 2012. The increase in lifeboats numbers coincides well with the increase in duration of service. Figure 5-3 shows the total service duration of the Severn class lifeboats, but rearranged to show duration as a function of Beaufort number.

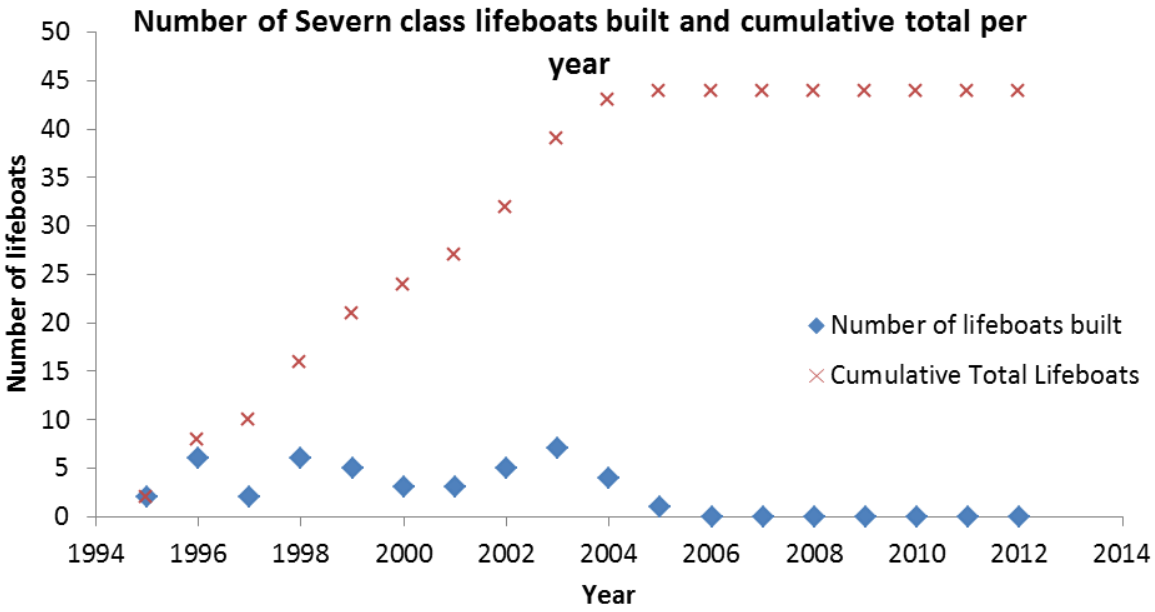

Figure 5-2: Number of lifeboats built per year and cumulative total number of lifeboats in fleet.

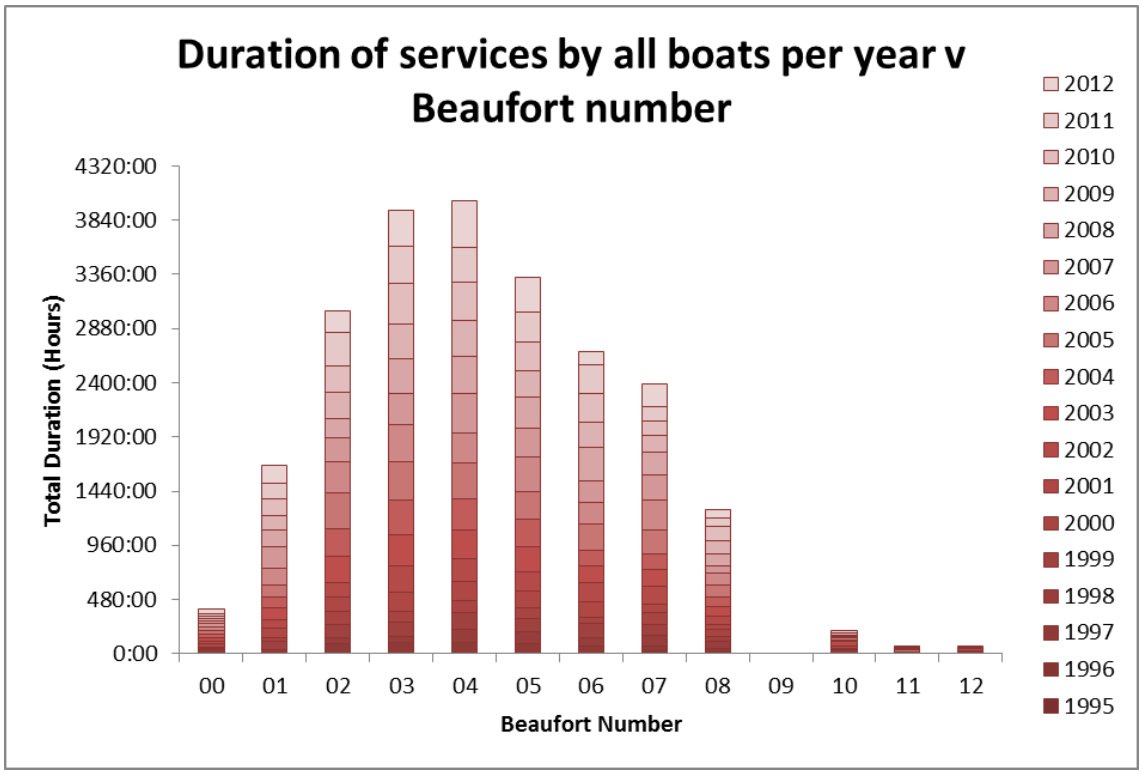

Figure 5-3: Duration of services by all lifeboats in a particular sea state per year.

The reasons for this distribution of services is unclear from the data available however it could be that in these sea states the weather conditions are such that general users of the littoral waters, whether professional or recreational, would consider their vessels safe and capable of dealing with the conditions and are therefore are likely to leave safe harbour. However sea states 9 and

above can be considered extreme by any standards, characterised by wave heights in excess of 10 meters and thus would make sea farers think twice before leaving a safe haven. Therefore services conducted in these Beaufort states are unlikely to occur and when they do occur as a result of people being caught out by quickly changing conditions or as a result of large vessels which could reasonably be expected to operate in extreme weather having some form of failure or accident that requires emergency help. Alternatively it could also be the result of inaccurate characterisation of the operating environment, this is further explored in section 5.2.

Initially hind casting of fatigue life used is suggested as being possible using known past histories of the individual Severn class lifeboats. Figure 5-1 shows us the duration of all lifeboats in all years; this can be used to understand the sort of use a lifeboat fleet under similar expected services might be subjected too, as well as the variation of total service time that can be expected year on year. In this case it tells us that from 2005 onwards the total duration of lifeboat services has remained fairly consistent. Prior to 2005 the number of lifeboats in the fleet was increasing in steps of between 2 and 6 a year as shown in Figure 5-2. The implications of this are that up until 2005 the expected total duration of the lifeboat fleet year on year had not reached a steady state, as one influencing factor (in this case the number of lifeboats in the fleet) is not constant. When considering the question being posed at this stage; what the expected useable life of the structure is, this representation doesn't really provide any useful information. From the data which is available it is possible to determine an expected usage profile which can show us the duration of service in any particular sea state, this is shown in Figure 5-3. This is a useful representation as it provides an initial understanding of the expected distribution of services in particular sea states.

There is some element of uncertainty within the data set provided since the durations shown are only representative of active duties, not for training, exercises, technical trials or passages, therefore it can be assumed the data provided is only a percentage of the actual time at sea experienced. Unfortunately getting an understanding on the size of this percentage is difficult due to the way the records are kept. With the introduction of AIS to the lifeboats it is suggested that it may be feasible to keep better, automated records of lifeboat movements in future.

Figure 5-1 to Figure 5-3 show an overall view of what services have happened to the Severn lifeboat fleet in the past, this does this not show us what the services of each individual lifeboat looks like. Due to the variation in the year on year service profiles it is definitely worth investigating the variation between lifeboats. This is easily done though by generating figures equivalent to Figure 5-1 and Figure 5-3 for each of the lifeboats.

Considering now the average duration shown in Figure 5-4, the total service time of 42 hours 9 minutes was preferred for two reasons. The first is that over time it is expected that the average using data from 1995 onwards will approach the 2005 onwards level as the relative influence of the first few years where there were very few boats in the fleet reduces and the second is that it provides a more pessimistic summary of the data which is preferable in the case of damage life prediction to optimistic assessments. However, this average itself may not be applicable to boats with known past histories if the spread of data is too large.

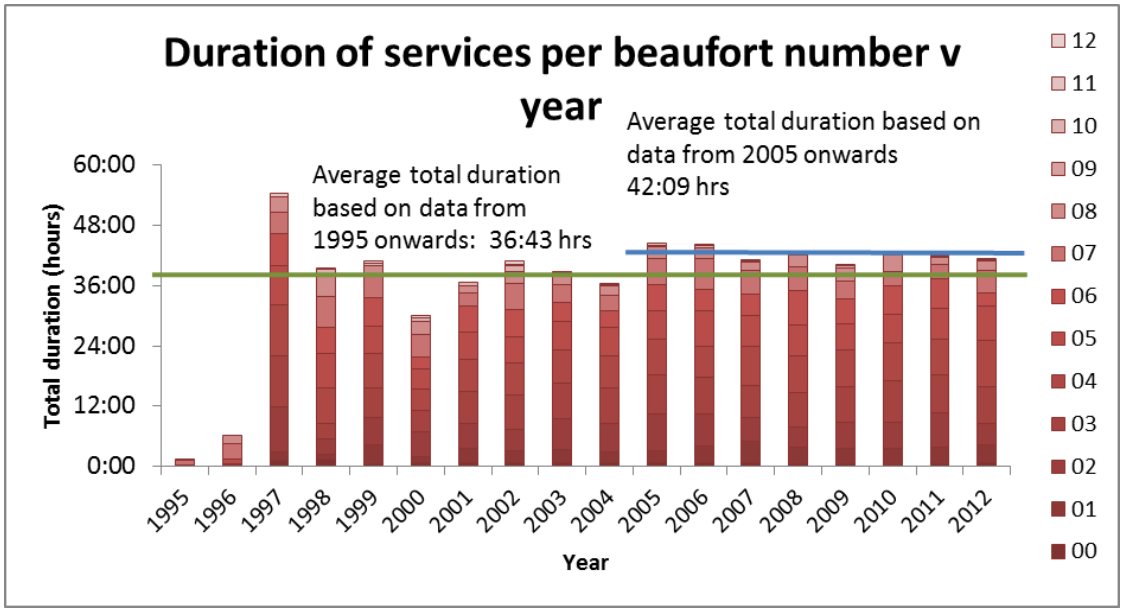

Figure 5-4: Duration of services by the average lifeboat per year. The blue line represents the average lifeboat service based on data from 2005 to 2012.

To determine if this is the case the average lifeboat duration per year was compared to the average duration per year for each of the individual lifeboats, shown in Figure 5-5. From this figure it can be seen indeed that the spread is extremely large with a standard deviation, σ of 41%, or 17 hours and 28 minutes. Figure 5-6 shows the spread of data about the average value, μ (42:09) in steps of 1 standard deviation, σ. It is clear from this graph that the majority of lifeboats (25 of 44) have an average service duration between 24 hours and 40 minutes and the average service. The size of the standard deviation suggests that using the average value of services as calculated could result in an over prediction for the majority of lifeboats (30 of 44) and an under prediction of 11 and severe under prediction of 2 lifeboats in the fleet.

Considering the data available for this study, this was considered an unnecessary compromise for roughly a quarter of the fleet. To alleviate the impact of this uncertainty the average service duration per year was then calculated for each of the different vessels and then compared to the

average calculated from Figure 5-4, shown in Figure 5-5. 4 particular Severns were selected for the analysis, one which has particularly high usage, one which is particularly low usage and one which closely matches the average of 42hrs per year average. This average was chosen as it represents the average obtained from a time when all the lifeboats were in service.

The chosen lifeboats are ON 1216, 1221, and 1248 respectively. Finally ON 1279 was also selected as it was used for the data acquisition of strain data discussed in chapter 7. ON 1279 is a relief lifeboat called "Margaret Joan and Fred Nye". This boat was selected as it was undergoing engineering trials when a vessel for structural monitoring was being sought. The other advantage to using this vessel is that it is a relief boat and therefore can be posted anywhere in the country making it likely to be exposed to a variety of sea conditions in a variety of geographical locations.

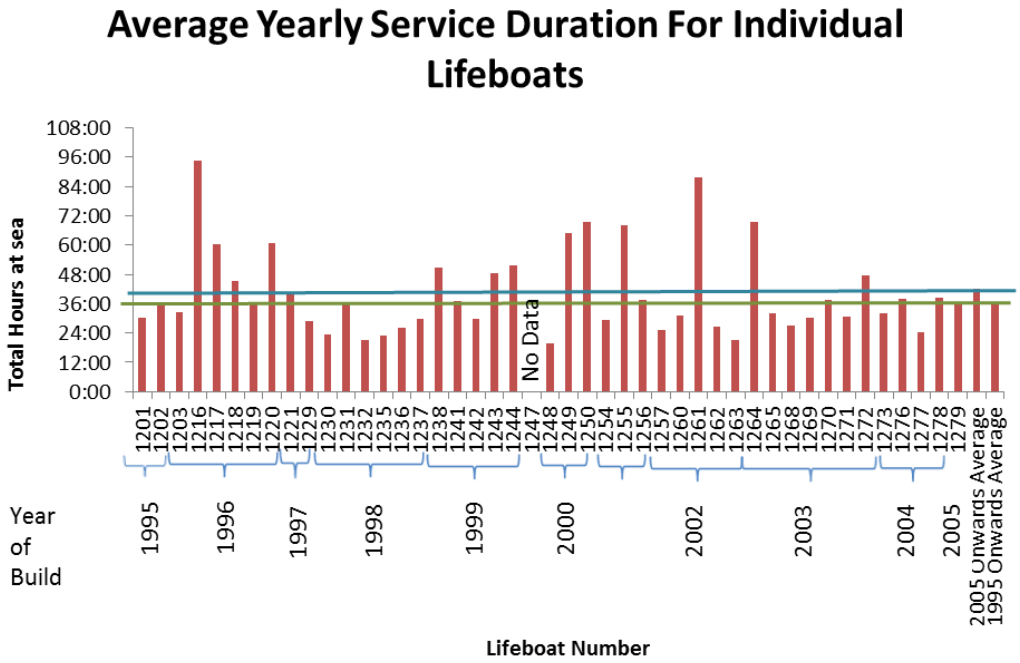

Figure 5-5: Average total service duration for the individual RNLI lifeboats. The blue and green lines indicate the average duration calculated including all years and from 2005 onwards respectively.

Figure 5-7 shows the total duration of lifeboat services per year for the first vessel under investigation, ON1216. It is obvious that for most years the number of services performed by this vessel is well above the average with only the year 2000 showing below average data. However the total duration of services is very variable from year to year with the average being 94:24 hrs. ON 1216 is the Severn lifeboat "The pride of Humber", this station is situated on a spit of land known as Spurn point and is crewed by the RNLI's only full time crew.

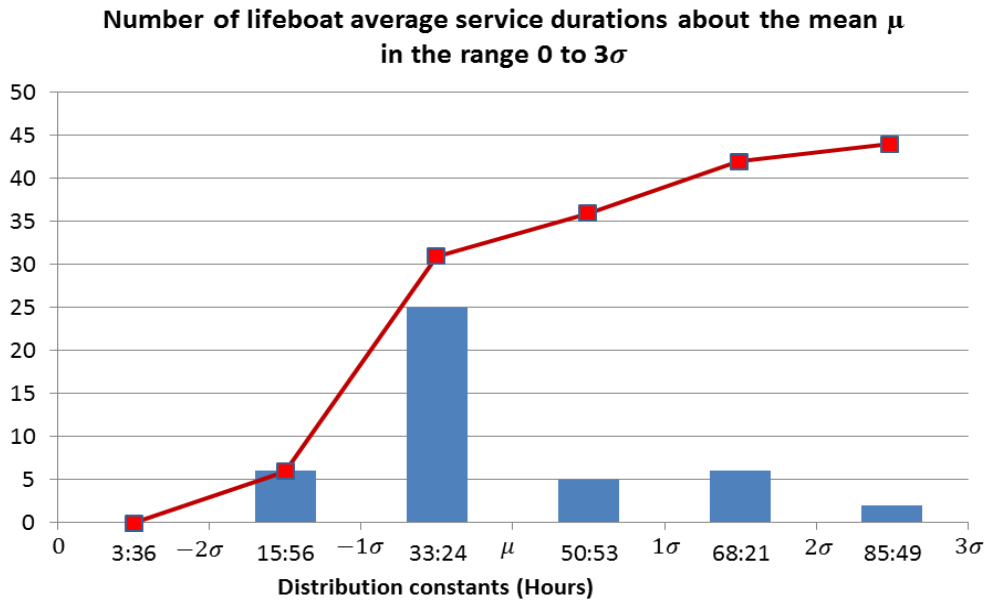

Figure 5-6: Spread of averages for each of the individual lifeboats using bin widths of multiples of σ either side of the average, μ. The line shows the cumulative number of lifeboats in the distribution.

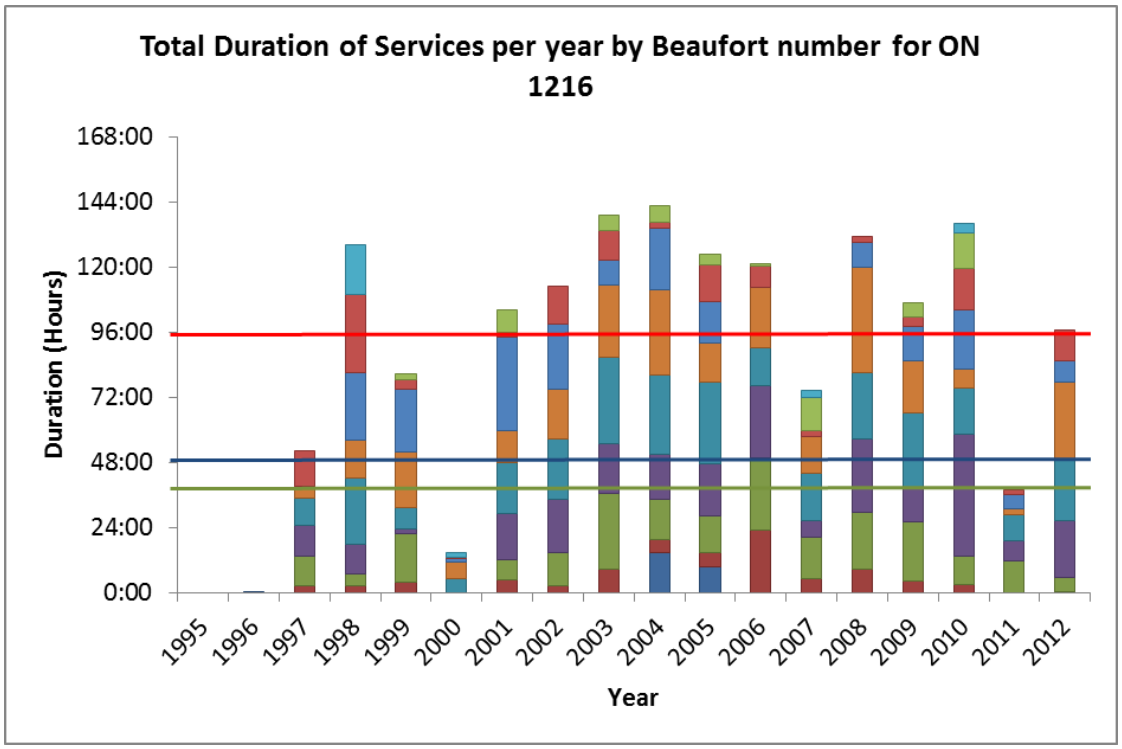

Figure 5-7: General pattern of boat services per year for ON 1216. The average for all Severn class lifeboats calculated from all available service data is shown in blue and that using data from 2005 onwards is shown in green. The red line represents the average for ON 1216.

Figure 5-8 shows that the distribution of services in each Beaufort state per year is variable between years. The data is difficult to visualise in this format, but it should be clear that each of the different distributions being quite unique for each year. Similar graphs for the On1221 and ON1248 can be found in the appendix, 11.2. Broadly the results are similar to those displayed for ON1216, however there are some slight differences. For instance for ON1221 the distributions tend to contain 2 peaks rather than a single peak, with peaks in a low and high sea state. This would suggest that the lifeboat attends to services regularly to both experienced commercial sea farer's who could reasonably be expected to passage in extreme weathers and inexperienced water users who can become easily caught out in more benign conditions. The variation in peak location from year to year could be due to the interpretation of the sea state as discussed in 5.2.

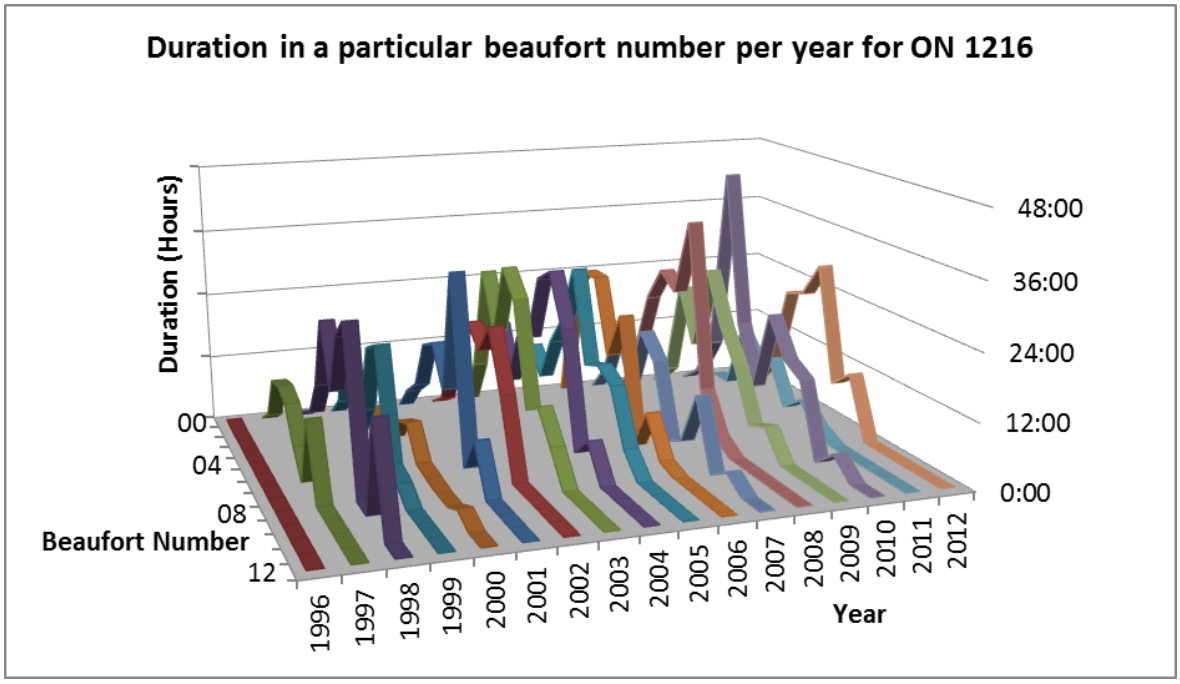

Figure 5-8: The distribution of service durations of ON 1216 for all years in service.

Figure 5-9 shows the total duration of the lifeboat services per year for ON1279. The interesting thing about a relief lifeboat is that the service history reflects the stations at which it was stationed throughout the year as well as the passage conditions between these stations. It is therefore likely that these vessels will show a greater variance in the total duration per year. This is confirmed by comparing the total duration of services in 2011 when the boat was stationed at the Humber for 6 months to previous years when she wasn't. There is a significant peak in duration of services in this year. Additionally investigating Figure 5-10 which shows the distribution of services per sea state per year doesn't show any particular increased variation

between years as might be expected from the variety of stations visited. The variation of distributions between years is still quite high as with the other lifeboats.

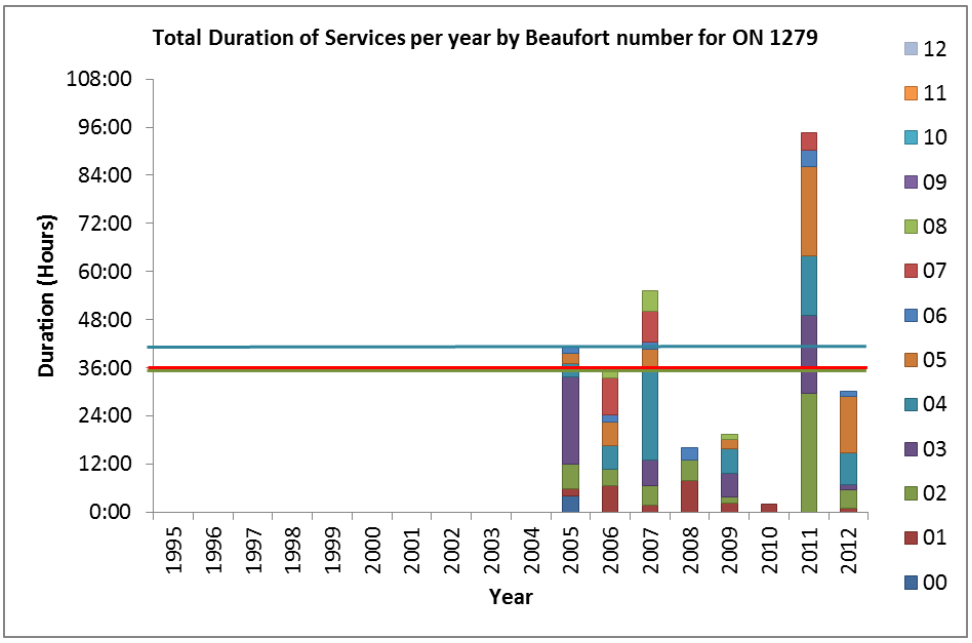

Figure 5-9: Total duration of services in all Beaufort conditions for lifeboat ON 1279. The average for all Severn class lifeboats calculated from all available service data is shown in blue and that using data from 2005 onwards is shown in green. The red line represents the average of ON 1279.

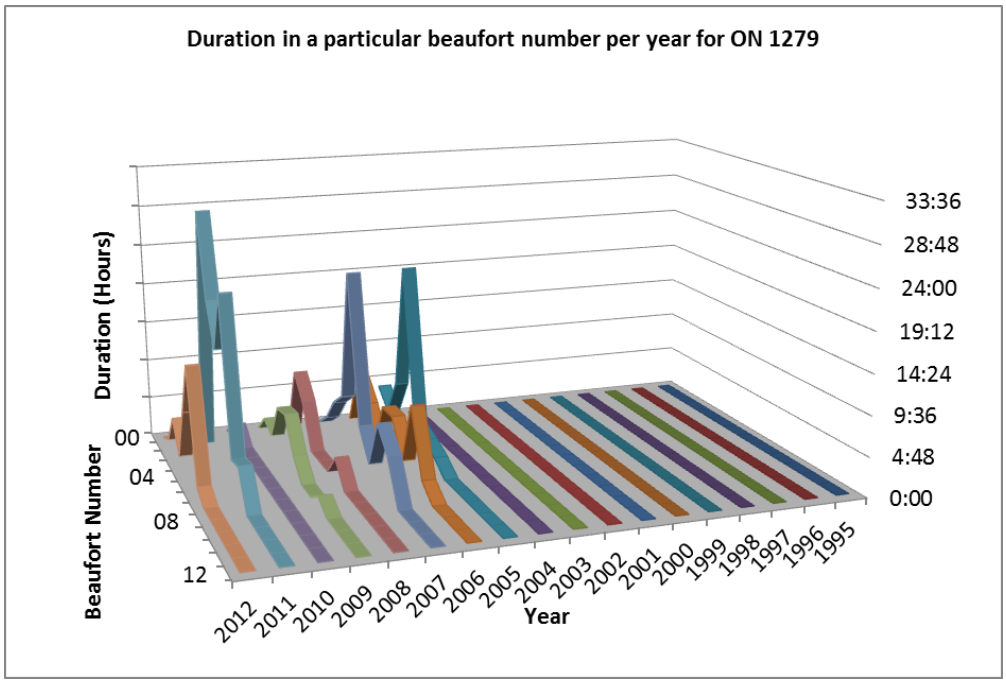

Figure 5-10: The distribution of service durations of ON 1279. The year axis is reversed when compared to other similar graphs in this chapter.

Figure 5-11 to Figure 5-14 show the distributions about the mean value of duration for each of the chosen lifeboats. 3 distinct distributions are shown, the first, ON 1216, is a skewed distribution with the biggest proportion of services occurring within one positive standard deviation of the mean and a standard deviation of 43 hours duration. The spread is quite large extending to 2 standard deviations. Figure 5-12 and Figure 5-13, from ON 1221 and 1248 respectively, are very different to that shown in Figure 5-11 with a much more even spread of services across the standard deviation widths. The final figure, Figure 5-14, shows that the total duration of services per year have occurred within a range one standard deviation less than the mean and the rest spread out over another two deviations greater than the mean.

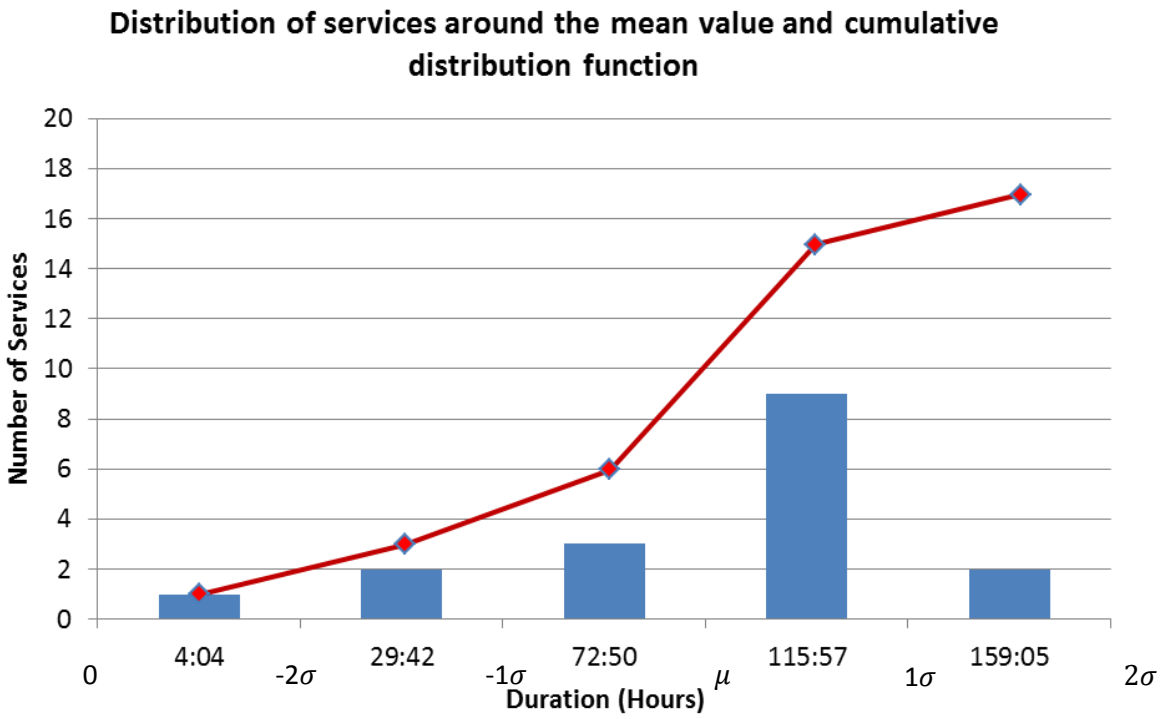

Figure 5-11: Distribution of services about the mean for ON 1216 and cumulative distribution function from discrete year by year values.

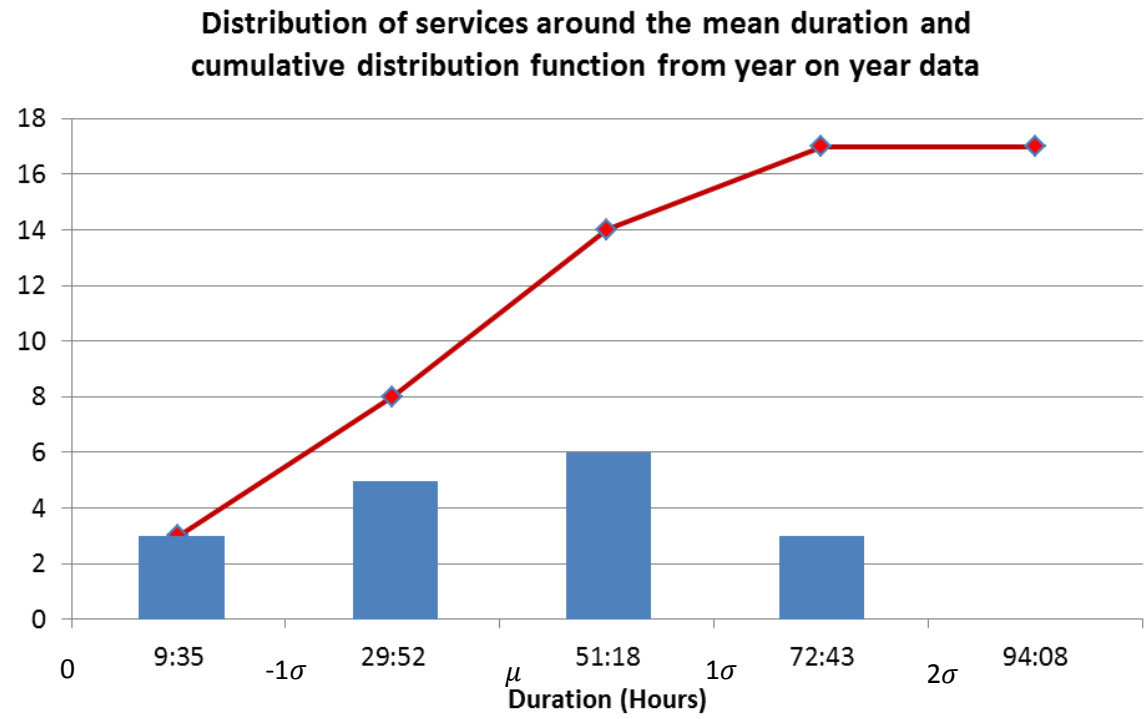

Figure 5-12: Distribution of services from the mean for all years for lifeboat ON 1221.

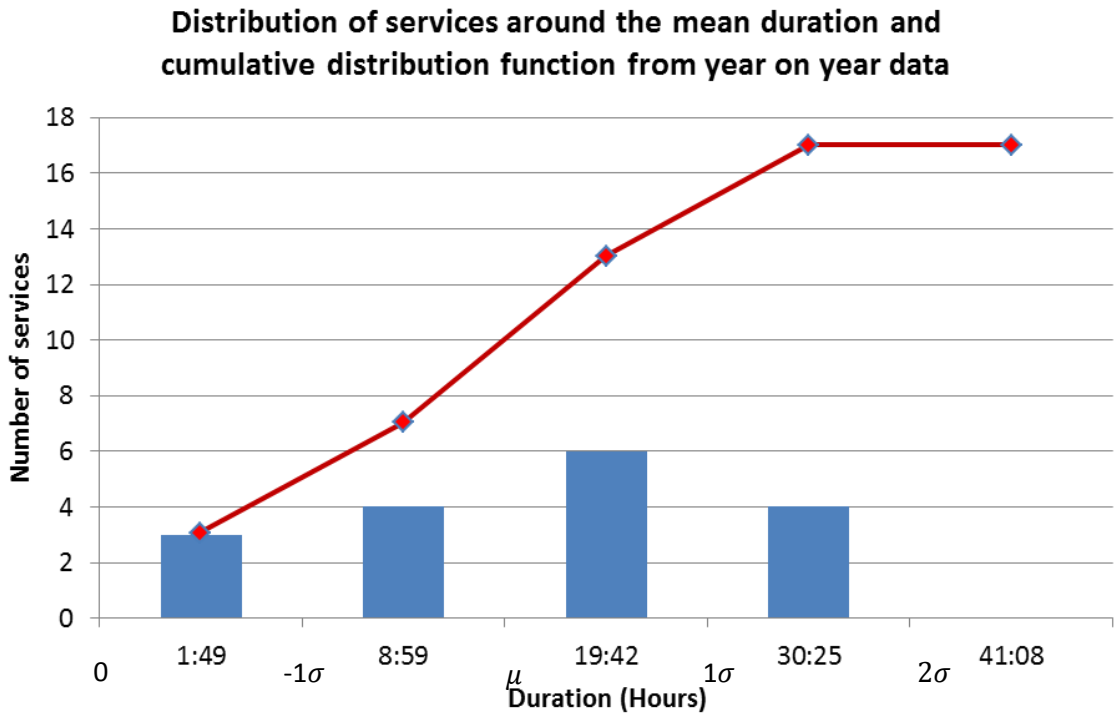

Figure 5-13: Distribution of services from the mean for all years for lifeboat ON 1248

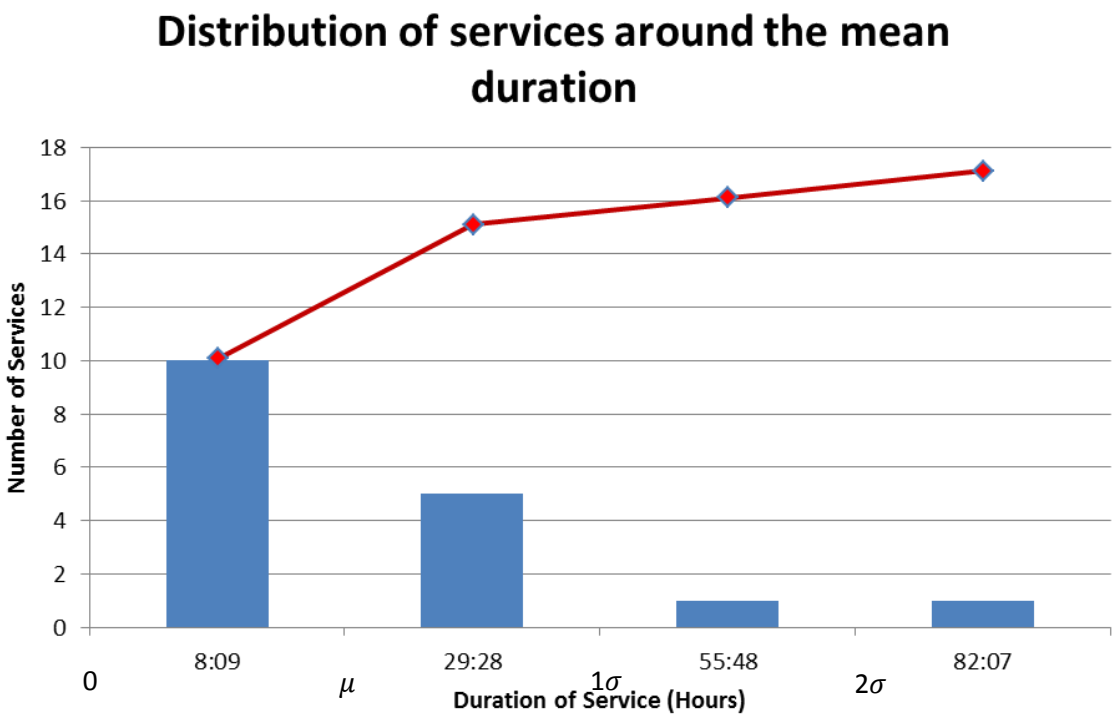

Figure 5-14: Distribution of services from the mean for all years for lifeboat ON 1279.

Hind casting the operating environments the lifeboats have served time in can be achieved as the past histories of the lifeboats are well documented. In this section this data has been introduced and analysed. Specific cases have been compared to the average case and shown to be different enough that individual records for each individual lifeboat should be used in the hind cast, not an average distribution of services based on all data.

Having identified the past services of the lifeboats which can be used along with an appropriate fatigue spectrum to determine the quantity of fatigue life used, the next step is to create a prediction for each individual boat which can be used to determine the expected remaining life. This is discussed in the next section.

5.1.2 Prediction of future operating environments

For prediction purposes an average total duration needs to be taken from the data presented. For an "Average life boat" this can be taken from Figure 5-1 and the outputs are shown in Figure 5-4. As discussed before two averages were considered to take into account the influence of the reduced number of lifeboats in the first ten years of the fleet history.

The average total duration per year using the data from 2005 onwards only was 42 hours and 9 minutes. The spread either side of this average ranges from 19 hours and 52 minutes for lifeboat ON 1248 to 94 hours and 24 minutes for ON 1216, a range from 16 hours and 51 minutes below

the lower average and 52 hours and 5 minutes above the higher average. There are 13 vessels which record durations over the average and 21 falling below with the rest falling between the two average lines.

Although this is useful in determining the expected total duration at sea for the average lifeboat it doesn't really help when the data available for the fatigue analysis is generated in terms of Beaufort number. The distribution of the duration in a particular Beaufort number is shown in Figure 5-15. This can be used if there is no other data available to predict the yearly average service for a lifeboat, as would be the case at design.

When there are assets already in existence that have been shown to have a significant variation in duration of services from the average, it is preferable to use their own service records to develop an average usage profile per year from which to make estimates on future services. The average service duration distribution across the different sea states for each of the different lifeboats discussed here is shown in Figure 5-16 to Figure 5-19.

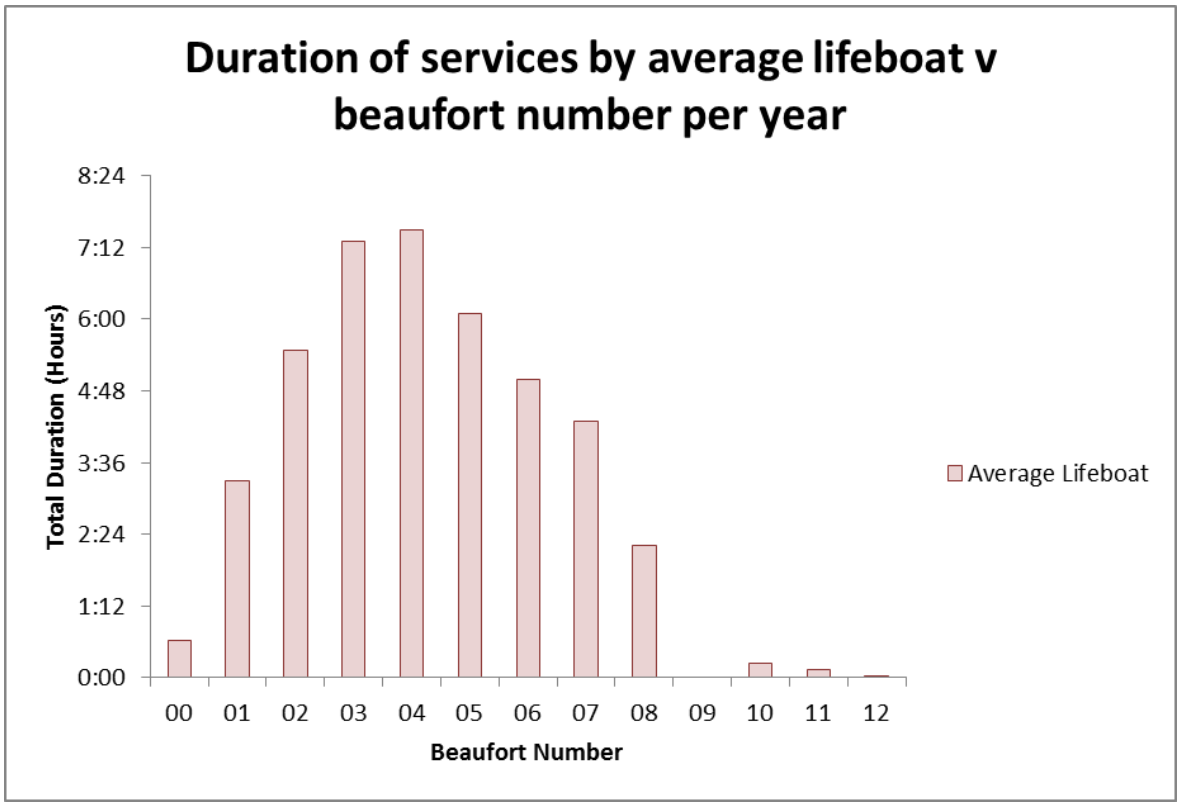

Figure 5-15: Distribution of total duration in each sea state for the average lifeboat per year.

Comparing the distribution of the different lifeboats to that of the average in Figure 5-15 it can be seen that for ON 1216, Figure 5-16, there are significant similarities. The distribution for ON 1221 is very different to that of the average lifeboat showing a bi-modal distribution, with two distinct

peaks at sea states 3 and 8. The distribution for ON 1248 is similar to that of the average lifeboat with a peak at sea state 3 rather than 4. The final average for ON 1279 has a roughly equal amount of service time in sea states 2 to 5 with significantly less in sea states 0, 1 and 6 to 8 with none recorded above this sea state.

The difference in shape between these graphs is significant enough to determine that using the average total duration and distribution in sea states for each individual asset will provide more detailed and useful information than taking the average value and distribution and applying it to all of the existing assets in the Severn lifeboat fleet.

To correctly use these distributions in their current state to predict future operational conditions the assumption must be made that in all cases the future trend will be similar to those shown in Figure 5-16 to Figure 5-19. Variation from these distributions on a year on year basis can be accounted for by continuously updating the distributions with the most recent service data.

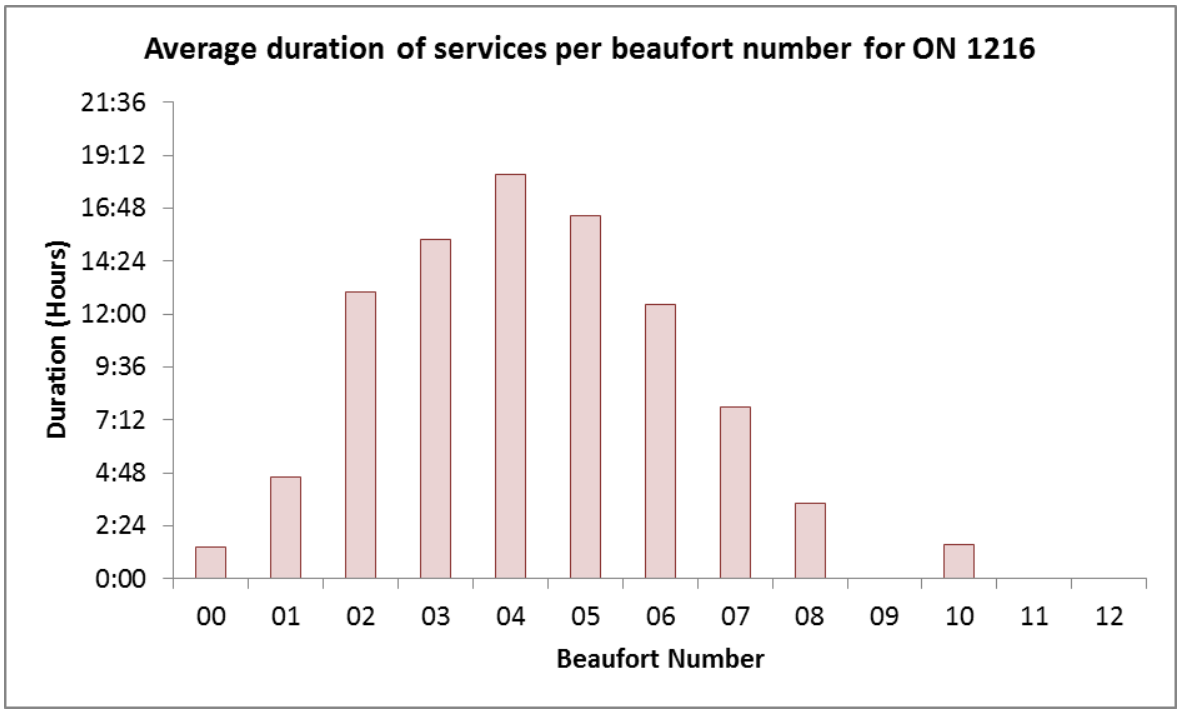

Figure 5-16: Average service history for lifeboat number ON 1216

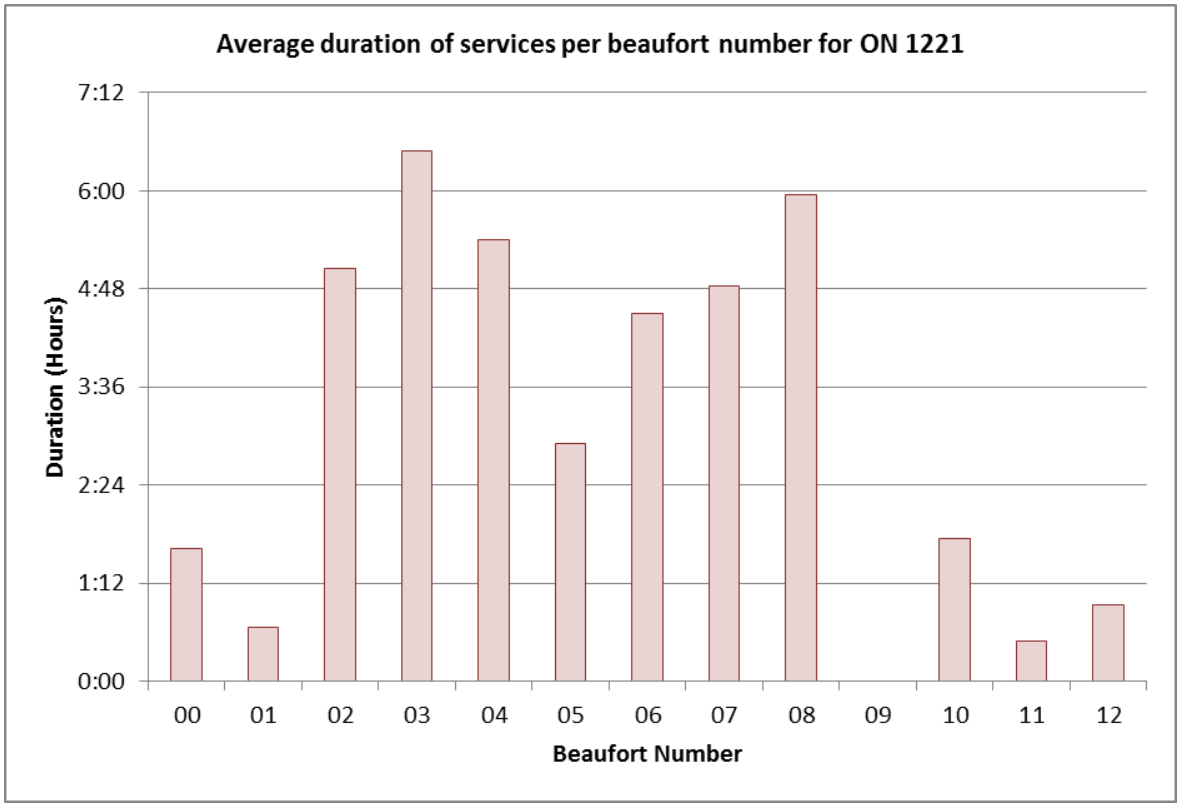

Figure 5-17: Average Services per year for lifeboat number ON 1221.

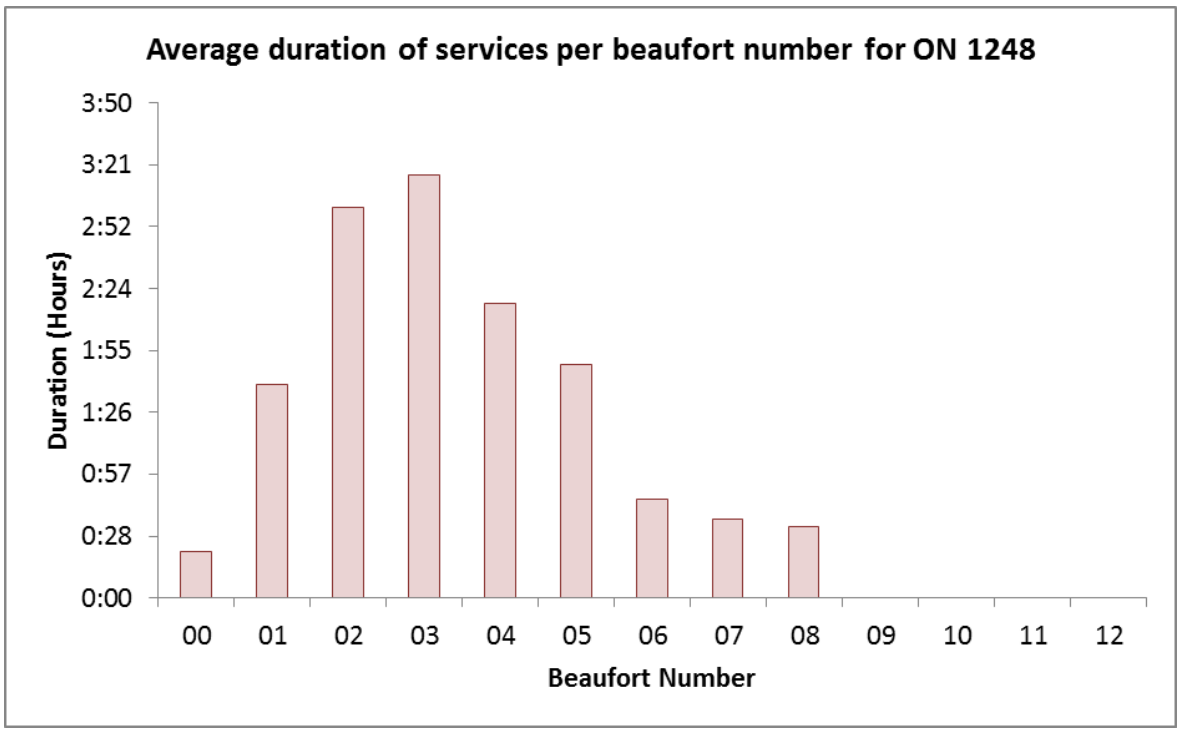

Figure 5-18: Average Services per year for lifeboat number ON 1248.

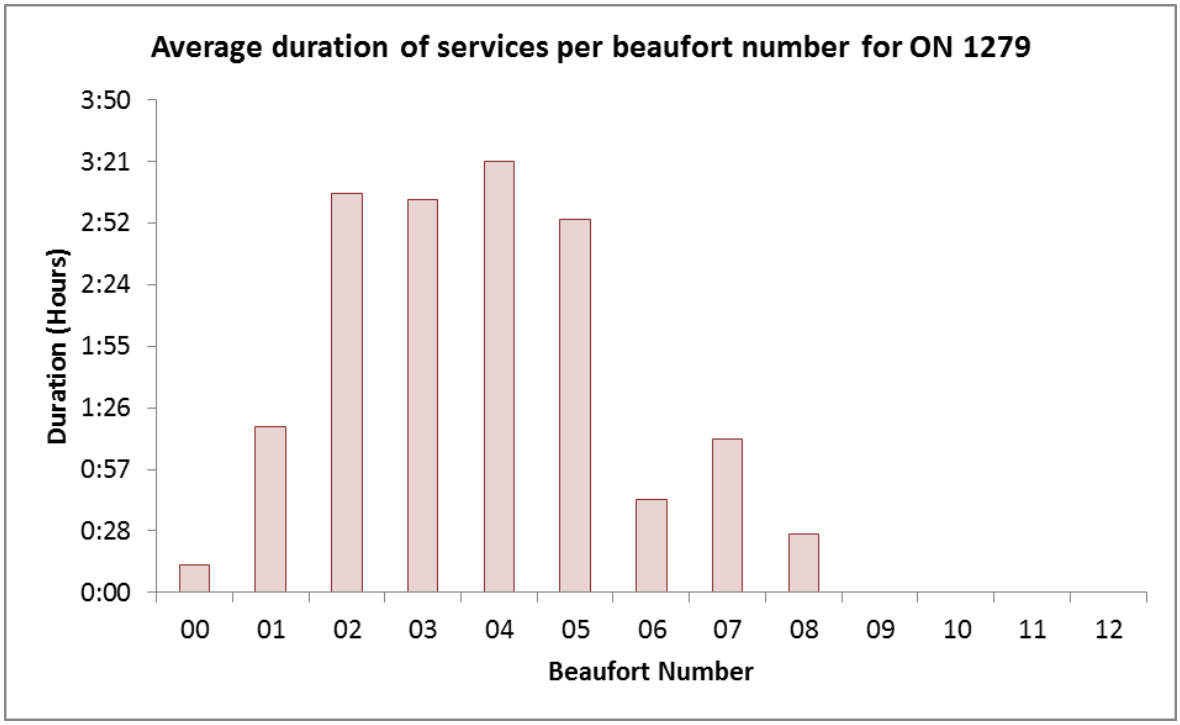

Figure 5-19: Average service duration for ON 1279 per Beaufort number.

This section has shown that the average yearly distributions of total time at sea for each declared Beaufort number for each of the individual assets will provide the best results when predicting the future operating environments expected. The distributions for four particular assets have then been identified to be used for life prediction purposes within the structural life assessment.

5.1.3 Section Summary

The aim of this section was to determine the variation in operating environment for the lifeboats and the duration of services in each of the variants. From the data available a number of average values and distributions were generated and evaluated. The fleet total duration, fleet wide average duration and fleet wide average duration per sea state have been discussed and dismissed as variables for use due to the coarseness of the data compared to that available.

Lifeboat average service durations per year and per sea state were identified as being suitable assuming the damage model does not take load history into account. If the damage model used in the structural life assessment model does take load history into account then the individual service histories for each year should be used to determine the damage for that year and then each value manipulated according to the damage model on a year by year basis.

One of the major assumptions of this work is that the reported sea states are correct and the resulting distributions can be relied upon to determine the service profile. This aspect is investigated in the subsequent section.

5.2 Assessing the Operating Environment

The previous section identified the duration of services in different sea states for different lifeboats, the main conclusion was that the service returns for each individual lifeboat be used to determine a used life for those vessels. From this past history an average for each individual vessel can then be used to determine the potential remaining life of each individual lifeboat in the fleet.

This process however relies on the accuracy of the people generating the service return forms when determining the sea state. Previous research by (Guedes Soares, 1986) has identified a possible variation of actual sea state when compared to the sea state as measured by wave buoys. This section investigates the likely variation from measured sea state as recorded by the crew's in their service returns, using the wave height as estimations of the sea state related to the Beaufort Wind Force parameters outlined in Table 2-1.

5.2.1 Methodology

The sea states identified by different crews from different lifeboat stations around the country were compared to wave buoy data, where there was a permanent wave buoy site. Station and Wave buoy locations were generated for various different stations using a combination of a map of the RNLI's stations around the UK and a map of wave buoy locations. All the stations considered suitable for analysis are shown in Table 5-1. The intention was to keep to stations with the wave buoys within 10 miles to try and negate the effects of topography, however this soon proved impractical so wave buoys were chosen based on distance from station, local topography and whether there were better opportunities for analysis in the near distance. Those identified for analysis are highlighted in brown. Wave data was gathered from the wavenet resource, (DEFRA, 2012). The date from the crew reports was used to search for information in the data base. The wave height data was then used to determine which sea state should be expected to be encountered. This was then correlated with the Sea State identified by the lifeboat crews. This correlation for all available data is shown in Figure 5-20.

Table 5-1: The location of selected wave buoys around the UK and Lifeboat stations which are in the vicinity along with the class of lifeboat stationed there. The highlighted columns show which wave buoy data is used for this analysis.

FROM (Station)	Lifeboat Type	TO (Buoy)	Dist	Bearing
Buckie	Severn	Moray Firth	21.1	325
Anstruther	Mersey	Firth of Forth	6.8	107
Hartlepool		Tyne / Tees	20.4	049
Tynemouth	Severn	Tyne / Tees	24.3	103
Humber	Severn	Dowsing	41.7	267
Skegness	Mersey	North Well	6.9	137
Wells		Blakeney Overfalls	10.4	069
Cromer	Tamar	Blakeney Overfalls	10.2	318
Walton & Frinton	Mersey	Sizewell	23.5	035
Walton & Frinton		Southwold Approach	33.9	034
Aldeburgh	Mersey	Sizewell	4.5	043
Aldeburgh	Mersey	Southwold Approach	11.8	034
Walton & Frinton		West Gabbard	31.1	075
Margate		South Knock	13.1	034
Dungeness	Mersey	Dungeness	2.3	181
Hastings		Hastings	9	137
Poole		Poole Bay	9.2	108
Swanage		Poole Bay	8.8	080
Barry Dock		Hinckley	10.5	159
The Mumbles		Scarweather	8.3	169
Hoylake		Liverpool Bay	10.3	323
Barrow	Tamar	Barrow	10.1	244
Oban		Blackstones	56.8	249
Islay	Severn	Blackstones	34.1	292
Barra Island	Severn	West of Hebrides	24.6	325

5.2.2 Results and Discussion

The blue crossed lines on Figure 5-20 represent the boundaries of the Beaufort scale, for data points which appear to the left of the Beaufort lower boundary, it can be concluded that the coxswain has over predicted the sea state, when compared to the wave buoy reading of the same date and time, for data points that appear to the right of the Beaufort upper boundary the conclusion is that the coxswain has under predicted the sea state. To confirm this, take two lines running vertically from the horizontal measured wave height axis and running vertically through two crosses adjacent to each other for any particular sea state indicated on the vertical axis. For the sea state number chosen there will be a number of data points between the crosses and a number of data points either side of the crosses. The data points to the left of the Beaufort Force Lower cross have been characterised as being that sea state by the coxswain, but measurements by the wave buoy suggest the characterisation should be lower. For data points to the right, measurements by the wave buoy suggest the coxswain should have characterised the sea state higher. The corresponding sea state for the data points in error can be determined by extending the vertical lines to the extremities of the graph and then identifying any data points which fall between them.

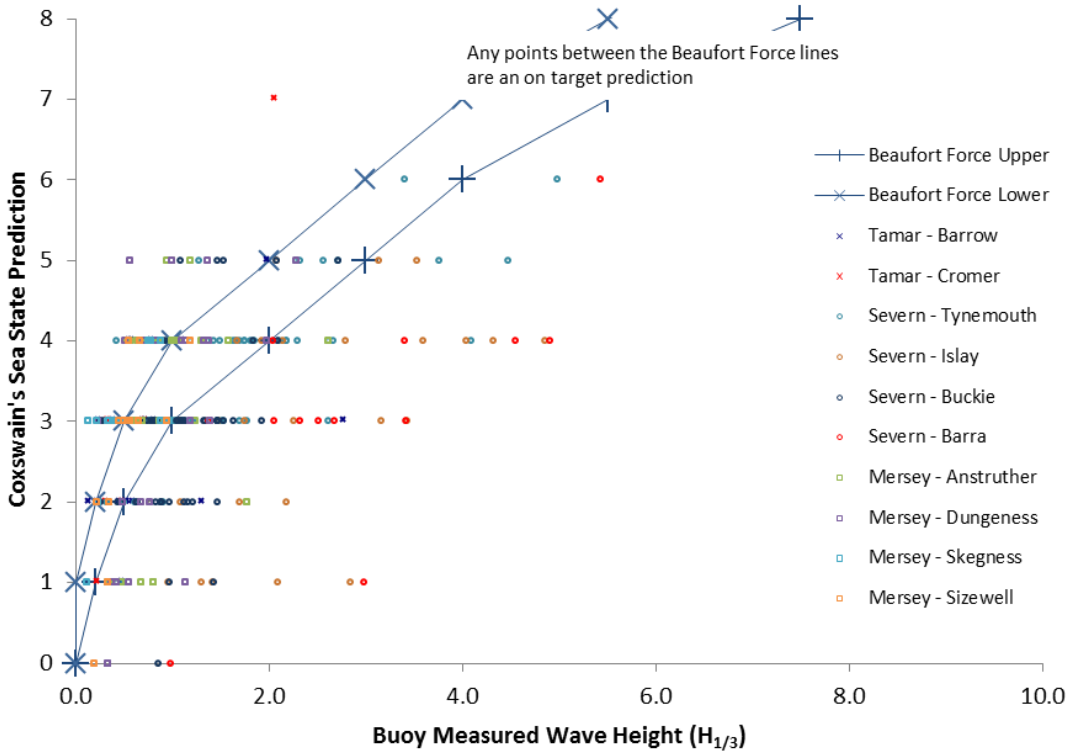

Figure 5-20: Coxswains recorded sea state versus wave buoy derived sea state for all of the stations combined. Any points above the upper line show an over prediction by the crew, any points below the lower line show an under prediction by the crew.

Data from three different class of lifeboat were available for the analysis, the Severn class, the Tamar class and the Mersey class Lifeboat. There are significant differences between the three classes of lifeboat in terms of profile, operating requirements and age of design. The Mersey Class Lifeboat is significantly shorter than the Tamar class lifeboat with the crew set inside a compartment which is very close to the waterline, the Tamar in turn is significantly shorter than the Severn class lifeboat and in a newer design with significantly more emphasis on crew comfort than either the Severn or the Mersey.

As can be seen there is significant spread for all of the sea states where there are recorded rescues that can be correlated against wave buoy data. The data also shows that there seems to be more occasions where the coxswain believes they are in a lower sea state than higher sea states. In general the spread either side of the boundaries appears fairly even for over and under predictions of the sea state for coxswain predicted sea states 3 and 4. For coxswain predicted sea states 0 to 2, it appears that more often than not the coxswain has under predicted. For coxswain predicted sea state 5 there is not enough data to draw any real conclusions, however at first glance it would appear the coxswains are generally either correct or over predicting. There is no data currently available for any sea states higher than a sea state 7, and there is not enough data for sea states 6 and 7 to draw any conclusions at all.

The next step was to try and generate an understanding of the expected general distribution of coxswain errors for all lifeboat services. This information was gathered by converting the measured wave height into a Beaufort number using the correlation in Table 2-1, then subtracting that number from the sea state number given by the lifeboat coxswain, this information is shown in Figure 5-21. The distribution presented shows a relatively peaky normal distribution centred around an error of 0, meaning 34% of the time the coxswain is correct and 31% of the time the coxswain over predicts by 1 sea state and 6% of the time by 2 or 3 sea states. This means that for 71% of the time using a damage state that has been developed for a particular sea state and applied based on the coxswains assessment of the conditions of the time will produce either an accurate, or over prediction of the potential damaged state or life used of the lifeboat. However this does mean that for 29% of the time the predicted sea state is an under prediction which could possibly lead to a non-conservative prediction of used life, of this 29%, 20% of the time the under prediction is by only 1 sea state whilst the remaining 9% is 2 or 3 sea states under predicted.

Having identified that there is the potential for an under prediction of the sea state for 30% of all services it was felt that it would be worth splitting the data in Figure 5-20 into the different classes of lifeboat. The data for the 4 Severn class lifeboats is shown in Figure 5-22. The

difference between the data displayed in Figure 5-20 and that displayed in Figure 5-22 is not obvious in this format; Figure 5-23 shows the percentage and magnitude of coxswain errors for the Severn class lifeboat specifically.

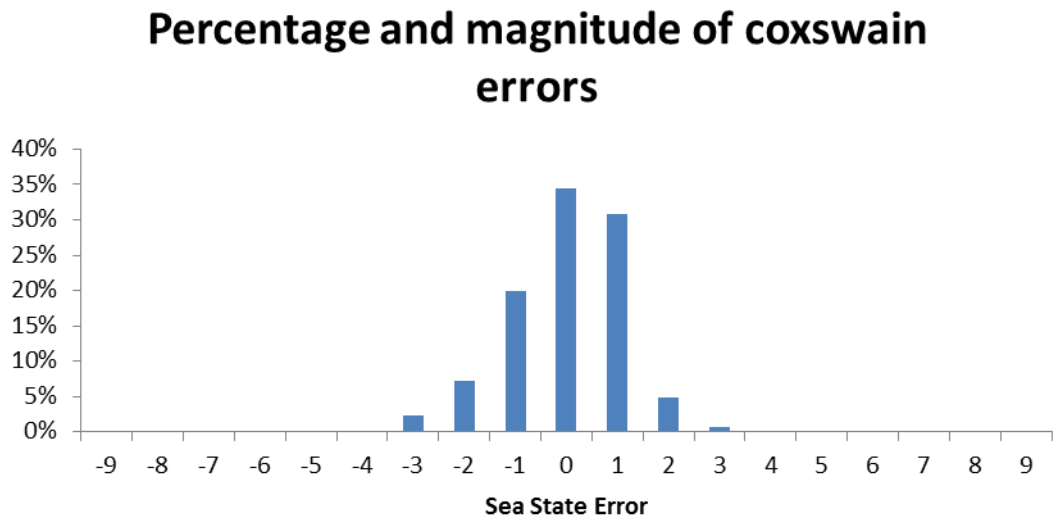

Figure 5-21: Number of sea states error in the coxswain's judgement along with the percentage of time it happens for all of the data presented in Figure 5-22.

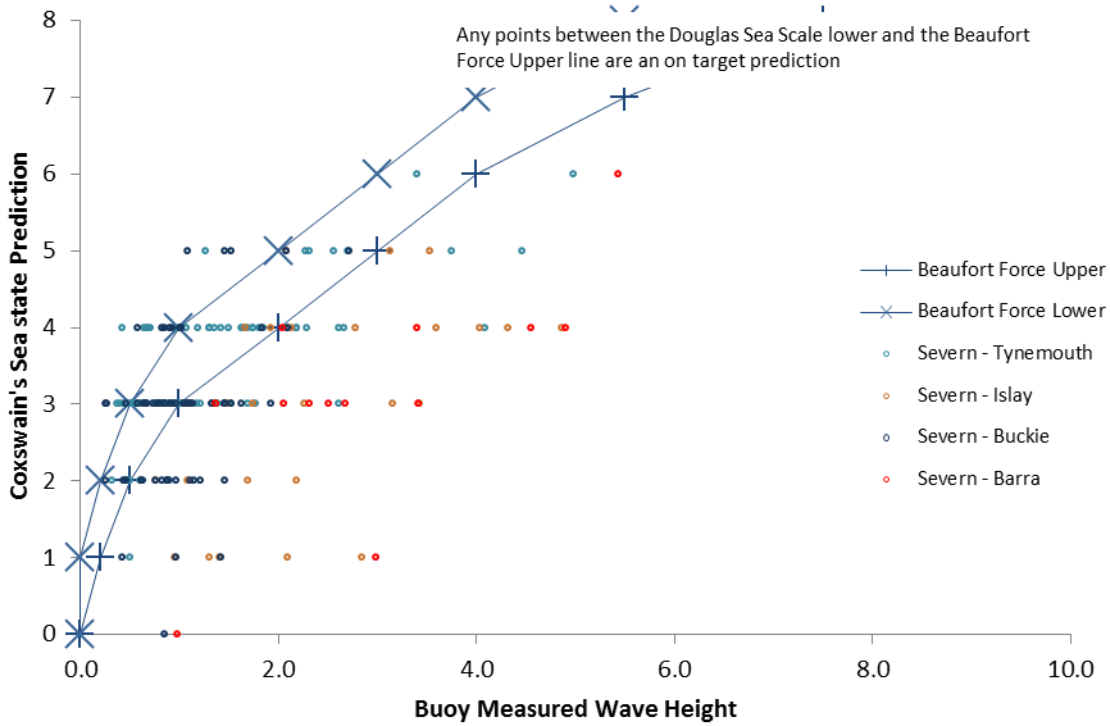

Figure 5-22: Coxswains recorded sea state versus wave buoy derived sea state for all of the Severn stations.

Comparing Figure 5-21 and Figure 5-23 the distributions are very similar with the recorded sea state being accurate 36% of the time over or under predicting by 1 sea state 27% and 22% of the time respectively and over or under predicting by 2 or more sea states 6% and 8% of the time respectively. This result can be explained in two ways, the first being that the size of the sample for Figure 5-21 was 337, with 106 from the Mersey data set, 26 from the Tamar data set and the final 205 from the Severn. With 61% of all the observations in this data set coming from the Severn lifeboat, the distributions shape would only be significantly changed if the data from the Mersey and Tamar lifeboats were significantly different (i.e. major over or under predictions by 2 or more sea states).

However, even if this was the case, since the case study of this thesis is the Severn lifeboat the results would not be relevant. As it stands the suggestion is that where data is not available i.e. for new vessels, the distribution shown in Figure 5-21 can be used to estimate the variability in suggested sea state compared to expected sea state. It is worth noting that this analysis does not take into account any localised effects which would need to be further investigated to further investigate the potential reasons for sea state misrepresentation. This could be caused by the local sea bed topography or the location of the station within the UK and Ireland. As an example, stations on the west coast of Ireland are more likely to be exposed to large rolling seas due to the several thousand mile fetch across the Atlantic ocean, than Dover lifeboat station where the fetch is limited by the comparative closeness of the European mainland.

Table 5-2 shows the total number of observations available for comparison of Beaufort numbers predicted from wave buoy measured wave heights to Beaufort numbers stated by crews on a Severn class lifeboat, it includes the percentage of those observations which do not agree with the wave buoy data, the % observed difference. From a statistical point of view, the size of the sample has a strong link to the confidence that can be placed in the trends drawn. For Beaufort sea states 3 to 5 there are a large number of results, enough that another single observation will not significantly change the shape of the resulting distribution. For Beaufort state 2 another observation will represent either an increase in % errors of 2% or a decrease of 4% depending on whether it is a correct estimation, under or over prediction. For Beaufort state 0, 1, 6 and 7 the total number of observations is very low (6 or 7) which means an individual observation will have a significantly higher impact for Beaufort state 1 and 6 a reduction in % observed differences of 12% and 14% respectively, and for Beaufort state 7, a decrease in observed differences of 10% or an increase of 4%. For sea state 0 it is fair to accept the assertion of 100% accuracy due to the very distinct physical appearance of the environment.

Table 5-2: Number of observations made by wave buoys per observed sea state and the number of errors from the coxswain within that data set.

Sea State	Number of Observations	% observed differences
0	6	0
1	6	100
2	15	67
3	68	53
4	69	67
5	28	82
6	7	100
7	6	67

From this table it can be seen that in general the amount of observations which are potentially wrong is very significant, and that as the sea state increases the problem gets worse. To investigate this the data was further broken down by sea state to determine the percentage of error observations in each one, which is presented in Figure 5-24. From this figure it can be gleaned that if a coxswain has determined a low sea state, 1 and 2, it is more likely that the disagreement between the coxswain and the wave buoy is through the coxswain underestimating the sea conditions by anything up to 4 sea states. The problem with this result is that with sea state 1 being almost the most benign sea state and sea state 5 containing wave heights up to 3m there could be significant under estimation of the damage condition if the data is taken directly from service returns. There is a chance that this could be due to a large swell which has a wavelength long enough that no breaking waves are visible. This may provide some evidence that due to the very subject nature of the Beaufort scale it may not be the best measure to use when predicting the sea state.

As the predicted sea states increases the peak number of observed differences increases by one sea state from -2 (2 sea state under prediction) to an over prediction of 1 sea state by sea state 4. The over prediction remains at 1 for sea state 5 but the bulk of the data is represented by this over prediction. For sea state 6 and 7 the relationship is difficult to determine, however this is clearly due to the small number of observations made. However for Beaufort state 6 29% (2 of 7) the observations are an under prediction by a single sea state and 71% (5 of 7) are an over prediction. This follows the general trend suggested by the data from the previous sea states, which continues with the data for Beaufort state 7 where of the 6 records 4 are over predictions

and 2 are in agreement. However, caution must be exercised when using the data from sea states 1, 6 and 7 until more data is captured and confidence built in the distributions for these sea states.

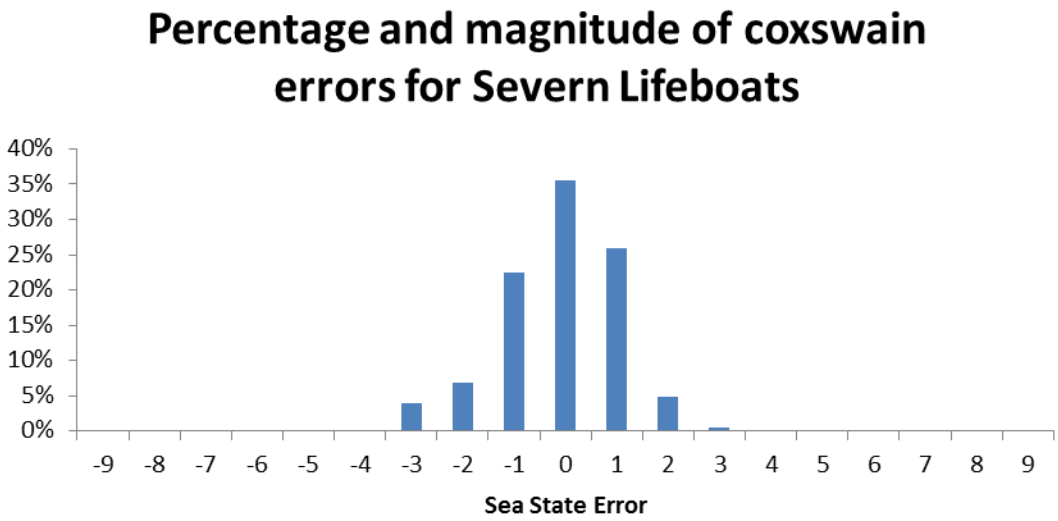

Figure 5-23: Number of sea states error in the coxswain's judgement along with the percentage of time it happens for all of the data presented in Figure 5-22

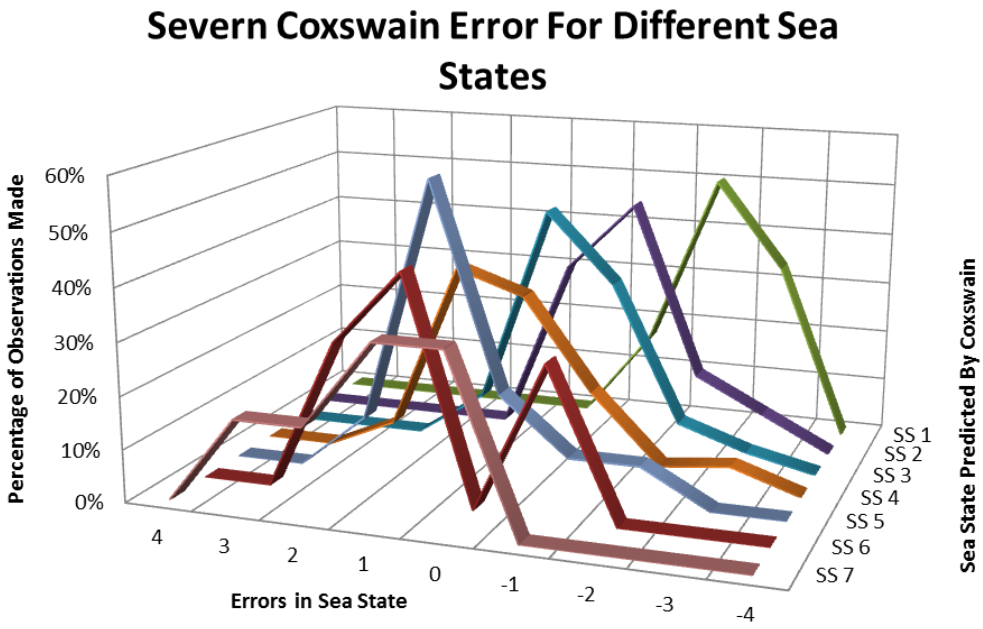

Figure 5-24: Errors in sea state observation that have been recorded by the coxswains of the Severn Lifeboats, a negative error suggests the coxswain has under predicted the sea state whilst a positive error suggests an over prediction of sea state.

5.2.3 Summary

Having completed this section it has been shown that properly understanding the correlation between the sea state predicted by the coxswain of the lifeboat and the sea state measured from the wave buoys, which is assumed to be correct, is extremely important. This is especially true for the predictions at the lower end of the sea state scale as the demonstrated scope for error can easily lead to an incorrect application of any structural response distribution developed.

Additionally there are other geographical influences on how the state of the sea will react to swell, wind and tidal changes. Areas where there is a change of depth from deep to shallow increases the likelihood of breaking waves or shorter seas which will increase the likelihood of slamming conditions. It is conceivable that in deep water such as that off the Atlantic coast the swell may be significant but occur over a long wavelength which is less likely to cause significant structural loading.

5.3 Application in Life Prediction

Two important results have been identified in this chapter;

1. The amount of time at sea, both in terms of time spent in the different sea states and cumulative duration at sea per year, is unique to each vessel.
2. In general it could be expected that errors when recording the sea state be made when comparing the estimation of the sea state based on crew observations to the estimation of sea state based on measurements by wave buoys.

Combining these two results will allow the potential error to be taken into account when deciding which sea state to use structural data from as well as ensuring the proportional weighting of each sea state, determined by the amount of time spent in it for that asset is correct. The first step is to declare a particular sea state, SS_{Dec}, for which the cumulative damage needs to be calculated. The second step involves determining the expected error for this instance SS_{Err} and summing it with SS_{Dec} to obtain the resultant sea state SS_{Res}, as shown in equation 5-1.

$$SS_{Res} = SS_{Dec} + SS_{Err} \qquad \textbf{5-1}$$

Where SS_{Err} is found from distributions in Figure 5-24, or Figure 5-23 where the distribution is undefined.

Finally the amount of time spent in the declared sea state needs to be taken into account to determine the total expected damage for the declared sea state. Correctly accounting for the

errors in sea state requires a technique which can build up an understanding of the likely values of sea state based on the distribution of error. In this case the Monte Carlo technique is chosen for the following reasons:

1. It allows uncertainty to be accounted for by generating a distribution of possible outcomes based on distributions of inputs.
2. It can account for numerous input distributions simultaneously in generating a single output distribution.
3. The number of iterations of the model can easily be managed to achieve greater understanding of the potential outcomes.

This is useful as the output from this analysis will act as one of a number of inputs into the structural life extension model discussed in chapter 7. Additionally the results of chapter 6 will also act as inputs to this model and will result in distributions of applied strain per sea state.

5.4 Summary

This chapter has identified the variability of the service histories in sea state based on Beaufort scale versus both time and for the different vessels. An average service life of the life boat fleet is presented and 4 vessels highlighted, which provide bounding and average service histories for which particular distributions are developed. These distributions can then be used to determine the quantity of time spent in the different environments which is identified as an important step in chapter 3.

Following on from that, an investigation into the relationship between sea states as determined by coxswain's and wave buoy measurements has found some discrepancy. Distributions representing the expected differences between coxswain and wave buoy measured sea conditions are presented.

Finally the method of application to a structural model is discussed, with subsequent chapters seeking to link a particular set of structural responses to the sea states identified in this chapter allowing the development of a fatigue spectrum which can be modified based on an individual vessel's service history. Combining this with the material's characterisation outputs of material strength and fatigue properties, the outcomes of this chapter and that following will allow an estimation of the used and predicted life of the vessel to be made. This combination is carried out in Chapter 8 as shown in Figure 5-25.

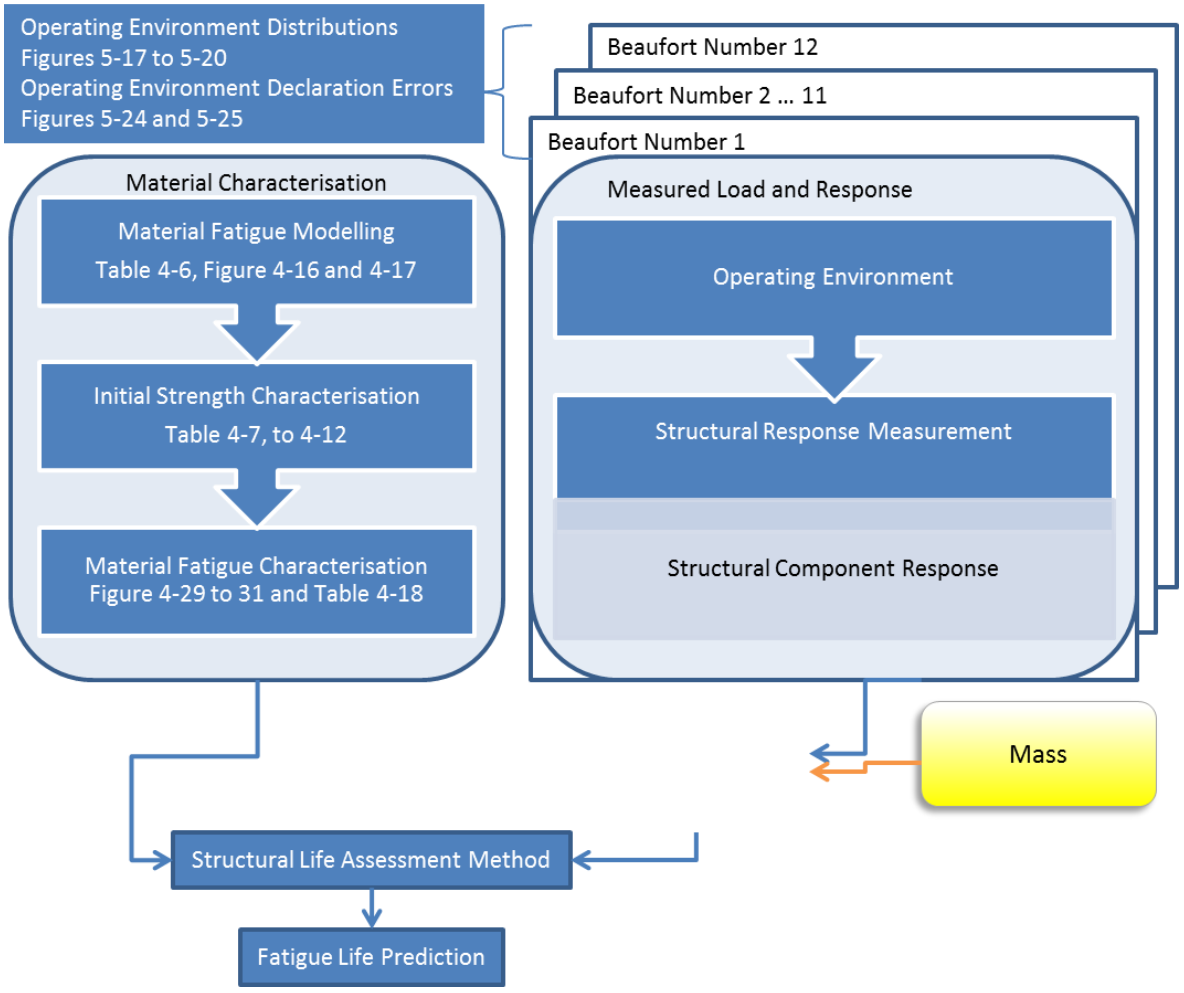

Figure 5-25: Areas identified within the methodology that are addressed so far.

6 Structural Response Monitoring

Having identified the relevant operating environments in terms of Beaufort number in the previous chapter, this chapter describes and demonstrates how structural monitoring can be used to generate the appropriate structural response inputs for each environment as shown in Figure 3-1. These are then applied in a fatigue life analysis, which is described and carried out in chapter 8.

Section 6.1 introduces a simple investigation to determine an accurate strain history for the Severn class lifeboat from direct measurement. The measurement of the interaction between the environment and the structure, which in the case of the Severn lifeboat is a pressure loading acting on the external face of the hull, is not conducted.

A previous investigation into the fatigue life prediction of the Trent class lifeboat used a fatigue spectrum of applied loads (Clark and Shenoi 1998), however the background to the source of the applied loads was not clear therefore relationship between the loads identified and the environment from which they were generated is not available making it difficult to use with the gathered environmental data. This can be remedied by understanding the expected variation of structural responses in each of the environments identified in the service returns. In addition to providing data which can be compared to the spectrum used in Clark (1998), the use of high speed data recording will allow the development of a refined fatigue spectrum from the measured structural responses.

The selection of appropriate response monitoring methods depends largely on the understanding of the loading condition the asset is subjected to and the availability of the asset. The easiest structural response to measure is strain and has been the response measured by a number of different investigations in the past (Bond and Farrow, 2000; Burman et al., 2010; Miller, 2001; ten Have, 1993).

6.1 Experimental Methodology

There are numerous technologies available for the measurement of strain, the selection of which is bound by practical issues, for instance optical methods which require a steady mounting platform and large amounts of light may not be appropriate in highly dynamic environments despite the potential gains in monitored area.

By their very nature monitored positions are limited to a finite area of monitoring. This feature means that without careful selection of the monitoring locations, important information about

the response of a structure to the applied loads could be lost and decisions made based on faulty information.

In an ideal world modelling methods would be used to determine areas of specific interest for further monitoring. This could be because they show a proportionally larger response to the loads applied than those around them or because there is significant uncertainty in the modelling process for that particular region.

However in this instance there is no model of the asset and no direct operational experience that may provide an insight into the areas which need monitoring, with the structure has proven to be reliable operationally in extreme conditions (a significant factor in its choice for lifetime extension investigation).. The choice of monitoring positions was therefore made based on the expectation of modelling methods being employed in the future which would need validation. Therefore engineering judgement was used to determine the structural detail monitored. In this case the shortest route to the directly applied load, that is it contains the least connections and opportunities for indirect loadings to have an effect on the results, i.e. hull panels was chosen.

The basic experimental methodology employed here is simply to continue using the asset as dictated by operational requirements whilst recording the appropriate structural response at an appropriate response rate. The lifeboat selected for the structural monitoring was a relief Lifeboat 17-46, Margaret, Joan and Fred Nye, one of 6 relief lifeboats operated by the RNLI. This lifeboat's role is to replace a station lifeboat when there is either a period of planned maintenance or an unexpected event puts the station boat out of action for a significant period of time. This lifeboat was chosen as at the time of hardware installation she was already undergoing maintenance work, as well as having a broad range of service locations programmed in for the coming years which would result in a large variation of geographic placements from which data could be taken, thus providing confidence that the developed distributions cover as broad a range of variables as possible.

The strains in the centre of a variety of individual panels were chosen for measurement as they provide the closest link to the applied load as defined previously. Although it is conceivable that certain areas of structure, such as bulkhead connections, may have a reduced lifetime due to the complex nature of the stress states associated with these details, they also provide a greater disconnect from the initial applied loads due to the complexity of the stress paths. This problem is exacerbated by the use of composite materials which are significantly more susceptible to manufacturing errors resulting in significant voids within the laminate if procedures are not

followed correctly. Regular structural inspection of the Severn class lifeboat hulls has found no evidence of any defects in the single skin hull area below the chine.

The strain gauges were located in the two major compartments within the lifeboat as shown in Figure 6-1. A total of 96 ¼ bridge strain gauges were fitted in a rectangular strain rosette configuration in 32 locations. 16 locations in the engine room and 16 locations in the survivors void space. The measuring positions cover the width of the engine room in the most forward and aft panels as well as measuring along the length of the engine room on panels immediately outboard of the prop tunnels. In the survivors void space, the strain gauge rosettes were placed symmetrically either side of the centre line in a 6, 6, 4 formation. In the foremost and aft most configurations the panelling was also symmetric either side. However in the centre row of panels, above the portside 3 is the structure containing the batteries for the lifeboat and as a result there is an extra support halving the length of these panels. The rearmost of the resulting set of 6 panels were monitored. Electrical strain gauges were chosen over optical gauges due to hardware limitations of the optical system at the time of installation.

The data acquisition units (DAQs) were set up in a master and slave configuration with the unit in the survivor's cabin being the master, handling the input from the Global Positioning System feed and acting as the master clock. Faltinsen (2000) who noted that structurally significant strain events (a single load and unload cycle) occurred on a flat aluminium panel over a period of no less than 5 milliseconds, with no further information relevant to the structure of interest, this was taken as a limiting value and 800 samples per second chosen for the speed of data acquisition. This would allow a minimum of 4 points to appear on any event which occurred over this duration. It was considered that under certain combinations of boat speed and operating environment it could be considered that the lifeboat would be platforming, effectively hoping from the crest of one wave to another. This can reasonably be expected to impart a large number of relatively low loads applied over short time periods, comparable to those found by Faltisen, which may have an impact on the long term structural integrity and therefore should be captured.

In addition to this the total expected service length for a lifeboat is expected to be 10 hours at a constant 25 knots, to ensure all data is captured, allowing a full structural response characterisation of the service, the system was required to operate for a minimum of 10 hours storing data continuously. The data was collected into individual files, 30 seconds in length and saved on the master DAQs, the data generated on the slave (Engine Room) DAQ was transferred to the Master (Survivors Cabin) DAQ using a standard network connection. The three files associated with one 30 second duration, containing engine room, survivor's space and GPS data

was then transferred through FTP to an external USB storage device. This set up was chosen as it allowed the storage to be expanded limitlessly and is visualised in Figure 6-1.

The software written to conduct the data acquisition can be found in Appendix 4 on the CD on the inside cover of this thesis. Once a service has been completed the data is collated by the crew onto a specific telemetry drive on the RNLI's system. From this point post processing is conducted offline. Simultaneously with the data acquisition the crew keep a record of the sea conditions throughout the passage. The data that the crew members recorded when on a service or training was as follows:

- Service / Training Date
- Sea State
- Duration of Service Conditions (Days, Hours, Minutes)

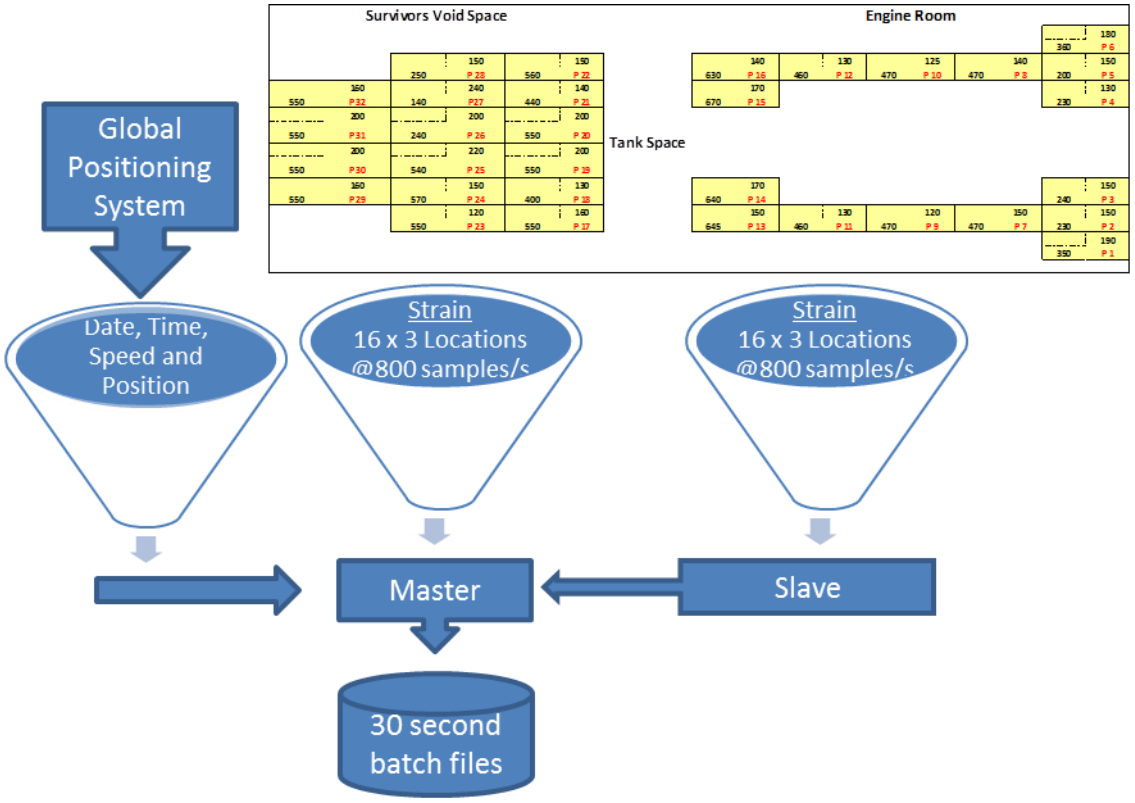

Figure 6-1: Visualisation of Data acquisition process and schematic of the monitored panels including dimensions of the panels from the base of the stiffening structure. The GPS data was used to time stamp the strain data and was taken from the Severn's GPS system.

6.2 Data Acquisition (DAQ) System and Validation

The data acquisition was undertaken by two standalone data acquisition units (DAQ's) with custom designed software, specific details for the system are found in Appendix 3. Typical

multipart systems contain several dummy DAQ's and a controlling PC configuration which would need to be accommodated in the Lifeboat. Due to the confined space and the fact the lifeboat would be conducting operations during the experimental period this was deemed un-suitable in this case. The system chosen is considerably more compact than a DAQ and PC configuration, comprising of a single "chassis" which contains both real time and deterministic programmable hardware. The data acquisition is taken care of using a Field Programmable Gate Array chip which allows the regular deterministic collection of the data, once triggered from the real time program. The computational load caused by collecting the data is isolated from the computational load associated with the real time software. This allows the initial data acquisition to be conducted at a far higher rate than is sustainable over long periods and then averaging the data according to a block size which result in a sustainable data acquisition rate. In this case the initial data acquisition rate was set to the maximum, 10,000 samples per second (SPS) and then averaged out to 800 SPS.

The data acquisition system was validated by comparing strain values measured by the DAQ using a strain gauge with those measured using a clip gauge attached to a composite test piece along with numerical calculations of expected strain in a laboratory environment. The test pieces used were constructed during student demonstrations and were expected to have a Young's modulus of between 21 and 23 GPa. This approach provided two independent sources of validation of the DAQ system. Although there are two data acquisition units in the system they are physically identical with the software determining the method of strain measurement also identical between the devices and the data channels used, therefore it was considered proving one channel would implicitly validate all other channels.

The attachment of the strain gauge to the specimen resulted in the inclusion of a bubble below the grid of the strain gauge. The effect of this was to interfere with the low strain readings during the test. Figure 6-2 shows the results of the validation process. The effect of the inclusion under the strain gauge is immediately obvious due to the confused strain trace of the gauge data below an applied load of around 2000N. It is also seen that the values of the clip and gauge measured strains are similar and within the bounds of the expected resultant strain.

Comparing the percentage error, Figure 6-2, between the clip and strain gauges using the expected strain line for a Young's Modulus of 23 GPa it can be seen that from an applied load of around 3000N there is a more or less constant difference of 5% between the measured strains. Considering the uncertainty in the material properties of the test piece and the potential interference with the recorded strain due to the included bubble below the grid it is considered

this comparison is acceptable and proves that the data acquisition system accurately measures strains. Ideally the experiment would have been repeated using specimen with better gauging however due to time constraints this was not possible.

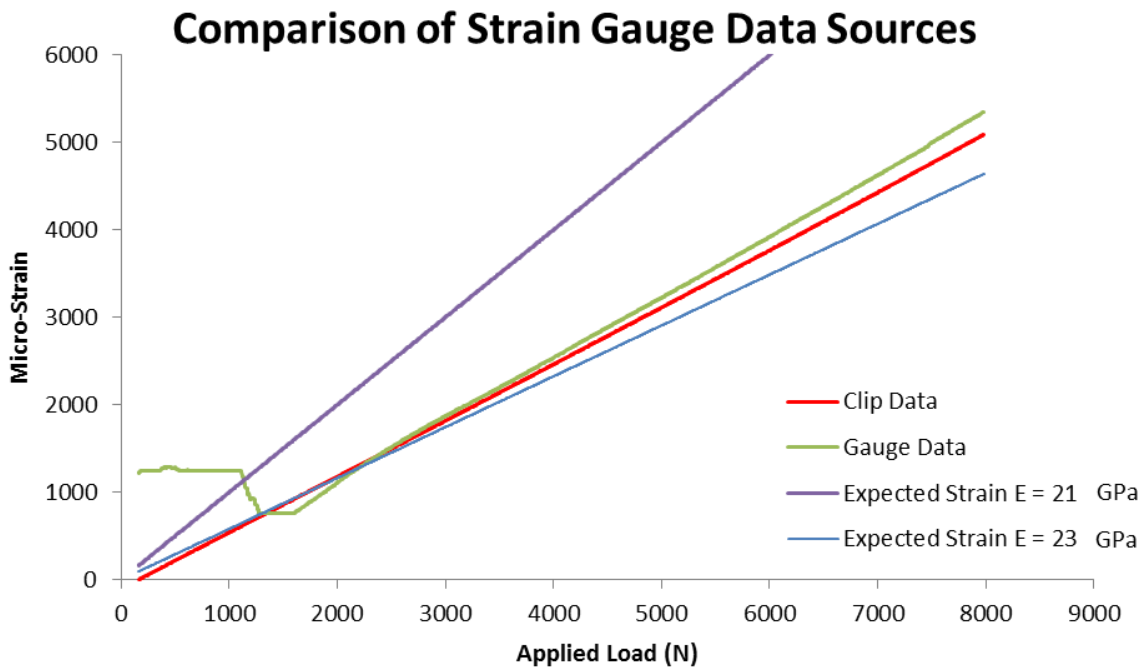

Figure 6-2: Comparison of Expected and Measured strains for validation of the DAQ system.

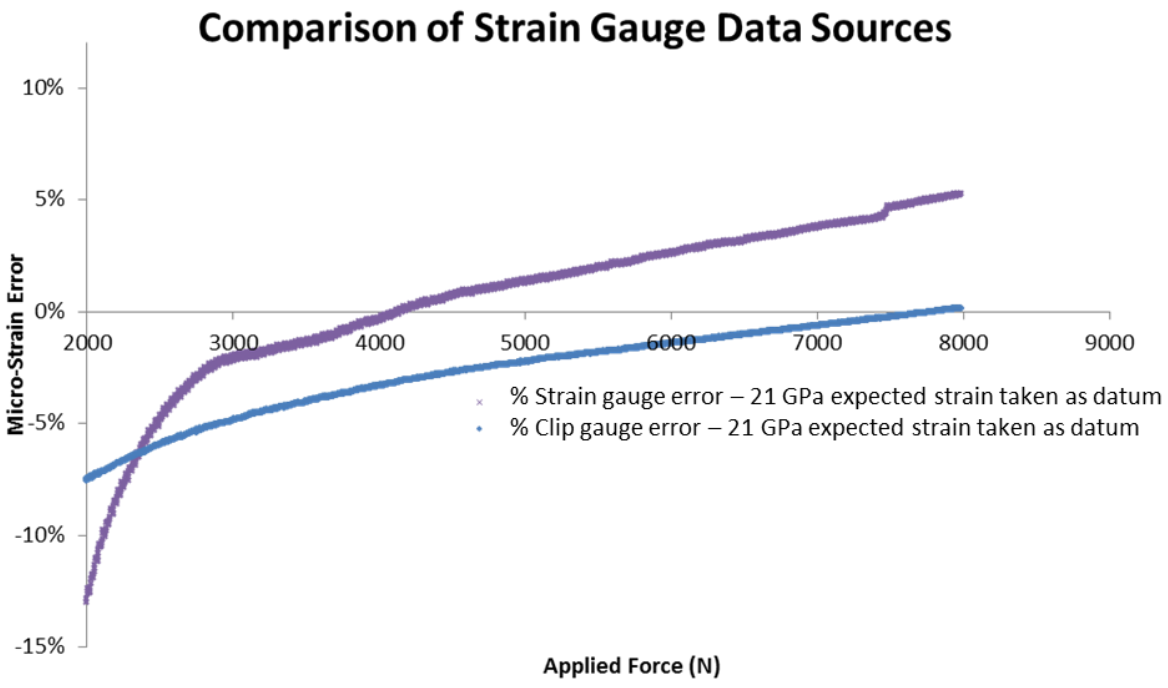

Figure 6-3: Comparison of error values between clip and strain gauges using the expected strain values assuming a 23 GPa Young's Modulus value.

6.3 Structural Installation

As can be seen from Figure 6-1 the strain gauge rosette installation layout of the strain sensors is symmetrical about the centre of the vessel, the gauges were installed by Strainstall, a third party installation specialist company. This was chosen to compare the variation from one side of the vessel to the other and also to mitigate the potential impact of failed gauges. Gauges were installed on around 25% of the available panels. There were numerous reasons for not adding more gauges some of which are outlined below:

- Data logging equipment costs
- Practical limitations
    - Limited breaching of watertight bulkheads
    - 46 of the remaining panels had limited or no access for installation of strain gauges
- Engineering considerations
    - 24 of the panels were in an area of high dead rise angle which can be reasonably expected to reduce applied load on impact with water.

The panels in the engine room were all considered to be more or less flat panels with very low dead rise angle, while the survivors space were also considered to be flat panels with an increasing dead rise angle from frame 9 to 12, both are shown in Figure 6-4.

The material construction of the panels nominally follows the layup described in the materials characterisation section, however the inclusion of stiffeners in the structure has resulted in overlaps extending almost to the middle of the panel in some cases resulting in a layup thickness of between 14 and just under 25 mm in places in the survivors space and early structural modification of the hull structure around the engine room resulted in an extra 20 layers of QE1200 glass being added resulting in a layup in excess of 30mm in some areas of the engine room. However beneath the stiffening structure in the survivors space the material thickness is expected to be consistent with the coupons created.

This increase in thickness compared to the coupons tested in the materials characterisation section may lead to some differences in material performance as compared to that determined experimentally. However it is expected that any differences will only go to strengthening the structure and therefore any errors resulting from the application of the recorded strains at the life assessment will result in under predictions rather than over prediction.

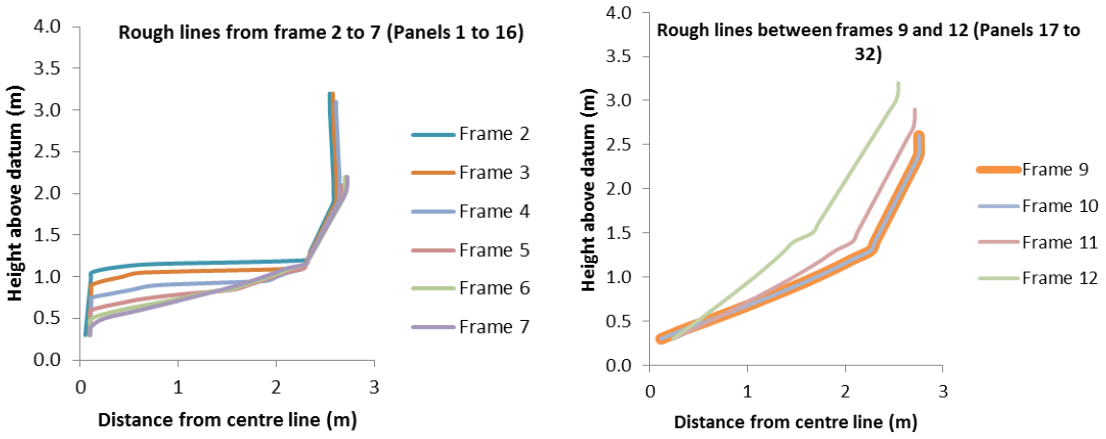

Figure 6-4: Lines plan for sections in the engine room bounded by Frames 2 and 7 and the survivors space bounded by Frames 9 and 12.

6.4 Data Post Processing

Figure 6-5 shows the data post processing method applied to the data once it has been transferred from the life boat to the central system, the V/V to ε equation comes from the user manual for the strain recording module (National Instruments, 2008). The software used to carry out the post processing is found in Appendix 5 on the CD at the back of this thesis. To fully implement the rainflow counting, the WAFO package for Matlab must be downloaded (Source: http://www.maths.lth.se/matstat/wafo/, Version 2.5 for Matlab 2010b used) and installed.

Once the data has been converted from the native V/V values to strain values then a zero correction is made. This correction is necessary as the strain gauges were placed on the boat when on hard standing during an engine change, when the vessel was lifted into the water the static stress condition will have changed. Therefore the readings taken, once zeroed are a best representation of the change in structural strain experienced from the hydrostatic strain measured, which itself represents a change from an unknown state of strain to a known state of strain, to the dynamic case at any instant in time. Because of this there is significant uncertainty in the absolute values of strain recorded however through the validation discussed in the previous section there is significant confidence that the change in strain is accurately represented by the difference between two values and therefore the outputs of the Rainflow calculation.

It is typical to temperature compensate strain gauges, however it is expected that the change in temperature will remain fairly low. In comparison to the transient loads which are likely to cause the most significant change in strain it is expected the changes in strain due to changes in temperature will be negligible.

The zero values were generated on a calm day on the pontoon at Lochinver lifeboat station[1], the data acquisition system was left running for 15 minutes using the same program used to collect the strain data during a trial period.

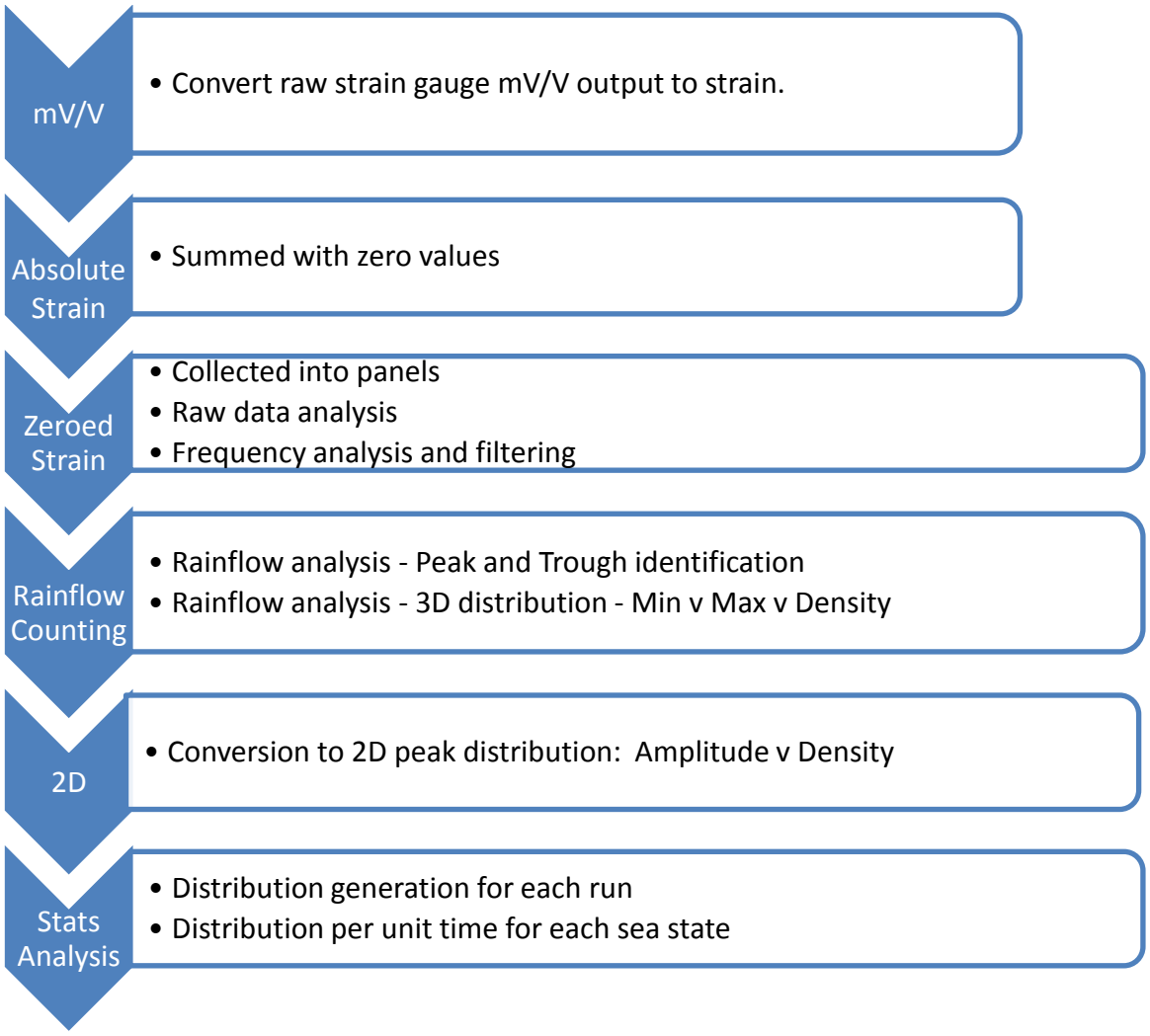

Date	Duration	Sea State	Distribution
dd-mm-yyyy	D:HH:MM	Beaufort Wind Force Scale (1 – 12)	Amplitude v Density

Figure 6-5: Flow diagram showing how the data is analysed in post processing to enable use with the S - N curves identified in the materials characterisation chapter and the damage models used in the structural life assessment chapter.

The process outlined in Figure 6-5 takes the raw output from each of the different strain gauges and generates a useable fatigue spectrum for each sea state data is collected in. This is made up

[1] 25/07/2013; Longitude: -5.248000145, Latitude: 58.14733505

of strain amplitude bins and the number of times a strain within this range is identified. Initially the raw input is converted to strain using equation 6-1.

$$\varepsilon = \frac{-4\frac{\mathrm{V}\times10^{-6}}{\mathrm{V}}}{G_f\left(1+2\frac{\mathrm{V}\times10^{-6}}{\mathrm{V}}\right)}\cdot\left(1+\left(\frac{R_l}{R_g}\right)\right) \qquad \textbf{6-1}$$

Where:

- $\frac{\mathrm{V}\times10^{-6}}{\mathrm{V}}$ is the gauge output, and V is volts.
- G_f is the gauge factor
- R_l is the lead resistance and
- R_g is the nominal gauge resistance (350 Ω)

The resultant strain is then summed with the zero values recorded at Lochinver. The zero values can be found in the Appendix, section 11.3. The resultant strain values were then collated into panel panels (Table 11-9) and raw data analysis was carried out on the zeroed strain. This analysis focused on the following questions:

1. Do the initial values of strain remain constant between runs?
2. Do changes in the mean value exceed 50 με? If yes, what is the cause?
3. Are any changes in the offset value comparable between runs?
4. Are the extreme values recorded plausible?

A visual inspection of the initial strain trace was used to answer these questions and frequency analysis of the transverse and longitudinal strain data followed. From this analysis confirmation of the consistency of the data and identification of any important frequencies of strain application is obtained and appropriate filter selection and limits made. Once the data has been verified as useable, the Rainflow analysis is conducted on the transverse and longitudinal strain.

The Rainflow analysis, a simplified example is shown in Figure 6-6, allows the capture of all open and closed loop cycles, the term “loop” refers to the hysteresis loop which is present when loading and unloading materials. By rotating the strain trace through 90 degrees, treating the two sides of the strain trace as a pagoda roof and imagining rain water emanating from the origin in both the positive and negative strain directions; the largest positive strains are matched with the largest minimum strains and counted as a cycle of a particular magnitude. A cycle is said to have been completed when the imagined flow of water will fall vertically from a peak value

uninterrupted to the end of the time series. The peak values are then removed from the strain trace and the analysis continued until all cycles have been accounted for.

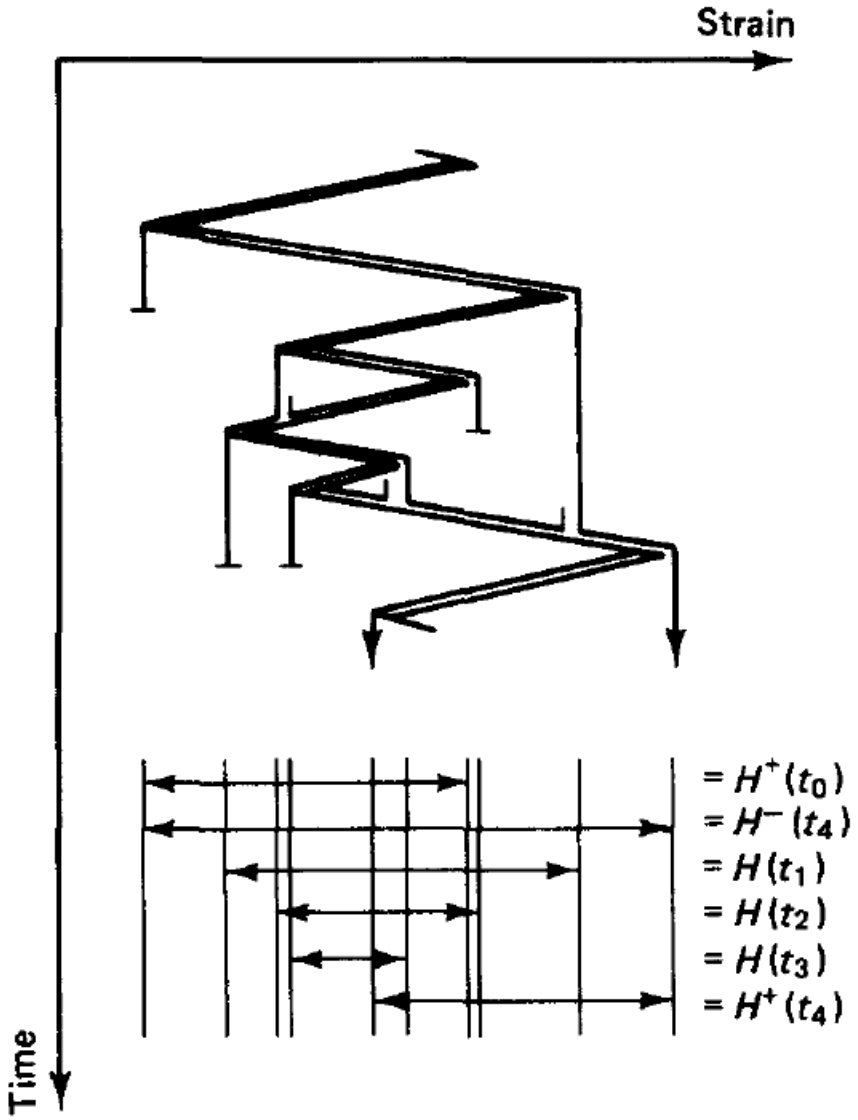

Figure 6-6: A simplified example of the Rainflow counting method, showing the strain trace rotated through 90 degrees and the result of the count shown below (Rychlik, 1987)

The output of a Rainflow analysis is a count of the number of times a strain occurs which falls between the boundaries of the class, the class width, for which the count is made. The number of classes used in previous investigations has ranged from 7 in the spectrum presented by Smith (1989) to 64 in the Wisper spectrum discussed by ten Have (1993) for 2D distributions and 15 x 11 for the 3D distribution suggested by ABS for the modelling of fatigue inducing wave encounters.

For this analysis the use of the Beaufort scale to determine the different distributions means potentially 12 different distributions for analysis.

The Rainflow analysis used was contained within the WAFO Toolbox for Matlab and is presented in (Brodtkorb et al., 2000) and was run using the University of Southampton High Performance Computing cluster.To allow the Rainflow count distributions to be comparable between runs the width of the classes was kept constant at 50 με, which meant changing the number of classes depending on the peak sizes encountered. 50 με was chosen as it is equivalent to a material stress of 0.76N/mm^2 (from $\sigma = E\varepsilon$, using the material constants identified in chapter 4) in the longitudinal direction, which is similar to the minimum calculated stress of 0.52N/mm^2 used in the fatigue spectrum presented in Shenoi and Clark (1998), which is also used for the first estimation of the fatigue life of the structure discussed in Chapter 8. This leads to an important assumption that, since the evidence obtained from the materials characterisation chapter did not conclusively identify a fatigue limit at any of the tested stress ratios, all applied stresses and therefore strains are important in the context of fatigue loading.

The output from the analysis implemented for this work is an $\left(N_i \times N_j\right)$ matrix where the value of N and N_j represent the centre of the 50 με bins (an example is shown in Table 6-3, page 169), where N is the number of bins determined from the difference between the maximum and minimum recorded strain value divided by 50. Since the number of bins has to be an integer value, the width of the bins at this stage is found to be 50 ± 1 με.

The value presented at the (n_i, n_j) location represents the number of up crossings recorded, i.e. the number of times there has been an instance where a strain has begun at a value in the bin centred about n_i and finishes in the bin centred about n_j. The reason for using the up crossings only is due to the limitation in this case of using the tensile strains for the fatigue life prediction, the material characterisation program has only identified a single S - N curve at an R ratio of 0.1 constructed from tensile and flexural fatigue curves. Therefore generating data which includes the down crossings, implicitly compressive element of cyclic loading, will produce a set of data that will not be used and is therefore unnecessary.

The two dimensional $\left(N_i \times N_j\right)$ matrix is reduced by calculating the amplitude values from the up-crossing start and finish values into a two dimensional distribution of strain amplitudes. As long as the assumption holds that the most damaging fatigue case is that of applied stresses at an R ratio of 0.1 then this will produce conservative results. The Rainflow package implemented in this work was first verified against the example problem found in the BS ISO standard (12110-2, 2012).

This verification showed that the WAFO (Brodtkorb et al., 2000) toolkit implementation was able to reproduce the results shown in Annex C of the standard. In this work the analysed data was presented in terms of the starting class to destination class table, Table C.2 from the standard.

As more services are recorded these distributions can then be combined according to sea state with the cumulative total of time at sea recorded. The more data that is gathered for each sea state (including varying location), the more confidence there can be in the distributions being truly representative of the vessel class in a particular sea state.

6.5 Results and Analysis

The data sets generated are listed in Table 6-1. The first 2 data sets were recorded during trials from Lochinver, in the north west of Scotland and each lasted 1 hour. The final set of data was recorded on a 2 day passage from Lochinver to Aberdeen via Scrabster. The duration of the passage was just over 4 hours on day one and just over 7 hours on day 2. The final data set was recorded on trials from Aberdeen lifeboat station at night lasting 1hour and 44 minutes. For the data sets recorded in sea state 8, 3 and 5 the journeys were out and back which meant both head sea and aft sea directions were experienced in the same conditions. For the longer journeys in sea states 4 and 6 the direction of travel was continuous with the exception of rounding Cape Wrath on the 30th September, rounding the headland into the North sea from the Atlantic ocean and rounding Peterhead on the 1st October. In all instances rounding the headlands changed the conditions the boat experienced as the relative direction of the travel of the vessel changed. On the 30th the conditions changed from a wind crossing the direction of water flow to wind over tide condition which whipped up and shortened the seas, although didn't dramatically change the conditions in terms of the Beaufort sea scale. On the 1st October the direction of the vessel with respect to the flow of the water changed from following to head seas. The service conducted in sea state 6 was split into two parts, one just under 6 hours and the other just over an hour and a half.

The complete data record cannot be included in this thesis due to the quantity of the data acquired (In excess of 34GB of binary data), the raw data is held at the RNLI engineering office and within the Fluid Structure Interactions research group at the University of Southampton.

Table 6-1: Summary of the operating environment data recorded by the crew.

Service / training Date	Beaufort Sea State	Duration	
		Hours	Minutes
2013/09/16	8	1	10
2013/09/22	3	1	
2013/09/30	4	4	15
2013/10/01	6	7	8
2013/10/10	5	1	44

6.5.1 Raw Data Analysis

An exemplar strain trace is shown in Figure 6-7. The results from considerations of the 4 questions posed in the previous section are shown in Table 6-2, based on this strict set of criteria only 5 of the 32 panels, 13, 18, 25, 26 and 27 (see Figure 6-1), measured fully satisfied all criteria. This does not mean the strain traces are necessarily unsuitable for use as an indication of the fatiguing strains experienced, merely that some limitation of the accuracy of the results is found, luckily due to the strict nature of the first two criteria any differences found are unlikely to have a significant adverse effect on the outcomes of the Rainflow analysis unless they are particularly extreme.

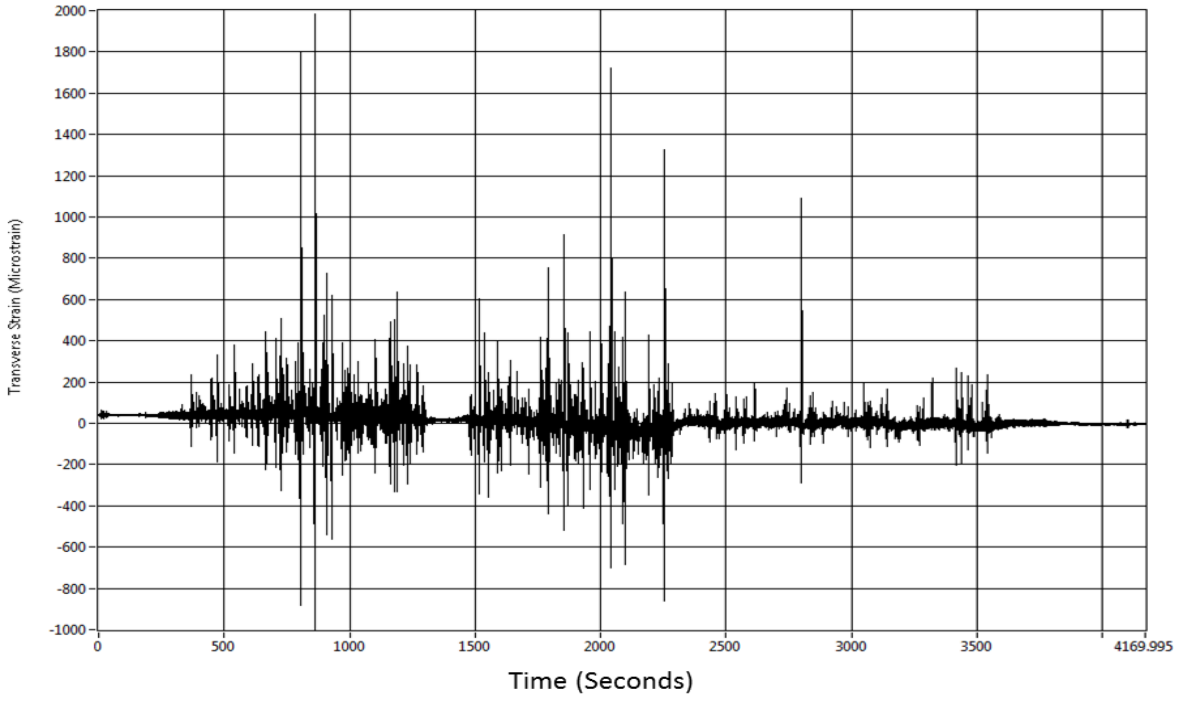

Figure 6-7 Transverse strain trace from the sea state 8 run taken from panel 18, located in the Survivors Space.

Table 6-2: Results of the visual analysis of the strain traces, carried out according to questions 1 to 4 with the results below the corresponding number, where the box is coloured green there is a favourable result, where red the result is not favourable and further investigation is required. The numbers in brackets below columns headed 1 show the minimum and maximum values of starting strain value.

[a] Caused by value drift

[b] Caused by value step changes

[c] 3+ traces comparable

[d] Change in drift direction ie positive to negative or vice versa.

*** Extreme value in SS6 trace greater than SS8 trace.**

**** Readings produced in ss3 greater than other sea states, generally greater than ss4, sometimes greater than SS5**

		Longitudinal Strain Analysis				Transverse Strain Analysis			
		1 (με)	2	3	4	1 (με)	2	3	4
Engine Room Panels	1	(-25, 80)	[b]		5, 6	(-160, 40)	[a][b]		
	2		[a][b]	[c]	5, 6				5, 6
	3		[a][b]		5, 6		[a]		5, 6
	4		[a][b]	[c]	5, 6		[b]		5, 6
	5				5, 6	(<50,>100)			5, 6
	6				5, 6				5, 6
	7		[a]		5, 6		[a]		5, 6
	8				5, 6	(30, 100)	[a]		5, 6
	9				5, 6	(-10, 50)	[b]		3, 5, 6, 8
	10		[a][b]		5, 6	(-40, 50)	[a]		8
	11	(150, 250)							**
	12				5, 6				
	13								
	14				*				3, 5, 6
	15	(-25, 40)			5, 6				5, 6
	16				5, 6				**
	17	Failed Strain Gauge							**
	18								**
	19		[a]	[c]					**
	20	(75, 150)							**
	21		[a]	[c]		Failed Strain Gauge			
Survivors Space Panels	22	Failed Strain Gauge				(-50, 50)	[a][b]		**
	23	(-50,60)	[a]	[c]		(-175, >-100)	[a]		**
	24			[d]		(-350, <-100)	[a]		**
	25								**
	26								**
	27								**
	28					(450, 1175)	[a][b]		**
	29	(440, 520)		[d]					**
	30	(-220,-25)	[b]	[c]					**
	31			[d]					**
	32	(0,100)							**

The reason it is important to investigate the initial value of the gauge is that gauges which do not return to a common zero value after use may well have imperfections in one way or another. In no cases did the start value for each run coincide exactly, however for this analysis changes of less than 50 με were considered negligible, therefore any range of start values that covered 50 με or less were considered comparable from one run to the next. For the majority of cases the starting strain was considered comparable, however for those that weren't the variation between extremes ranged from 65 με, so just outside the limit of accuracy to 725 με, nearly 15 times the limit. However even so this still represents a small value in terms of the applied stresses, a variation of roughly 11 N/mm^2. In comparison to the strain gauge with a defect beneath the change in strain is less, but still comparable to that of the validation test. Therefore results for the worst performing gauges, those with variations in the hundreds of με, should be treated with caution.

Investigating the change in mean value of the data is one way to help determine whether there are imperfections within each gauge location. From Table 6-2 under heading "2" it is obvious that for the Longitudinal Strain gauges 11 out of 32 panels have some sort of change in mean value which exceeds the limit of 50 με imposed and for the Transverse strain gauges a further 11 exceeded the limit. Of the Longitudinal 11, 4 are through value drift, 2 are through value step change and 5 are due to a combination of drift and step change. Of the Transverse 11, 6 were through Drift, 2 were through a step change in value and the remaining 3 were a combination of the two. In truth all of the gauges were subject to some degree of drift in the results, it is just that the majority did not exceed the nominal 50 με limit.

Drift is caused by the heating of both the environment close to the strain gauge, which modifies the response of that gauge with time, and the heat generated within the data logging hardware, modifying its response to the strain gauge input. Best practice is to measure the temperature of the environment or measure a dummy gauge which reacts only to temperature. Both of these techniques allow the modification of the resultant readings allowing for temperature. This is more important in applications such as bridges where the gauges are to be left in place throughout the seasons and a steady state is recorded with very small dynamic variations. In this case the measured variation is expected to be dominated by the dynamic loads on the structure; therefore the effect of temperature change is less important as the influence is a much smaller part of the dynamic signal. This difference is further increased in the survivors space where the response of the panels is increased as expected with the position of the panels being in the third forward mid quarter of the vessel where slamming loads are expected to be increased.

Additionally the temperature in the different gauged parts of the engine room is unlikely to be constant due to restricted airflow around the room and the proximity of the gauges to different pieces of machinery all of which have varying heat signatures which could affect the gauges, accounting for all of these would have at least halved the number of strained locations due to the use of the data logging hardware to measure the dummy gauges, therefore this was dismissed as an option, instead the drift was handled using filters.

Comparing the changes in mean value (heading 3 in Table 6-2) between runs allows an understanding of the consistency of the system as if all of the changes across all of the runs are directly comparable then even if there is an issue as described in the previous paragraph; at least the issue is consistent. Of the 32 panels tested 13 had some kind of comparison issues. 3 were related to a change in direction of the drift either from positive to negative or vice versa and for 6 of the remaining, 3 out of the 5 runs were comparable and generally the remaining two were also comparable. Generally where the runs are not comparable a single run is the culprit, where this is associated with the step change of mean value it is normally this change which makes the mean value of the runs incompatible with the previous. Initially this suggests we can have limited confidence in the system and the results. A very unusual result which is hard to explain is the change from a positive drift over time to a negative drift which occurred on panels 24, 29 and 31, if the change was due to temperature variations then it could be reasonably expected across all gauges in this compartment, or at least for the panels where this occurs to be blocked together. However neither of these options are true.

Checking the value of the extreme strains measured for all of the working gauges in the survivors space the extreme values seemed plausible. For the engine room however for runs in sea states 5 and 6 there were some extreme values which were unbelievable. Further investigation found that for these values there seemed to be a regular step change in the signal for a very short space of time. This can be traced back through the unfiltered data to a point where the data logger has recorded 0 values rather than strain values. This is an intermittent problem which can be caused by the interaction between the real time data processing side of the data logging software, which can run into memory issues, and the deterministic data capture of the FPGA chip which will carry on pumping data to the real time part of the program irrelevant of the point in the process it is in. Thankfully these occurrences are small and can be easily factored into the Rainflow analysis. However it does suggest that this will have happened for panels 11, 13 and 14, but the value change is much smaller and therefore harder to identify.

One aspect worth noting is that in general the extreme values measured by the transverse strains were significantly larger than those measured for the longitudinal strains. This result is expected when considering plates where the maximum normal stresses (and therefore strains) are found on the tensile surface in the centre of a plate and that for both fixed and simply supported plates made of homogenous materials the absolute maximum is found in the shorter orientation (Young and Budynas, 2011, pp. 502, 508). With the material in this case being neither specially orthotropic nor homogenous, in truth it could be expected that the maximum stresses in the plate will be somewhere within the composite plate structure, geometrically below the centre. This is because of the inherent stress discontinuities that are found through the thickness of the material. Combining these stress discontinuities with the stress imposed by the bending of the plate will result in a very specific position within the laminate structure containing the maximum stress.

Before discussing the frequency response it is a worthwhile exercise determining which of the frequencies presented in 6.5.3 coincide with specific structural events for this vessel, by understanding the time duration of a series of events as recorded, it may be conceivable that a specific frequency range can be determined for future use of structural monitoring, which outside this range it can be expected that either the amplitude of the response will be small enough that it can be dismissed as structurally insignificant.

To keep the consistency this analysis will be kept to the strain trace shown in Figure 6-7. From this trace it can be seen there are some very clear transient loads which change in magnitude at around 2300 seconds. This coincides with the time at which the boat about turned and headed for home resulting in a change from head seas to following seas. The period of around 100 seconds from just over 1250 and just under 1500 shows a relatively quiet period for the vessel from a structural point of view, however there are still a clear number of structural events at low, less than 1Hz frequencies. The amplitudes of these events are very small and significantly less than the 50 με limit set for this analysis. This type of response is very typical across each of the panels in both the engine room and the survivors space. Refining this plot further to cover a period of 1 second from 1305 to 1306 seconds (Figure 6-9) reveals a large amount of high frequency fluctuations, again this is typical for all other panels.

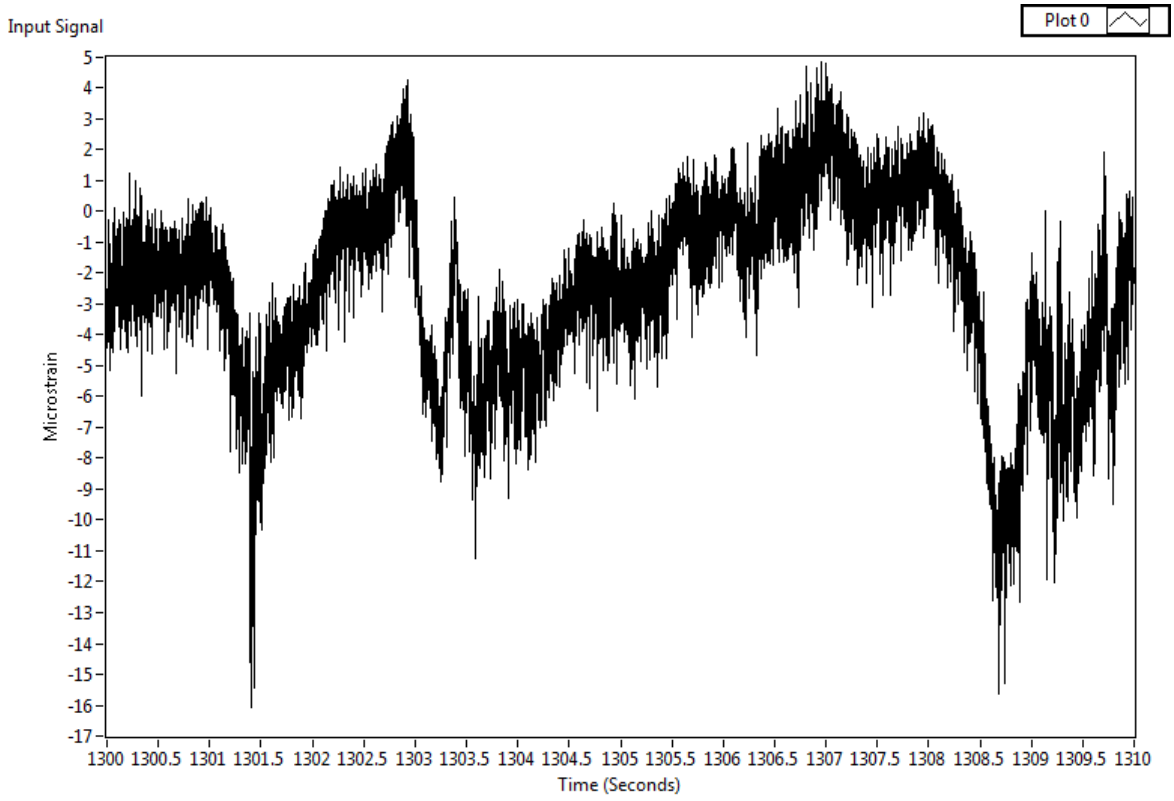

Figure 6-8: Transverse strain response of panel 18 for a structurally quiet 10 second period.

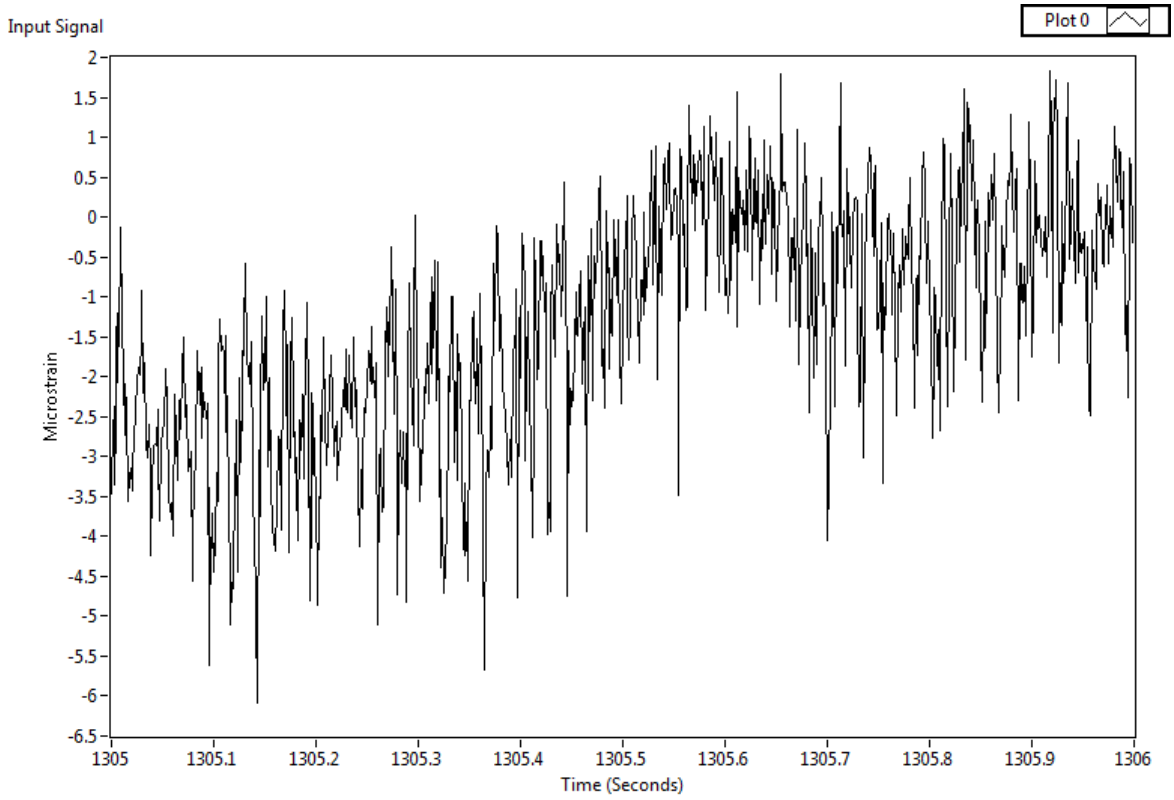

Figure 6-9: Transverse strain response of panel 18 from Figure 6-8 refined further to a 1 second period.

Before ruling any particular frequency out as “noise”, identifying and analysing the period of specific peaks will ensure those frequencies are allowed to remain. The first peak investigated is the largest peak in the data set which occurs at around 1551 seconds and has a minimum of just under -650 με and a maximum of just over 2000 με, this is shown in Figure 6-10.

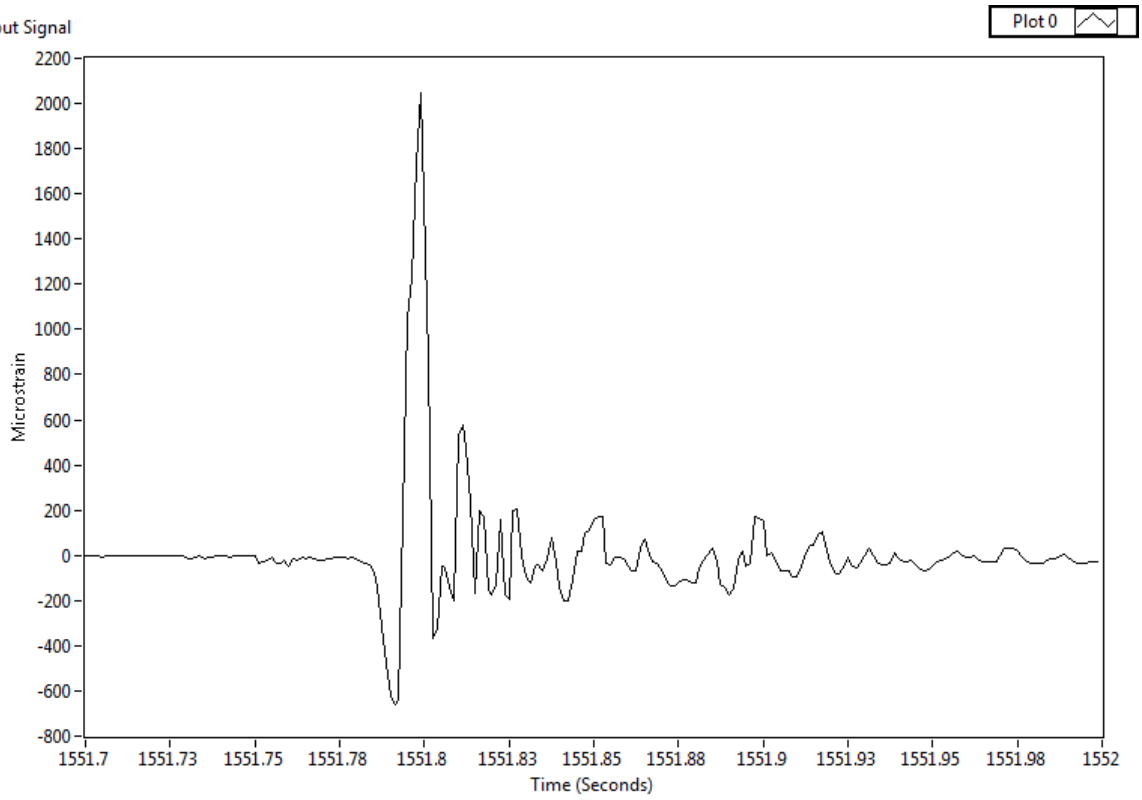

Figure 6-10: strain trace for the largest peak in the strain trace shown in Figure 6-8.

From this figure it is obvious that the event itself is made up of an initial compressive response followed very quickly by the tensile response achieving its maximum and returning back to the equilibrium point over a period of a little over 0.03seconds, or at a frequency of 33Hz. This is followed by a series of half cycles which continue over a period of 0.2 seconds before settling down to the zero point again. Considering another point between 1000 and 1500s peaking at just over 800 με, the strain trace is consistent with that shown in Figure 6-10 except there is a slight plateau at just over 400 με which extends the response to around 0.07 seconds or 14 Hz. For other responses of history in this and other strain traces, those that exceed the cut off of 50 με show a similar strain trace.

6.5.2 Filtering

With any time history of a phenomenon recorded there is often noise associated with different systems. This noise can manifest itself in different forms; i.e. 50Hz vibrations caused by AC power, very low power but very high frequency vibrations through a system or mixing of frequencies in vibration or acceleration analysis. If a particular recurrent signal can be attributed to one source or another then often they are removed as not being part of the system under investigation. However when considering strain response, responses within the structure whether the result of forced oscillations through rotating machinery or of an individual impact under certain conditions, they still represent a significant proportion of the response of the structure and therefore do not necessarily want to be removed.

Additionally the rules applied to the Rainflow counting algorithm mean that any change of less than 50 με will be dismissed which in itself is a form of filter. However for ease of analysis some filtering should be applied which will, at least remove the drift within the data. An initial frequency analysis highlighted a large proportion of the signal between 0 and 2 Hz, removing all of this had an undesired effect on the peak values within the signal, removing some of the smaller peaks. However applying a filter between 0 and 0.05Hz removed the unwanted drift in the data without effecting the important information.

Therefore for this analysis a 5^{th} order Butterworth filter was used as a high pass filter, with a pass frequency of 0.05 Hz to remove the drift and any step changes that had been identified in the previous analysis thus removing the potential impact of the negative results to questions 2 and 3 in section 6.5.1. It was found through trial and error that the 5^{th} order Butterworth filter provided the best compromise between filtering the unwanted low frequency responses whilst maintaining the peak values which are important in the Rainflow analysis.

6.5.3 Frequency analysis

Generating the power spectrum for the different strain traces allowed an understanding to be developed as to which frequencies contain the majority of the power within the time history, this in turn will allow the identification of particular response which may be used in the future to narrow down investigations into structural response and thus reduce the memory requirements and improve the time for post processing and analysis by discarding uninformative responses.

This analysis was achieved through the implementation of the Labview, Auto Power Spectrum VI[2] which computes the single sided power spectrum from the result of the following equation:

$$\frac{\mathrm{FFT}^{*}(\mathrm{Signal}) \times \mathrm{FFT}(\mathrm{Signal})}{n^2}$$

Where:

- FFT is the Fast Fourier Transform of the time history signal
- n is the number of points in the Signal
- $*$ denotes the complex conjugate

With the resulting output being power with units of $\mu\varepsilon_{rms^2}$

The results presented are limited to a comparison of the transverse and longitudinal frequency responses for Panels 13 (Figure 6-11) and 18 (Figure 6-12) in a sea state 8, comparison of the frequency response between panels 18 and 25 to 27 in sea state 8 for both the longitudinal (Figure 6-13) and transversely (Figure 6-14) measured strain directions, comparison of transverse strains between panels 13 and 18 in sea state 8 (Figure 6-15) and finally a comparison of the frequency response between runs for panels 13 (Figure 6-16) and 18 (Figure 6-17) for the transverse direction.

The frequency analysis was conducted with a change in frequency of 1Hz, such that the % total power presented at 10.5 Hz represents the sum of total power in the range 10 to 11 Hz. This was considered accurate enough for this analysis. To produce the plots in a meaningful format the data was normalised against the sum of total power in the spectrum. The graphical representation was then limited to a window between 2 and 220 Hz as the proportion of the signal below 2Hz was found to be large compared to that in the window potentially swamping the results, but at the same time generally having amplitudes of less than 50 με and therefore not likely to have an impact on the total count. The proportion of signal beyond 220Hz was many magnitudes less and was considered insignificant in comparison to the windowed section.

[2] VI is the term used by National Instruments to define a program or function within the LabVIEW software suite.

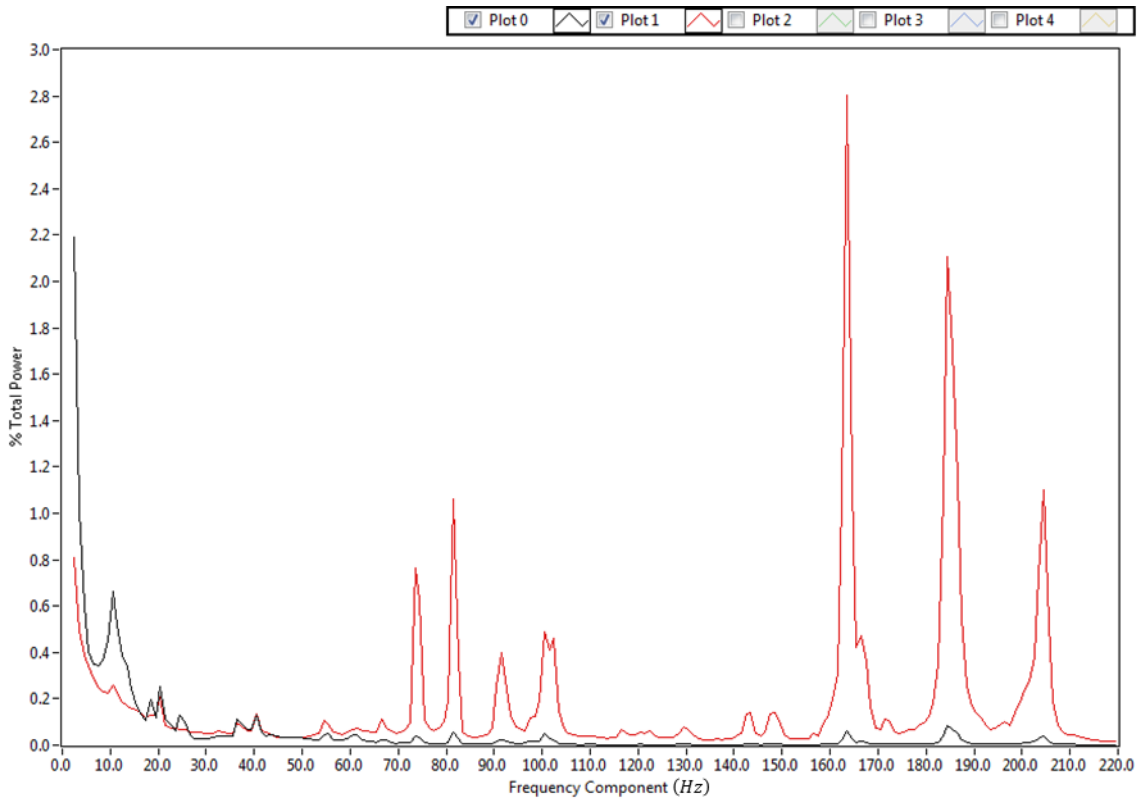

Figure 6-11: Comparison of the % of total $\mu\varepsilon_{rms^2}$ for each frequency for the Longitudinal (Plot 0) and Transverse (Plot 1) responses for panel 13 in a sea state 8.

Comparing the spectra in Figure 6-11 it is clear that in the transverse direction there is a lot more power in the frequency domain above 60Hz with the total proportion of power in this region many magnitudes larger than that below. There are also very clear frequency response peaks in the longitudinal spectrum at the same frequency, but not as large in proportion as for the transverse strains. For the longitudinal strains the dominant frequencies seem to be below 30 Hz with a number of small peaks in this region. At a frequency of between 35 and 40 Hz the two frequency responses match almost exactly.

For Panel 18, Figure 6-12, the responses for the transverse and longitudinal strains are significantly different. For the transverse strain there is a much broader spread of power across the frequencies, with some distinct spikes. For the longitudinal strain the majority of the signal above the 2Hz frequency cut off is also focused below 110Hz with a number of peaks at frequencies coinciding with peaks in the transverse signal. However there are also peaks around 10 and 20 Hz which do not seem to be present within the transverse strain analysis.

Comparing the panels in the survivors space to each other, as in Figure 6-13 for Longitudinal strain response and Figure 6-14 for transverse strain response, it is clear, for the longitudinal case, there

is a lot of similarity between the traces. There is very little of the total signal above a frequency of about 30 Hz and spikes between 10 and 25 Hz are present.

Considering the comparison of transverse strains between panels there are three clearly different frequency responses present. The frequency response for panel 18, which is described for Figure 6-12 (Plot 1), is very different to that of Panels 25 and 26 which have a much quicker drop off in frequency response but still retain small peaks which coincide with those of panel 18 above 40 Hz. The response of panel 27 is somewhere between the two with a comparable frequency response to panel 18 at frequencies below 50 Hz moving to a response comparable to that of panels 25 and 26 for frequencies above this.

Comparing the frequency response of the transverse strain values between panels 13 and 18, Figure 6-15, there are a number of clear differences and similarities. The proportion of signal below around 70Hz is significantly greater for panel 18, however the peaks which do occur above this region generally coincide with peaks found in panel 13.

The total proportion of the signal associated with these peaks is in all cases significantly lower for panel 18 than panel 13, especially in the very high frequency domain where the difference is an order of magnitude or more. Additionally for panel 13 there is an extra significant peak at a frequency of around 205Hz which does not appear in the spectrum for panel 18. Finally at a frequency of 100 to 105 Hz there is a double peak in the panel 13 response where there is a single peak in the panel 18 response.

Figure 6-13 and Figure 6-14 compare the longitudinal and transverse strain frequency response between the different panels in the survivors space; 18, 25 to 26, in a sea state 8. For these panels the frequency response matches extremely well. This is an important result since the dimensions of the panels are quite different, with panels 26 and 27 being 480 and 500 mm from the rearmost to the foremost boundary. The rear most bulkhead in this case is a supporting structure for the battery box which is located directly above panels 26 to 28 and which effectively divides a single panel into 2. This is clear from the dimensions of panel 25, which other than the supporting structure for the battery box is bounded by the same bulkheads. The length of this panel is 1080 mm. The length of panel 18 is between panels 26/27 and 25 at 800mm. The reason for this reduction in length for this panel is the inclusion of housings for the speed log and echo sounder, which penetrate through the hull shell in this location, and act as the rearmost boundary for these panels. Considering that it would be reasonable to expect the frequency response of a plate to change with its dimensions, it is reasonable to suggest these inclusions have very little or no effect on the response of the plate to the structural loadings.

This is further backed up by the inspection of Figure 6-14 where the frequency response of panels 18 and 27, which have a width of 560 and 300 mm respectively between boundaries, are directly comparable up until about 50 Hz beyond which there is a transition where the response of panel 27 takes on similarities to 25 and 26 and are directly comparable beyond a frequency range of around 85. Panels 25 and 26 have a width of 440 and 400 mm respectively and their frequency response matches very closely throughout the entire spectrum, with the exception of specific points where panel 25 shows peaks not visible in panel 26 at around 75 and 82 Hz. Beyond this range the comparison is extremely reliable. The inclusion of these peaks in all of the responses suggests that at this frequency the whole structure is undergoing a forced oscillation of some sort.

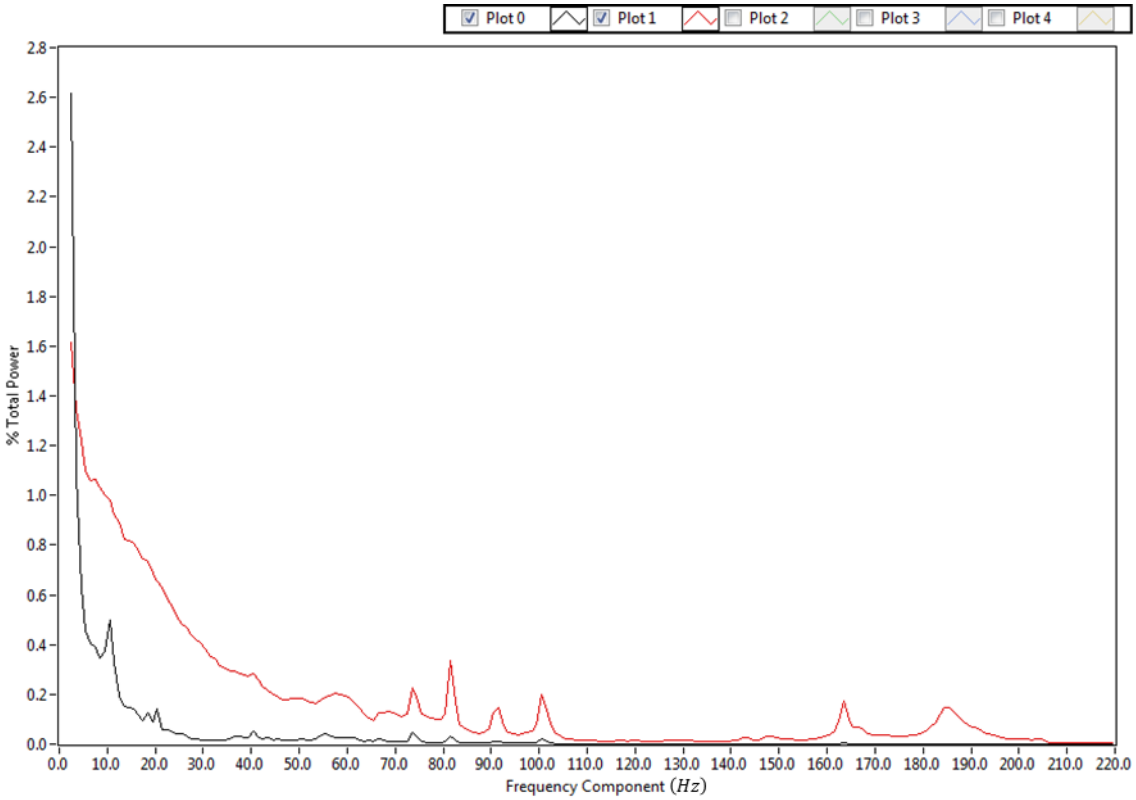

Figure 6-12: Comparison of the % of total $\mu\varepsilon_{rms^2}$ for each frequency for the Longitudinal (Plot 0) and Transverse (Plot 1) responses for panel 18 in a sea state 8.

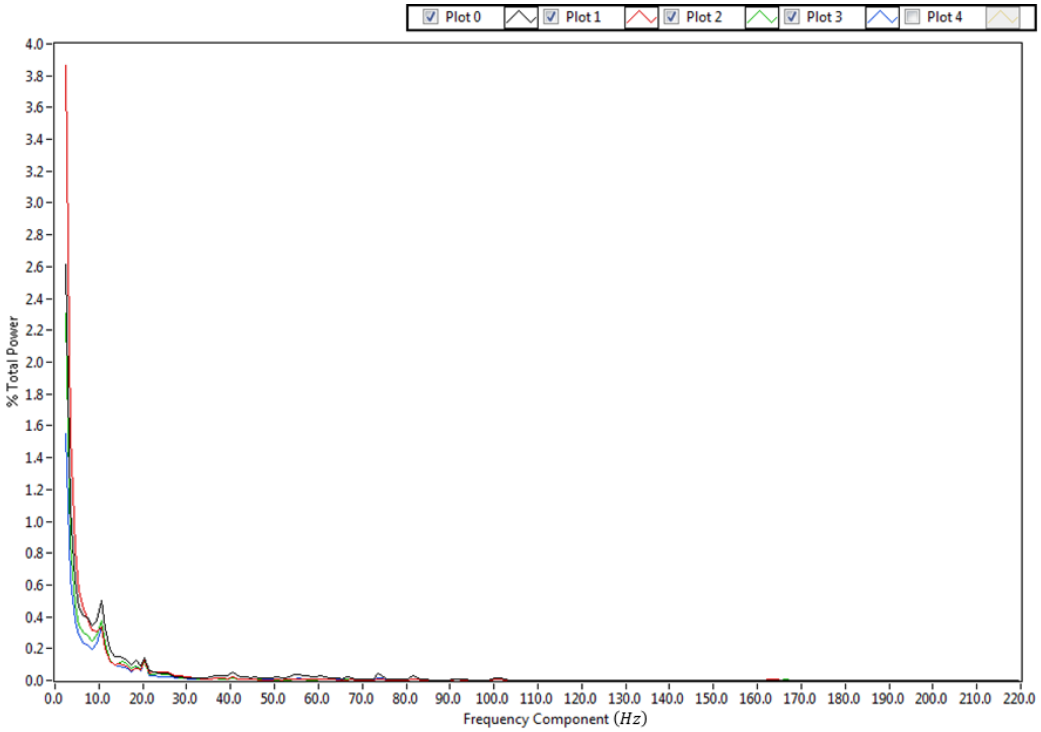

Figure 6-13: Comparison of the % of total $\mu\varepsilon_{rms^2}$ at each frequency for the Longitudinal strain of panels 18 (Plot 0), 25 (Plot 1), 26 (Plot 2) and 27 (Plot 3) in a sea state 8.

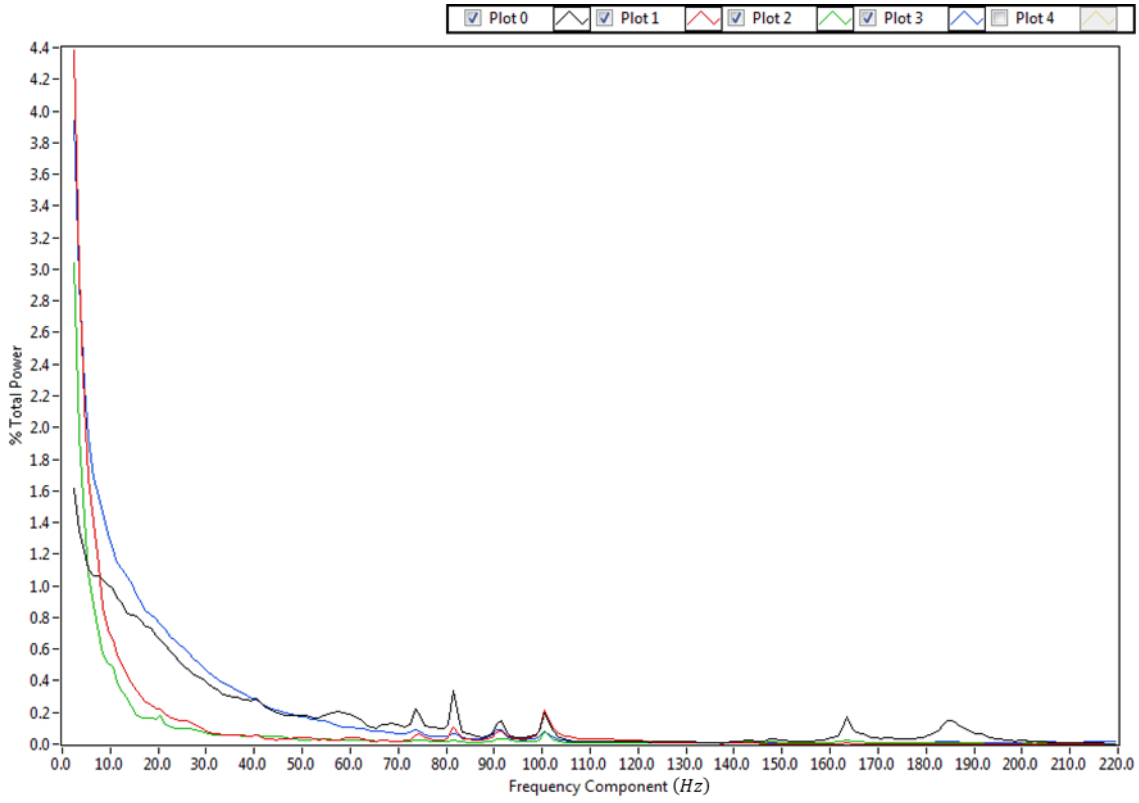

Figure 6-14: Comparison of the % of total $\mu\varepsilon_{rms^2}$ at each frequency for the transverse strain of panels 18 (Plot 0), 25 (Plot 1), 26 (Plot 2) and 27 (Plot 3) in a sea state 8.

Comparing the frequency responses for panel 13, Figure 6-16, in each sea state the most interesting observation is that each sea state seems to have a unique frequency response for this type of vessel. But between these responses there are a number of similarities. In all cases there are significant frequency peaks between 65 and 105 HZ and between 155 and 210Hz, below 60 Hz there are some peaks, notably between 30 and 45 Hz, which are common to all sea states. Between the two distinct bands are peaks at 128 and 146 Hz for sea state 4, closer inspection reveals that there are peaks around these frequencies for the other sea states but of a much reduced magnitude in comparison.

Figure 6-17 shows the frequency response for the different sea states of panel 18. In this figure there are 2 distinct blocks of response as with the previous analysis, however there is also a general large increase in the amount of low frequency response, with the exception of the sea state 4 response which as with the previous analysis shows very distinct peaks. Beyond the regular broad band of responses previously identified there is very little in regular recurring peaks at very specific frequencies within this plot. There are occasionally coincidental peaks which include up to 3 of the different sea states but the frequency response of the other sea states at this frequency precludes it from being considered common to all.

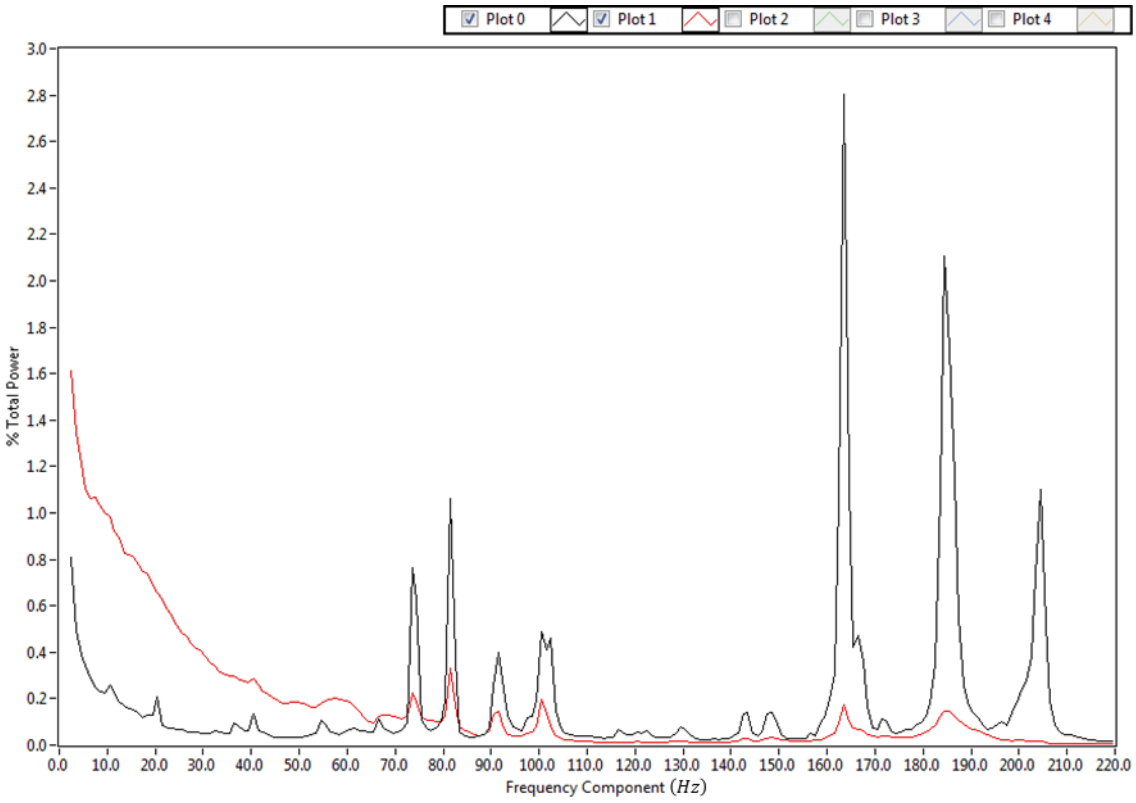

Figure 6-15: Comparison of the % of total $\mu\varepsilon_{rms^2}$ at each frequency for the transverse strain of panels 13 (Plot 0), 18 (Plot 1) in a sea state 8.

Figure 6-16 and Figure 6-17 shows that there are clear differences between the responses depending on sea states encountered. This may be due to many factors such as the way the boat is driven, the amount of time spent in head seas compared to following or quartering seas or it may be a characteristic of this vessels response to the sea way at that time in particular. Unfortunately to fully test this hypothesis a significant number of runs would need to be carried out in a particular declared sea state at different times in multiple directions to the sea and under pilotage of different coxswains. The major result of a positive correlation between sea state and frequency response is that a much more accurate declaration of the sea conditions, which would be relevant to the structural response and therefore fatigue history could be made.

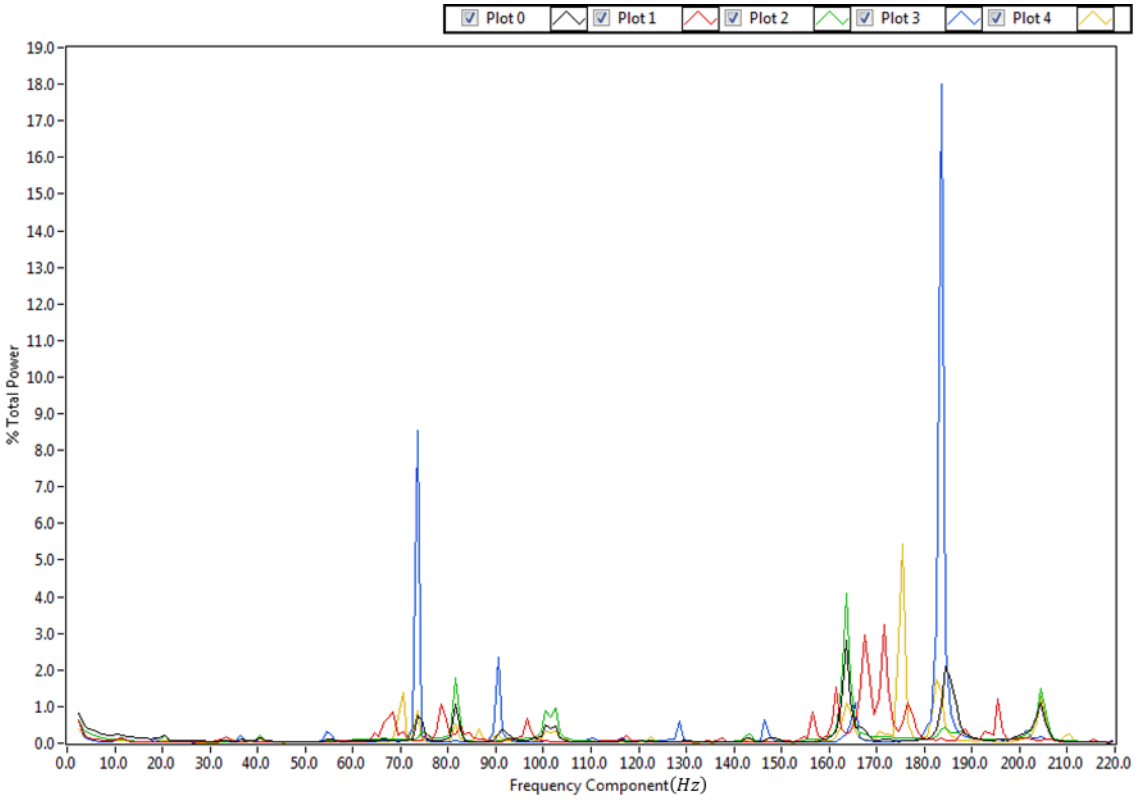

Figure 6-16: Comparison of the % of total $\mu\varepsilon_{rms^2}$ at each frequency for the transverse strain of panel 13 for runs in Beaufort sea state 8 (Plot 0), 6 (Plot 1), 5 (Plot 2), 4 (Plot 3) and 3 (Plot 4).

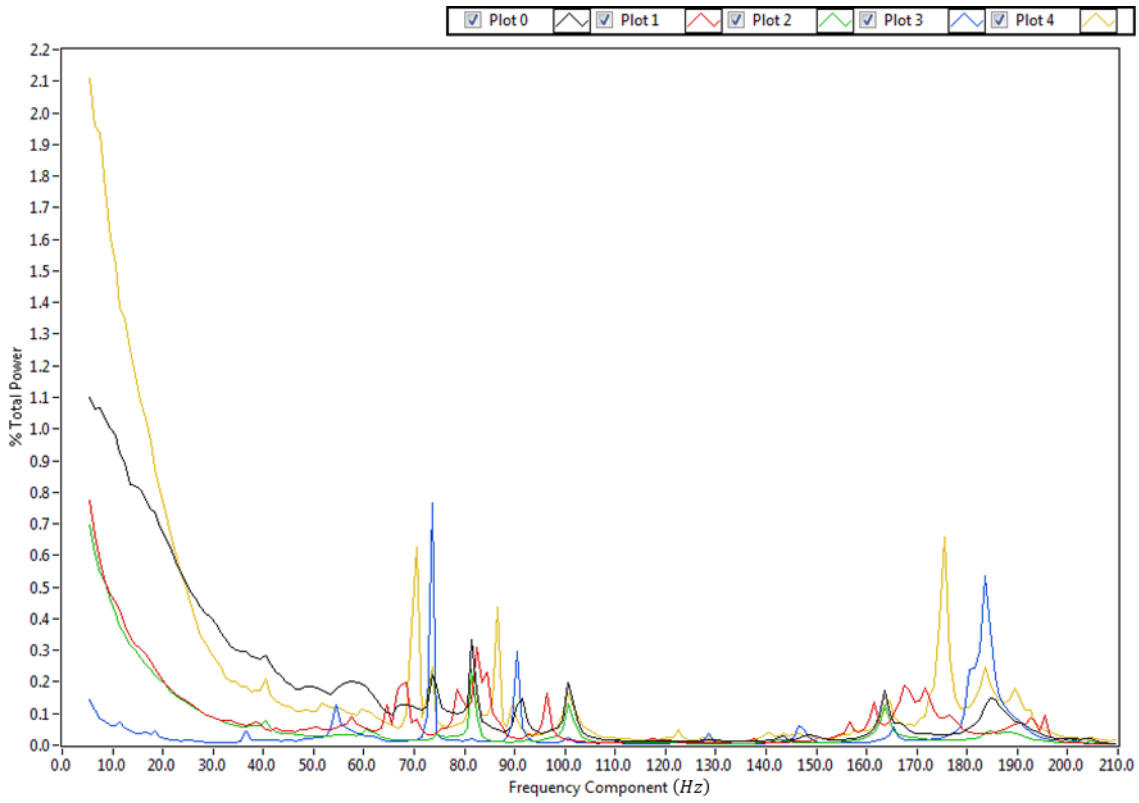

Figure 6-17: Comparison of the % of total $\mu\varepsilon_{rms^2}$ at each frequency for the transverse strain of panel 18 for runs in Beaufort sea state 8 (Plot 0), 6 (Plot 1), 5 (Plot 2), 4 (Plot 3) and 3 (Plot 4).

One of the reasons for conducting the analysis was to try and understand whether or not there are any particularly dominant or differing responses based on the direction of measurement; transverse or longitudinal, the panel chosen; 13, 18 or 25 to 27 or sea state encountered.

Comparison of the longitudinal and transverse response for panel 13 is shown in Figure 6-11 and panel 18,Figure 6-12. In both cases the frequency responses are markedly different, however for panel 13 these differences are generally related to the magnitude of total signal at a particular frequency rather than the value of the peak frequencies. Above a value of 50Hz the magnitude of the peaks in the longitudinal strain frequency response is at least an order of magnitude smaller than those of the transverse response, this could be due to the smaller dimension of the width of the plate resulting in the comparatively greater stiffness in this direction. This increased stiffness will reduce the attenuation rate of higher frequency signals allowing them to propagate for longer and resulting in a higher proportion of the total spectrum power, whereas the lower frequencies will be proportionally less, this will be reinforced by the material layup which is predominantly stiffer transversely than longitudinally. Between 35 and 50 Hz the traces for the two strain directions compare very well suggesting that whatever is causing this oscillation is acting in a common way in both directions. This can be put down to the engine speed which has a maximum

of 2450 RPM or 40.83Hz and can operate anywhere between 600 RPM and this value, since the response between 35 and 50 Hz is directly comparable to both strain measurement directions it is conceivable this response may be due to engine speed.

In the transverse direction the magnitude of the frequency peaks between 70 – 110 HZ and 160 – 210 Hz are harder to explain. Not only are they not coincident with the frequency of any system on board the boat significantly larger than the frequencies preceding them. The dominance of the signal at these frequencies is significantly greater in the engine room suggesting that the source of is located here. However it is also present in the analysis of the transverse strain of panel 18, in the survivors space, at a much reduced power suggesting propagation to this point, however for the other plates analysed in the survivors space there seems to be very little signal in the 160 – 210 Hz range, and some commonality in the 70 to 110 Hz range.

This would suggest that whatever is generating the powerful high frequency signal is doing so from the Engine room. Surrounding all rotating machinery there will be bearings which, if they contain some defect may result in significant vibration. Also the Severn is fitted with 5 bladed propellers which are situated beneath the structure within tunnels which are bounded by bilge keels. This has the potential of creating a signal at 5 times the drive shaft rotation speed, the gear box has a reduction ration of just over 2:1 thus the prop rotation frequency is from 5 to 20 Hz and the blade passing frequency 25 to just over 100Hz. It is plausible to suggest that the very large peaks identified in the lower block are specifically due to the propeller passing the hull bottom and there enough energy is imparted to the structure through this that even in the survivors space the oscillations have not fully attenuated.

6.5.4 Rainflow Analysis

An example of the output is found in Table 6-3. The result of reducing this to a 2D distribution is shown in Table 6-4. Equivalent distributions are created for each of the different panels for each of the different sea states in both the transverse and longitudinal directions, the complete rainflow outputs of each of the different runs can be found in appendix 6.

To try to understand how the counts may vary between panels and runs a comparison must be made; the easiest comparison is the total number of counts in any one run for any one panel. This will allow a comparison between panels for a single run but does not allow a comparison between runs since each of the runs were of a different length, therefore the results are

presented in terms of counts per minute or counts per second depending on the analysis being undertaken.

Table 6-3: An example of the output from the Rainflow analysis up crossing count for the tensile strains on Panel 7 during the sea state 8 run. The row and column header values are all in με and the table entries are counts.

0	-9	41.375	91.75	142.12	192.5	242.88	293.25	343.62	394
-9							2		1
41.375			3224	95	3				
91.75				46472	2	1			
142.12					4				
192.5						2			
242.88									
293.25									
343.62									
394									

Table 6-4: 2D distribution of cycle counts generated from Table 6 3.

Amplitude Lower Boundary (με)	Number of cycles encountered
50	49702
100	0
150	97
200	4
250	0
300	0
350	2
400	1
450	1

Figure 6-18 shows the number of counts per minute for the transverse strain on panel 18 in the different sea states, BSS 6a refers to the first part of the journey and BSS 6b refers to the second part of the journey. The figures presented represent the expected number of cycles of any

particular strain range; 50 – 100 με, 150 - 200 με, etc, per minute in each of the sea states for which data was collected. The first thing that is noticeable is the extremely high count per minute in all sea states at the very low strain range which are in the hundreds to thousands. However in this representation the data is not particularly clear.

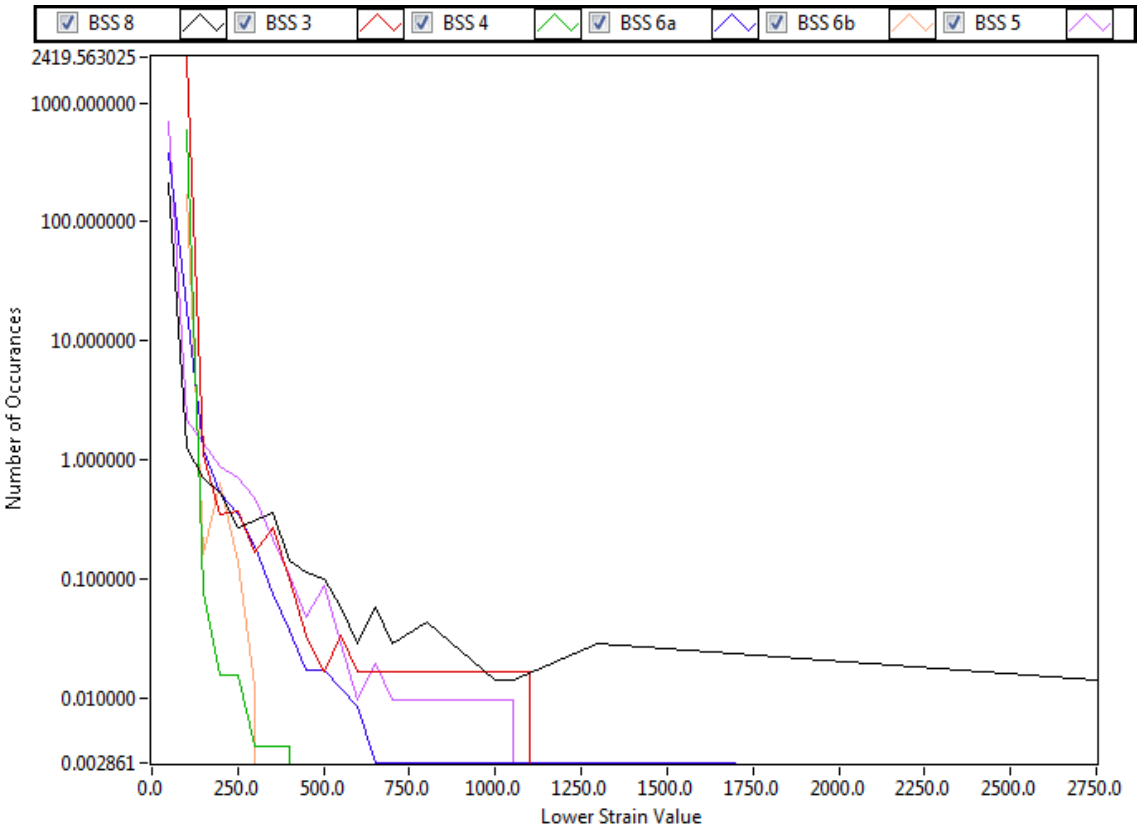

Figure 6-18: Number of transverse strain cycles per minute on panel 18 in the different sea states.

Table 6-5 contains a comparison of the minimum applied strain range for the panels identified as being most consistent in the previous analysis. The representation is changed from counts per minute to counts per second as it shows the data in a slightly more compact format. This allows an easier comparison for the lowest recorded strains between runs and between panels. In all cases, with the exception of 1 panel at 1 sea state, the lowest recorded range is either between 50 and 100 με or 100 to 150 με. The only exception is for panel 13 in sea state 6, run a, which has a lowest recorded strain range of between 150 and 200 με. However, for this particular panel and sea state the count per second value is less than three, which is a very low count when compared to all other sea states where it ranges from just over 33 to just over 78 counts per second for this panel.

Considering the panels in the survivors space the range of cycles per second is considerably reduced for all but one panel in one sea state (panel 18, BSS 3) to a minimum of 0.01 counts per second and a maximum of just over 20 counts per second, significantly less than Panel 13. Panel 27 is unique in both its consistency in lowest recorded strain range being 100 to 150 με and containing low count rates, ranging from less than one a 0.01 per second to just under 8 a second. To understand the consistency of the data the standard deviation was calculated from the count per second data normalised by the largest count per second present across all panels, presenting it as a percentage of the largest value. In all cases the standard deviation was between 32% and 38% with the exception of Panel 25 which had a standard deviation of 18% of the max value.

Table 6-5: Minimum amplitudes measured in the tensile direction and associated cycles per second for the different sea states encountered and the panels identified as being most consistent in the previous analysis. The data presented here is representative of other panels. The starred values are considered outlying results.

Panel		13	18	25	26	27
BSS 8	Amplitude (με)	100	50	50	100	100
	Count / Sec	75.4	3.51	10.18	1.59	4.7
BSS 6a	Amplitude (με)	150*	50	50	50	100
	Count / Sec	2.72*	6.37	15.31	6.84	0.06
BSS 6b	Amplitude (με)	100	100	100	50	100
	Count / Sec	49.01	2.85	19.19	1.58	0.01
BSS 5	Amplitude (με)	100	50	100	100	100
	Count / Sec	78.18	11.45	20.02	3.54	0.26
BSS 4	Amplitude (με)	100	100	100	100	100
	Count / Sec	33.16	9.93	11.66	6.56	7.88
BSS 3	Amplitude (με)	100	100*	100	100*	100
	Count / Sec	64.08	40.33*	15.19	0.21*	0.93
Average		50.43	12.41	15.26	3.39	2.31
Standard Deviation		34%	32%	18%	37%	38%

Figure 6-20 shows the normalised count per minute for the longitudinal strain of each panel for each separate run. The numbered squares represent the panels and their locations relative to one another, within each box there are up to 6 individual bars. The thickness of these bars represents the normalised value of the number of counts per minute. The counts per minute

were normalised against the largest value in the entire data set. For this case the absolute maximum number of cycles per minute was just over 3483 and was found on panel 4, during the 2nd of the two runs in the sea state 6, 6(b). An equivalent representation for the transverse strain trace is found in Figure 6-21, for this figure the largest number of strains per minute was also found on panel 4 during the run in sea state 6(b) and was just under 5165 cycles per minute.

Comparing the panels either side of the vessel it would appear that from run to run there is little consistency in the number of cycles per second for any individual panel. The best conclusion that can be drawn from this is that the panels in the engine room tend to experience much higher total numbers of strain counts than those in the survivors space.

It is evident from Figure 6-18 and Table 6-5 that the very low strains, in the range 50 – 150 με, contain the majority of the applied strain cycle counts, at least 79% of the total count but generally over 99% of the total cycle count can be attributed to this very low applied strain, which corresponds to an applied stress ratio (r_{app}) of 0.011 or less for both the transverse and longitudinal applied stress ratio, or very little in terms of fatigue. This is still however an extremely conservative assumption to make. Challenging it for the moment and removing the very low strains from the analysis reveals a slightly different story.

Figure 6-19 shows how the data has been combined to allow comparisons between both the different sea states in which trials were conducted and between all panels. The bar graph is representative of the relative size of the number of samples per minute. This is achieved by normalising the number of samples per minute at a particular condition against the largest number of cycles per minute in that condition, giving the y axis a maximum value of 1.

Within each panel there are 6 bar graphs, these individual bar graphs show the comparative value of number of samples per second for the different trials conducted. These have been identified by the sea states they were conducted in. Sea states 6(a) and 6(b) are from the same day, but were split by a lunch time stop off.

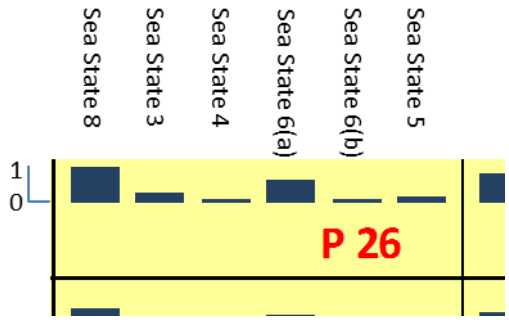

Figure 6-19: Focused view of panel 26 from Figure 6-23 which shows how the axis on the bar charts work. Along the x axis the bars are representative of the different trials conducted and the y axis is scaled against the largest value of counts per minute within that particular data set. This representation is valid for Figure 6-20, Figure 6-21, Figure 6-23 and Figure 6-25.

Figure 6-20 and Figure 6-21 show the cycles per minute for longitudinal and transverse strains respectively. These figures seem to suggest that the majority of the strain events will be found in the engine room.

For a planing vessel like the Severn class lifeboat it is reasonable to expect, and has been experimentally shown as identified in the literature review that the most severe loads can be expected in the forward 3rd of the vessel (Jasper, 1949). If the assumption is made that as you move forward in the boat from the stern there is a higher chance of encountering a large strain until the dead rise angle increases to such a point that the angle of incidence with the water surface is great enough to significantly reduce the applied pressure, then the likelihood of encountering a particular strain event is:

- equal for panels 1 to 6 but less than
- panels 7 and 8 which are equal but less than etc…
- …
- panels 29 to 32 which are likely to be highest, unless the deadrise angle is great enough to result in a reduced applied pressure.

Therefore the results shown in Figure 6-20 and Figure 6-21 should be treated with caution. Within the engine room there is a lot of machinery which could result in a large amount of low, but high frequency strain events which may explain the results shown. By removing strain events below a certain magnitude it is possible that the relationship previously identified by Jasper may be seen here.

Investigating Figure 6-22, this hypothesis is shown to be correct for longitudinal strains, with a relatively clear rise in count number from panel 8 until panel 26 where the count number starts to

fall off and become more irregular, this is also shown in Figure 6-23 which clearly shows the consistency of panels 1 to 10, 11 and 12 and 13 to 16 in the engine room and panels 17 to 32 in the survivors space. For transverse strains, shown in Figure 6-24, there is still a general increase from aft forward, but the counts for panels 19, 20, 25, 26, 30 and 31, are significantly reduced when compared to the rest of the panels. Referring to Figure 6-25 the pattern is very obvious, these panels are in the centre of the vessel either side of the keel which provides an additional stiffness against global bending moments, but also provides significant stiffness to the local structure either side, thus the response of these panels to impacts will be much reduced compared to others in the survivor's space.

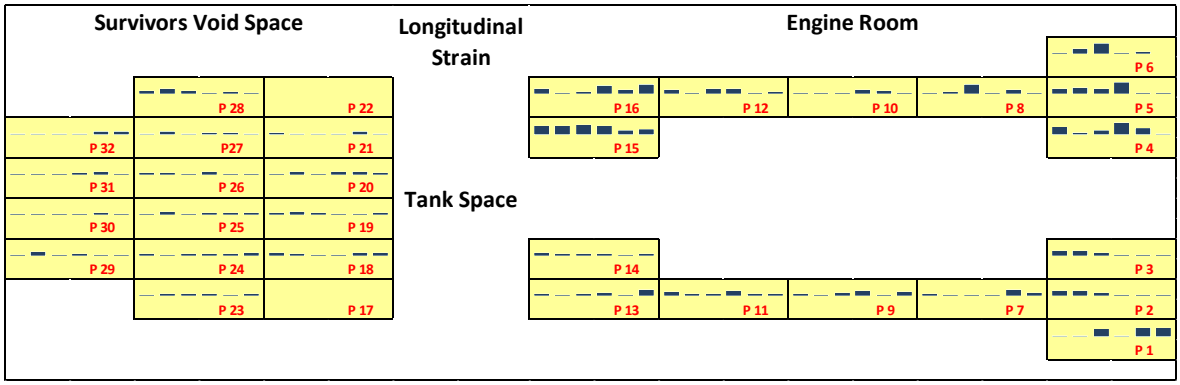

Figure 6-20: Normalised count of longitudinal strain cycles per minute for each panel.

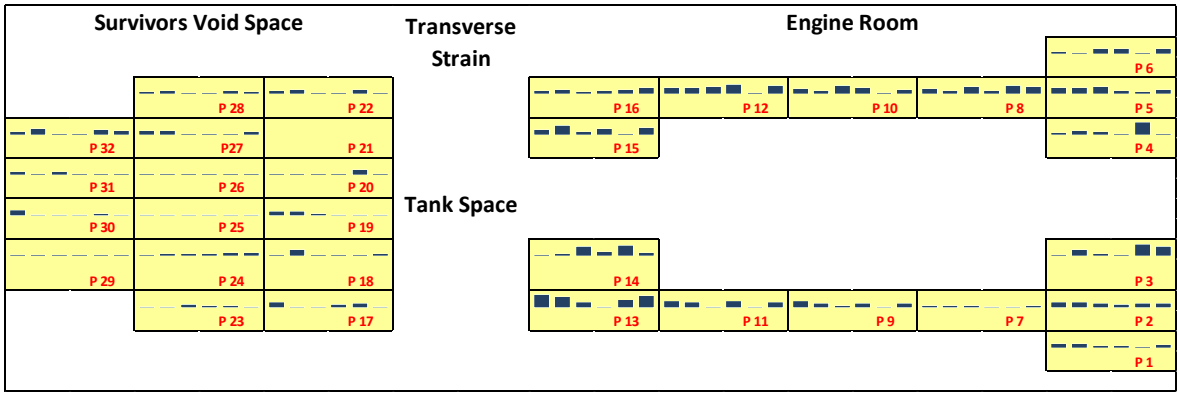

Figure 6-21: Normalised count of transverse strain cycles per minute for each panel.

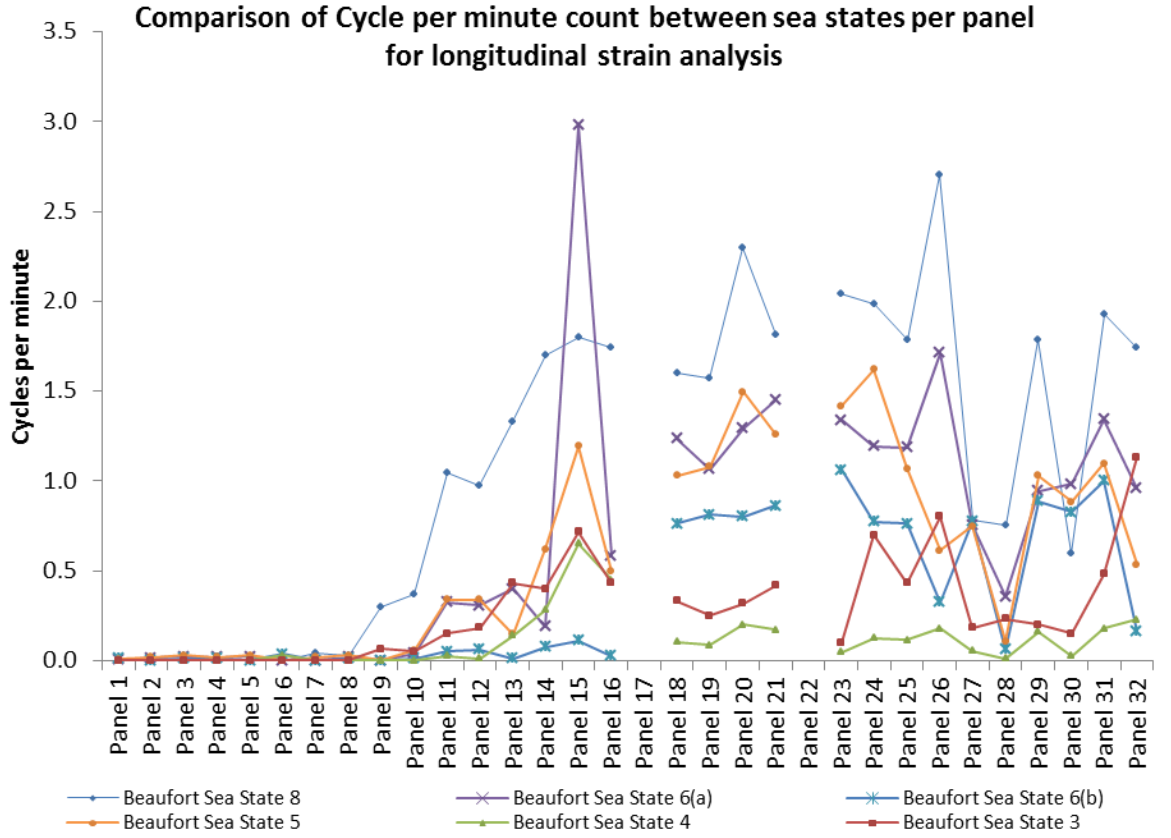

Figure 6-22: Number of cycle counts per minute for the longitudinal strain measurement in the different sea states and the different panels, with values below 200με removed.

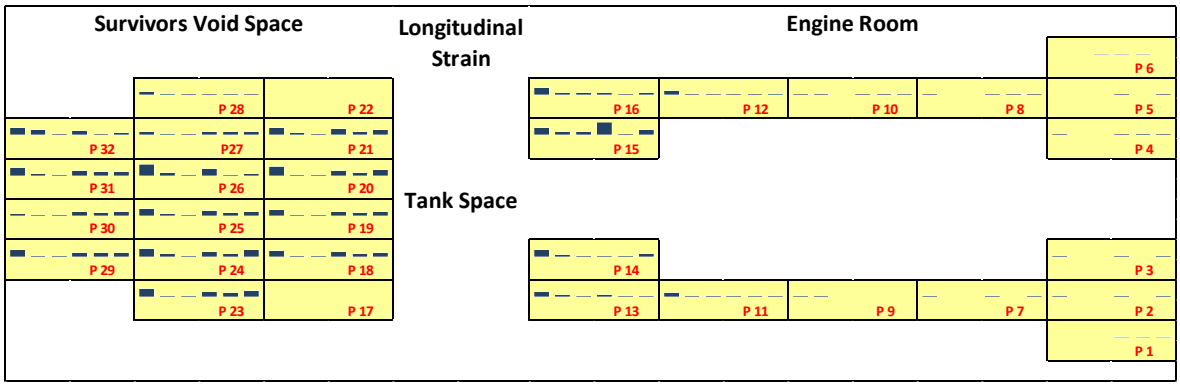

Figure 6-23: Normalised count of longitudinal strain cycles per minute for each panel, with values below 200με removed.

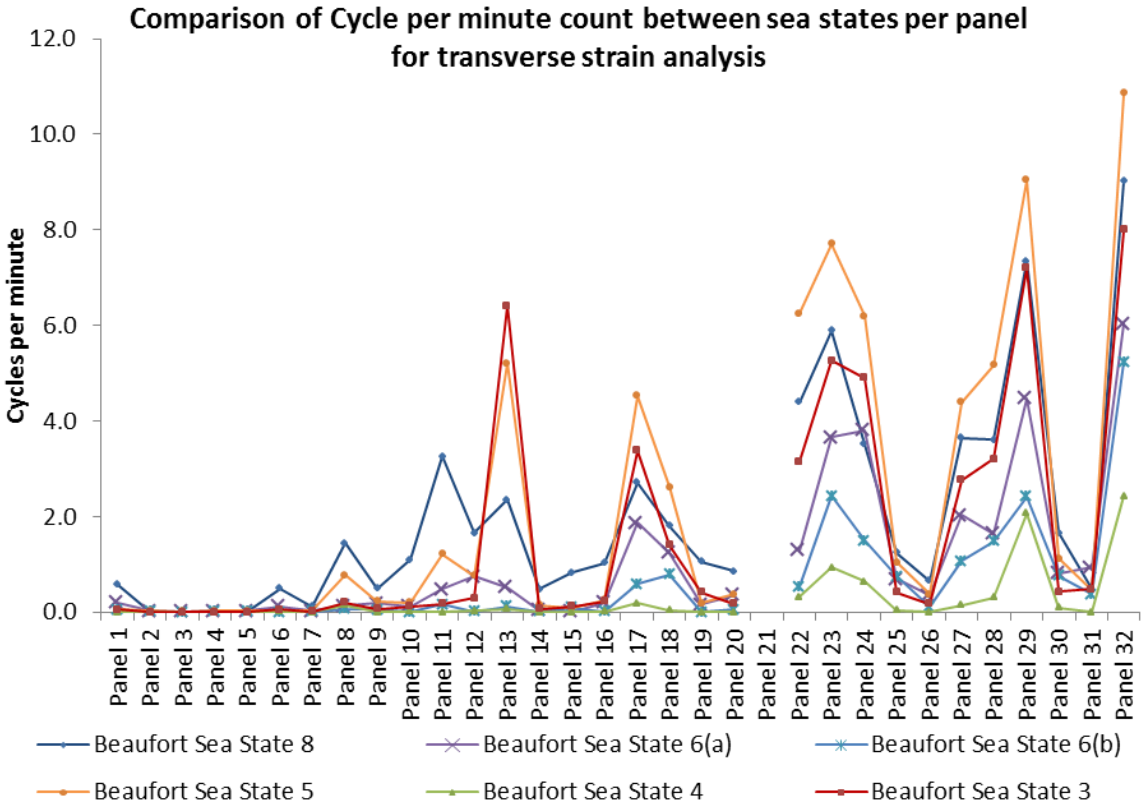

Figure 6-24: Number of cycle counts per minute for the transverse strain measurement in the different sea states and the different panels, with values below 200με removed.

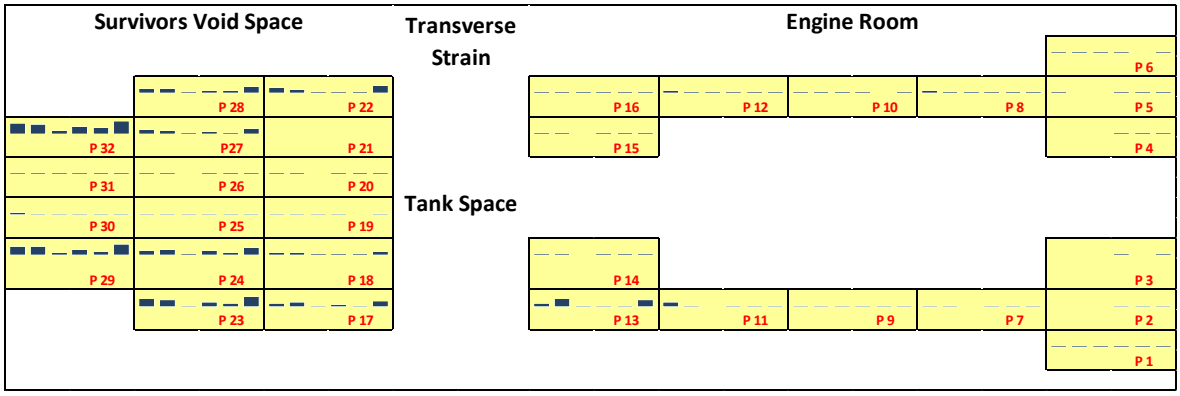

Figure 6-25: Normalised count of transverse strain cycles per minute for each panel, with values below 200με removed.

The analysis of the cycle count was split into two parts, analysis of the number of cycles attributed to the lowest relevant strains recorded and the cycle count per second without these included. Focusing on the lowest recorded strains and panel 13 in the engine room it would seem that there are a lot of repetitive events going on, this is confirmed within the frequency analysis with the

high proportion of signal power in the higher frequencies. However as discussed previously this panel is located in the engine room near rotating mechanical equipment and it is conceivable that forced vibration due to the engines and the gearbox could cause the very high count rate in this case.

The reduction of counts in panel 27 may well be due to the size and location of the panel. The panel is shorter than most due to the location of the battery box above, which is supported by an extra bulkhead running along the middle of the bottom and attached to the hull skin at the boundary of panels 26 and 27. Not only is 27 shorter than most, it is also narrower by 100mm than any of the others bar panel 18. This combination of reduced width and reduced length will result in a panel subjected to a reduced total load, due to reduced area, but also increased stiffness due to the reduced length and width.

However, comparing the counts per second of panel 27 with the results from panel 28 (see Table 6-6), which are of identical dimensions and neighbour one another does not generate corroborative evidence. Although panel 28 was highlighted as one of the worst performing panels in terms of the analysis presented in Table 6-2, the issues highlighted are not expected to play a significant role in this particular analysis since none of the errors highlighted are based around high speed fluctuations of strain.

A comparison between panels 13 and 14 which are also geometrically extremely similar and in geometrically similar positions but either side of the centre line of the vessel is also conducted. As with the previous comparison the results are inconclusive.

One possible explanation for the variation in the results panel to panel and sea state to sea state is that the global response of the structure, hull girder bending and torsional forces in particular, do provide a significant influence on the results of the panel strain state, enough to significantly affect the results at the lowest strains. To prove this either computational modelling or conducting drop tests from known heights to understand the panel response to known transient loading conditions and separately inducing global bending moments, both whilst measuring the panel response should be conducted. Then comparing the strain readings under global bending and transient loading conditions will help confirm the hypothesis above.

However, the larger strains, which are shown to be more consistent with the expected results as in Figure 6-22 and Figure 6-24 are not dominated by the global structural response and are therefore more consistent. However whilst there is no fatigue limit identified for this material, it is not right to dismiss these cycles from the fatigue analysis as being spurious results.

Table 6-6: Count per second comparison of panels 27 and 28 and 13 and 14.

Panel		27	28	13	14
BSS 8	Amplitude	100	100	100	100
	Count / Sec	4.7	75.4	75.4	10.18
BSS 6a	Amplitude	100	150	150	100
	Count / Sec	0.06	2.72	2.72	26.99
BSS 6b	Amplitude	100	100	100	100
	Count / Sec	0.01	49.01	49.01	71.71
BSS 5	Amplitude	100	100	100	100
	Count / Sec	0.26	78.18	78.18	21.49
BSS 4	Amplitude	100	100	100	100
	Count / Sec	7.88	33.16	33.16	67.24
BSS 3	Amplitude	100	100	100	100
	Count / Sec	0.93	64.08	64.08	13.69

6.6 Data Grouping

The results of data analysis of the monitored strain traces, are used to define a distribution of cycle counts for each individual panel in each individual sea state, for which there is data. For the sea states where there is data, this data represents only one combination of all the possible variations within the sea state that could affect the resultant strain history and therefore applied strain distribution.

To try to account for this the following assumptions were made:

- Under particular circumstances the panels measured can be grouped together.
- Within this group, each panel can then be considered to represent one version of the possible variations within the sea state.

Therefore it can be considered that the distributions developed for each different panel in a particular grouping can be combined to generate a larger pool of data from which an analysis can be conducted on what would be an average, representative panel for that group.

The frequency response graphs shown in Figure 6-14 show that for longitudinal responses there is significant similarities between the panels, however for the transverse strain response shown in Figure 6-15 there is more variation in the response, but still some compatibility is identified.

Based on this analysis it is confirmed that some amount of grouping of the panels is possible, however careful selection of the groups is required and the groups are likely to be different between transverse and longitudinal strains. The panels are grouped by balancing the following criteria.

- The strain direction being considered.
- The panel location in the boat.
- Change in deadrise angle between panels.
- The size of the panel.
- Observations from Figure 6-24 to Figure 6-8.

Based on the location, initial grouping puts panels 1 to 16 and 17 to 32 together. Nominally the panels should be mirrored port to starboard and combining this with the findings of Jasper (1948), that the further forward in the vessel the higher the likelihood of encountering a large slam event, then the engine room should be split further into 5 groups based on longitudinal distance forward and the survivors space into 3.

As can be seen from Figure 6-4 the deadrise angle of the panels in the engine room does not vary dramatically from one frame to the next. However this figure does not capture the slightly concave nature of the hull where the propeller tunnels run, bounded by the keel in the centre and bilge keels, which varies slightly between frames. It is expected that the influence of this will not be as significant in changing the response between panels as the influence of the relatively consistent dead rise angle between frames on keeping them similar. Although the longitudinal position changes, which is expected to increase the loading on the panels during a slam event there will be very little influence due to changes in deadrise angle suggesting that all the panels can be grouped together from this perspective, thus the case for 5 different groupings for the engine room panels is weakened.

Figure 6-6 shows the change in dead rise angle between frames 9 and 12 which changes quite considerably between frame 10 and 11 and again between frame 11 and 12. This strengthens the case for keeping the groupings based on longitudinal separation, as the influence due to dead rise angle will also change with longitudinal distance along the hull.

The overall panel dimensions are important as the proportion of the total applied load at any longitudinal distance along the hull will be directly proportional to the area covered by the panel in question. Nominally the length of the panels bounded by the same frames should be the same and the width of panels bounded by the same longitudinal stiffeners should also be constant. The only exception to this rule is panels 26 to 28 which are halved in length by the extra supporting

structure for the battery box. Therefore in the survivors space the second group is split further in two creating a total of 9 groups, one for each longitudinal variation between panels plus an extra one due to the reduction in length of panels 26 to 28 when compared to 23 to 25.

Finally the distribution of the number of applied strain cycles per minute, greater than 200 με, as shown in Figure 6-24 and Figure 6-25 for the longitudinal strains and Figure 6-23 and Figure 6-8 for the transverse strains is taken into account. Firstly from Figure 6-24 and Figure 6-25 it can be seen that there are three very clear groupings within the engine room group. Panels 1 to 6 have consistently low numbers of cycles per minute over 200με. Panels 7 to 12, are comparable and, although there is more variability panels 13, 14 and 16 are comparable. Panel 15 shows a general increase in cycle count when compared to these panels. This increase is difficult to explain as nominally it should be directly comparable to panel 14. The distribution of cycles per minute within the engine room recorded matches the expectations when considering the similarities or differences between location, dead rise angle and panel size which supports the use of these 3 groups (Panels 1 to 6, 7 to 12 and 13 to 16) for data pooling within this analysis.

Within the survivors space 4 groups had previously been identified based on longitudinal location, change in dead rise angle and panel size, since the strain gauges for panel 17 and 22 failed they will not be included in comparison of cycle counts per minute. The results of the analysis support the use of 4 separate groupings in the survivors space for pooling of data in the survivors space with panels 18 to 21 having directly comparable cycle counts per minute, as do panel 23 to 25 and 29 to 32 supporting the banding of panels into these three distinct groups in the survivors space. Comparing panels 26, 27 and 28, which are nominal equivalent in length, whilst being around half the length of panels 23 to 25 but in the same longitudinal ordinate, the pattern of cycle count for panel 26 seems to compare more closely with panels 23 to 25, than 27 or 28, this is likely to be due to one of the boundaries of the panel being the keel, which whilst expecting to act to increase the stiffness of the boat as a whole also acts as a boundary to this panel. The keel runs between panel 19 and 20, 25 and 26 and 30 and 31, however panel 26 is the only one which shows a significant difference to the others with which it is grouped, ie panels 23 to 25 are consistently comparable as are 23 to 25 and 18 to 21. Therefore the conclusion must be drawn that the boundary itself, the keel, experiences strains which are coupled with the longitudinal strains on the surrounding panels. This influence is not significantly dominant on most of the panels when compared to other factors, however for panel 26 the influence of the changing boundary due to the global response of the boat is greater than the influence of the reduction in size of the panels. Therefore the grouping for the survivors space is as follows: 17 to 22 (with the assumption that panels 17 and 22 will be comparable); 23 to 26; 27 and 28; 29 to 32.

Comparing Figure 6-24, longitudinal counts per second, and Figure 6-23, transverse counts per second, it is clear that an appropriate group for the longitudinal strains is not an appropriate group for the transverse strains when considering the counts per minute. Within the engine room grouping there is good consistency between panels 1 to 6 with a general increase in count as the longitudinal ordinate increases grouping panels 7 and 8, 9 and 10, 11 and 12. The grouping of panels 13 to 16 is not quite so straight forward as although panel 14, 15 and 16 are comparable panel 13 consistently has a much higher count rate. There is no clear reason for the count rate to be significantly higher for this panel compared to panel 16 which should be similar. For the engine room the grouping for the transverse strains will be as follows: 1 to 6; 7 and 8; 9 and 10; 11 and 12; 13 to 16.

Moving into the survivor's space, where in this direction gauge 21 failed, there is a significant drop in the number of counts per minute over 200με for the panels bounding the keel line (19, 20, 25, 26, 30 and 31) when compared to others of the same longitudinal position. The influence of the keel on these panels is very easily seen in Figure 6-8. If the assumption is made that the global response has a minimal impact on the transverse strains either in terms of maximum strain or number of strains applied, then only the local impact of the plate on the water will give rise to strain readings. Unlike in the longitudinal direction where the keel imposes a change in the boundary conditions along the keel edge, in the transverse direction the influence of the keel will be to stiffen the plate boundary. This will have the influence of reducing the local plate deflection when a local pressure loading is applied, therefore creating a reduced strain response in all directions. In the longitudinal direction this reduction is outweighed by the influence of the global bending on the panel, but in the transverse direction there is no other influence, therefore the panel sees a significant reduction in the number of applied strain cycles greater than 200με. Therefore the groups for data pooling in the survivors space will be will be as follows: 17, 18, 21 and 22; 23 and 24; 27 and 28; 29 and 32; 19, 20, 25, 26, 30 and 31. All the groups are shown in Table 6-7 for the longitudinal and transverse groupings.

Once the group has been selected the applied strain per minute distribution for each group can be combined for each sea state to create a new distribution which represents all values within that particular group, for that particular sea state. The use of Monte Carlo analysis as chosen in the previous chapter allows the distribution of strains to be used effectively to select a number of different possible inputs into the structural life assessment model simultaneously with the selection of different environmental variations based on the different distributions.

Table 6-7: Grouping of panels from the lifeboat for data pooling of longitudinal strain measurements.

Group	Longitudinal Group Panels	Transverse Group Panels
1	1 – 6	1 – 6
2	7 – 12	7, 8
3	13 – 16	9, 10
4	17 – 22	11, 12
5	23 – 26	13 – 16
6	27, 28	17, 18, 21 and 22
7	29 – 32	23, 24, 27 and 28
8	-	29, 32
9	-	19, 20, 25, 26, 30 and 31

6.7 Lifeboat Mass Variation

In this case the assumption made is that the weight variation found from vessel to vessel can be limited to the amount of material used to fill and fair the structure, variations in equipment levels and variations in non-structural fit out items. If the assumption is made that none of the extra, or reduction in weight directly contributes to a change in stiffness or hydrodynamic profile and that the structure behaves in a linear fashion and behaves in accordance with Hooke's Law then a simple normalisation of the measured structural response by the weight of the measured vessel will provide a variable which can be applied to each of the individual boats in class using the vessel weight to determine the appropriate value for each vessel.

Based on the hydrostatic case where the applied pressure to the hull structure is linearly related to the draught, which in turn is linearly related to the vessel weight, the assumption is made that even at service speeds for vessels geometrically similar, like the Severn lifeboats, the variation of applied load will vary only with vessel mass. Therefore to expand the results of the cycle counting from one vessel to another the following equation is applied:

$$\varepsilon_i = \alpha \varepsilon_m$$

Where:

- $\alpha = \frac{\nabla_i}{\nabla_m} =$ Lifeboat weight variation
- ε_m is the measured strain
- ∇_m is the displacement of the vessel measured
- ∇_i is the displacement of the vessel of interest
- ε_i is the value of strain to be applied to the vessel of interest

The weight of the Severn lifeboat fleet ranges from 40.52 to 43.33 tonnes a range of 2.81 tonnes. The lifeboat used in measuring the structural response weighs 41.44 tonnes. The application of the variation can either be performed pre or post counting. The effect of applying the variation prior to the count would be to change the measured strains themselves which may result in one value changing bin if the change increases or decreases the value across a boundary of 50με. The alternative is to leave the strain count as it is, but modify the value of the strain represented by a particular bin. Considering the maximum variation from the measured vessel, the strains applied in calculation will be at most 2.3% smaller than those measured and 4.6% larger. The weight and change from the measured vessel of the vessels chosen for investigation is shown in Table 6-8.

To apply the change due to weight prior to the counting analysis would result in a significant increase in processing time for the method, as the Rainflow count would have to be performed for each different vessel investigated. Applying the change after the completion of the cycle counting will result in the methodology being able to be applied to the different vessels in a much simpler and quicker fashion.

Table 6-8: Variation of weights for different vessels.

Vessel	Weight (Tonnes)	α
Most Used	41.63	1.005
Average Used	41.97	1.013
Least Used	42.14	1.016

6.8 Summary

In this chapter the methodology for determining and interpreting strain traces to output the number of applied strains in a particular strain range for a composite asset was introduced and implemented on a Severn class lifeboat. 5 different sea states were encountered and the lifeboat operated for between 1 and just over 7 hours in the different sea states.

The data was analysed using frequency analysis and Rainflow counting. The frequency analysis revealed that there are a large number of different frequencies detected within the measured strains. Removing the higher frequency components dramatically changed the peak values of the strain output. For all panels there were blocks of frequency response between 160 and 210 Hz that were very difficult to explain, however although the blocks were fairly consistent in overall width, the location of the peaks was subtly different between runs suggesting they are a function of the sea state at the time rather than a function of the structure or other asset based source.

The Rainflow counting revealed that there were an extraordinarily high number of very low strain events across all panels, however removing these and focusing on the more extreme events revealed an increase in number of events the further forward in the vessel the plate is. However, as the material characterisation chapter has not identified a fatigue limit for this material, it must be considered that all structural loadings are relevant and therefore even the very low strains cannot be dismissed.

The final output from this chapter is the fatigue spectrum which contains the number of counts for each different 50 με block for each panel in each sea state the vessel spent time in. Combining

this with the known amount of time in each sea state and predicted amount of time in each sea state per year identified in chapter 6 and the results of the material fatigue testing in chapter 5 an estimate of the total life used and remaining life of the vessel can be made. This is conducted in Chapter 8 and the method developed so far shown in Figure 6-26.

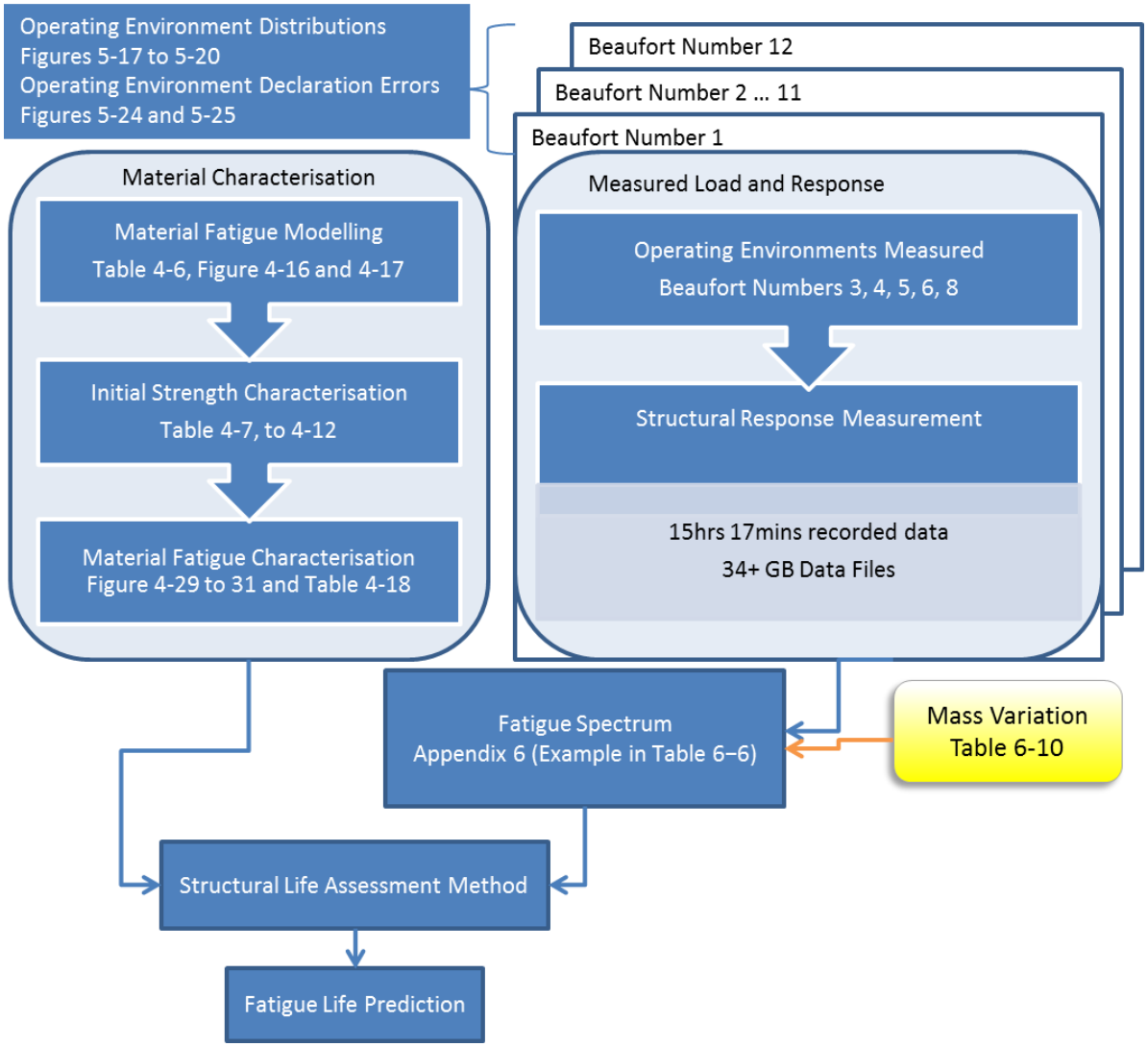

Figure 6-26: Areas identified within the methodology that are addressed so far.

Intentionally left blank

7 Structural Life Assessment Modelling (SLAM)

The SLAM process brings all of the work together that was presented in the chapters 4 to 6, as shown in Figure 3-1 to generate the inputs for a chosen fatigue model thus developing a baseline structural life prediction identified in the literature as being a core investigation for life extension assessment. The material characterisation process, chapter 4, provides the fatigue understanding required of the materials. The environment identification process identifies the environments peculiar to the asset, which in this case is the sea and comes with its own identification issues which are tackled in chapter 4. The structural response monitoring process measures the variation in responses for each of the environments identified and generates fatigue spectra for them from this data as conducted in chapter 6. This chapter takes the results of the work described and updates the initial life prediction bit by bit assessing the change in predicted life as more information becomes available. Section 7.1 discusses the life extension based on information obtained from various sources but without a direct relationship to the asset under investigation. Section 7.2 looks at how the life prediction changes with the application of the material data, section 7.3 completes the process by generating and applying a method of life prediction based on all of the data available using Monte Carlo analysis to help generate an understanding of the uncertainty in the process.

7.1 Initial Fatigue Life Prediction

To understand whether an asset is worth life extending beyond the original design life, an initial estimate of the structural life is required. The design life and structural life should ideally coincide. However there may be any number of reasons why they wouldn't therefore an estimation of the structural life based on the best information available should be made at the design stage.

For the Severn class lifeboat an initial design life was determined to be 25 years, however there is no evidence available for a detailed structural life prediction having been conducted at the time. Therefore an initial structural life prediction was made based on information similar to that which may be available to designers during the early stages of development.

7.1.1 Method

As a baseline investigation an initial fatigue life prediction for the Severn class lifeboat was presented by Roberton et al (2009). This was found from the combination of static material data from calculations, fatigue data taken from literature and a previously defined structural load distribution developed for a different class of lifeboat, the Trent class as presented by Clark et al (1999).

The values used for the fatigue life prediction are those found from the modelling conducted in Chapter 4 and presented in Table 4-6. The fatigue life diagram used for the analysis presented in Roberton et al (2009) was a predecessor curve to that which is presented in Figure 4-16 and Figure 4-17. The applied pressures applied to a simply supported plate with dimensions of 1230mm x 460mm x 11.06 mm, which was considered representative of a plate within the Severn hull. The maximum stresses were obtained from a third order shear deformation tool developed by Sobey et al (2009) and a simple Miners rule calculation used to determine the fatigue life.

7.1.2 Results

The initial life prediction based on the findings in Roberton et al (2009) is shown in Table 7-1. From this table the initial used life over the 20 year period defined by the fatigue spectrum was 6.66%, generating a total useful life of $20/0.0666 = 300$ years.

Table 7-1: Initial Severn Life prediction as presented by Roberton et al (2009), the number of applied cycles are considered the cycles developed over a period of 20 years.

Applied Pressure (kPa)	Stress (N/mm^2)	R_{app}	Applied Cycles (n)	Cycles to Failure (N)	% Life Used
8	0.52	N/A	1,400,000	36,307,805	3.86
27	1.77	N/A	577,500	35,481,339	1.63
61	3.99	N/A	208,500	28,183,829	0.74
101	6.61	N/A	54,300	23,442,288	0.23
178	11.66	N/A	13,770	15,848,932	0.09
178	11.66	N/A	13,770	15,848,932	0.09
239	15.65	N/A	2,535	11,481,536	0.02
325	21.28	N/A	500	7,244,360	0.01
386	25.28	N/A	100	5,370,318	<0.01
463	30.32	N/A	15	3,548,134	<0.01
596	39.03	N/A	1	1,1778,279	<0.01
				Total Used Life	6.66

Further data gathering identified two possible S-N curves which could be used, shown in Figure 4-16 and Figure 4-17, the lower prediction lines were used as in the previous life prediction, and the R_{app} values were obtained from the predicted material constant values shown in Table 4-6 with an assumed failure strain of 3%. The results are shown in Table 7-2 using the lower prediction line from Figure 4-16 and Table 7-3 using the lower prediction line from Error! Reference source not found.. The results outlined in Table 7-2 suggest that a period of 20 years will be too great for the Severn lifeboat, with a total % of life used being 243%. This suggests that Severn lifeboat could be expected to become structurally unsound after 8.2 years.

Table 7-2: Initial Severn Life prediction using data from the Trent lifeboat for applied pressure presented in (Roberton D.M.V et al., 2009) and the number of applied cycles, modelled ultimate material properties from section 4.3 and the lower prediction line equation 4-18 from Figure 4-16 using the Miner's rule for damage estimation. The change from Table 7-1 is highlighted in pink.

Pressure (kPa)	Stress (N/mm^2)	R_{app}	Applied Cycles (n)	Cycles to Failure (N)	% Life Used
(Roberton D.M.V et al., 2009)		$\frac{\text{(Roberton D. M. V et al., 2009)}}{\text{Table 4-6}}$	(Roberton D.M.V et al., 2009)	Figure 4-16	(Miner, 1945)
8	0.52	0.10%	1,400,000	976924	143.31%
27	1.77	0.35%	577,500	923607	62.53%
61	3.99	0.78%	208,500	835987	24.94%
101	6.61	1.29%	54,300	743211	7.31%
178	11.66	2.27%	13,770	592438	2.32%
178	11.66	2.27%	13,770	592438	2.32%
239	15.65	3.05%	2,535	495271	0.51%
325	21.28	4.15%	500	384648	0.13%
386	25.28	4.93%	100	321417	0.03%
463	30.32	5.91%	15	256327	0.01%
596	39.03	7.61%	1	173364	<0.01%
				Total Used Life	243%

Table 7-3: Initial Severn Life prediction using data from the Trent lifeboat for applied pressure presented in Table 7-1 and the number of applied cycles, modelled ultimate material properties from section 4.2 and the lower prediction line equation 4-19, using equation the Miner's rule for damage estimation The change from Table 7-2 is highlighted in pink.

Pressure (kPa)	Stress (N/mm^2)	R_{app}	Applied Cycles (n)	Cycles to Failure (N)	% Life Used
(Roberton D.M.V et al., 2009)		$\frac{\text{(Roberton D. M. V et al., 2009)}}{\text{Table 4-2}}$	(Roberton D.M.V et al., 2009)	Figure 4-17	(Miner, 1945)
8	0.52	0.10%	1,400,000	3071325	45.58%
27	1.77	0.35%	577,500	2863246	20.17%
61	3.99	0.78%	208,500	2527839	8.25%
101	6.61	1.29%	54,300	2182180	2.49%
178	11.66	2.27%	13,770	1643629	0.84%
178	11.66	2.27%	13,770	1643629	0.84%
239	15.65	3.05%	2,535	1313872	0.19%
325	21.28	4.15%	500	957921	0.05%
386	25.28	4.93%	100	765307	0.01%
463	30.32	5.91%	15	576756	<0.01%
596	39.03	7.61%	1	353752	<0.01%
				Total Used Life	78.43%

The results from Table 7-3 are more encouraging with a total used life after 20 years of just over 78%, suggesting the Severn lifeboat will maintain structural integrity for 25 years, the current design life of the vessel.

7.1.3 Discussion

The total life expectancy based on the different data sources varies wildly from 300 years to just over 8 years. The source of the discrepancy is entirely the S - N graphs used. The two sources have very different lines representing the 95% prediction limit which is used in this analysis. These differences come from the different source materials. In order to overcome this, the most appropriate data sets should be identified to produce the most accurate prediction based on the data available.

One of the benefits of composite materials is the ability to build the structure in such a way that the material properties can be precisely arranged to match the direction and to some extent magnitude of expected stresses. However, this does have the drawback that every time a new part is made, the material is made with it and the uniqueness of that particular build is not captured by the methods captured here. The ideal would be to conduct tests on each new build, however this may prove impractical so testing similar to that carried out in section 4.3 is a good compromise between practical limitations and achieving representative material properties.

7.1.4 Summary

Use of data from literature will generate a huge range in results depending on how data has been chosen. Careful choice of data may result in too few points being captured. It is expected that the method presented in this section and the results generated will merely provide designers with an order of magnitude of the expected life of the vessel rather than a definitive value.

The results here range from what is known to be unrealistically conservative at 8 years, proven by the fact a large proportion of the fleet are over 8 years old and still floating, to a high but not unbelievable value of 300 years. It is difficult to determine how realistic this value is at this stage.

The only way to determine what is the most appropriate data is to conduct material testing for the materials used, this can then be used to augment other data of similar materials or generate S-N curves specific to be used in this application. This choice depends on whether more data or more specificity is required for the application under investigation.

7.2 Influence of Material Characterisation

Having identified that using estimated data sources provided an enormous range in possible life expectancies for the Severn, the influence of this unknown was reduced by embarking on a

material characterisation of the materials used within the Severn class lifeboat. In this section the material properties calculated are replaced by the material properties found from the tests conducted in the materials characterisation chapter.

7.2.1 Method

The applied stress ratio, R_{app}, was recalculated using the applied stress values first proposed in Roberton et al (2009) as with the previous tables, but then normalising them using the tested ultimate failure stress values determined from both tensile and flexural tests in the material characterisation chapter, found in Table 4-8 to Table 4-12.

First the expected life prediction using the tensile and flexural values determined for the [0] direction are compared, followed by the [90] direction tests. The number of cycles to failure was determined from the graph in Figure 4-17 as the graph in Figure 4-16 is clearly ultra conservative to the point of being unrealistic.

7.2.2 Results

Table 7-4 shows the life time prediction results of the application of the tensile strength data in the [0] direction and Table 7-5 shows the lifetime prediction results of the application of the flexural strength data.

Table 7-4: Modification of Table 7-3 Life prediction using updated ultimate tensile material properties as tested in the [0] direction from 4.3. The changed data is highlighted in pink.

Pressure (kPa)	Stress (N/mm^2)	R_{app}	Number of Cycles (n)	Number of Cycles to Failure (N)	% Life Used
(Roberton D.M.V et al., 2009)		$\frac{\text{(Roberton D. M. V et al., 2009)}}{\text{Table 4 – 7}}$	(Roberton D.M.V et al., 2009)	Figure 4-17	(Miner, 1945)
8	0.52	0.34%	1,400,000	2867585	49%
27	1.77	1.16%	577,500	2266690	25%
61	3.99	2.61%	208,500	1492862	14%
101	6.61	4.32%	54,300	911942	6%
178	11.66	7.62%	13,770	352684	4%
178	11.66	7.62%	13,770	352684	4%
239	15.65	10.23%	2,535	166497	2%
325	21.28	13.91%	500	57735	1%
386	25.28	16.52%	100	27204	0%
463	30.32	19.82%	15	10541	0%
596	39.03	25.51%	1	2048	0%
				Total Used Life	105%

Table 7-5: Modification of Table 7-4 life prediction using updated ultimate flexural material properties as tested in the [0] direction from section 4.3. Changed data is highlighted in pink.

Applied Pressure (kPa)	Calculated Stress (N/mm^2)	R_{app}	Number of applied Cycles (n)	Number of Cycles to Failure (N)	% Life Used
(Roberton D.M.V et al., 2009)		$\frac{\text{(Roberton D. M. V et al., 2009)}}{\text{Table 4-9}}$	(Roberton D.M.V et al., 2009)	Figure 4-17	(Miner, 1945)
8	0.52	0.35%	1,400,000	2856159	49%
27	1.77	1.20%	577,500	2236093	26%
61	3.99	2.71%	208,500	1447819	14%
101	6.61	4.50%	54,300	866813	6%
178	11.66	7.93%	13,770	322480	4%
178	11.66	7.93%	13,770	322480	4%
239	15.65	10.65%	2,535	147645	2%
325	21.28	14.48%	500	49032	1%
386	25.28	17.20%	100	22405	0%
463	30.32	20.63%	15	8352	0%
596	39.03	26.55%	1	1517	0%
				Total Used Life	107%

Table 7-6: Modification of Table 7-5 Life prediction using updated ultimate tensile material properties as tested in the [90] direction from section 4.3. Changed data is highlighted in pink.

Applied Pressure (kPa)	Calculated Stress (N/mm^2)	R_{app}	Number of applied Cycles (n)	Number of Cycles to Failure (N)	% Life Used
(Roberton D.M.V et al., 2009)		$\frac{\text{(Roberton D. M. V et al., 2009)}}{\text{Table 4-8}}$	(Roberton D.M.V et al., 2009)	Figure 4-17	(Miner, 1945)
8	0.52	0.15%	1,400,000	3032443	46%
27	1.77	0.50%	577,500	2741733	21%
61	3.99	1.12%	208,500	2292420	9%
101	6.61	1.85%	54,300	1855912	3%
178	11.66	3.27%	13,770	1235198	1%
178	11.66	3.27%	13,770	1235198	1%
239	15.65	4.38%	2,535	895428	0%
325	21.28	5.96%	500	568725	0%
386	25.28	7.08%	100	411951	0%
463	30.32	8.49%	15	274394	0%
596	39.03	10.93%	1	135958	0%
				Total Used Life	82%

Table 7-7: Modification of Table 7 5 life prediction using updated ultimate flexural material properties as tested in the [90] direction from section 4.3. Changed data is highlighted in pink.

Applied Pressure, (kPa)	Calculated Stress (N/mm^2)	R_{app}	Number of applied Cycles (n)	Number of Cycles to Failure (N)	% Life Used
(Roberton D.M.V et al., 2009)		(Roberton D. M. V et al., 2009) / Table 4-10	(Roberton D.M.V et al., 2009)	Figure 4-17	(Miner, 1945)
8	0.52	0.15%	1,400,000	3032086	46%
27	1.77	0.50%	577,500	2740635	21%
61	3.99	1.12%	208,500	2290349	9%
101	6.61	1.86%	54,300	1853136	3%
178	11.66	3.28%	13,770	1231941	1%
178	11.66	3.28%	13,770	1231941	1%
239	15.65	4.40%	2,535	892260	0%
325	21.28	5.98%	500	565990	0%
386	25.28	7.10%	100	409600	0%
463	30.32	8.52%	15	272517	0%
596	39.03	10.96%	1	134761	0%
				Total Used Life	82%

The actual used life prediction over the 20 year period represented by the fatigue spectrum increases from just over 78% in Table 7-3 to 105% in Table 7-4 and 107% in Table 7-5 which represent the fatigue life calculated using the measured failure stress in the [0] direction using tensile and flexural tests respectively. Using the results of the tensile and flexural failure stresses in Table 7-6 and Table 7-7 respectively the life used of the vessel fell to 82% in both cases.

In addition to the ultimate failure strength tests fatigue tests were also carried out in the chapter 4. Fatigue curves for the materials were developed in the [0] direction in both tension and flexure with the results found in Figure 4-29 and Figure 4-30, flexural fatigue tests were conducted on coupons representing the [90] direction and the results are shown in Figure 4-31**.**

The 95% confidence limits from these graphs were used to modify the number of cycles to failure at the different stress ratios presented in Table 7-4 using the 95% confidence limit in Figure 4-29, Table 7-5 using the 95% confidence limit in Figure 4-31 and Table 7-7 using the 95% confidence limit in Figure 4-30**.**

Using these confidence limits the total used life after applying the 20 year representative fatigue spectrum is 2.4%, 6.8% and 0.03% for the [0] direction tensile, flexural and [90] flexural 95% confidence limits respectively shown in Table 7-8, Table 7-9 and Table 7-10. This translates into a potential useful life of 833, 294 and more than 60 milennia.

Table 7-8: Life prediction updated from Table 7-4 using the equation for the tensile fatigue curve as tested in the [0] direction from section 4.4 using the 95% prediction line equation from Figure 4-29 found in Table 4-19.

Applied Pressure (kPa)	Calculated Stress (N/mm^2)	R_{app}	Number of applied Cycles (n)	Number of Cycles to Failure (N)	% Life Used
(Roberton D.M.V et al., 2009)		$\frac{\text{(Roberton D. M. V et al., 2009)}}{\text{Table 4 – 7}}$	(Roberton D.M.V et al., 2009)	Figure 4-29	(Miner, 1945)
8	0.52	0.35%	1,400,000	114818504	1.2%
27	1.77	1.20%	577,500	96769779	0.6%
61	3.99	2.71%	208,500	71422071	0.3%
101	6.61	4.50%	54,300	49906608	0.1%
178	11.66	7.93%	13,770	25009133	0.1%
178	11.66	7.93%	13,770	25009133	0.1%
239	15.65	10.65%	2,535	14488452	0.0%
325	21.28	14.48%	500	6706567	0.0%
386	25.28	17.20%	100	3879980	0.0%
463	30.32	20.63%	15	1946992	0.0%
596	39.03	26.55%	1	591338	0.0%
				Total Used Life	2.4%

Table 7-9: Life prediction updated from Table 7-5 using the equation for the flexural fatigue curve as tested in the [0] direction from section 4.4 using the 95% prediction line equation from Figure 4-31 found in Table 4-19.

Applied Pressure (kPa)	Calculated Stress (N/mm^2)	R_{app}	Number of applied Cycles (n)	Number of Cycles to Failure (N)	% Life Used
(Roberton D.M.V et al., 2009)		$\frac{\text{(Roberton D. M. V et al., 2009)}}{\text{Table 4 – 9}}$	(Roberton D.M.V et al., 2009)	Figure 4-31	(Miner, 1945)
8	0.52	0.35%	1,400,000	40314978	3.5%
27	1.77	1.20%	577,500	33977725	1.7%
61	3.99	2.71%	208,500	25077659	0.9%
101	6.61	4.50%	54,300	17523167	0.3%
178	11.66	7.93%	13,770	8781186	0.2%
178	11.66	7.93%	13,770	8781186	0.2%
239	15.65	10.65%	2,535	5087173	0.1%
325	21.28	14.48%	500	2354804	0.0%
386	25.28	17.20%	100	1362335	0.0%
463	30.32	20.63%	15	683626	0.0%
596	39.03	26.55%	1	207630	0.0%
				Total Used Life	6.8%

Table 7-10: Life prediction updated from Table 7 7 using the equation for the flexural fatigue curve as tested in the [90] direction from section 4.4 using the 95% prediction line equation from Figure 4 30 found in Table 4 18.

Applied Pressure (kPa) (Roberton D.M.V et al., 2009)	Calculated Stress (N/mm^2)	R_{app} $\frac{\text{(Roberton D. M. V et al., 2009)}}{\text{Table 4-10}}$	Number of applied Cycles (n) (Roberton D.M.V et al., 2009)	Number of Cycles to Failure (N) Figure 4-30	% Life Used (Miner, 1945)
8	0.52	0.15%	1,400,000	6800116292	0.02%
27	1.77	0.50%	577,500	5375169414	0.01%
61	3.99	1.12%	208,500	3540133240	0.00%
101	6.61	1.86%	54,300	2162555790	0.00%
178	11.66	3.28%	13,770	836345301	0.00%
178	11.66	3.28%	13,770	836345301	0.00%
239	15.65	4.40%	2,535	394825532	0.00%
325	21.28	5.98%	500	136910863	0.00%
386	25.28	7.10%	100	64512002	0.00%
463	30.32	8.52%	15	24996305	0.00%
596	39.03	10.96%	1	4855953	0.00%
				Total Used Life	0.03%

7.2.3 Discussion

Having tested the material properties some of the unknowns identified in section 7.1 have been accounted for. This approach can have the impact of reducing the uncertainty, if the tested points produce results close together, or increasing the uncertainty if the tested points are spread widely. An example of the former is with the [90] direction material where the points are very close together and an example of the latter is with the [0] direction testing where there is a large spread. Ideally further testing would be conducted on materials with larger spread to try to reduce the uncertainty however this is not always possible.

Comparing the flexural and tensile fatigue results in the [0] direction shows that the tensile provides less conservative results, 2.4% used life compared to 6.8% for the flexural fatigue results. This difference comes from the different equations used to determine the number of cycles to failure at each of the different stress ranges.

The difference between the [0] and [90] direction fatigue results are extremely large with the [90] results being less, a factor of 100 smaller. The reason for the differences is due to the consistency of the results for the fatigue tests of the [90] specimens when compared to the [0] specimens. Comparing the results to previous investigations of (Clark et al., 1999), the results from the [0] direction fatigue tests are an order of 4 to 8 times greater than that produced for the Trent lifeboat, with the prediction from the [90] fatigue results being an order of 1000 times greater.

In the above analysis the assumption is made that the developed stresses within the hull will be consistent in magnitude. However with the complex stress states that can be expected within the hull response this is unlikely, indeed this is confirmed in the results in chapter 6, therefore these results are still implicitly unreliable due to the application of the fixed fatigue spectrum which cannot be considered representative of the real life situation. To fully understand the implication of the different fatigue results, the stresses developed within the structure need to match the direction of testing for the material itself as has been conducted in chapter **6**.

7.2.4 Summary

In this section the importance of the material properties is investigated. The main findings are that doing specific tests with the materials used in the construction will generate a fatigue life prediction more specific to the asset in question. However this fatigue investigation will generally result in reduced number of test points on the graph itself.

Having developed a fatigue life prediction based on material information directly relevant to the Severn class lifeboat, the next step is to use a developed load profile representative of the actual stresses experienced by the boat during services, to make best use of the data obtained in the material characterisation work, the structural response should be measured in the [0] and [90] directions as a minimum to generate information of the stress state of the plate. This was conducted in chapter 6 and the results are discussed in the following section.

7.3 Application of operating environment definitions and structural response monitoring

Sections 7.1 and 7.2 have been completed using an assumed loading profile, from which stresses have been calculated. This approach makes perfect sense at the design stage of an asset, however throughout the asset's life the intended operation may change or the extreme design cases may not be encountered. Therefore to fully understand the service life used by an asset some method for determining the structural response should be used. In this case the approach taken has been to monitor the structure of the asset in use.

Having now taken into account the material characterisation study to produce an estimate of the fatigue life, the measured data can be used to update the fatigue spectrum to one which is representative of the asset's usage profile. This has been achieved by measuring the Severn's structural response in 32 separate locations during operation in as many of the different operating environments as possible. In this case each of the 12 different sea states, as determined by the Beaufort scale, defines a different operating environment and as such there are 12 possible fatigue spectra that could be defined.

In addition to the different sea states, there are also a fleet of Severn class lifeboats of which only one has been subjected to structural monitoring. As a result the differences between the vessels needed understanding, since the vessels are of a single class, it can be considered that structurally they are all identical and therefore structural responses measured on one boat can be considered representative of those which would be experienced by another boat in the same conditions. However as pointed out in section 3.7 the vessel's weights are not consistent and since the weight of a vessel is directly proportional to the force exerted on it there needs to be some way to allow for this variation.

7.3.1 Method

The total life of the lifeboat is predicted using a Monte Carlo analysis, the implementation of which is shown in Figure 7-1 and Figure 7-2. The Monte Carlo analysis picks a value of different variables based on the distributions provided. In this case the variables simulated were:

- The total number of cycles expected in any minute for each panel in a particular group for each sea state where recorded data was available.
- The total damage experienced in any sea state where recorded data was not available.
- The error in recorded sea state as defined by sea state specific distributions where available and a standard distribution where not.

In addition to these simulated variables data pooling was used through the panel grouping identified previously in Chapter 7 to improve the data density and overcome some of the statistical uncertainty found using limited data sets.

The **first step** in the simulation takes the measurement data found in section 7.5.4 for each of the different panels within a particular grouping, identified in section 7.7 and pools it together. The pooling is achieved by summing the counts per minute for each different panel in a particular group at each different strain level for each different sea state resulting in a single distribution where there had previously been two or more. These values were then normalised by the total of this distribution providing a normalised distribution which is then considered representative of all of the panels within the group. This remains the same for each iteration of the Monte Carlo simulation.

For each different panel within the group there was a unique number of counts per minute. Although the variation above 200με is used as part of the analysis for the grouping due to its consistency, for the measured strains below 200με there is no pattern within the groups as shown in Table 7-7, figure 7-18 and figure 7-19, therefore it is considered that the strains at this level are

the result of very complex pseudorandom loading. This could be the result of complex hydrodynamic loads or the direction of the sea way for these particular runs and as such can be considered to occur on any of the panels within the group if the conditions at the time had been different.

To account for this the **second step** takes the variation of the counts per minute across each of the different panels within the group, identifies the maximum and minimum values and uses these to bound a distribution of equal likelihood. A distribution of equal likelihood was chosen due to the small number of data points available, ranging from 2 to 6, for this variable. The distributions generated remain the same for each iteration of the Monte Carlo analysis.

The **third step** selects a value for the total number of cycles per minute to apply from the distribution set up in the second step, the selected value chosen changes with each iteration of the Monte Carlo analysis. This value is then multiplied with the normalised distribution to give a distribution of cycles per minute which will be applied for this iteration. This value changes for each iteration of the Monte Carlo analysis.

The **fourth step** takes the resultant distribution of applied strain cycles per minute and converts it into a distribution of applied stresses using material constants and the lifeboat weight variation, α. Following this a total number of cycles to failure using fatigue constants is determined before combining them to calculate a single value for damage per minute. The applied stress σ_{app} is calculated for each strain level through Equation 7-1.

$$\sigma_{app} = E\alpha\varepsilon \qquad \text{Equation 7-1}$$

Where the Young's modulus E is found from Table Table 4-6, the weight variation α is unique to each lifeboat and is discussed in section 7.8, the applied strain is the upper value of the bin used for each different count, ie 50με, 100 με, 150 με … etc.

The reality of the situation is that the plate will be subjected to a mixture of bending stresses found through $\delta_{bend} = \frac{My}{I}$ and tensile membrane stress found using $\sigma_{membrane} = \frac{P}{y}$. However with the method used in this thesis of measuring the strain values on the surface of the plate, without fully understanding the loading conditions both locally and globally it is impossible to determine the proportion of measured strain to apportion to the bending moments and to the membrane forces. Therefore sticking to the most basic Young's modulus equation will provide the most appropriate stress result for this investigation.

Simulation Model Walk Through Part 1

Step 1: Generate normalised distributions of combined strain cycles per minute for each group

ε_i	SS 3	SS 4	SS 5	SS 6	SS 8
$\varepsilon_{m,k} \times \alpha$	$\sum_{j=1}^{G} n_{j,k}$	$\sum_{j=1}^{G} n_{j,k}$	$\sum_{j=1}^{G} n_{j,k}$	$\sum_{j=1}^{G} n_{j,k}$	$\sum_{j=1}^{G} n_{j,k}$

Normalised by the total number of resultant cycles, n_T

$\varepsilon_{m,k}$ is the measured strain level.
α is the chosen lifeboat weight variation.
G is the number of panels in a group.
$n_{j,k}$ is the cycles per second for each group at $\varepsilon_{m,k}$.

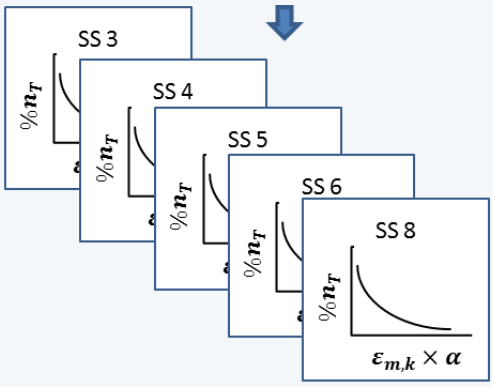

Step 2: Set up distribution of total strain cycles per minute for simulation

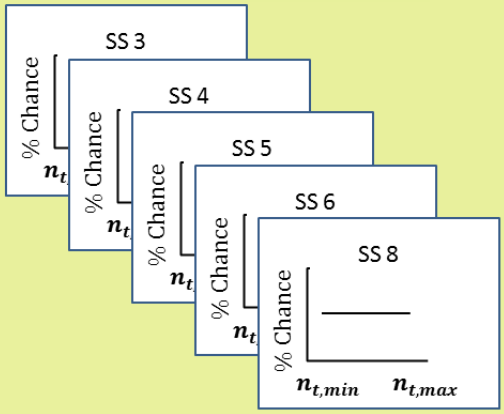

Step 3: Simulate a value of total cycles per minute for each sea state using distributions generated in Step 2 and multiply with the normalised distribution from Step 1.

Step 4: Calculate the damage per minute for each group in each sea state using the results from Step 3, material and S v N constants found in chapter 5 and chosen damage equation, in this case Palmgren-Miner's rule.

Group	SS 3	SS 4	SS 5	SS 6	SS 8
1	$D_{SS3,min}$	$D_{SS4,min}$	$D_{SS5,min}$	$D_{SS6,min}$	$D_{SS8,min}$
m	$D_{SS3,min}$	$D_{SS4,min}$	$D_{SS5,min}$	$D_{SS6,min}$	$D_{SS8,min}$

Step 5: Simulate damage per minute for sea states 0 – 2, 7 and 9 – 12 for each group using the results from Step 4.

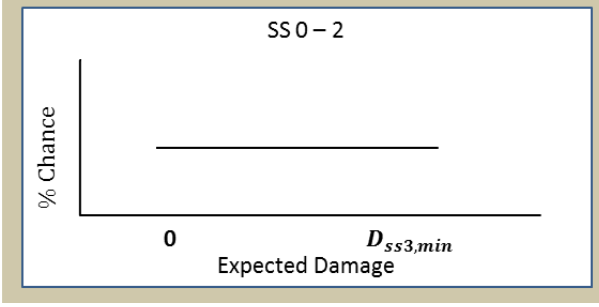

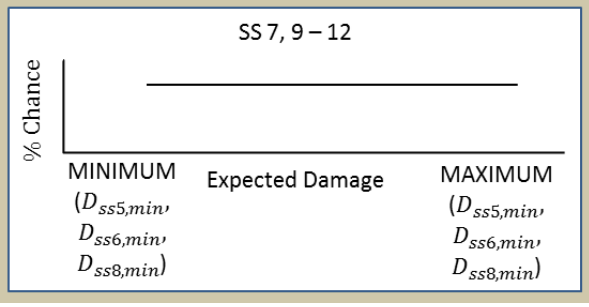

Figure 7-1: Part 1 of the walk through for 1 iteration of the simulation model developed to determine a value of the Severn life expectation from the data gathered in the preceding chapters.

Simulation Model Walk Through Part 2

Step 6: From error distributions identified in Chapter 6, for specific sea states where available and average distribution where not, simulate an expected error for each sea state.

Declared Sea State	1	2 … 11	12
Simulated Error	± Err_{SS1}	± $Err_{SS2\ \ldots 11}$	± Err_{SS12}

Step 7: Modify declared sea state by simulated error and select damage per cycle value based on the resulting sea state value:

Declared Sea State	Example Error	Example Resultant Sea State
3	-1	2
4	1	5
5	2	7
6	-2	4

Damage Selection

Sea State	Damage per minute
2	D_{ss2}
3	D_{ss3}
4	D_{ss4}
5	D_{ss5}
6	D_{ss6}
7	D_{ss7}
8	D_{ss8}

The resultant output is the simulated damage per minute for each sea state declared for that particular iteration.

Step 8: Multiply the results from step 6 by the proportional amount of time spent in each sea state for the chosen lifeboat as determined in Chapter 6.

Declared Sea State	Selected Damage per minute	Proportion of time spent in declared sea state	Proportional Damage per Minute
3	D_{ss2}	$\%T_{ss3}$	$D_{ss2} \times \%T_{ss3}$
4	D_{ss5}	$\%T_{ss4}$	$D_{ss5} \times \%T_{ss4}$
5	D_{ss7}	$\%T_{ss5}$	$D_{ss7} \times \%T_{ss5}$
6	D_{ss4}	$\%T_{ss6}$	$D_{ss4} \times \%T_{ss6}$
	Expected Damage Per Minute		Σ

Summing the proportional damage per minute for each of the declared sea states gives an output of expected damage per minute for the lifeboat under investigation for that particular iteration.

Step 9: Multiply the results from step 7 by the total time at sea (minutes) for the lifeboat selected to give the total damage experienced in that time period.

$$D_{Total} = D_{per\ min} \times T_{at\ sea}$$

Step 10: Determine the total life in years by dividing the number of years in service by the total damage simulated.

$$\text{Life}_{years} = \frac{Y_{served}}{D_{Total}}$$

Figure 7-2: Part 2 of the walk through for 1 iteration of the simulation model developed to determine a value of the Severn life expectation from the data gathered in the preceding chapters.

The number of cycles to failure, N, is then determined for each of the different applied stresses by rearranging Equation 7-2.

$$\frac{\sigma_{app}}{\sigma_{ult}} = C + M\log_{10}(N) \qquad \text{Equation 7-2}$$

Where σ_{ult} is a material constant and found in Table 5-9, C is the y axis crossing point and M is the gradient of the representative S - N curve the values of which are selected from the results of Error! Reference source not found. and Error! Reference source not found. shown in Table 4-19. The constants developed remain the same in each iteration of the Monte Carlo analysis.

Combining the calculated number of cycles to failure, N, for each applied stress value with the simulated value of applied cycles per minute, from step 3, allows an expected value of damage per minute to be determined for each stress level. This can be calculated using an appropriate fatigue damage calculation, in this case the applied damage rule used is the Miner's rule. This value changes for each iteration of the Monte Carlo analysis as the number of cycles at each applied stress will change as described in the third step.

Having calculated a value of damage per minute for the sea states where recorded strain data is available, rather than assuming no damage occurs for the remaining states the assumption is made that the damage will be similar to that experienced by similar sea states. This is accounted for in the **fifth step**. For sea states 0 – 2 a distribution of equal likelihood is generated using 0 as the minimum value and the expected damage per minute for sea state 3 as the maximum value and a unique value for the three unknown sea states generated from this distribution.

For sea states 7 and 9 – 12 there is a little more uncertainty as arguably there isn't an upper limit available. However it can be expected that as the size of the sea state increases the actions of the crew on board will reduce the likelihood of extreme events. However they are still likely to occur, due to the cumulative nature of fatigue, many small events which might be experienced in a lower sea state such as 4, 5 or 6 can be considered to have a similar total damage effect as few large events such as those which might be expected in large sea states such as 10, 11 or 12. Therefore a distribution of equal likelihood is determined using the maximum and minimum values of damage per minute determined for sea states 5, 6 and 8 and a unique value for the 5 unknown sea states generated from this distribution. However this needs to be tested through further data acquisition.

Having determined an expected value of damage per minute for the different sea states the next step is to apply the damage to the asset selected. The difference in weight from the measurement vessel has been accounted for in the lifeboat weight variation, α, but the different

operational experience needs to be accounted for. In chapter 6 the different boats are shown to have significantly varying operating conditions and a variation between the declared and actual sea state is found. The following steps take this into account.

The **sixth step** uses the error distributions determined in chapter 6 to pick an expected error in declared sea state for each of the different sea states where a distribution has been identified as shown in figure 6-32. Where there is no distribution identified the average distribution shown in figure 6-31 is used to determine the error. For each iteration of the Monte Carlo analysis a value of the expected error is chosen.

In the **seventh step** the value of the declared sea state (1 to 12) is modified by the sea state error identified in the sixth step, with the limit that the resultant sea state can never be less than 0 or more than 12. This is then used to choose the value of damage per minute identified as the result of steps 1 to 5. This results in an expected value of damage per minute for each of the 12 possible declared sea states. The value of damage selected to be applied to each declared sea state changes each iteration based on the error chosen in step six.

To determine the value of damage for the combined sea states requires summing the values of damage per minute identified for each sea state. However, through dimensional analysis it is easy to see that summing the values as they are would result in a value of damage per 12 minute interval, not per minute. To account for this in **step eight** the normalised proportion of time the asset spends in anyone sea state, as discussed in section 6.1 is multiplied by the value of damage for that sea state resulting in an expected proportion of damage per minute for that sea state. Summing these values for each sea state results in a single value for expected damage per minute for the vessel under investigation.

To turn this into an expected value of damage for the vessel based on its historical use **step nine** multiplies the value from step eight with the total time at sea. To turn this into a total expected service life, the assumption is made that the average operating profile used to generate the damage per minute for the particular vessel will remain close enough to future operating profiles. In which case the total service life is then calculated using Equation 7-3 which is the final step, **step ten**.

$$Total\ Life_{Years} = D_{Failure} / \frac{D_{Total}}{Service\ Life_{Years}}$$ Equation 7-3

Where:

- $D_{Failure}$ is a value which determines material failure
- D_{Total} is the total damage sustained during the service life in years

7.3.2 Results

The outputs for the method are a series of distributions of life, one for each group in each direction, for each of the four lifeboats selected for investigation. These graphs are summarised by three values in the table below. The first value is the 95% Confidence value, the second the mean and the last the 5% Confidence value. For maximum conservatism the 95% confidence value should be used, however by reporting this value only, the spread of the data will be lost and an understanding of the potential life of the assets will not be possible. The panel groupings referred to in the table below can be found in Table 6-7, but as a reminder for the life predictions based on longitudinal strains groups 1 to 3 contain panels in the engine room and groups 4 to 7 panels in the survivors space. For the life predictions made from the transverse strain recordings groups 1 to 5 contain panels from the engine room and 6 to 9 those from the survivors space.

Firstly taking the most conservative figure that of 95% confidence and assuming that the lowest value of life prediction represents the limiting state, in all boats assessed the boats can already have considered to fail. This is because group 5 in the transverse direction returns a life prediction value of 1 to 2 years as can be seen in Table 7-12, Table 7-14, Table 7-16 and Table 7-18.

Looking at the spread for this particular panel grouping it can be seen that for:

- ON1216 there is a spread in life of 8 years, from a lower limit of 1, with a mean at 3.
- ON1221 and ON1248 there is a spread in life of 8 years, from a lower limit of 1, with a mean at 4.
- ON1279 there is a spread in life of 12 years, from a lower limit of 2, with a mean at 6.

Considering now the best case scenario which is presented by group 9 at a 5% confidence level the boats could be expected to last anything from 92 to 148 years. Considering the spread for these values it can be seen that for:

- ON1216 there is a spread in life of 70 years, from an upper limit of 95, with a mean at 50.

- ON1221 there is a spread in life of 83 years, from an upper limit of 110, with a mean at 55.
- ON1248 there is a spread in life of 93 years, from an upper limit of 123, with a mean at 62.
- ON1279 there is a spread in life of 115 years, from an upper limit of 148, with a mean at 71.

Comparing these results to those from the previous sections there is a certain amount of consistency with these results falling below the upper boundary in Table 7-9 of 294 years but also below the boundary set in Table 7-5 of just under 19 years. However as discussed in the previous section it is difficult to believe the lower values due to the evidence of 45 Severn class lifeboats, all of whom have conducted sea time in excess of that accounted for in this analysis, still being used operationally on a regular basis with little or no cause for concern over the structure of the vessel.

Table 7-11: Predicted lifetimes based on the methodology applied in Figure 7-1 and Figure 7-2 using the longitudinally measured strains for ON1216.

Panel Group	Mean lifetime value (Years)	95% Confidence (Years)	5% Confidence (Years)
1	16	5	35
2	44	25	74
3	17	11	26
4	46	34	63
5	47	33	66
6	46	30	69
7	52	30	82

Table 7-12: Predicted lifetimes based on the methodology applied in Figure 7-1 and Figure 7-2 using the transversely measured strains for ON1216.

Panel Group	Mean lifetime value (Years)	95% Confidence (Years)	5% Confidence (Years)
1	16	8	26
2	16	10	23
3	13	11	17
4	10	7	12
5	3	1	9
6	38	19	71
7	30	18	49
8	30	16	53
9	50	25	95

Table 7-13: Predicted lifetimes based on the methodology applied in Figure 7-1 and Figure 7-2 using the longitudinally measured strains for ON1221.

Panel Group	Mean lifetime value (Years)	95% Confidence (Years)	5% Confidence (Years)
1	28	15	50
2	50	29	83
3	20	13	29
4	53	39	72
5	53	38	73
6	51	34	77
7	59	36	92

Table 7-14: Predicted lifetimes based on the methodology applied in Figure 7-1 and Figure 7-2 using the transversely measured strains for ON1221.

Panel Group	Mean lifetime value (Years)	95% Confidence (Years)	5% Confidence (Years)
1	18	10	29
2	19	12	26
3	15	13	19
4	11	9	15
5	4	1	9
6	42	21	82
7	34	21	55
8	34	19	59
9	55	27	110

Table 7-15: Predicted lifetimes based on the methodology applied in Figure 7-1 and Figure 7-2 using the longitudinally measured strains for ON1248.

Panel Group	Mean lifetime value (Years)	95% Confidence (Years)	5% Confidence (Years)
1	33	18	58
2	57	36	88
3	23	15	34
4	61	46	80
5	63	46	87
6	63	44	92
7	70	43	107

Table 7-16: Predicted lifetimes based on the methodology applied in Figure 7-1 and Figure 7-2 using the transversely measured strains for ON1248.

Panel Group	Mean lifetime value (Years)	95% Confidence (Years)	5% Confidence (Years)
1	21	12	34
2	22	15	31
3	18	15	21
4	13	10	16
5	4	1	9
6	49	25	92
7	39	25	60
8	39	23	67
9	62	30	123

Table 7-17: Predicted lifetimes based on the methodology applied in Figure 7-1 and Figure 7-2 using the longitudinally measured strains for ON1279.

Panel Group	Mean lifetime value (Years)	95% Confidence (Years)	5% Confidence (Years)
1	34	18	61
2	65	34	113
3	25	15	41
4	64	46	90
5	65	45	96
6	58	36	90
7	72	40	125

Table 7-18: Predicted lifetimes based on the methodology applied in Figure 7-1 and Figure 7-2 using the transversely measured strains for ON1279.

Panel Group	Mean lifetime value (Years)	95% Confidence (Years)	5% Confidence (Years)
1	22	12	38
2	23	15	34
3	19	15	25
4	14	10	19
5	6	2	14
6	54	23	109
7	43	24	80
8	41	20	78
9	71	33	148

7.3.3 Discussion

The biggest cause for discussion is the exceptionally low value of expected life in some areas of the vessel, specifically those panels that are contained within group 5 of the transverse strain measurement. The biggest problem with this, as mentioned in the previous section, is that there are Severn class lifeboats which were built in the late 1990's which have performed extremely well on the coast for the whole of their lives and are continuing to do so until this day. The crew's trust them and the evidence of the strength of the structure is well documented with the grounding of the Port Rush Severn class lifeboat in 2008 (Harman et al., 2011). Although the Port Rush incident does not directly demonstrate the resistance to fatigue failure it does illustrate the strength of these vessels and therefore an expected long service life. In addition to this structural non-destructive testing in the form of shearography has been being carried out on the vessel topsides for some years now. Although disbands have been being found these are generally either found to have been either defects at build or caused by serious collisions. Additionally the shearography has found that no areas of delamination have grown significantly in the time period before repairs could be carried out.

Considering this, the source of the uncertainty must come in the form of the measured strains and the limits applied in determining what actually consists of a stress which generates fatigue induced damage. Nominally, until proven otherwise, it must be considered that all applied loads contribute in some way to fatigue damage of a material. As discussed in section 6.4, In the work

conducted by Clark et al (1999) it was considered that the minimum applied load which would cause a fatiguing stress was an applied pressure of 8 KPa, this was converted into a plate stress of just over 0.5 N/mm^2 using a method proposed by Sobey et al (2009)**.** It was this which prompted the decision to define the bin size as 50με in chapter 6, as using the young's modulus in the [0] direction as defined in chapter 5 resulted in an applied stress of 0.76N/mm^2.

However, there is evidence (Cavatorta, 2007) that below values of up to 20% of the ultimate failure strength there is unlikely to be noticeable fatigue up to 10^6 cycles. For the materials used in this investigation this equates to an applied stress of 33.4 N/mm^2 in the [0] direction and between 80.5 N/mm^2 in the [90] direction. Converting from stress into strain using the Young's modulus equation as there is no way of determining the proportion of stress due to bending and membrane forces, and using the modulus values from section 4.3, this would result in an applied strain of between 2408με in the longitudinal direction and between 2349με in the transverse measured direction.

Therefore if the materials were considered to have no significant fatigue response below 20% of the applied maximum strain, strains below this limit would not be counted in the fatiguing cycles. Considering the implication now that as discovered in section 6.5.2 between 79 and 99% of all cycles encountered across all panels were in the strain range between 50 με and 150με it can be considered the current results are extremely conservative and a further investigation into the material characterisation to identify the fatigue limit of the materials used should be conducted. If a fatigue limit is found then all measured strains below this limit can be disregarded. Such an analysis cannot be conducted through the data gathered from this investigation.

An alternative option is that in the areas covered by panel grouping number 5 there has indeed been material failure, it is just that this failure has not been catastrophic in any way. This is possible if you consider the fatigue failure mode of the flexural samples, which had minimal visual damage on the material surface at the lowest loads, but had failed through delamination within the samples. If this type of failure mode was occurring within the hull structure it would result in voids within the laminate in the aramid fibre layers. However without significant structural investigation it would be very difficult to prove if this is the case or not.

Even if it was the case, it would seem that the resulting voids within the structure are not affecting the operation of the lifeboats unduly. However the growth of these voids may eventually lead to serious structural instability although further postulation is not possible from the evidence generated in this report.

7.3.4 Summary

In this section a method has been developed which is then applied using the data gathered from chapters 4 and 5. The results are extremely conservative with the lower bound being just one year and the upper bound being in the region of 150 years.

The lower boundary for expected life is not considered to be realistic due to the 45 examples of Severn class lifeboats being used all over the coast of the UK in some of the most extreme conditions imaginable, all being over 1 year old. Additionally between 79% and 99% of all cycles recorded across all panels represent values of less than 10% of a strain which can be reasonably expected to cause fatigue damage (assuming a fatigue limit of 20% ultimate strength). These two points together suggest that further material investigations are required to determine the fatigue limit for the materials used, remove all cycles below this limit from the investigation and re-evaluate using the same method.

7.4 Summary

In this chapter two methods for the final structural life assessment are investigated. The first, used in sections 7.1 and 7.2 are directly comparable to that used by Clark and Shenoi (1998) and is based on a simple table of applied loads. The results from this were variable resulting in an expected life of between 8 and 300 years from modelled constants applied in 7.1, and just under 20 years to over 30 Millenia in 7.2 using the loading profile from Clark and Shenoi (1998) but applying material constants generated in chapter 4. However there were limitations in the application of this model in that the loading profile did not fit easily into any of the possible operating environments encountered by the RNLI's lifeboats.

The second method sought to address this and applied the definitions of sea sate as defined by the RNLI operationally, namely the 12 stages in the Beaufort scale and used the results from structural monitoring to determine fatigue spectra for these sea states. The sea states for which structural monitoring data was available was limited to Beaufort numbers 3 to 6 and 8. To address this, and to take into account the potential error in defining sea states identified in chapter 6 Monte Carlo analysis was used to fill the gaps in the data as described in Figure 7-1 and Figure 7-2.

However the results were not considered realistic considering the evidence of 45 Severn class lifeboats operating around the shores of Great Britain, all exceeding the lower limit representing 95% confidence in the output. Reasons for this are suggested and a further material characterisation focusing on identifying the fatigue limit for the materials used in the construction

of the Severn class lifeboat is suggested to address the unrealistic results. Figure 7-3 shows the data sources and outputs of the completed methodology.

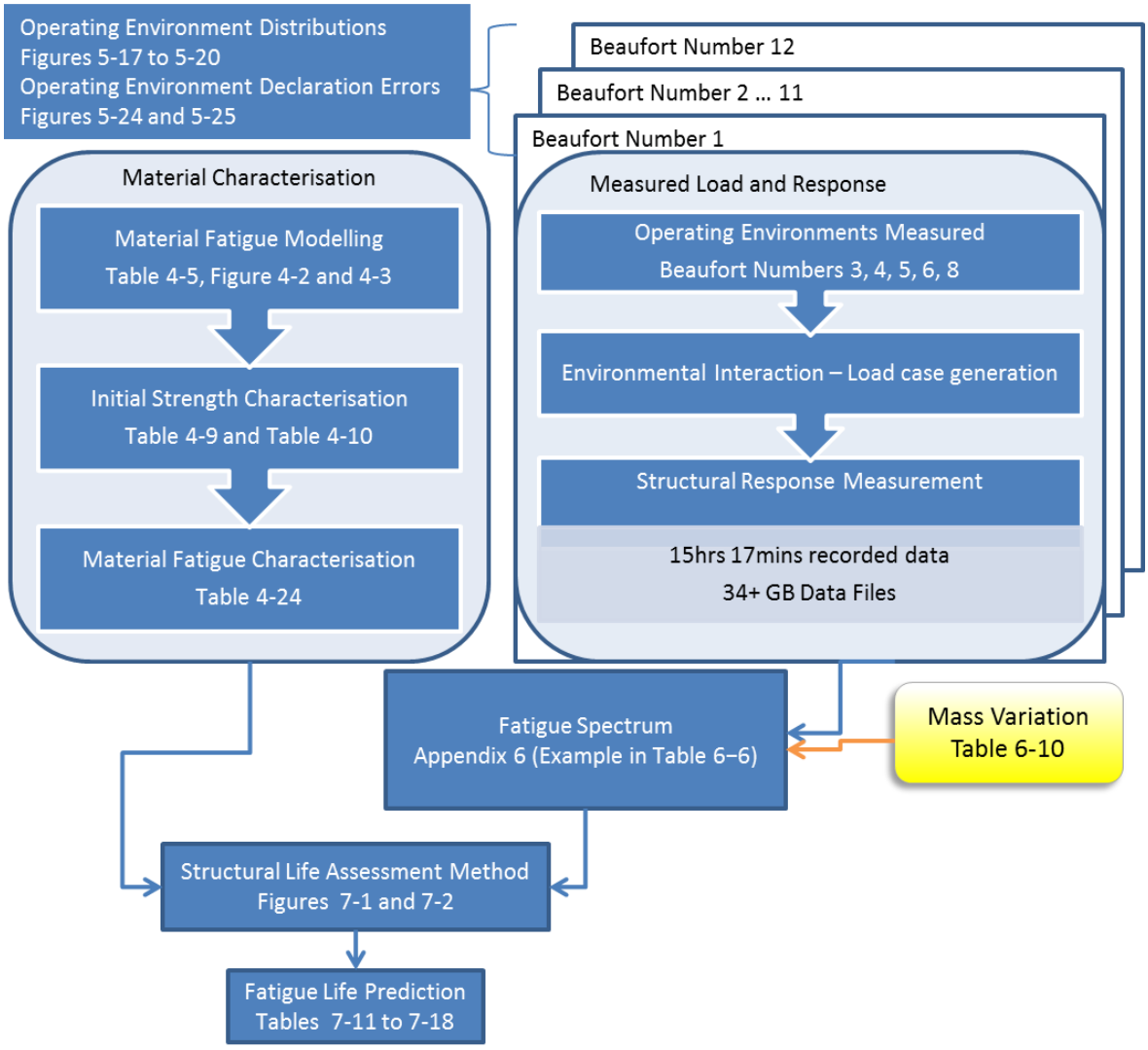

Figure 7-3: Areas identified within the methodology that are addressed within the thesis.

8 Discussion

In chapter 3, a methodology to investigate degradation due to fatigue was proposed as this was considered the most pressing of all the potential investigations identified from the literature review. Three variables were suggested as being important to understand when developing an understanding for fatigue of a structure:

1. What events cause fatigue response within the structure, a collection of these events is defined as a fatigue spectrum?
2. What aspects will cause modifications to these events?
3. How much damage is likely to be imparted by the different events?

Figure 3-1 shows the process undertaken in this thesis to address these three points. In Chapter 4 the question "How much damage is likely to be imparted by the different events?" is answered. This is achieved by modelling the material engineering constants initially before carrying out fatigue testing to confirm the results of the modelling.

The material constants were modelled using a simple rule of mixtures calculation and classical laminate theory. Due to the unavailability of original material for fatigue testing, a replicate had to be created. An initial comparison between the layup used during the original build and the proposed material found some slight differences between the two with the most significant being in the longitudinal boat direction. Material tests were conducted for comparison to the modelled constants, the results of the tensile tests are shown in Table 4-8 and the results of the flexural tests in Table 4-9 to Table 4-12. Comparing the predicted material constants to the tested values found that for $E_{[0]}$ the tested values fell between the values predicted for the original and replicate laminate, for $E_{[90]}$ it was found that the tested values were larger than predicted for both the original and replicate laminates. Both of the preceding statements were also found to be true for the flexural tests. The average failure stress was used to determine the ultimate value for use in the fatigue tests. Comparison of the standard deviation of the tests conducted and for other tests within literature showed similarities and therefore improved confidence in the results of the tests carried out in this work.

To model the material fatigue diagram a data trawl through published literature was conducted and appropriate fatigue data was collected from papers shown in Table 2-8. The resulting S-N curves are shown in Figure 4-16 to Figure 4-19 and equations 4-18 to 4-20 provide the values of linear regression line for comparison to the results from testing. To test the applicability of these curves to the material in question fatigue tests were carried out on representative material. Ultimate tensile and flexural strength tests were carried out on coupons to produce S-N curves for

comparison to those modelled with the results of these tests are shown in Table 4-16 for tensile fatigue and Table 4-17 and Table 4-18 for the flexural fatigue results. A comparison of the modelled fatigue life diagrams and the resulting diagrams from the testing is made in Table 4-19 and Figure 4-32, which also includes results from a similar study carried out in the literature. The general conclusion was drawn that the test data fitted well around the linear regression line shown in Figure 4-17, therefore using the lower 95% confidence boundary limit from this figure to provide an estimate of cycles to failure in the design stage would provide a suitably conservative estimate for life at the design stage. However where actual material fatigue life data is available this will provide a more realistic life prediction as shown in Figure 4-32. The areas of the methodology addressed in chapter 4 are highlighted in Figure 4-33 which shows how the data will be used in combination with the data from chapter 5 and 6 in chapter 8 to determine the fatigue life of the structure.

Having determined the material fatigue characteristics the next step required understanding the size and number of damaging events seen by the structure. Based on the assumption that the damage is directly related to the size of the structural strains and therefore stresses experienced, and that these strains are the result of loads imposed by the operating environment, understanding how the operating environment is defined and then measuring the structural strains within these different operating environments were decided to be the focus of this side of the investigation. For the Severn class lifeboat the operating environment was defined as the littoral waters around the UK, additionally the lifeboat crews are trained to use the Beaufort scale to determine variations in operating condition. This scale then provided 12 possible different operating conditions the vessels could be subjected to. These 12 different options were used to determine the fatigue spectrum to use as defined in chapter 7.

Once the different operating conditions had been defined discovering how much time was spent in each of these different conditions for the different lifeboats became important. Figure 5-3 shows that taking into account all services conducted by Severn class lifeboats there is a bias towards the lower end of the sea state spectrum, with sea states 3 and 4 containing the largest amount of time spent at sea in total. From this an average total time at sea was determined to be 42 hours 9 minutes, however once the variation of services between lifeboats was taken into account (Figure 5-5 and Figure 5-6) it was found that just over a quarter of the fleet's yearly service averages do not fall within 1 standard deviation of 42 hours and 9 minutes. This was considered an unnecessary compromise and therefore a selection of vessels were chosen which represented the lifeboats that were most, least and closest to average use thus providing bounding and average times at sea to be used in the life prediction. As well as the range of

average yearly time at sea for the different vessels, the distribution of this time at sea across the different Beaufort states also varies from vessel to vessel as is seen in Figure 5-16 to Figure 5-19. Thus to provide a good estimate of the average time at sea and service profile per year for each individual vessel, it is not enough to use the fleet average data, but the data available for that individual vessel.

The previous analysis is only as accurate as the accounts of the crews at sea at the time. To test the accuracy of the crews at sea a comparison between the crew stated sea state and the measured wave height, by a wave buoy in the near vicinity, was made. The results of the comparison for Severn class lifeboats are shown in Figure 5-22. It was found that 36% of the time the crew were accurate, and over or under predicting the sea state by 1 27% and 22% of the time respectively and an over or under prediction by 2 to 3 sea states making up the final 15%. However the difference between sea states is not constant in terms of the wave height, therefore a misrepresentation at a low sea state will have less of an impact on the attempt to assess lifetime than one at a higher sea state. Therefore distributions of error expectation for each of the sea states were made where data was readily available, Figure 5-25.

This piece of work provides the environmental boundaries which are to be used in the structural life assessment model. These boundaries take into account the differences in both yearly average time at sea and distribution of time across the Beaufort numbers according to the lifeboat crews. Additionally an assessment is made of the likely correlation between the sea state declared by the crew and the actual sea state as recorded by wave buoys. These bits of information used together will allow the life assessment model to provide a range of expected lifetimes for the Severn lifeboat when combined with the structural response modelling results.

Having developed an understanding of the fatigue characteristics of the materials used in the structure, and understood the operating environment definition in terms of Beaufort number and the distributions time spent in each of the different cases, structural monitoring was used to investigate the strain, these values were then converted to stress using the basic youngs modulus equation as there was no way of determining what proportion of the measured strains were as a result of applied bending moments, and would therefore result in bending stresses, or tensile forces, producing membrane stresses. Therefore the stress calculated from the measured strains using the young's modulus equation were considered a composite of the bending and membrane stresses, which makes up the fatigue cycles. A very simple experimental methodology was employed that involved identifying different panels for measurement, mounting strain gauges and recording the strain experienced during routine operations in the different operating

environments. Once the measured strains had been verified power spectra were developed for the different data sets. This analysis revealed that different frequency responses were evident between panels in different compartments within the boat and for the same panel in different sea states, but that there was enough consistency between gauges within the same compartment to ensure confidence in the results.

To convert the strain traces into a format that could be used for a life prediction, a rainflow cycle counting algorithm was carried out on the data for each of the different panels in both the transverse and longitudinal strain directions. The analysis was conducted using a bin size of 50με which resulted in a different number of bins depending on the size of the maximum strain event seen for a particular panel strain trace in a particular run, however it did mean that the bin sizes were consistent for all runs. Analysis of the number of cycles counted by the rainflow analysis revealed that in all cases the vast majority of the cycles were at the lowest strains, however when panels of similar dimensions were compared there were some significant differences found.

An explanation for these differences is that the global response of the structure has a significant influence on the panel strain state, however this has not been tested. This was considered to be a function of the direction of the sea way in relation to the vessel and under different conditions the same sea state could produce a different strain state within the panels. Under this assumption, the measured strain state is just one of a multitude of potential strain states for the same sea state, but varied by other parameters that were uncontrollable during the tests. Therefore it is conceivable that panels with similar characteristics could be subjected to any strain response measured by other panels with similar characteristics. To allow for this, panels were grouped together based on 5 criteria and then the distributions of measured strains for each panel combined to generate a distribution that represents the average panel within that group. Table 6-7 shows the resultant panel grouping and identifies 7 groups when considering longitudinal strains and 9 groups when considering transverse strains. The analysis so far takes account of variations between the different panels, however in this case we are also concerned in the differences between vessels within the fleet. Nominally the Severn class lifeboats are identical, however there is a significant weight variation between them. This is taken into account by multiplying the applied strains by a value determined by normalising the weight of the vessel of interest by the weight of the vessel the measurement took place on.

Finally a structural life assessment methodology was developed which combined the results of the preceding pieces of work as shown in Figure 7-1 and Figure 7-2. But to show the impact of the different pieces of work life predictions were made based on the data available prior to this

research. The first life prediction was made using data from Roberton et al (2009) and provided an initial assessment typical of one which might be considered during the design stage of an asset. This was then modified based on the materials data generated in chapter 4 and the results of the inclusion of all available data are shown in Table 7-8, Table 7-9 and Table 7-10. There was shown to be a large increase in expected life based on this data which can be explained by the vast reduction in scatter of the fatigue diagrams used in the generation of the results and therefore reduced width of the 95% confidence interval.

Due to the representation of the fatigue spectrum used in these calculations, there was no way to determine how they may match with to the operational environments distributions developed so the operating environment and structural monitoring work was accounted for in the same analysis. This analysis consisted of a 10 step simulation model with each step taking place during one iteration of a Monte Carlo analysis. The results of this analysis produced a large variation of life expectation for the panels as shown in Table 7-11 to Table 7-18, but importantly a large reduction in expected life compared to the results in the previous analysis. This reduction in fatigue life is caused by the lack of endurance limit found during the material investigation work meaning not even the smallest of cycles can be dismissed as not damaging. If a fatigue endurance limit for these materials was to be found that would enable a proportion of the recorded cycles to be dismissed and therefore a reduction in estimated damage can be expected.

Intentionally left blank

9 Conclusion

The RNLI has an interest in life extending its fleet of Severn class lifeboats from a design lifetime of 25 years to an expected lifetime of 50 years. As was identified in the Literature Review, life extension of high value assets is an area of industry lead investigation, containing many facets, which are complex and often conflicting. However it is clear that the most fundamental result required for life extension is that the structure can be expected to last the required amount of time.

Thus the focus of this thesis was to generate a structural life expectancy for the RNLI's fleet of Severn class lifeboats. The process developed to achieve this is shown schematically in Figure 3-1 and involved; generating an understanding of the material strength and fatigue characteristics, defining and understanding the asset operating environments, generating a fatigue spectrum for the asset and then developing a method which can bring these very different sources of information together to produce a used life prediction. From this, and under the assumption an average year can be generated from the operationally gathered data, a total life prediction can be made.

The life expectancy determined for the different panel groups ranged from a minimum of 1 year, considered unrealistically conservative since there are lifeboats in service without issue that are nearly 20 years old, to a maximum of 148 years. The reason for the extreme conservatism was that no fatigue limit for the materials in question was identified during the material characterisation process. This meant all cycles identified as a result of the structural response monitoring had to be taken into account in the fatigue spectrum. Further analysis identified that if there was a fatigue limit at 20% of the ultimate tensile strength then any strains below a value in the region of 2000με could be dismissed. Considering that between 79% and 99% of all recorded strain values were in the region of between 50με and 150με, determining this fatigue limit will instantly reduce the conservatism and provide a more realistic result.

Intentionally left blank

10 Future Work

As identified in section 2.7 there are 4 further areas of investigation to complete based on the state of the art from the literature review. These are

1. The structural loading of semi planing craft for application to fatigue load prediction.
2. Understanding the structural response for application to fatigue life prediction.
3. The description of the waters around the coastal regions of the UK which are affected by significant changes in local topology.
4. The development of a methodology to address the holistic aspects of life extension such as maintenance, economics, systems and management methods.

By completing these investigations a method will be made available which can be used throughout an assets lifetime. Using state of the art modelling (investigations 1 and 2) at the design stage to predict an assets life based on assumed operational requirements, following the approach in chapter 4 to confirm material properties and applying the methods from chapter 5 (modified by the result of investigation 3) to 7 over the lifetime of the boat to continuously update the expected structural life. Combining this with a methodology designed to account for the more holistic aspects of life extension (investigation 4) would allow decision makers to have up to date information on expected life of the structure, current costs, maintenance burdens and other important criteria from which they can decide between life extension, purchase new or any other option available to fulfil operational requirements.

In addition to this work carried out in this thesis identified further areas of research which should be pursued. The material characterisation section focused on understanding the fatigue characteristics of the materials used. But in reality the environment that the structure sits in, sea water, may have an effect on these properties. Further work should be undertaken to ensure the fatigue characteristics are not modified by the sea water in a way which will mean the results of the material characterisation chapter are non-conservative. Also within the realm of materials characterisation would be identifying a fatigue limit for the materials. This would enable a minimum stress and therefore strain level to be identified below which structural responses could be dismissed. This would benefit the load and response monitoring analysis by potentially significantly reducing the memory requirements of the hardware and reducing the post processing time due to the reduced quantity of data.

One aspect which is outside the scope of this work, but would be interesting to pursue is the impact of individual waves there would be a wave encounter frequency where individual waves encountered can be identified, then attributed an interaction load or response value. If an individual wave type could be attributed to a specific strain response then over time a data base of wave profiles and responses could be built up. As technology improves so image processing could identify a wave type based on videos or other images and therefore expected strains and stresses applied to the asset from which the video came. Additionally the data base could be used for validation purposes of modelling techniques as they evolve and become more powerful.

11 Appendix

11.1 Material Characterisation Results

11.1.1 Ultimate Tensile Strength Results

Table 11-1: Specimen dimensions for the static tests. Specimens T-01 to T-10 are tensile and T-11 to T20 are Flexural samples. Mean values were calculated in blocks according to specimen orientation and test type

Specimen Name	Specimen Orientation	Average Width (mm)	Average Thickness (mm)	Thickness Diff. from mean (%)
T[0]-01	0	25.89	9.71	-2%
T[0]-02	0	25.91	9.59	-1%
T[0]-03	0	25.55	9.61	-1%
T[0]-04	0	25.66	9.77	-2%
T[0]-05*	0	25.79	9.93	-4%
T[90]-06	90	26.36	9.44	1%
T[90]-07	90	25.94	9.41	1%
T[90]-08	90	26.09	9.33	2%
T[90]-09*	90	25.91	9.23	3%
T[90]-10	90	25.91	9.36	2%

Table 11-2: Detailed results for tensile strength test results for the individual test coupons. *The maximum load and calculated strength values were not used to calculate the Standard Deviation or Coefficient due to known issues with the test resulting in premature test ending.

Sample Number	Max Load (kN)	Strength (Mpa)	Transverse Strain At 2500 με Longitudinal		Optical Strains for poisons ratio calculation	
			SG2 (με)	SG4 (με)	long (με)	trans (με)
T[0]-01	39.5	**157.1**	-505	-416	2306	-451
T[0]-02	39.3	**158.1**	-513	-420	1784	-231
T[0]-03	40.3	**164.1**	-500	-433	3738	-648
T[0]-04	33.3	**132.9**	-551	-442	3418	-455
T[0]-05	38.7	**151.0**	-549	-441	2291	-392
Average	**38.2**	**152.6**	**-524**	**-430**	**N/A**	**N/A**
Standard Deviation	**2.8**	**12.0**	**24.54**	**11.90**	**N/A**	**N/A**
Coeff of variation	**7%**	**8%**	**5%**	**3%**	**N/A**	**N/A**
T[90]-06	88.0	**353.8**	-804	-1015	3676	-1011
T[90]-07	86.3	**353.5**	-951	-1015	4102	-1237
T[90]-08*	83.4	**342.4**	-866	-1012	4292	-1152
T[90]-09	86.5	**361.7**	-890	-1012	3649	-1233
T[90]-10	87.1	**359.3**	-904	-1007	4380	-1287
Average	**87.0**	**357.1**	**-883.1**	**-1012.1**	**N/A**	**N/A**
Standard Deviation	**0.66**	**4.05**	**53.77**	**3.21**	**N/A**	**N/A**
Coeff of variation	**1%**	**1%**	**6%**	**0%**	**N/A**	**N/A**

Table 11-3: Detailed results for tensile strength test results for the individual test coupons.

Sample Number	Poissons Ratio, μ_b			Modulus		
	SG2 / SG1	SG4 / SG3	Trans / Long	SG1 (Gpa)	SG3 (Gpa)	Opt Long
T[0]-01	**-0.20**	**-0.17**	**-0.20**	**16.0**	**15.3**	**9.07**
T[0]-02	**-0.21**	**-0.17**	**-0.13**	**13.9**	**16.4**	**5.96**
T[0]-03	**-0.20**	**-0.17**	**-0.17**	**12.8**	**16.8**	**6.35**
T[0]-04	**-0.22**	**-0.18**	**-0.13**	**19.7**	**13.4**	**7.94**
T[0]-05	**-0.22**	**-0.18**	**-0.17**	**12.9**	**15.3**	**7.44**
Average	**-0.21**	**-0.17**	**-0.16**	**15.1**	**15.4**	**7**
Standard Deviation	**0.01**	**0.00**	**0.03**	**2.90**	**1.31**	**1.25**
Coeff of variation	**4%**	**3%**	**17%**	**17%**	**8%**	**17%**
T[90]-06	**-0.35**	**-0.41**	**-0.28**	**27.84**	**29.8**	**31.06**
T[90]-07	**-0.42**	**-0.41**	**-0.30**	**29.44**	**29.1**	**20.13**
T[90]-08*	**-0.36**	**-0.41**	**-0.27**	**29.18**	**29.8**	**17.15**
T[90]-09	**-0.38**	**-0.41**	**-0.34**	**29.75**	**29.4**	**20.10**
T[90]-10	**-0.41**	**-0.40**	**-0.29**	**29.09**	**29.2**	**17.76**
Average	**-0.38**	**-0.4**	**-0.3**	**29.06**	**29.4**	**21.2**
Standard Deviation	**0.03**	**0.00**	**0.03**	**0.73**	**0.32**	**5.65**
Coeff of variation	**6%**	**1%**	**9%**	**3%**	**1%**	**27%**

11.1.1.1 [0] Direction Individual Results

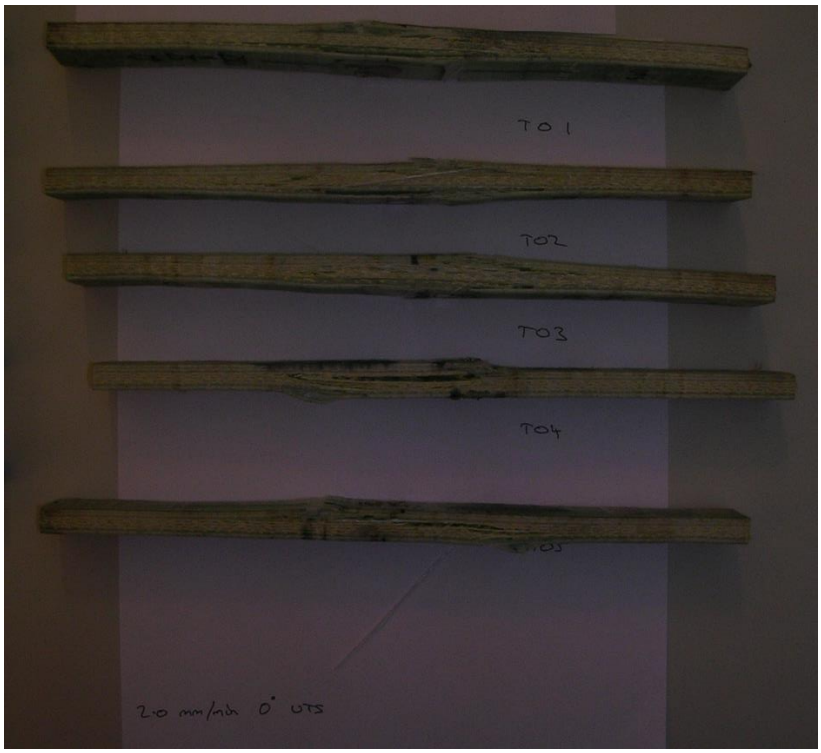

Figure 11-1: [0] direction ultimate tensile samples post failure.

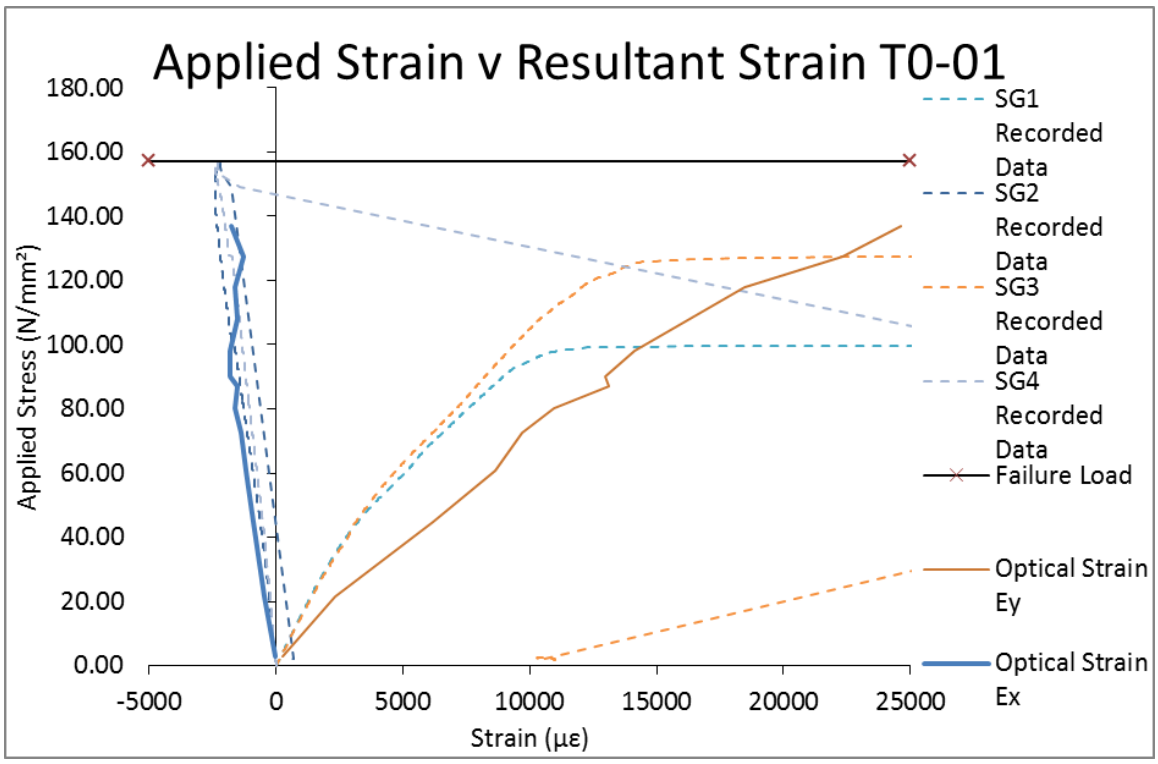

Figure 11-2: Strain gauge and optical strain measurement values for tensile test conducted on sample T[0]-01

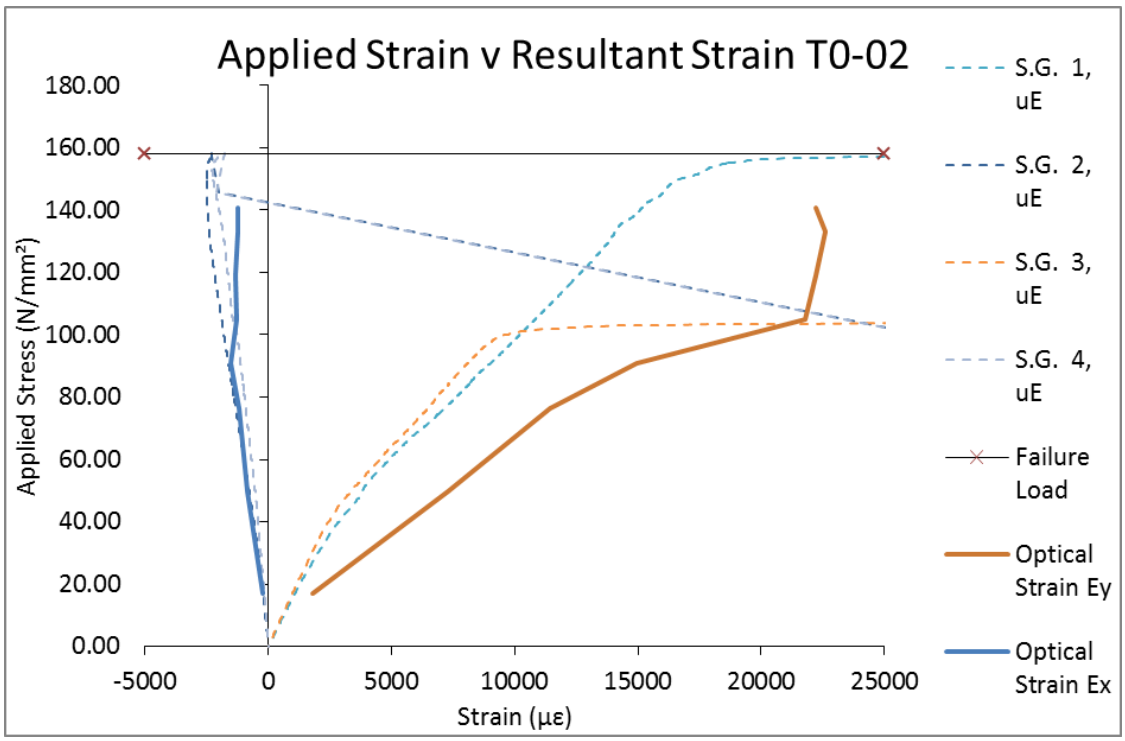

Figure 11-3: Strain gauge and optical strain measurement values for tensile test conducted on sample T[0]-02

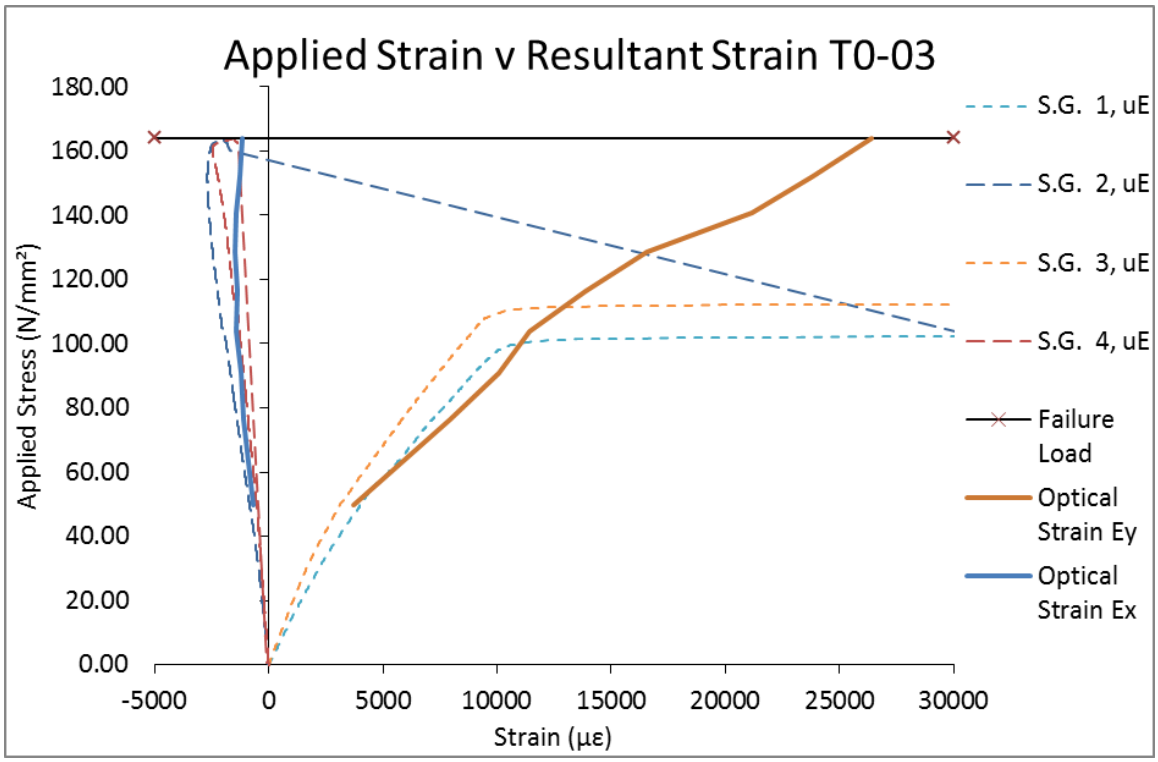

Figure 11-4: Strain gauge and optical strain measurement values for tensile test conducted on sample T[0]-03

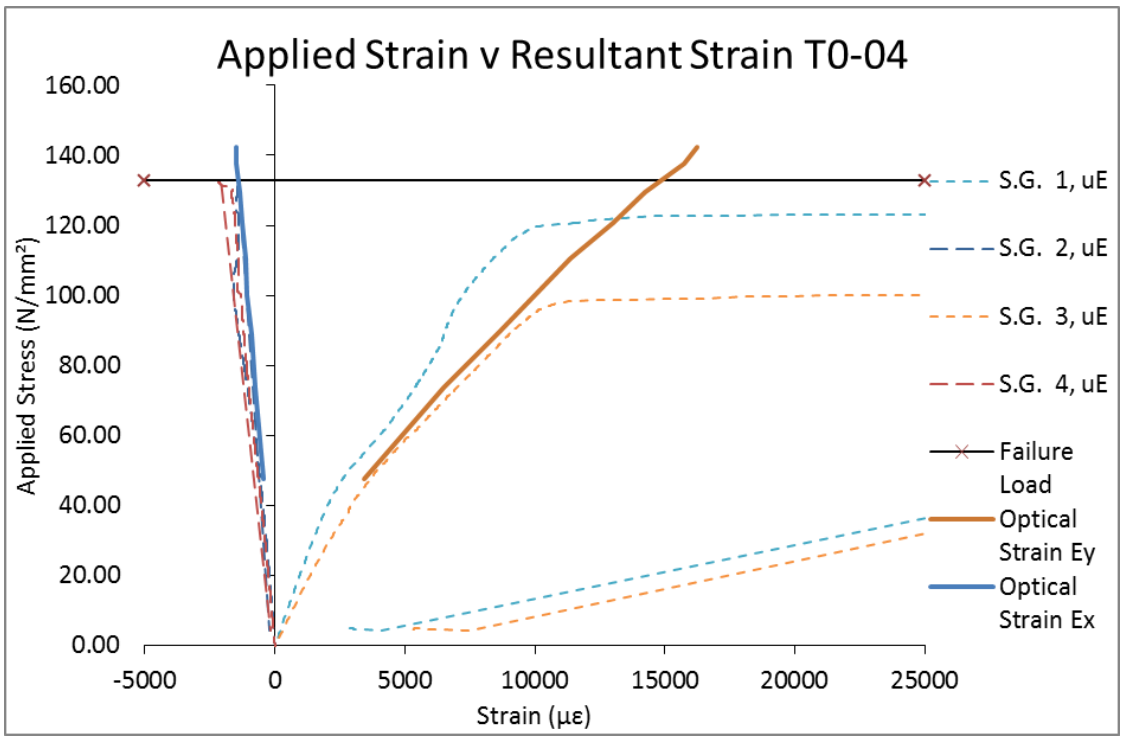

Figure 11-5: Strain gauge and optical strain measurement values for tensile test conducted on sample T[0]-04

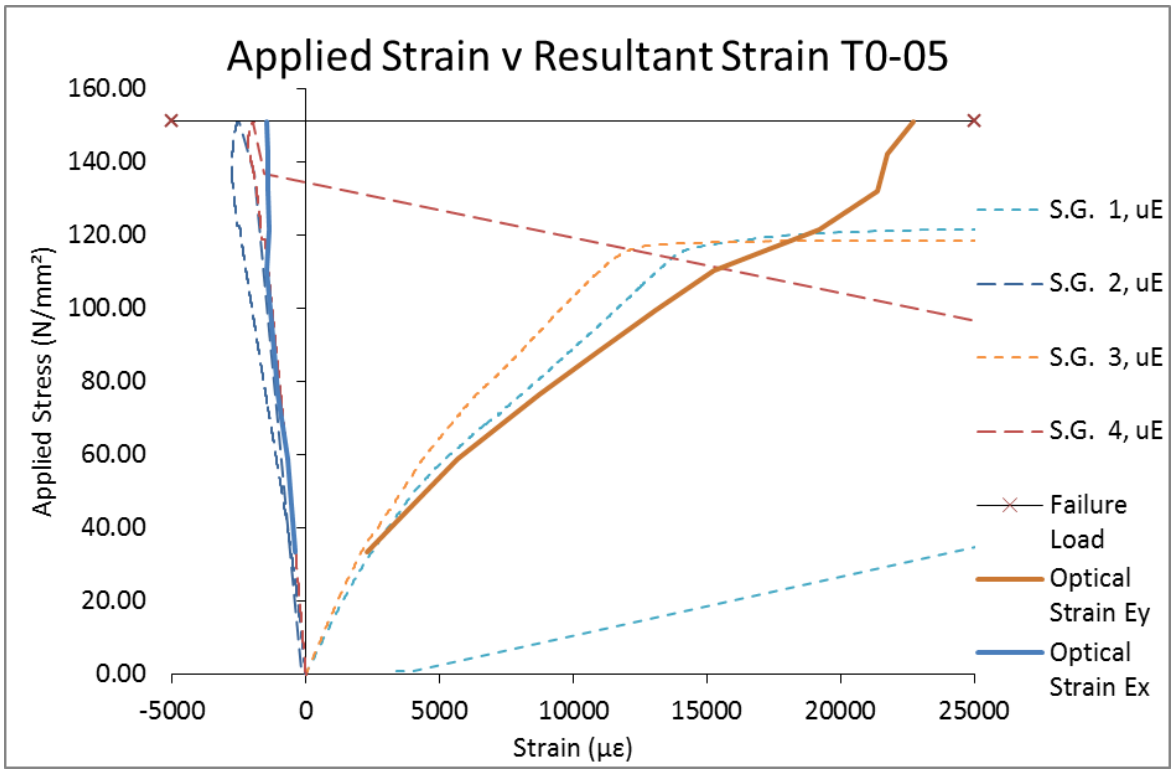

Figure 11-6: Strain gauge and optical strain measurement values for tensile test conducted on sample T[0]-05

11.1.1.2 [90] Direction Individual Results

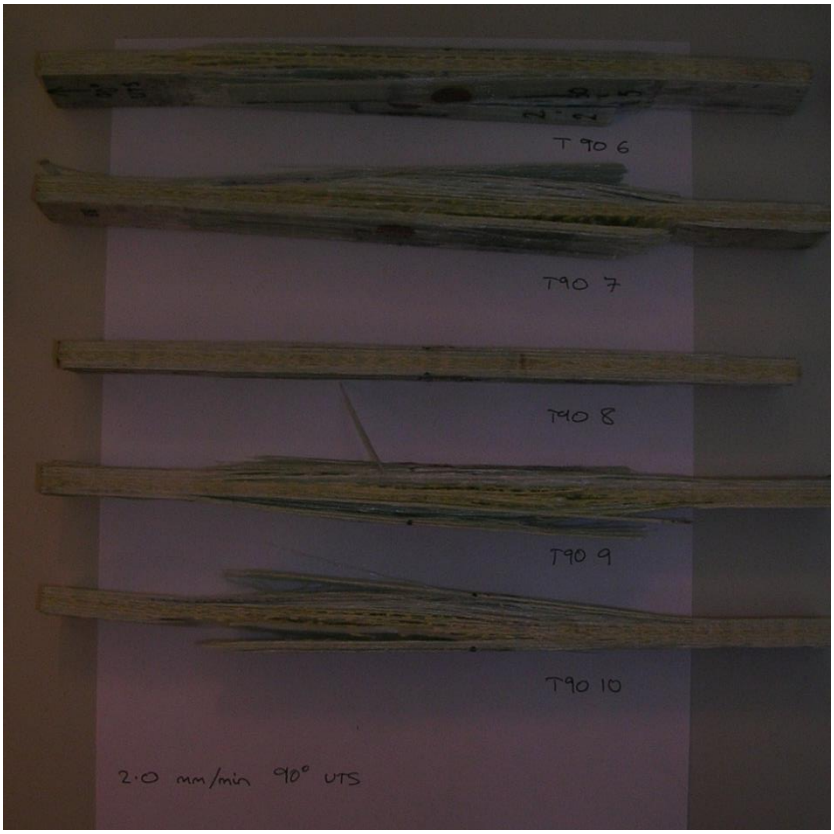

Figure 11-7: Final failure of ultimate tensile strength experiments.

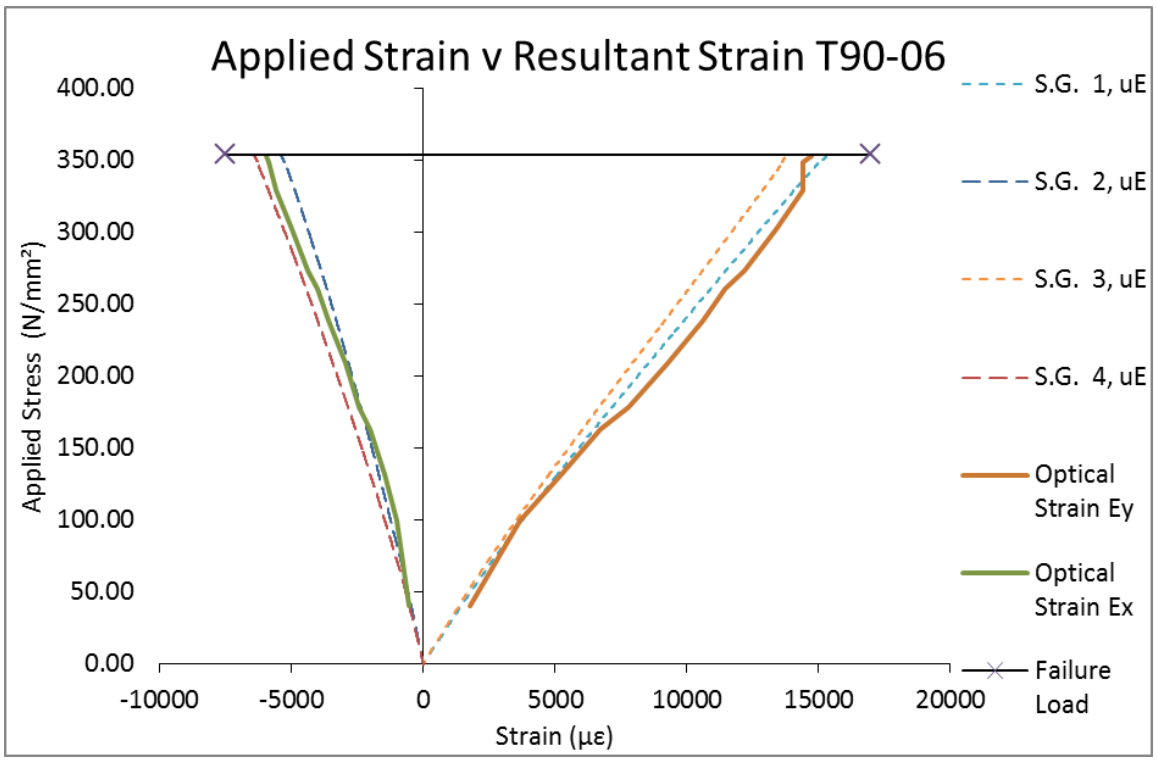

Figure 11-8: Strain gauge and optical strain measurement values for tensile test conducted on sample T[90]-06

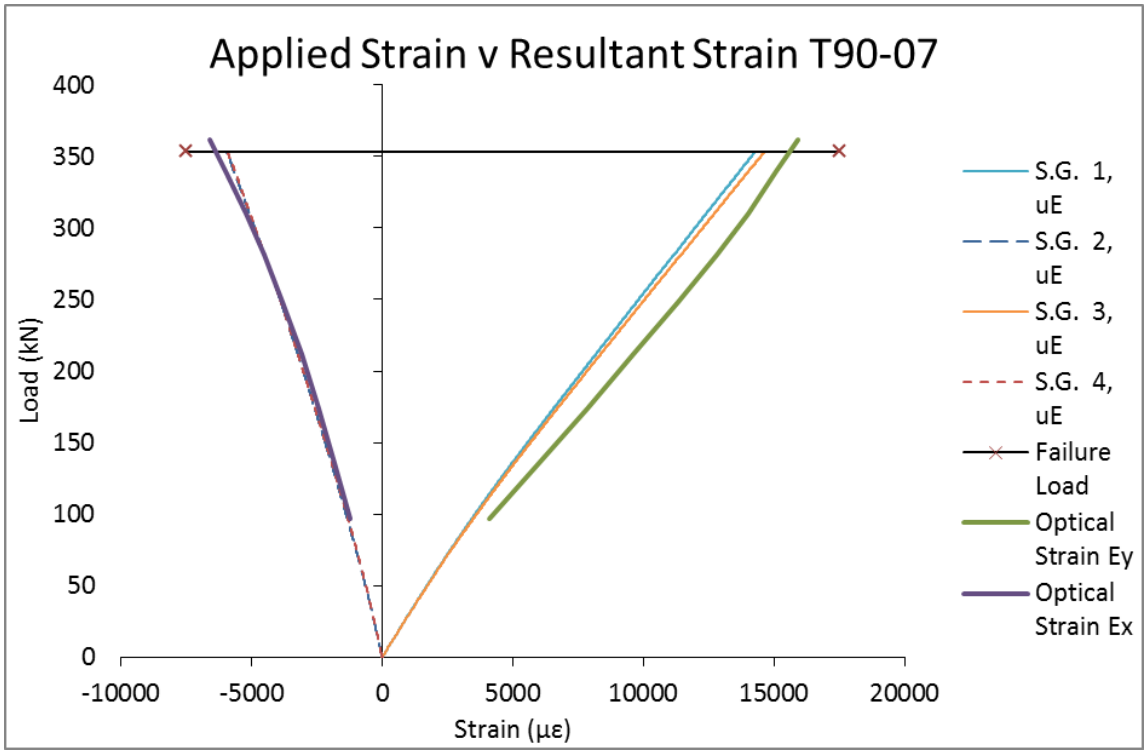

Figure 11-9: Strain gauge and optical strain measurement values for tensile test conducted on sample T[90]-07

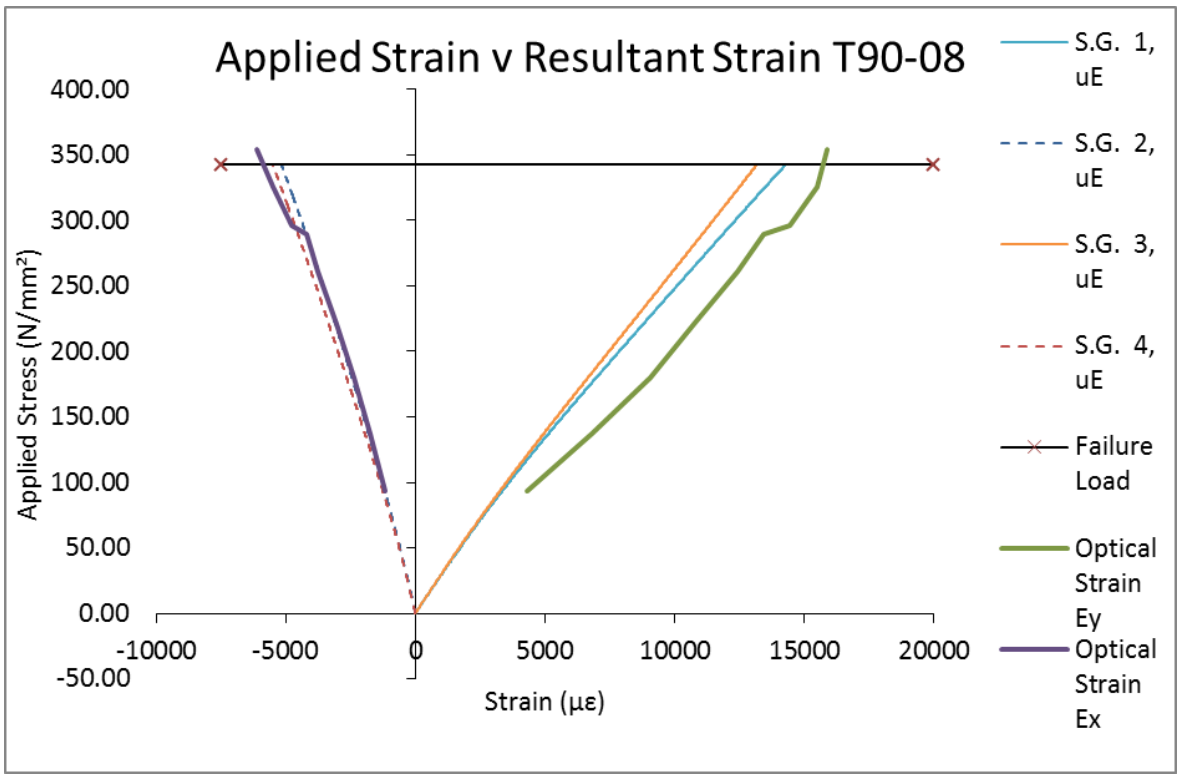

Figure 11-10: Strain gauge and optical strain measurement values for tensile test conducted on sample T[90]-08

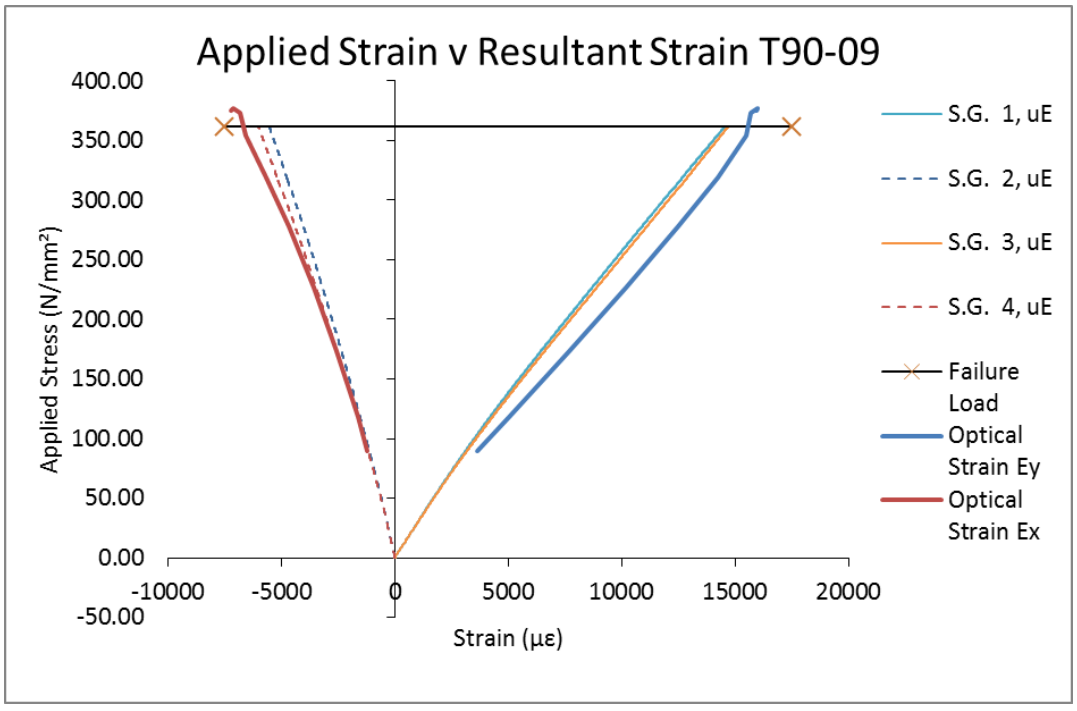

Figure 11-11: Strain gauge and optical strain measurement values for tensile test conducted on sample T[90]-09

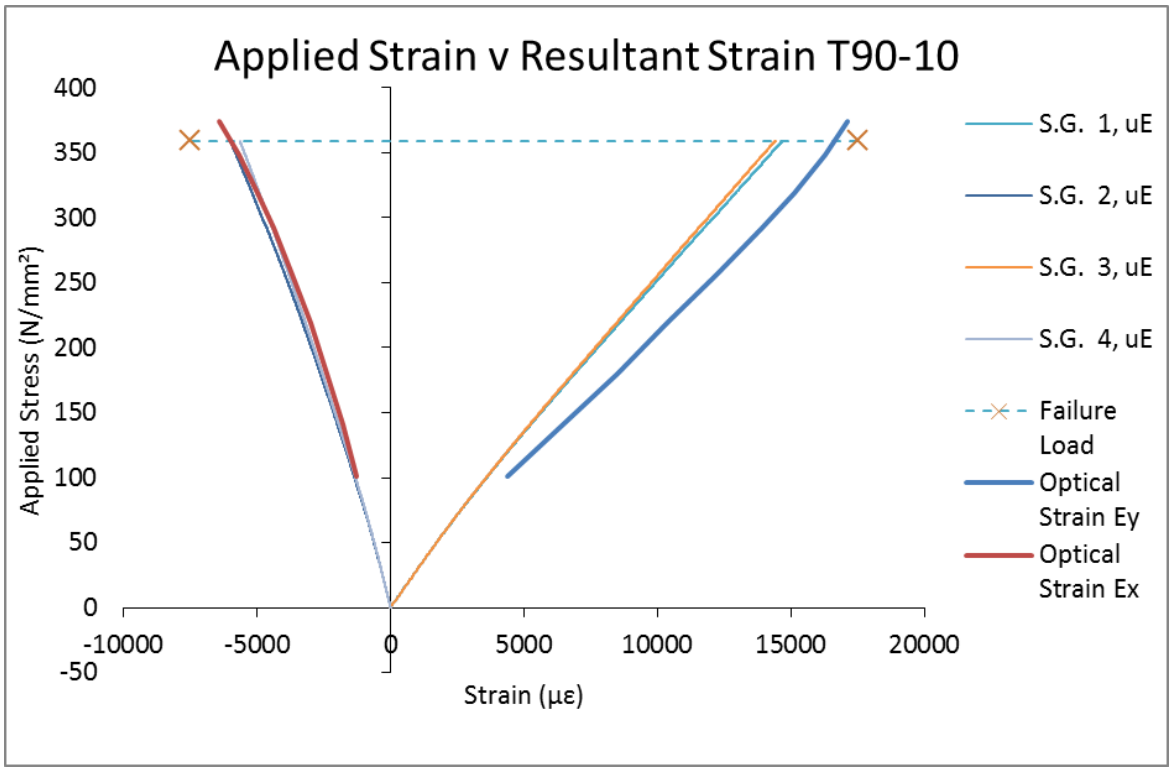

Figure 11-12: Strain gauge and optical strain measurement values for tensile test conducted on sample T[90]-10

11.1.2 Tensile Fatigue Results [0]

Table 11-4: Specimen identification and their specific dimensions for tests

Specimen Name	Specimen Orientation	Average Width (mm)	Average Thickness (mm)	Thickness Diff. from mean (%)
T-11	0	25.8	9.84	0%
T-12	0	26.58	9.74	-1%
T-13	0	26.27	9.68	-1%
T-14	0	26.41	9.93	1%
T-15	0	26.02	9.8	0%
T-16	0	26.14	9.84	0%
T-17	0	26.23	9.97	1%
T-18	0	26.18	9.75	-1%
T-19	0	26.09	9.88	0%
T-20	0	26.13	9.82	0%
T-21	0	25.67	9.68	0%
T-22	0	26.03	9.84	2%
T-23	0	25.81	9.52	-2%
T-24	0	26.57	9.74	1%
T-25	0	26.3	9.65	0%
T-26	0	26.11	9.72	0%
T-27	0	26.1	9.64	-1%
T-28	0	26.52	9.71	0%
T-29	0	25.99	9.65	-1%
T-30	0	25.75	9.8	1%
T-31	0	25.9	9.63	0%
T-32	0	25.33	9.55	-1%
T-33	0	25.7	9.74	1%
T-34	0	25.72	9.72	1%
T-35	0	26.2	9.7	0%

11.1.2.1 Samples T[0]-11 – T[0]-15

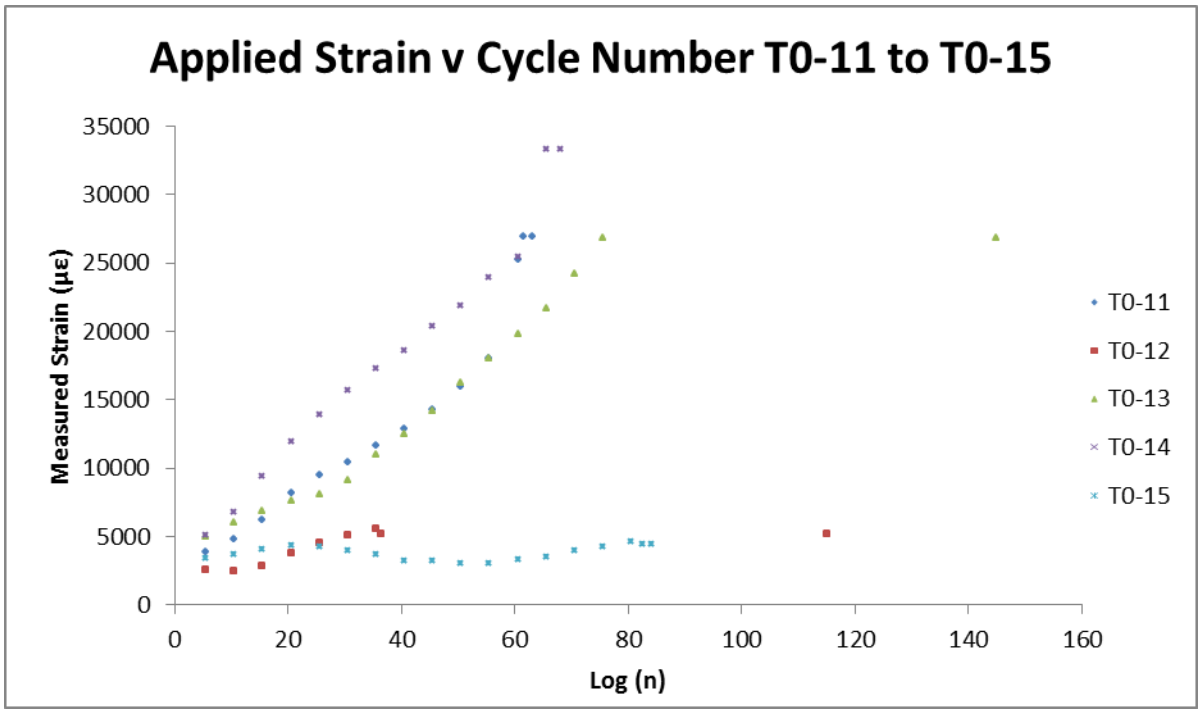

Figure 11-13: Increase in strain response of the coupons as the applied cycles increase for the coupons fatigued at 90% of Ultimate Tensile Strength.

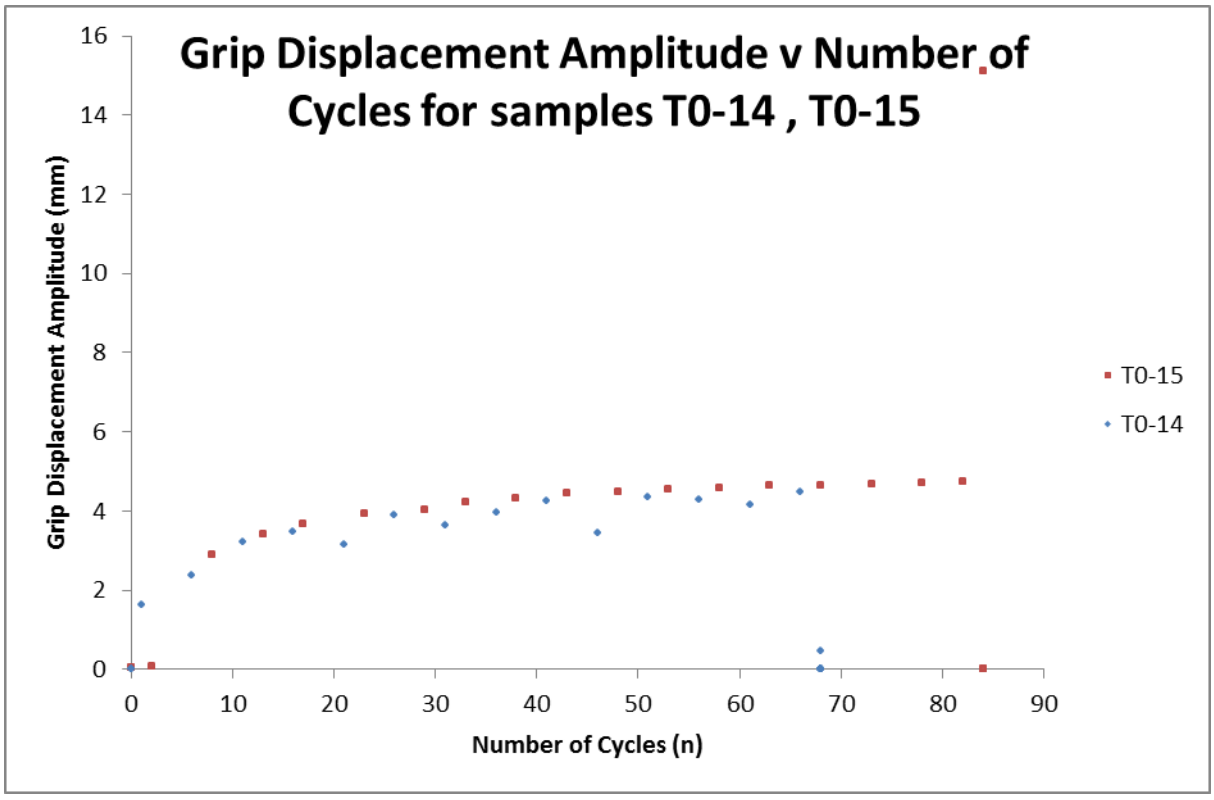

Figure 11-14: Change in grip displacement amplitude as the number of cycles increase to failure for coupons T[0]-14 and T[0]-15.

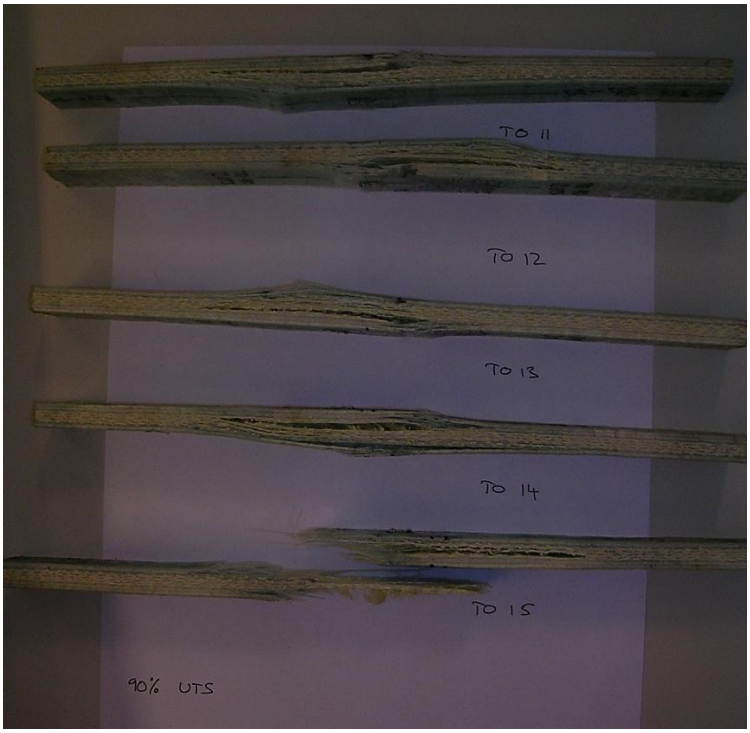

Figure 11-15: final failure damage of coupons T[0]11 to T[0]15

11.1.2.2 Samples T[0]-16 – T[0]-20

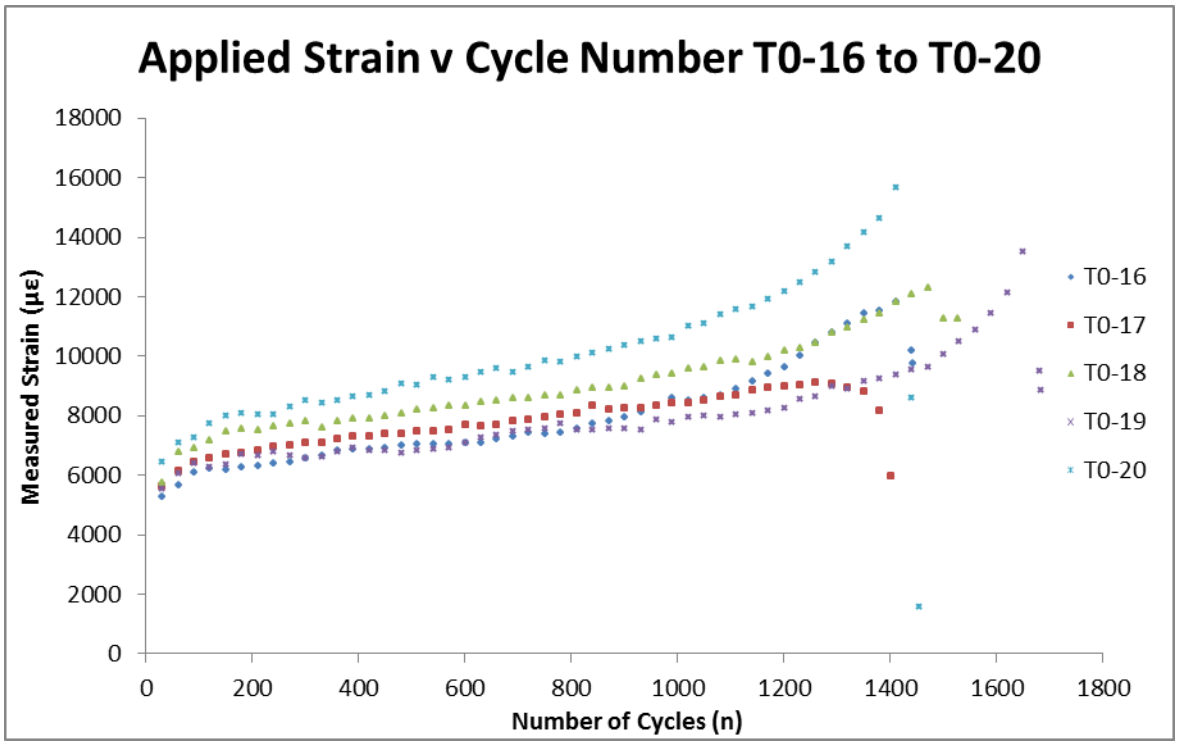

Figure 11-16: Increase in strain response of the coupons as the applied cycles increase for the coupons fatigued at 80% of Ultimate Tensile Strength.

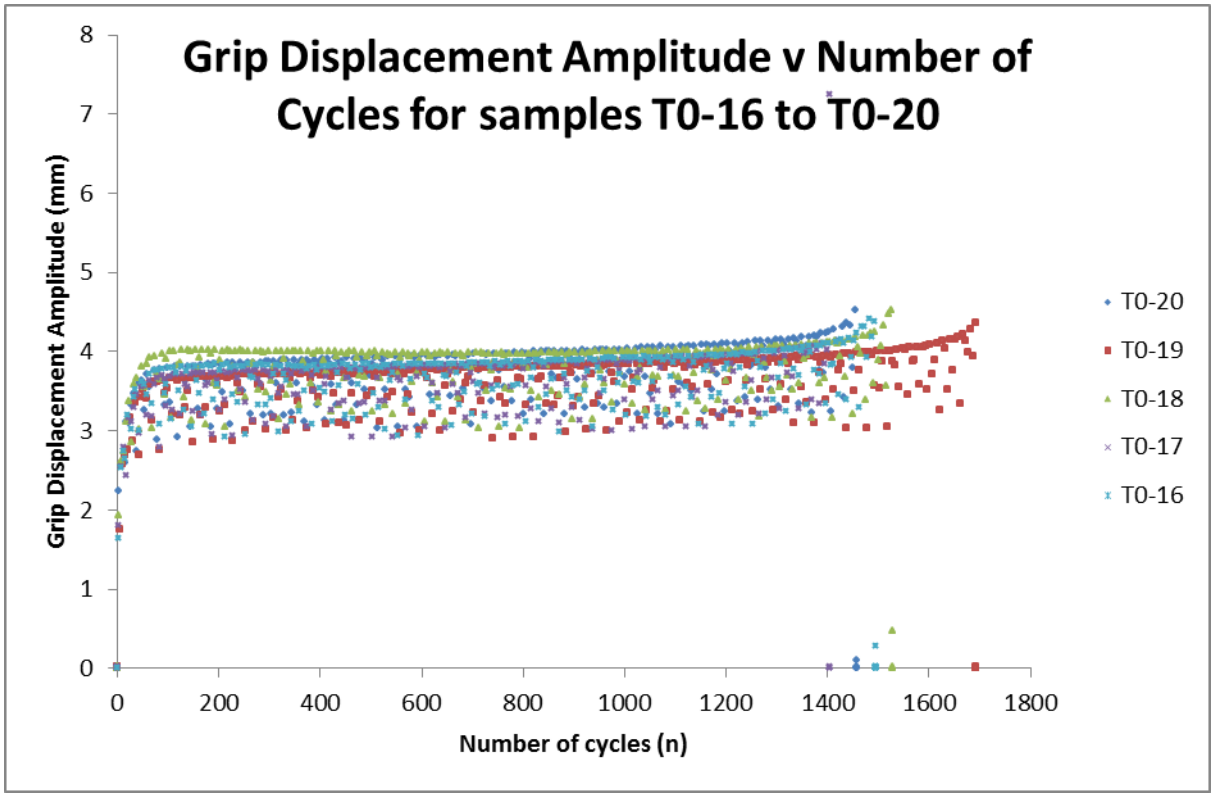

Figure 11-17: Change in grip displacement amplitude as the number of cycles increase to failure for coupons T[0]-16 to T[0]-20.

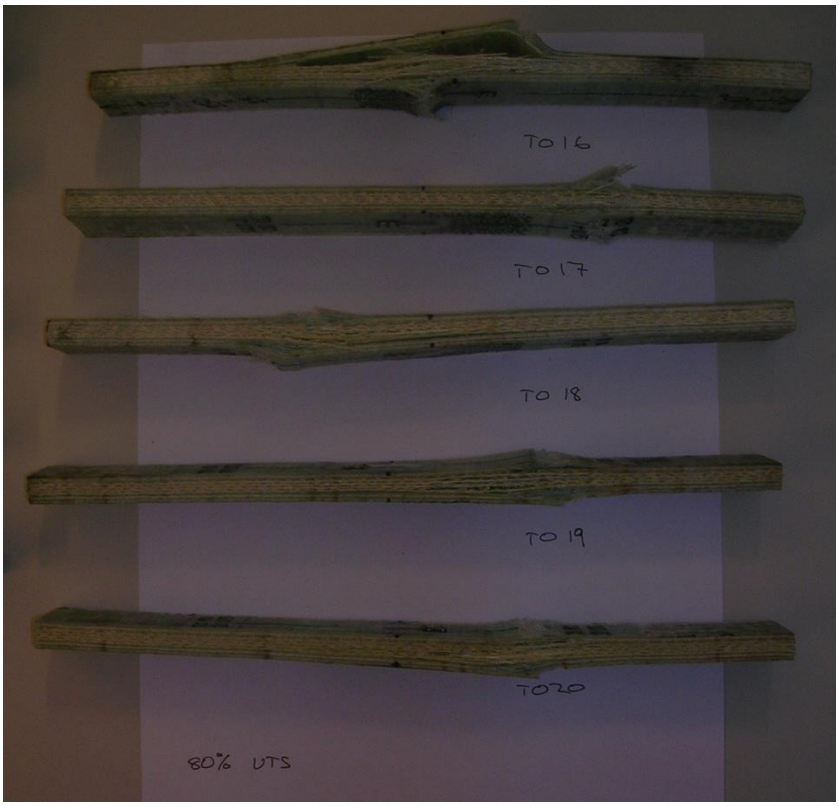

Figure 11-18: final failure damage of coupons T[0]16 to T[0]20

11.1.2.3 Samples T[0]-21 – T[0]-25

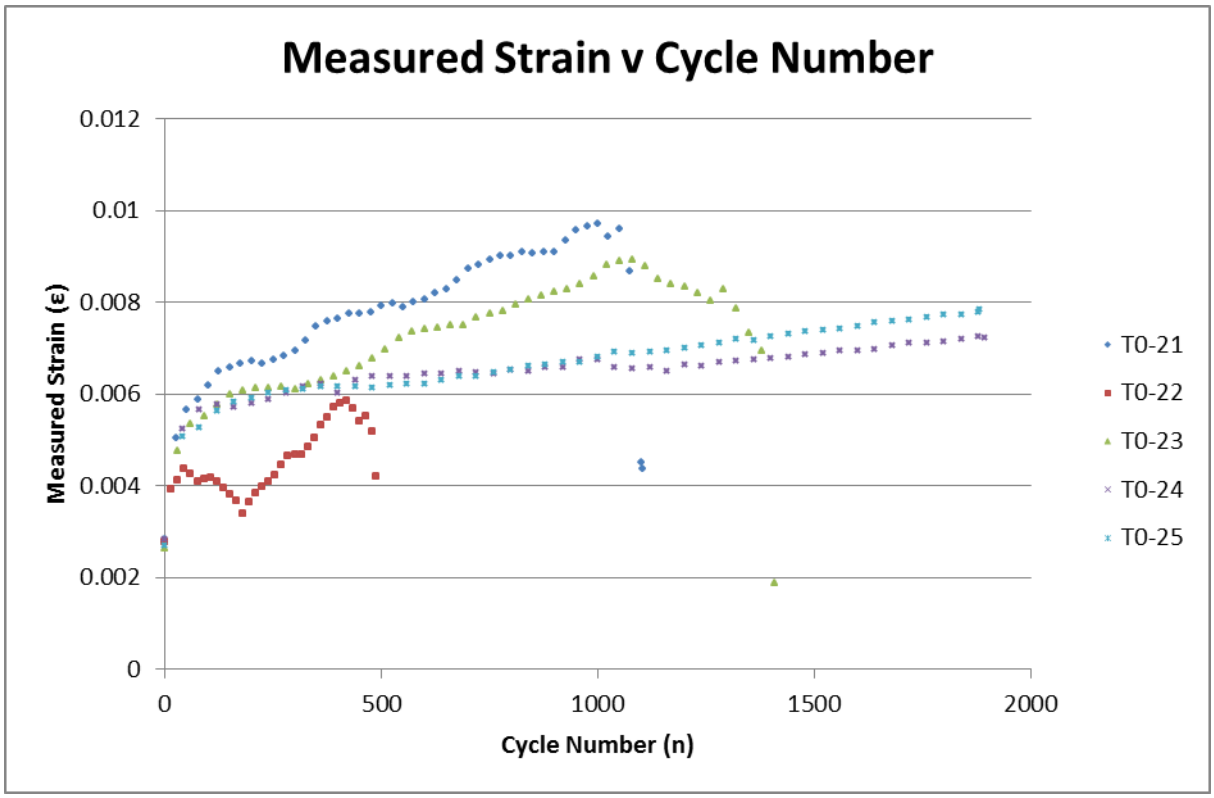

Figure 11-19: Increase in strain response of the coupons as the applied cycles increase for the coupons fatigued at 70% of Ultimate Tensile Strength.

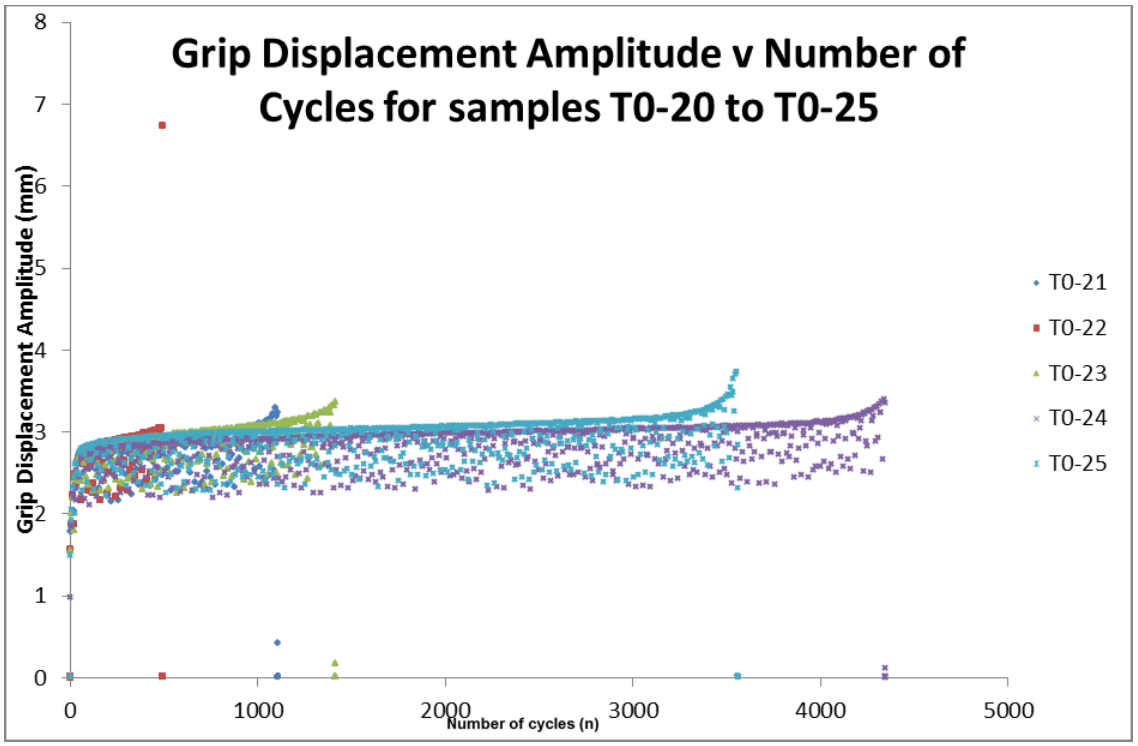

Figure 11-20: Change in grip displacement amplitude as the number of cycles increase to failure for coupons tested at 70% Ultimate Tensile Strength

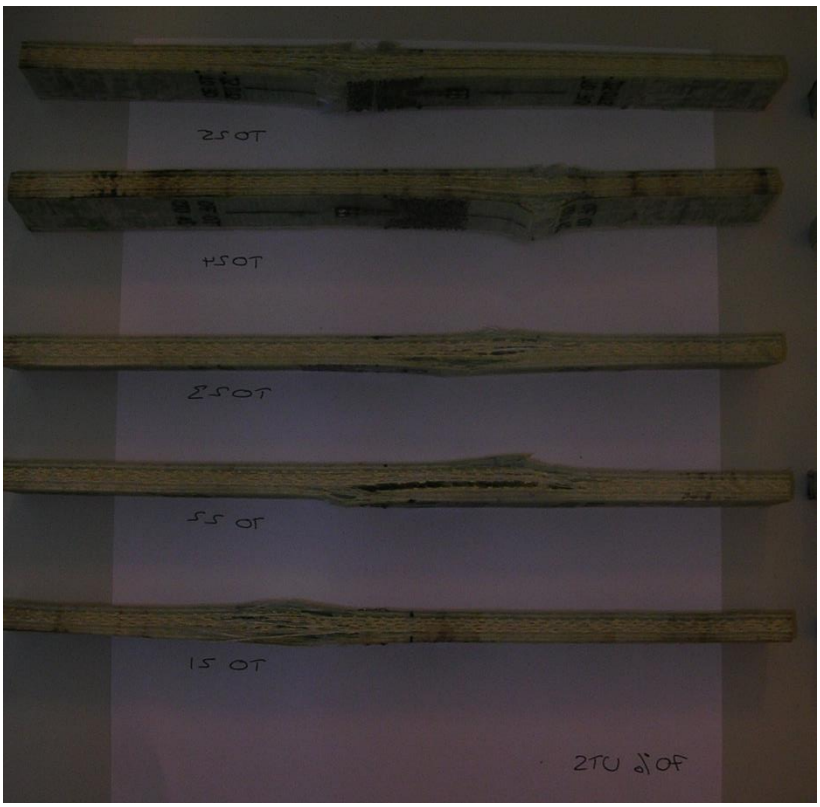

Figure 11-21: final failure damage of coupons T[0]21 to T[0]25

11.1.2.4 Samples T[0]-26 – T[0]-30

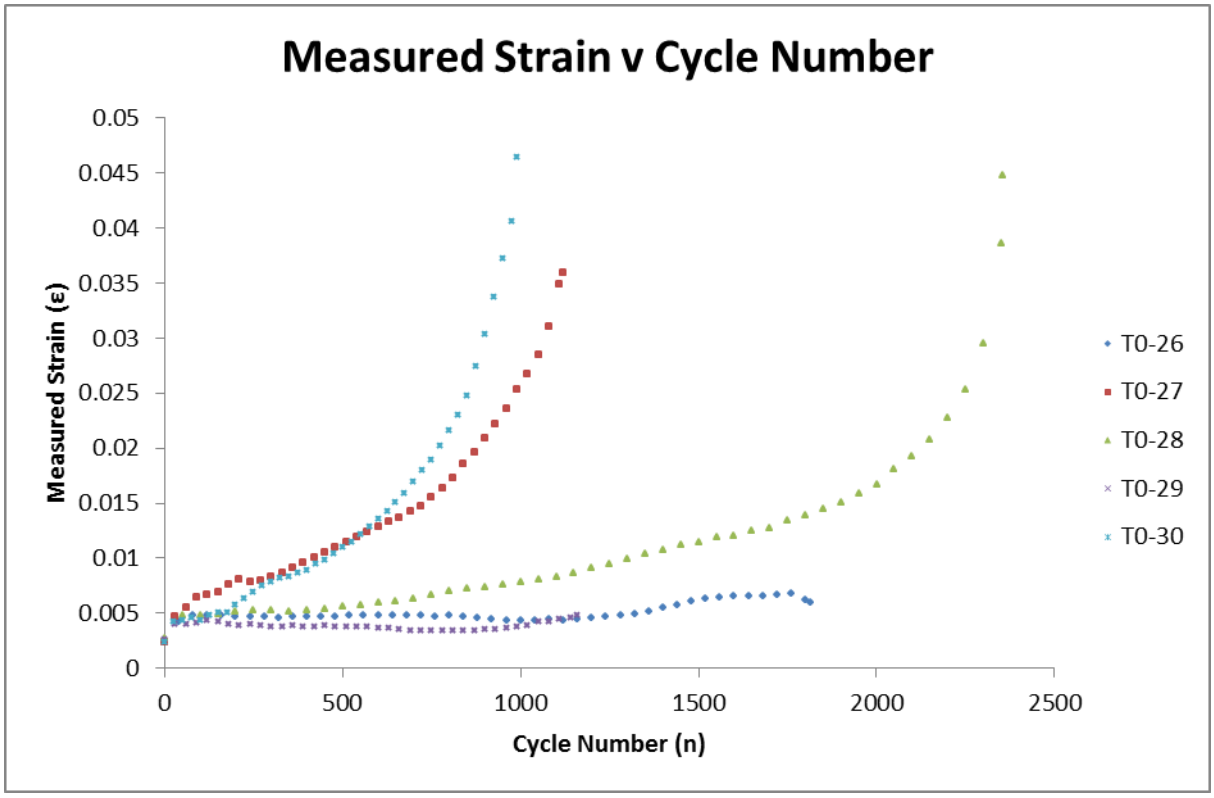

Figure 11-22: Increase in strain response of the coupons as the applied cycles increase for the coupons fatigued at 60% of Ultimate Tensile Strength.

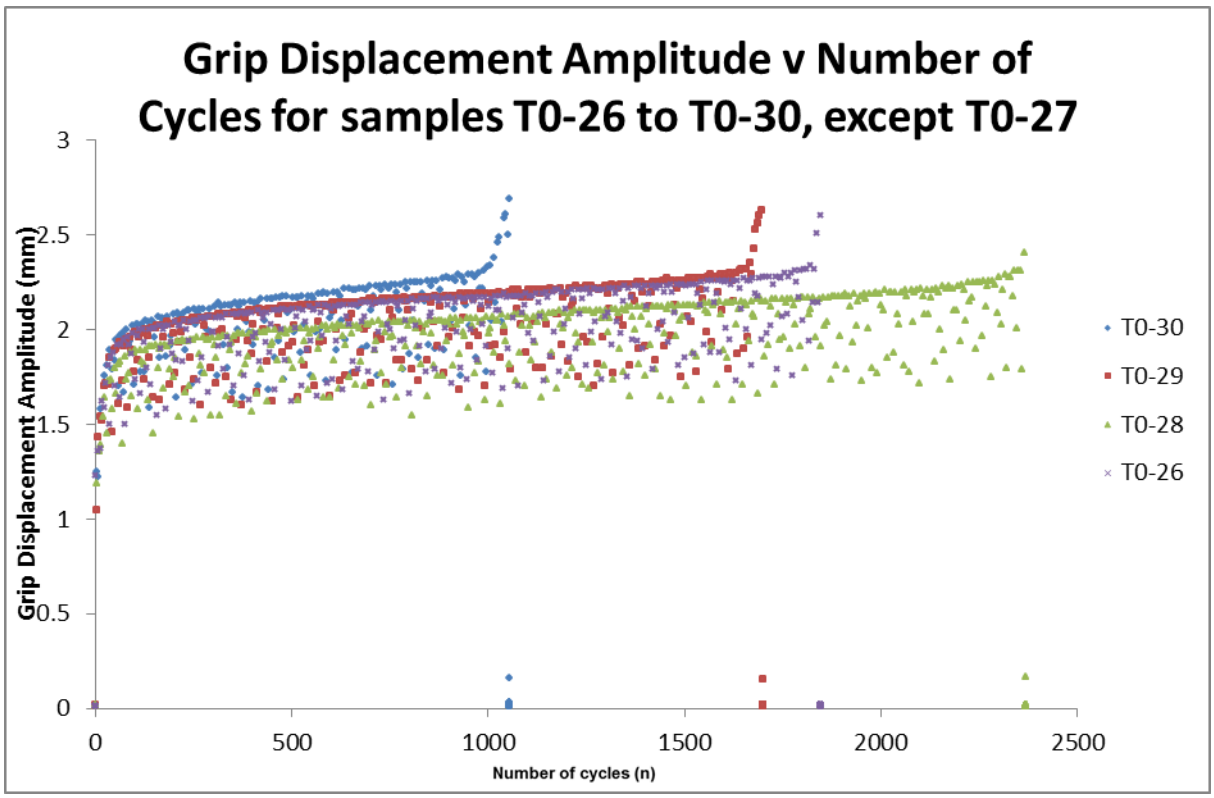

Figure 11-23: Change in grip displacement amplitude as the number of cycles increase to failure for coupons tested at 60% Ultimate Tensile Strength

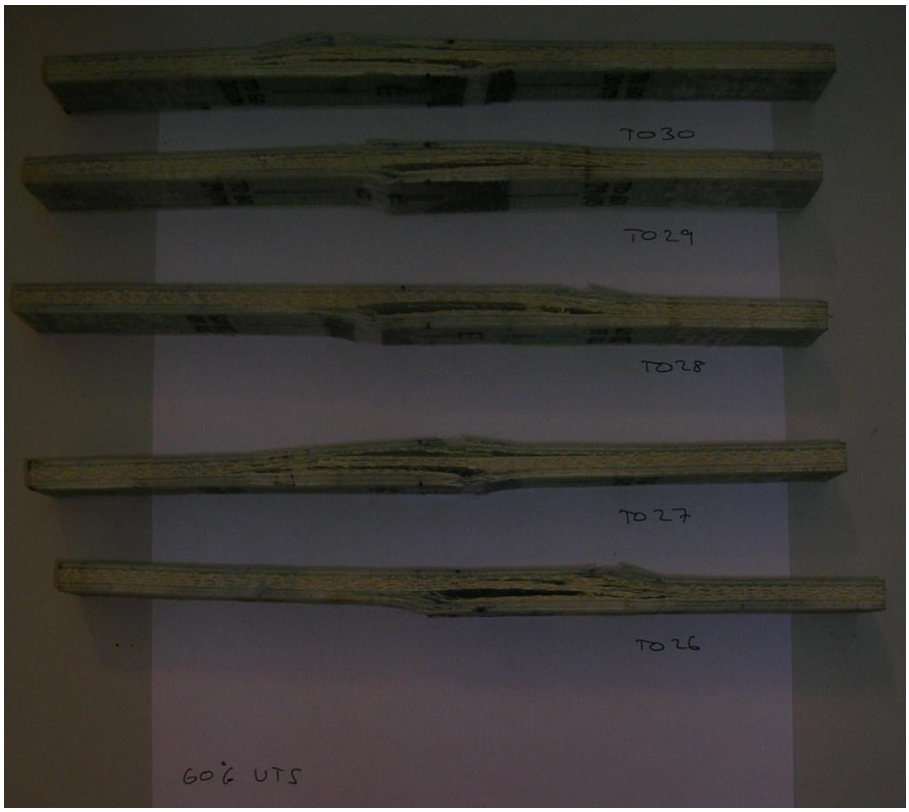

Figure 11-24: final failure damage of coupons T[0]26 to T[0]30

11.1.2.5 Samples T[0]-31 – T[0]-35

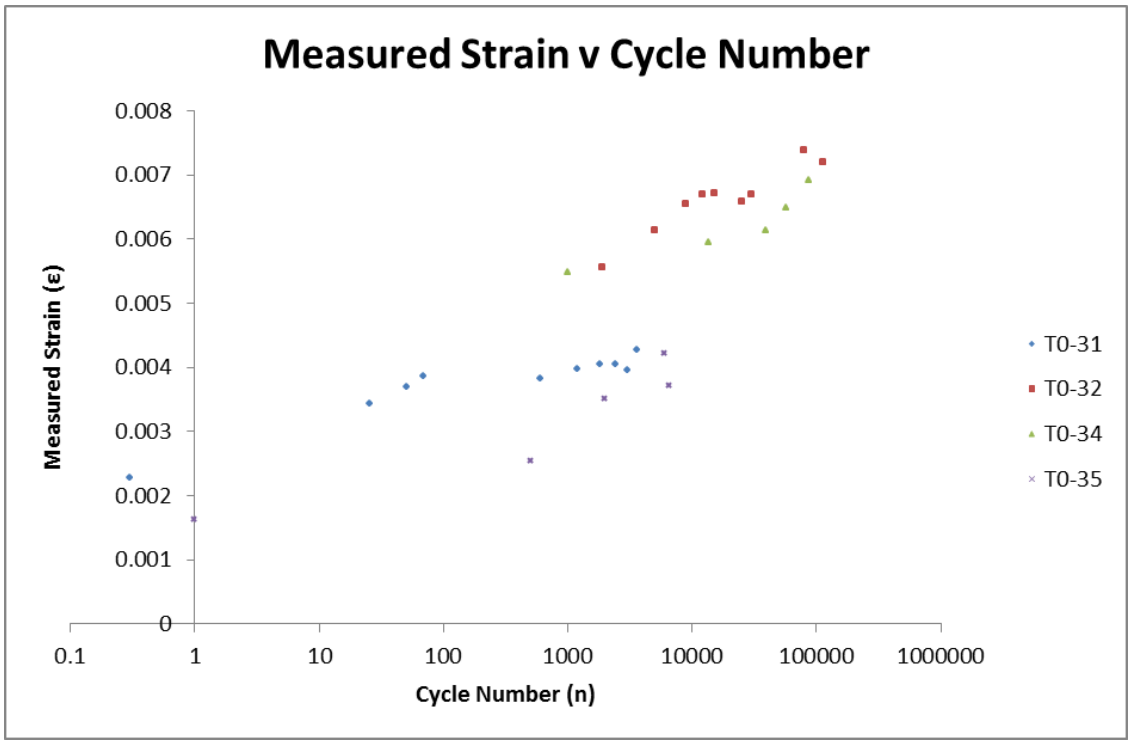

Figure 11-25: Increase in strain response of the coupons as the applied cycles increase for the coupons fatigued at 50% of Ultimate Tensile Strength.

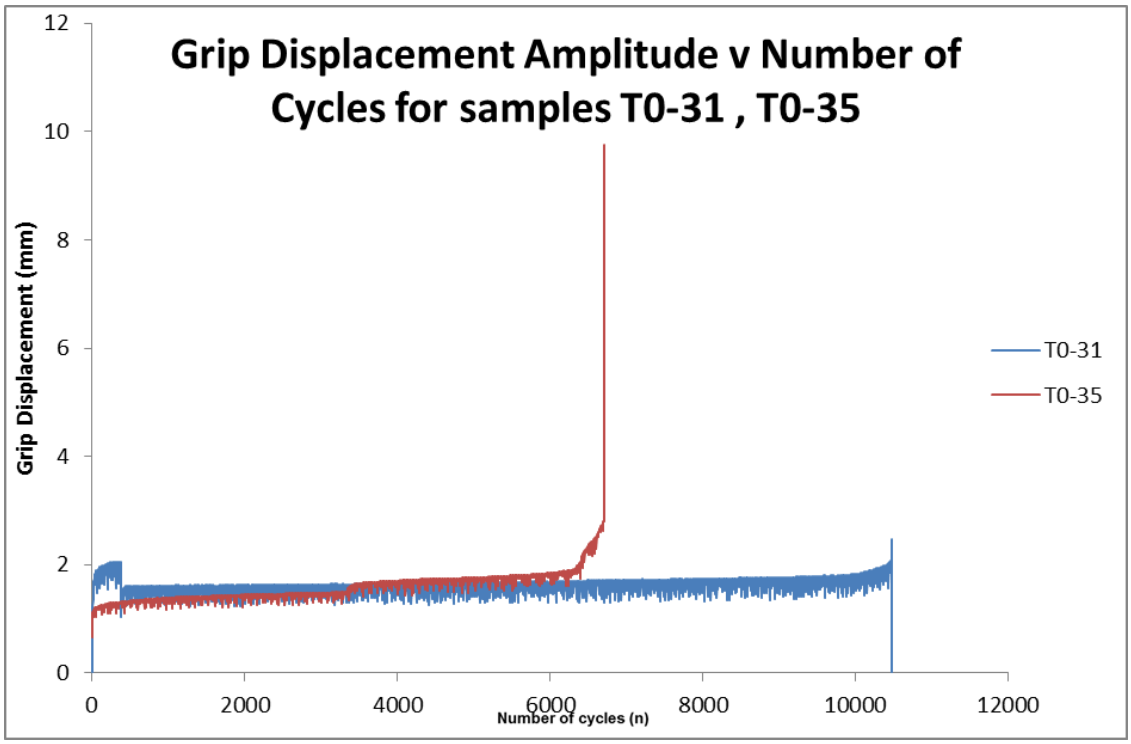

Figure 11-26: Change in grip displacement amplitude as the number of cycles increase to failure for 2 of the coupons tested at 50% Ultimate Tensile Strength

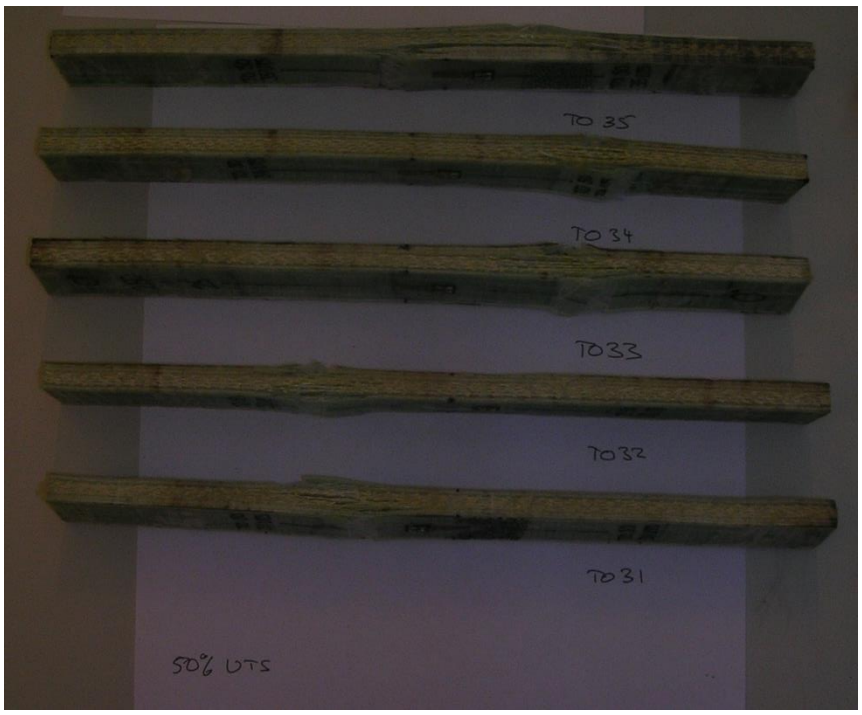

Figure 11-27: final failure damage of coupons T[0]31 to T[0]35

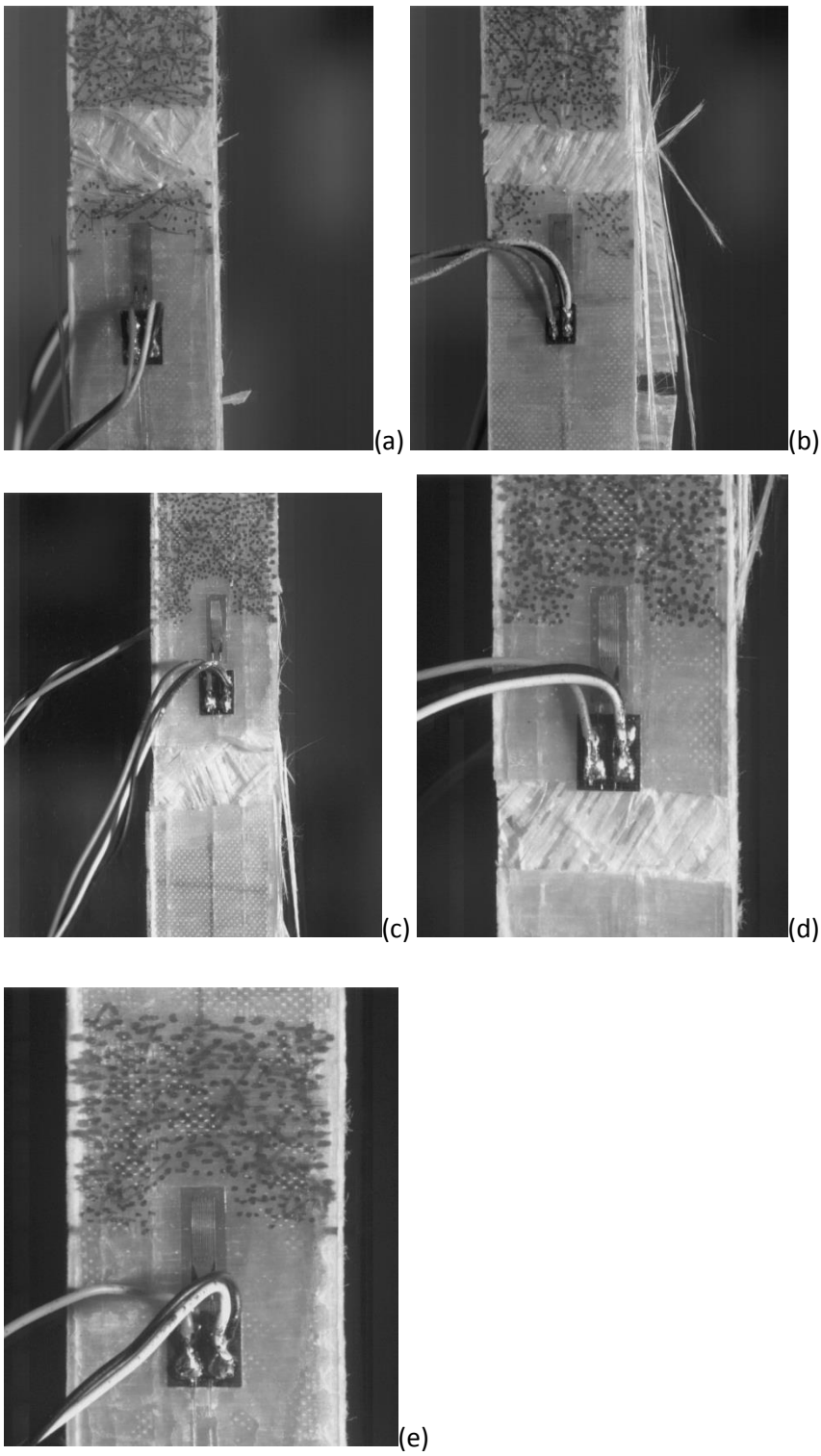

Figure 11-28: DIC images for failed tensile fatigue test coupons (a) T[0]-11 (b) T[0]-16 (c) T[0]-21 (d) T[0]-26 (e) T[0]-31

11.1.3 Ultimate Flexural Strength Results

Table 11-5: Specimen dimensions for the static flexural tests. Mean values were calculated in blocks according to specimen orientation

Specimen Name	Specimen Orientation	Average Width (mm)	Average Thickness (mm)	Thickness Diff. from mean (%)
F[0]-01	0	20.73	9.60	-2%
F[0]-02	0	20.65	9.50	-1%
F[0]-03	0	21.04	9.50	-1%
F[0]-04	0	20.60	9.60	-2%
F[0]-05	0	20.40	9.50	-1%
F[90]-06	90	20.80	9.40	1%
F[90]-07	90	20.75	9.30	2%
F[90]-08*	90	20.44	9.20	3%
F[90]-09	90	20.81	9.40	1%
F[0]-10	90	20.45	9.50	-1%
F[0]-11	0	21.08	9.52	-1%
F[0]-12	0	20.36	9.61	0%
F[0]-13	0	20.54	9.65	0%
F[0]-14	0	20.73	9.61	0%
F[0]-15	0	20.56	9.73	1%
F[90]-36	90	19.99	9.47	-1%
F[90]-37	90	21.07	9.57	0%
F[90]-38	90	20.8	9.62	1%
F[90]-39	90	20.45	9.58	0%
F[90]-40	90	20.57	9.5	-1%
F[0]-30	0	21.14	9.6	-1%
F[90]-55*	90	20.8	9.89	4%

Table 11-6: Recorded data for the [0] direction 4 point bend static tests.

Coupon	Max Load (kN)	Displacement at Failure	Max Fibre stress at Failure σ_f	Failure Strain Calculated ε_{calc}	Failure Strain Measured ε_{meas}	Modulus from ε_{calc} E_{meas}	Modulus from ε_{meas} E_{meas}
F[0]-01	1.22	22.2	150.38	1.99%	-	13.0	13.0
F[0]-02	1.23	22.9	154.98	2.03%	-	13.3	13.2
F[0]-03	1.18	20.0	142.88	1.79%	-	13.9	12.7
F[0]-04	1.11	20.6	134.88	1.86%	-	13.1	13.0
F[0]-05	1.20	21.7	153.13	1.92%	-	14.1	13.1
Average	1.19	21.48	147.25	1.91%	-	13.47	13.00
sd	0.05	1.18	8.31	0.00	-	0.47	0.22
Coeff. Of Var	4.20	5.47	5.64	5.06	-	3.53	1.65
F[0]-11	2.23	12.7	185.18	2.86%	-	10.0	10.1
F[0]-12	2.02	11.2	170.65	2.56%	-	9.4	6.4
F[0]-13	2.01	11.0	166.92	2.53%	2.38%	10.8	14.0
F[0]-14	2.10	11.5	174.10	2.63%	-	11.2	13.9
F[0]-15	2.03	11.5	165.94	2.65%	-	10.7	13.6
Average	2.08	11.58	172.56	0.03	-	10.41	11.60
sd	0.09	0.64	7.76	0.00	-	0.74	3.34
Coeff. Of Var	4.35	5.48	4.50	4.93	-	7.13	28.81
F[0]-30	1.80	11.1	146.56	2.52	-	14.1	19.4

Table 11-7: Recorded data for the [90] direction 4 point bend static tests.

Coupon	Max Load (kN)	Displacement at Failure	Max Fibre stress at Failure σ_f	Failure Strain Calculated ε_{calc}	Failure Strain Measured ε_{meas}	Modulus from ε_{calc} E_{meas}	Modulus from ε_{meas} E_{meas}
F[90]-06	2.93	13.2	355.64	1.52%	1.32%	27.5	31.8
F[90]-07	2.88	12.1	353.78	1.39%	1.20%	26.2	31.2
F[90]-08	2.90	12.3	371.37	1.39%	1.14%	28.5	33.9
F[90]-09	2.86	12.2	341.60	1.41%	1.27%	24.6	29.8
F[90]-10	2.87	11.8	340.58	1.38%	1.27%	27.4	31.0
Average	2.89	12.32	352.59	1.42%	1.24%	26.83	31.53
sd	0.03	0.54	12.53	0.00	0.00	1.51	1.49
Coeff. Of Var	0.87	4.38	3.55	4.10	5.78	5.62	4.74
F[90]-36	4.84	7.6	429.55	1.71%	1.31%	23.6	35.3
F[90]-37	5.21	7.3	435.53	1.67%	1.28%	25.4	34.3
F[90]-38	5.16	8.1	431.03	1.85%	1.48%	23.8	32.8
F[90]-39	5.07	7.5	423.53	1.70%	1.34%	24.9	32.4
F[90]-40	5.18	8.0	432.95	1.82%	1.37%	24.2	34.6
Average	5.09	7.72	430.52	0.02	0.01	24.38	33.88
sd	0.15	0.34	4.50	0.00	0.00	0.75	1.22
Coeff. Of Var	2.95	4.45	1.05	4.58	5.65	3.06	3.61
F[90]-55	4.36	6.9	340.82	1.62%	1.18%	28.8	43.8

11.1.3.1 [0] Coupons Graphical Results

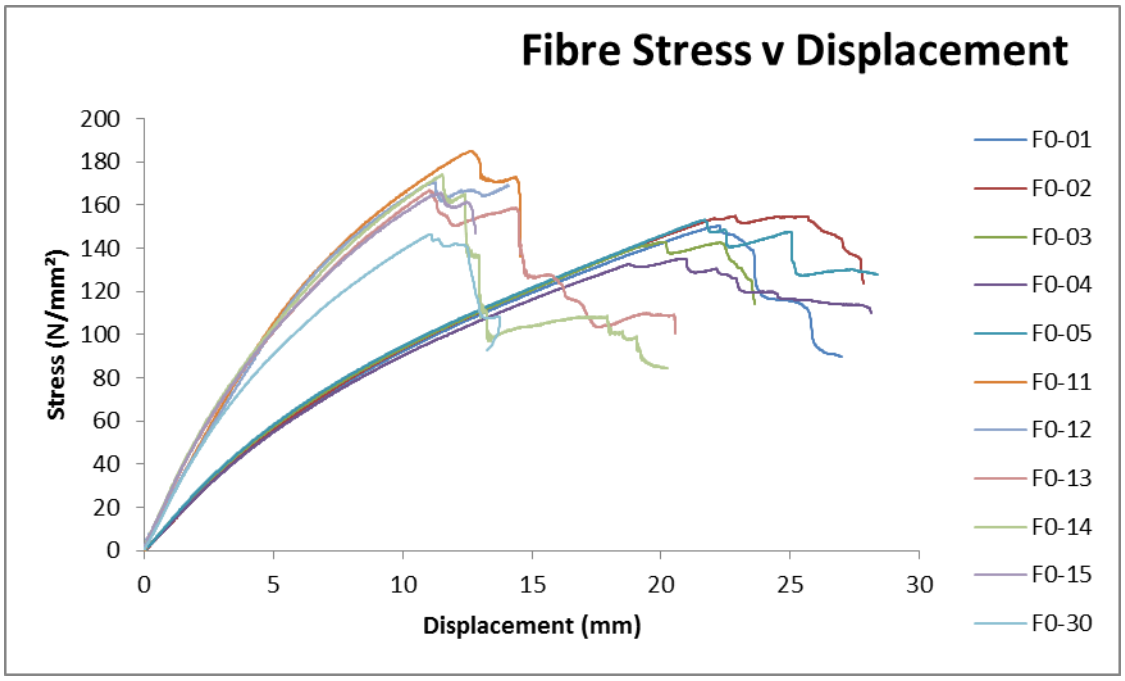

Figure 11-29: Relationship between the applied stress and the resulting displacement due to 4 point bend test for coupons in the [0] direction.

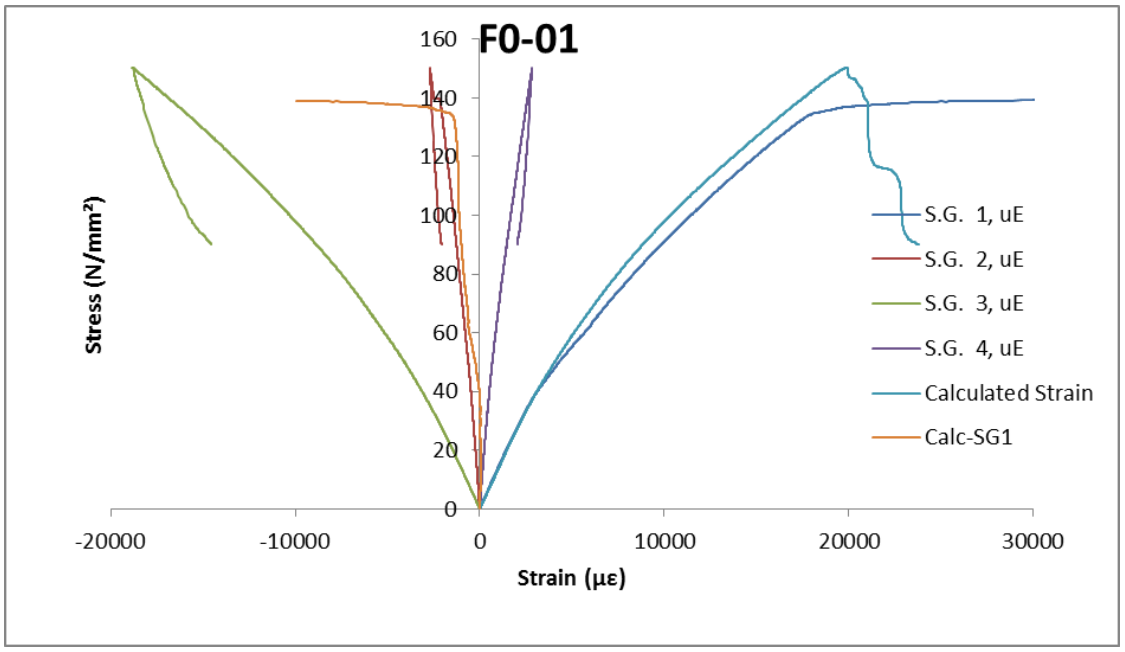

Figure 11-30: Applied Fibre Stress v Resulting strain for sample F[0]-01.

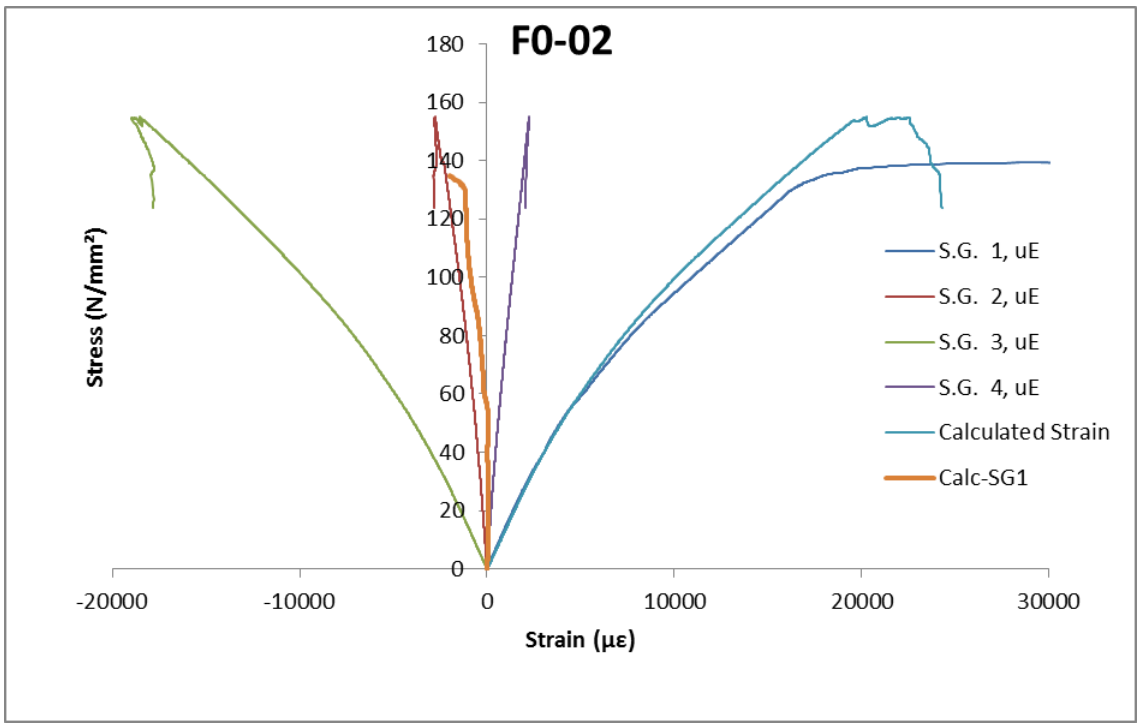

Figure 11-31: Applied Fibre Stress v Resulting strain for sample F[0]-02.

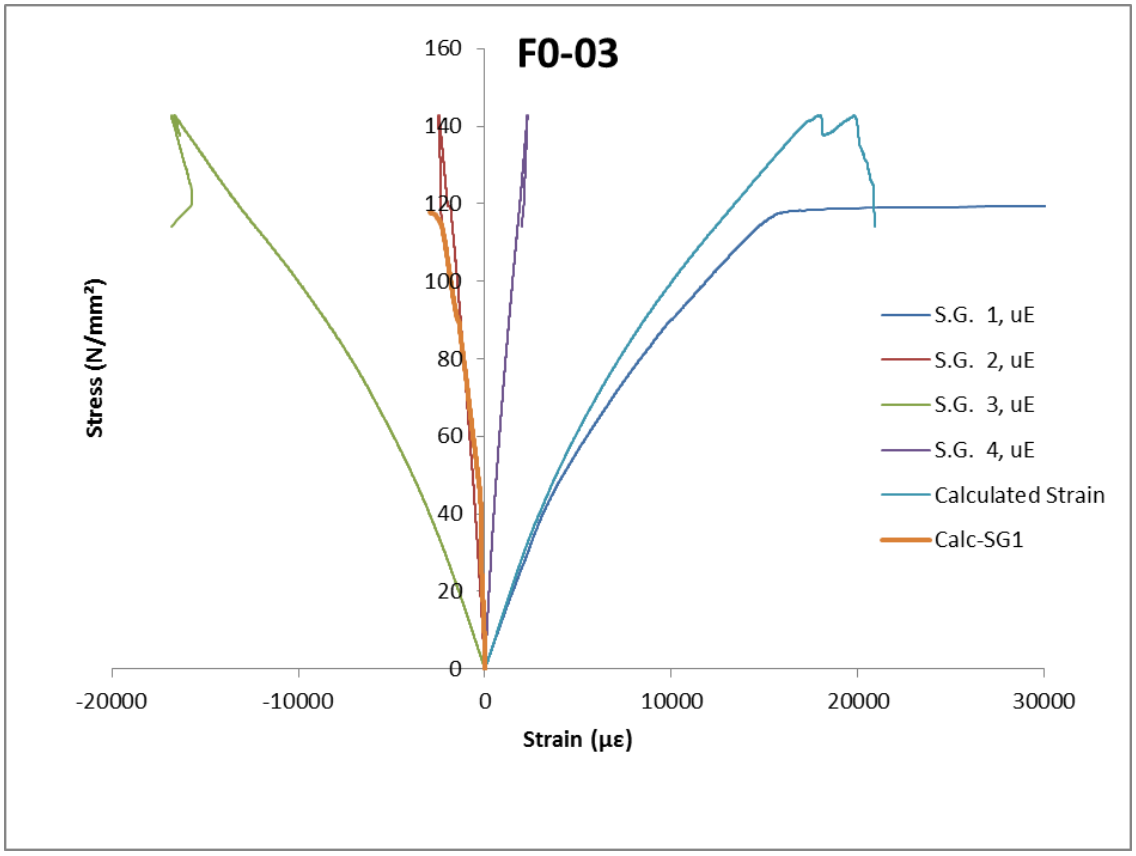

Figure 11-32: Applied Fibre Stress v Resulting strain for sample F[0]-03.

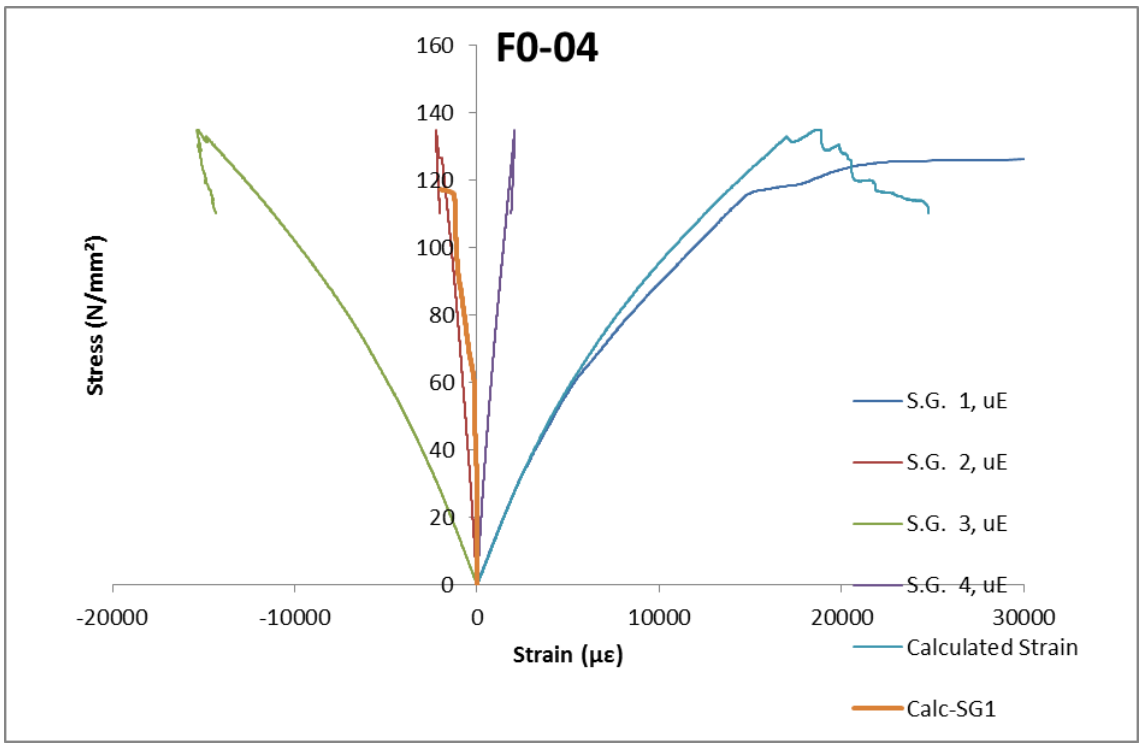

Figure 11-33: Applied Fibre Stress v Resulting strain for sample F[0]-04.

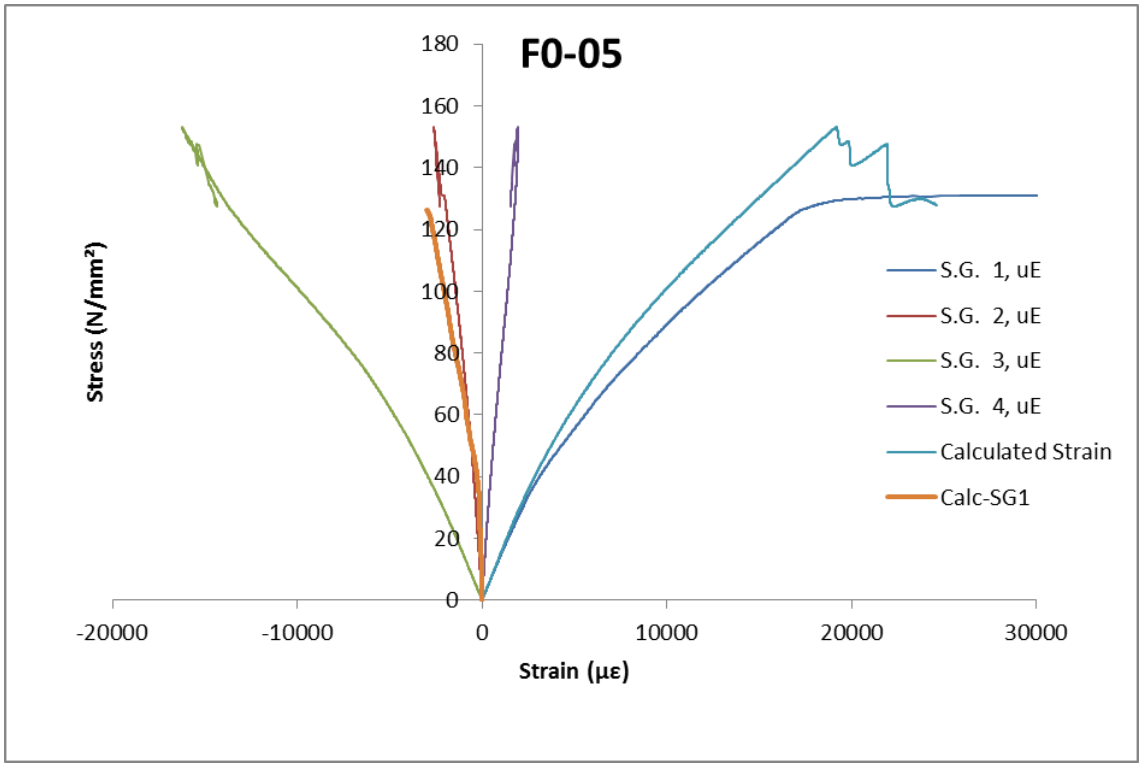

Figure 11-34: Applied Fibre Stress v Resulting strain for sample F[0]-05

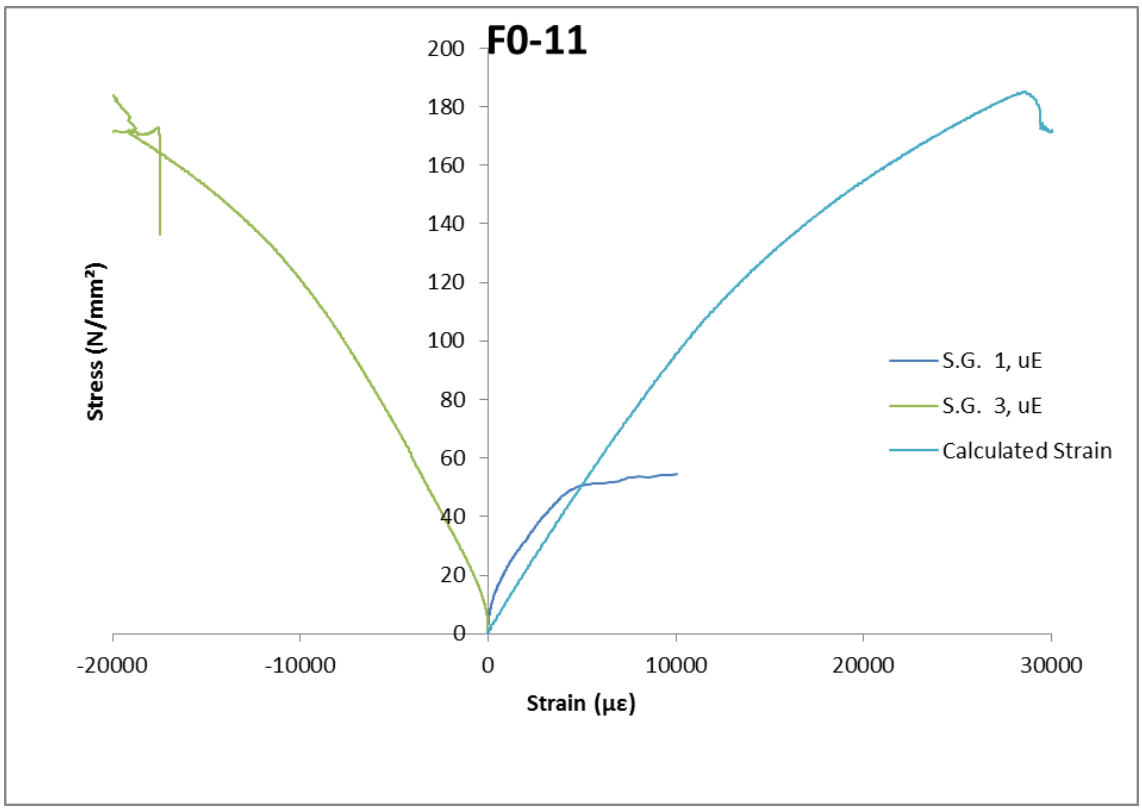

Figure 11-35: Applied stress v resulting strain for sample F[0]-11

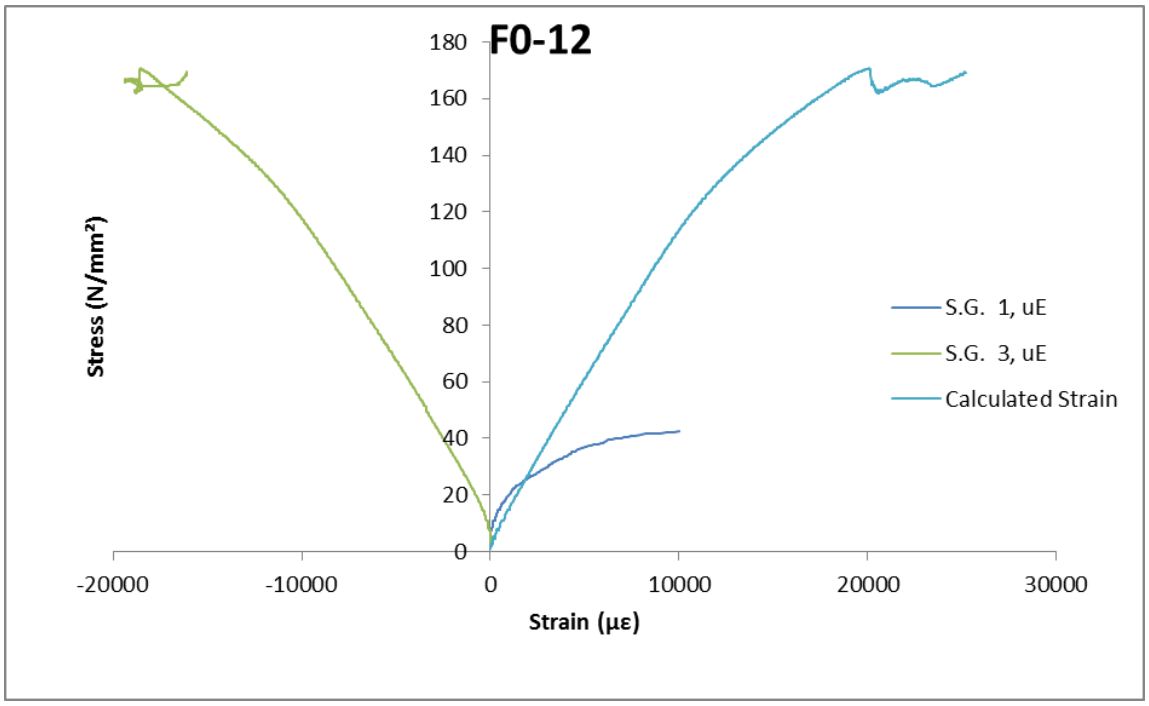

Figure 11-36: Applied stress v resulting strain for sample F[0]-12

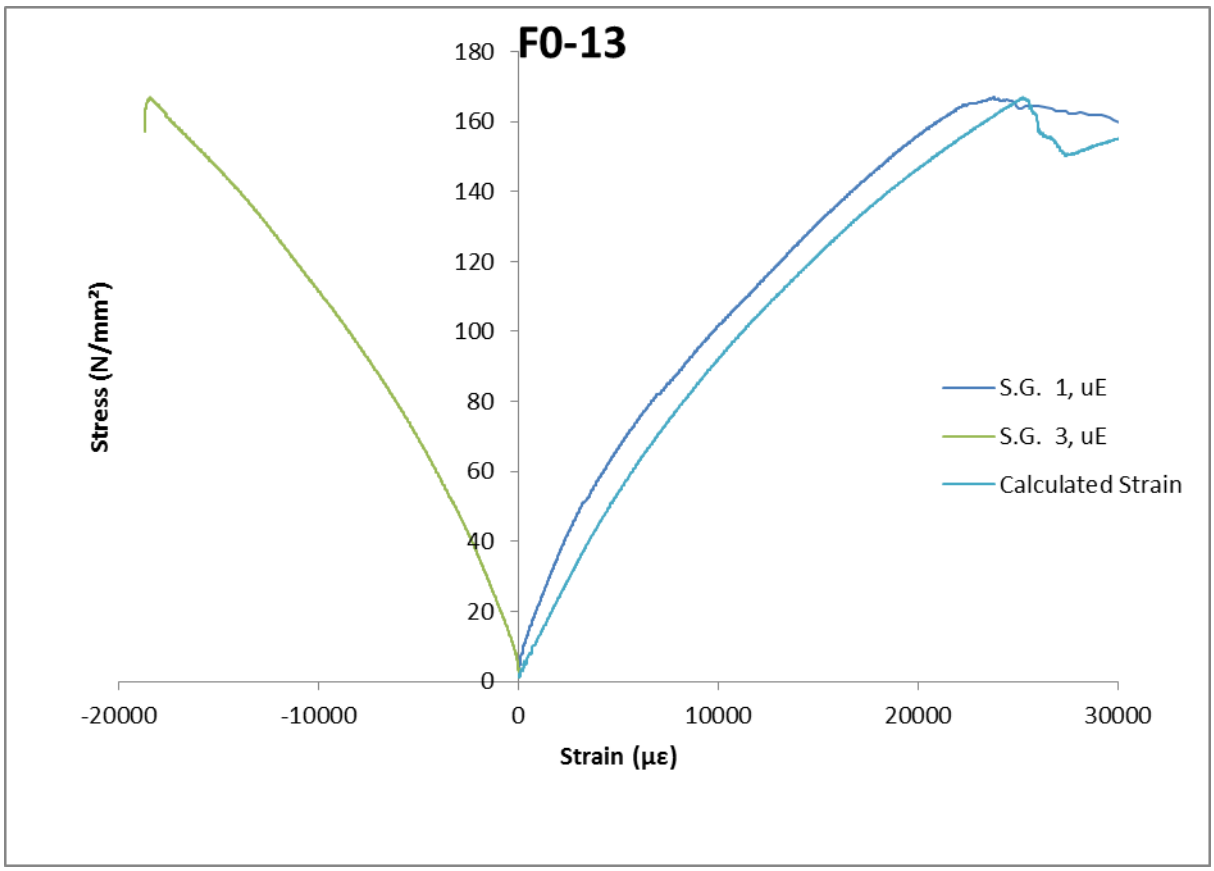

Figure 11-37: Applied stress v resulting strain for sample F[0]-13

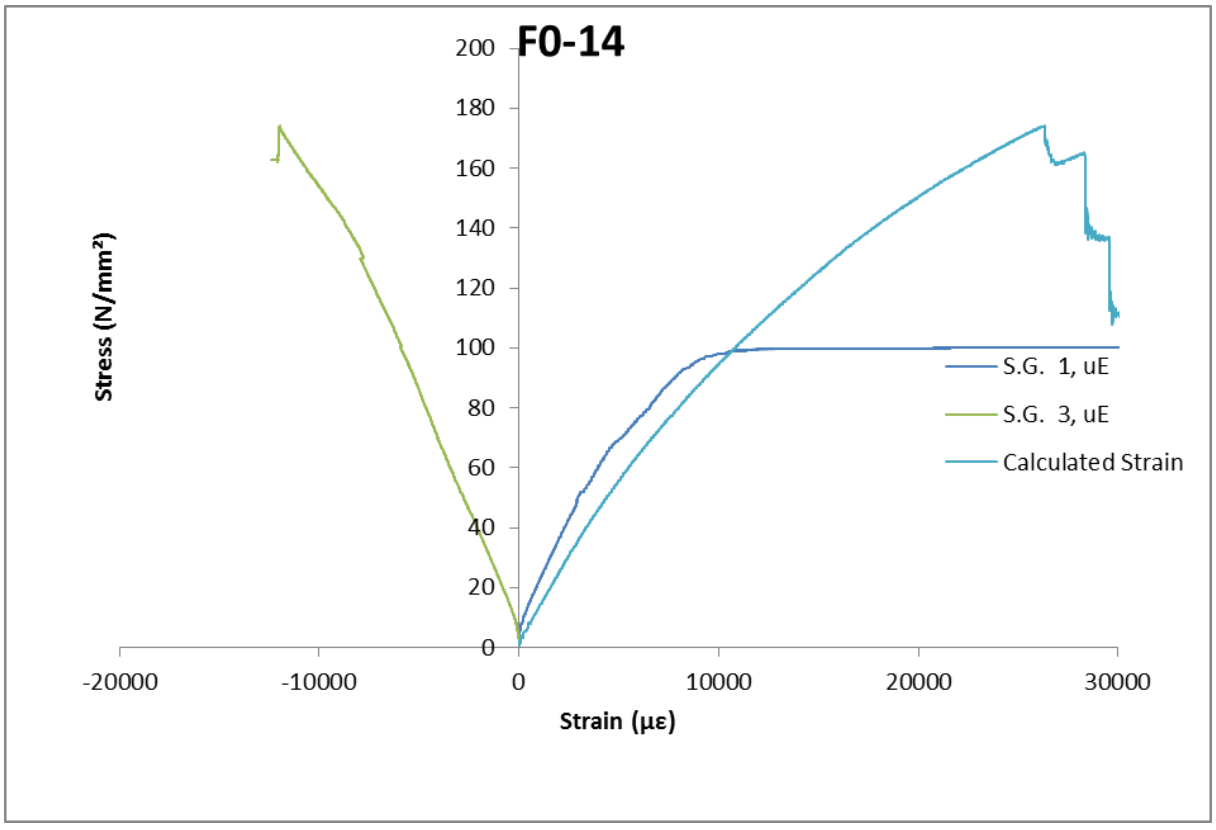

Figure 11-38: Applied stress v resulting strain for sample F[0]-14

CCL

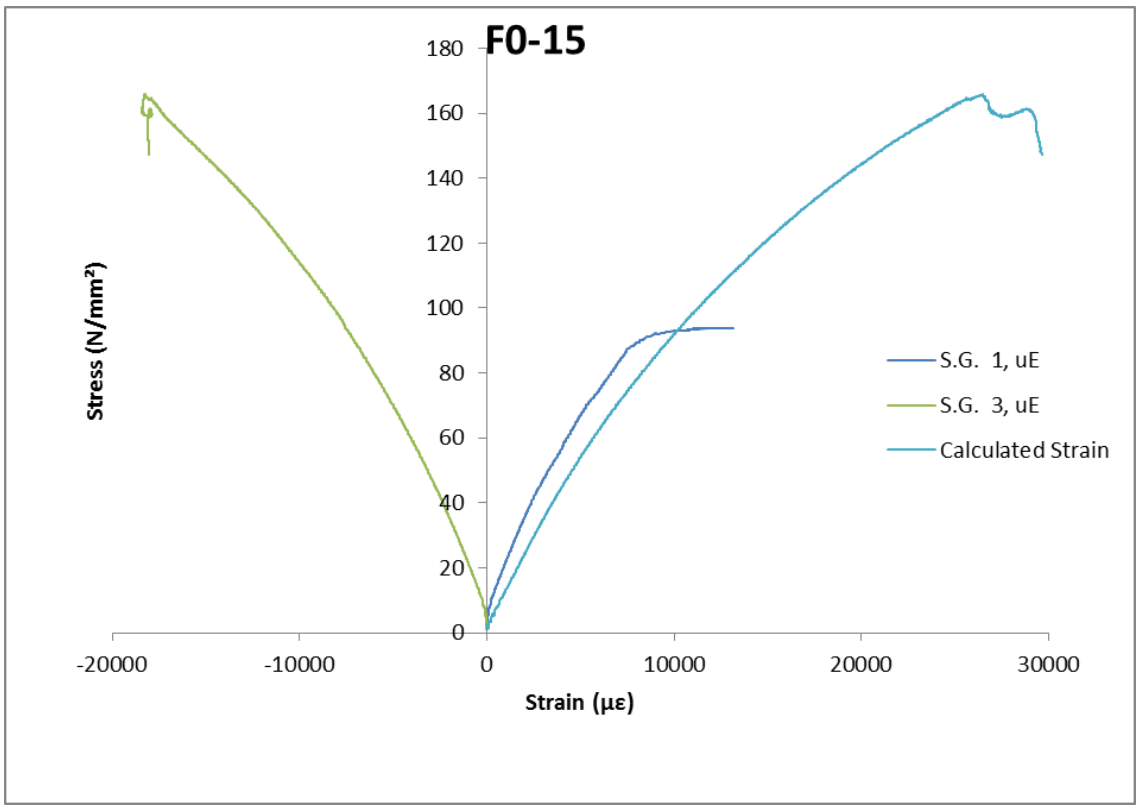

Figure 11-39: Applied stress v resulting strain for sample F[0]-15

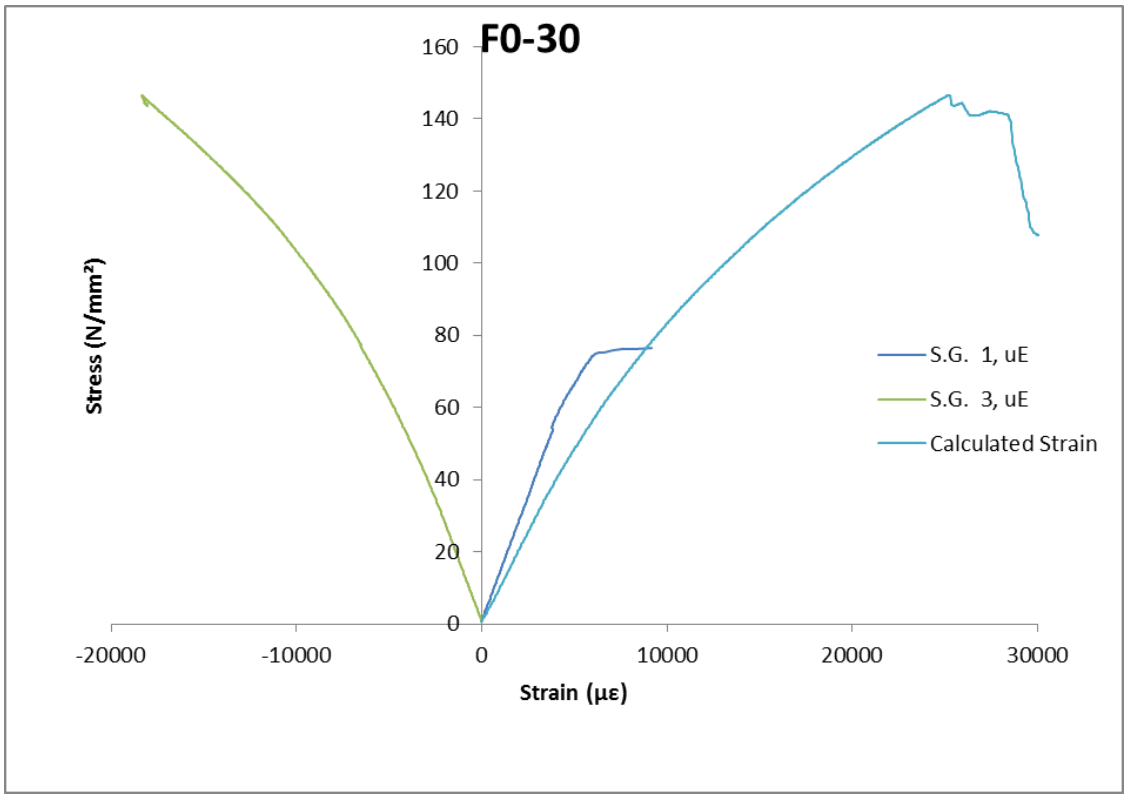

Figure 11-40: Applied fibre stress v resulting strain for sample F[0]-30

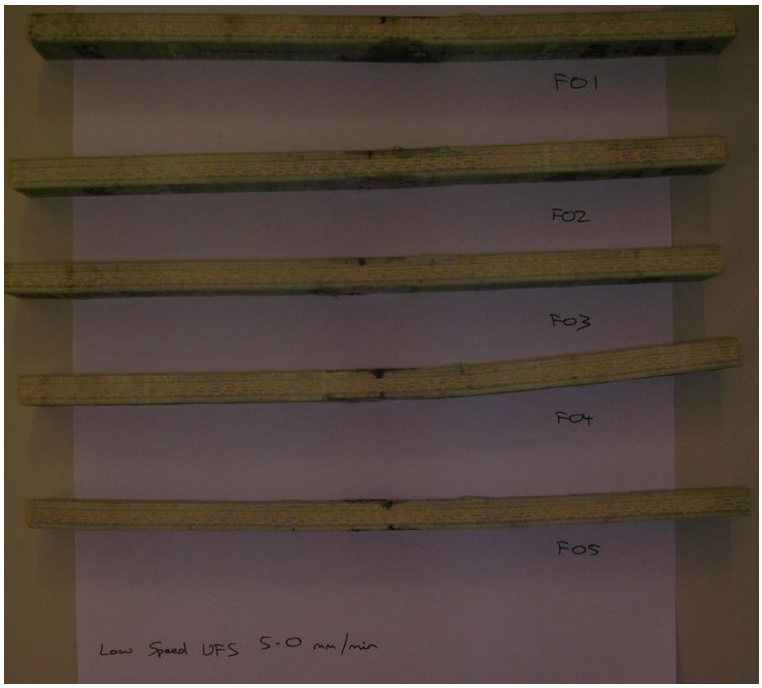

Figure 11-41: UFS results for [0] direction coupons F[0]-1 to F[0]-5 tested at a strain rate of 5mm/min

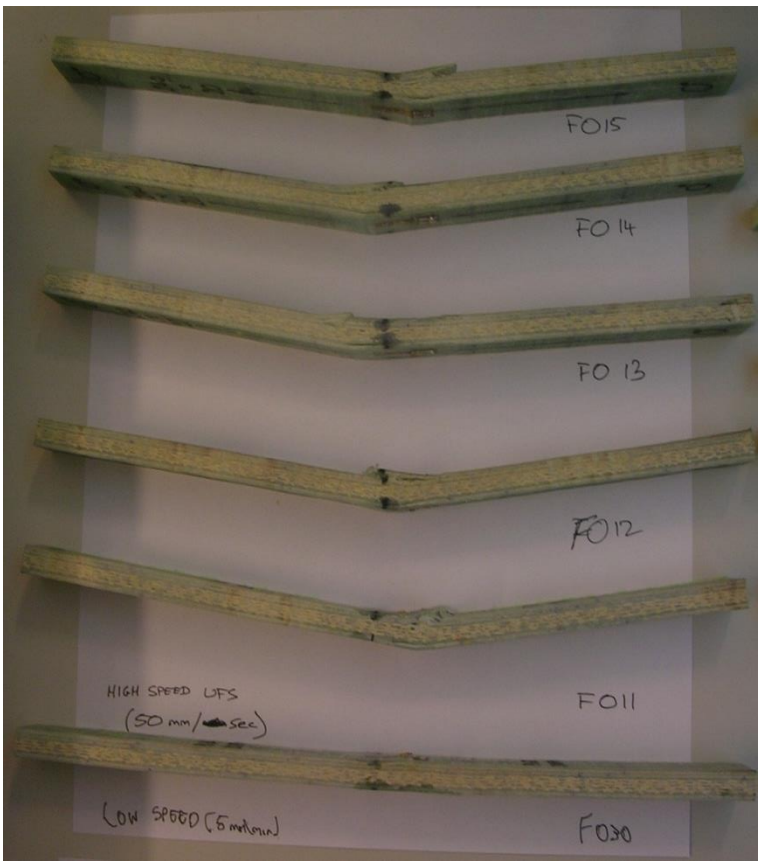

Figure 11-42: UFS results for [0] direction coupons F[0]-11 to F[0]-15 tested at a strain rate of 30mm/min

11.1.3.2 [90] Coupon Graphical Results

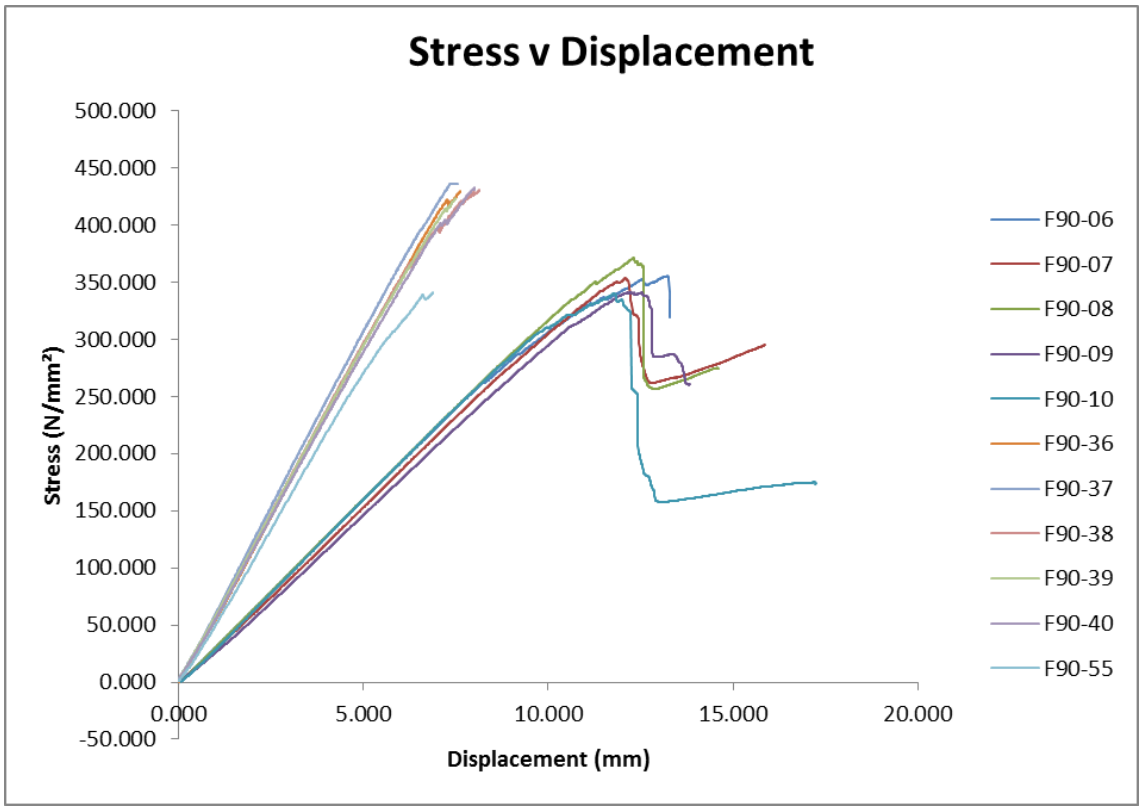

Figure 11-43: Relationship between the applied stress and the resulting displacement due to 4 point bend test for coupons in the [90] direction.

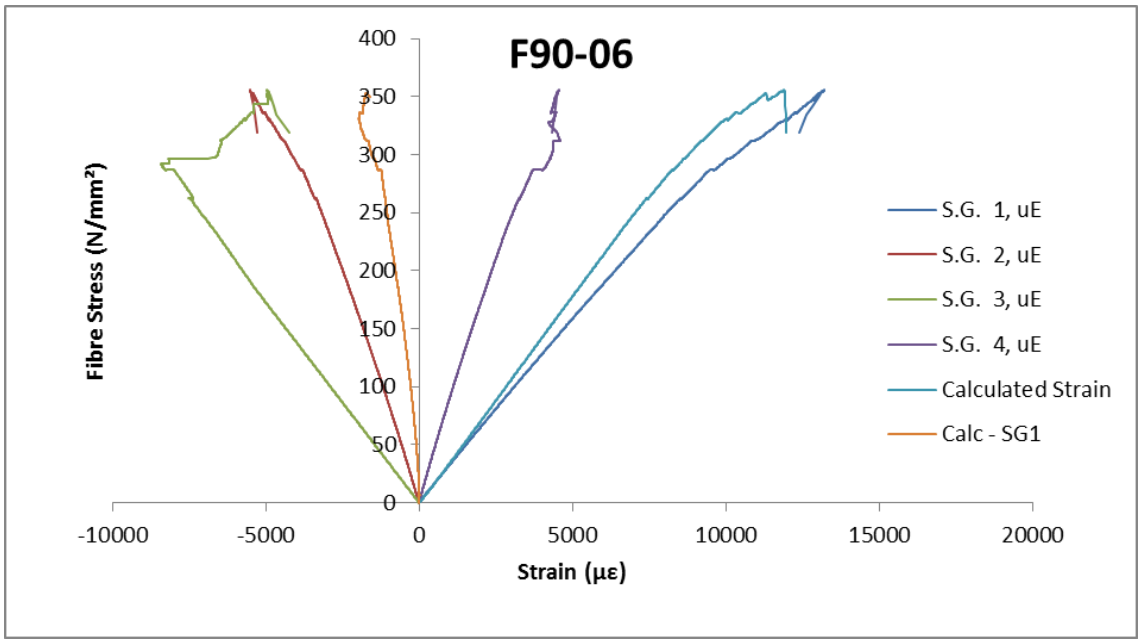

Figure 11-44: Applied Fibre Stress v Resulting strain for sample F[90]-06

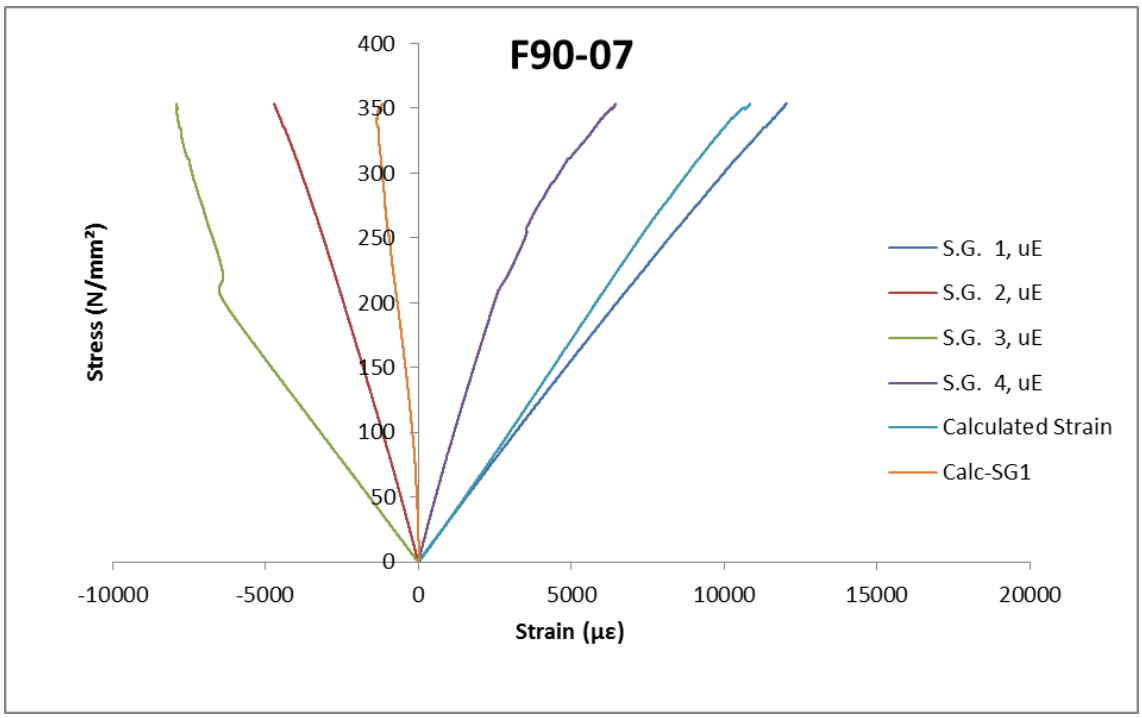

Figure 11-45: Applied Fibre Stress v Resulting strain for sample F[90]-07

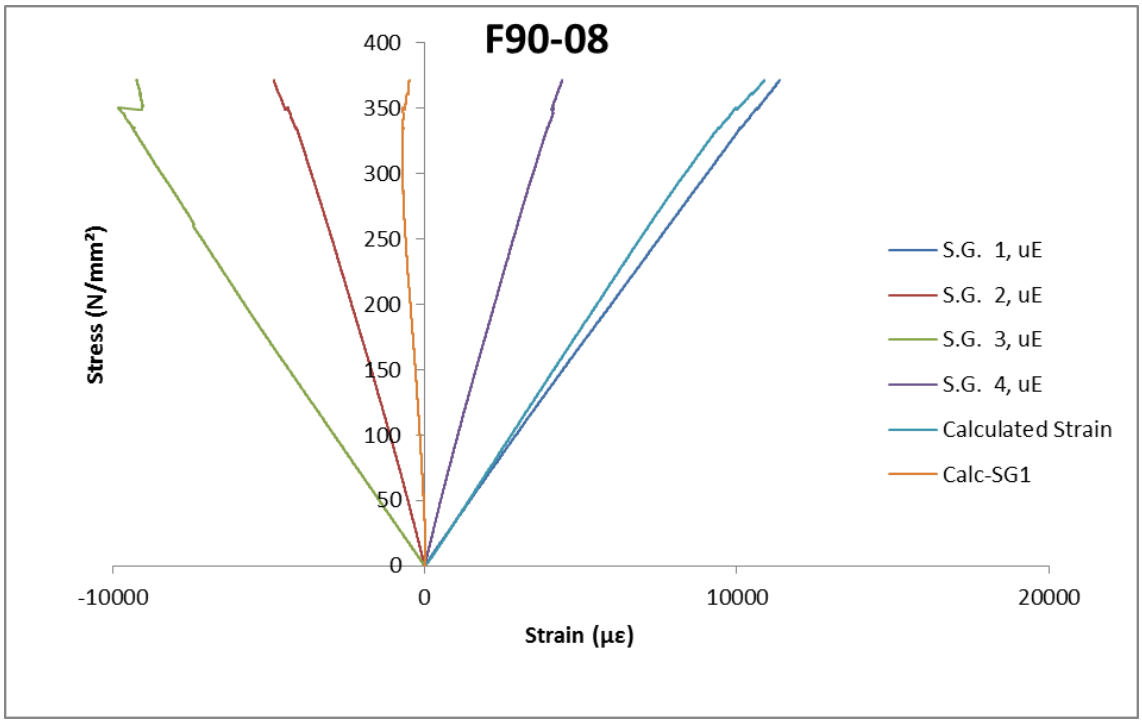

Figure 11-46: Applied Fibre Stress v Resulting strain for sample F[90]-08

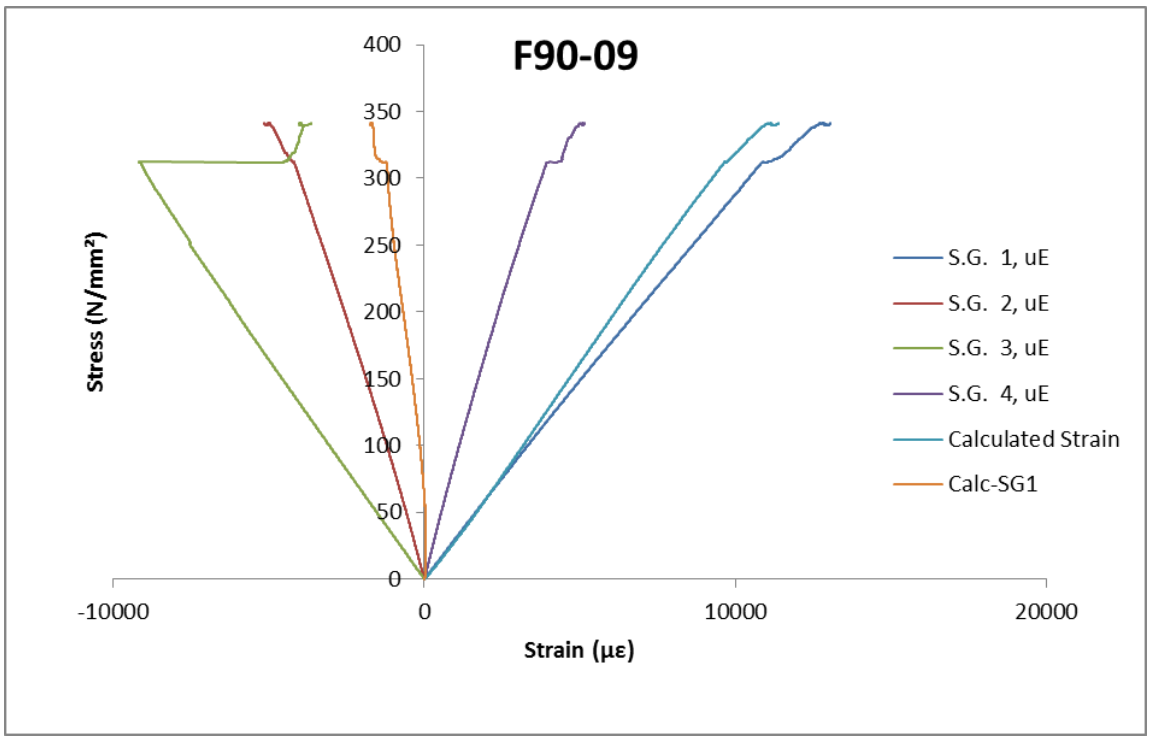

Figure 11-47: Applied Fibre Stress v Resulting strain for sample F[90]-09

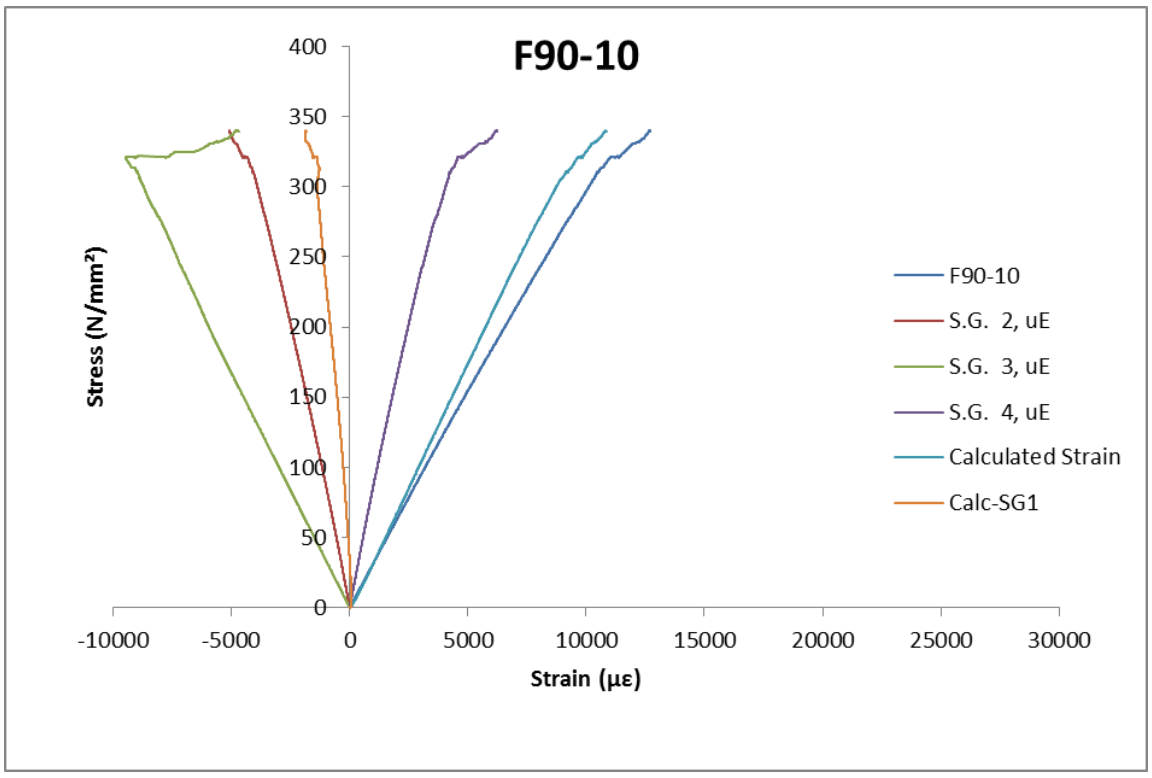

Figure 11-48: Applied Fibre Stress v Resulting strain for sample F[90]-10

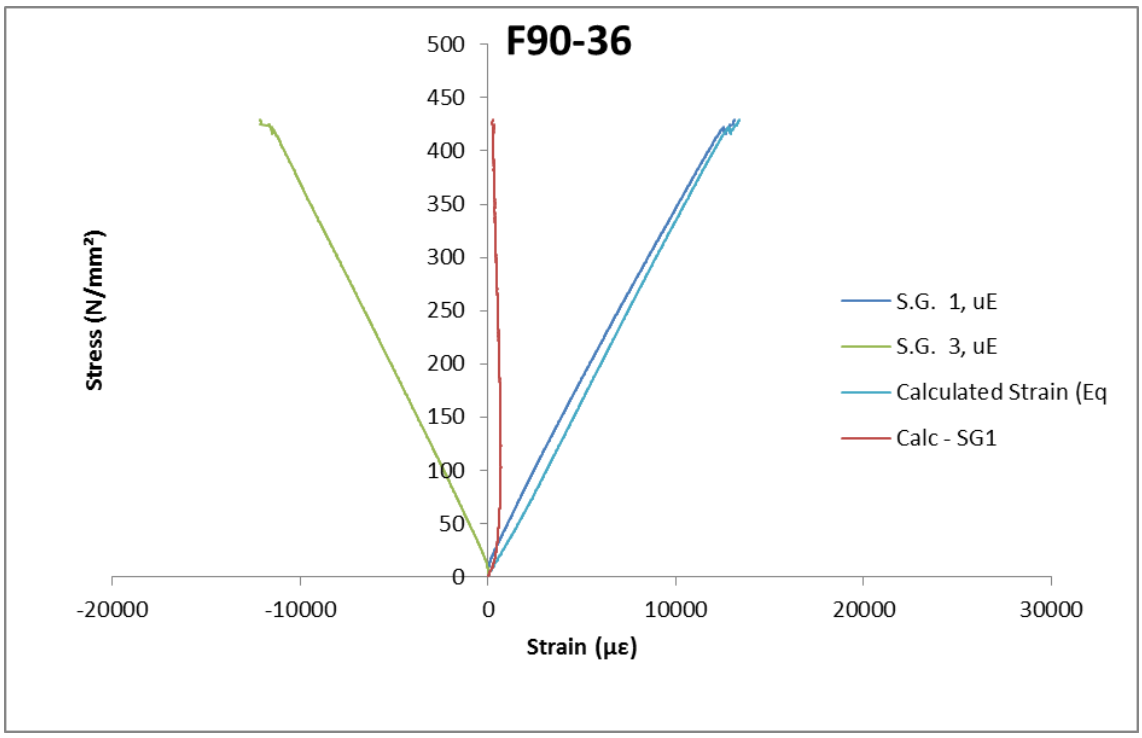

Figure 11-49: Applied stress v Resulting strain for sample F[90]-36.

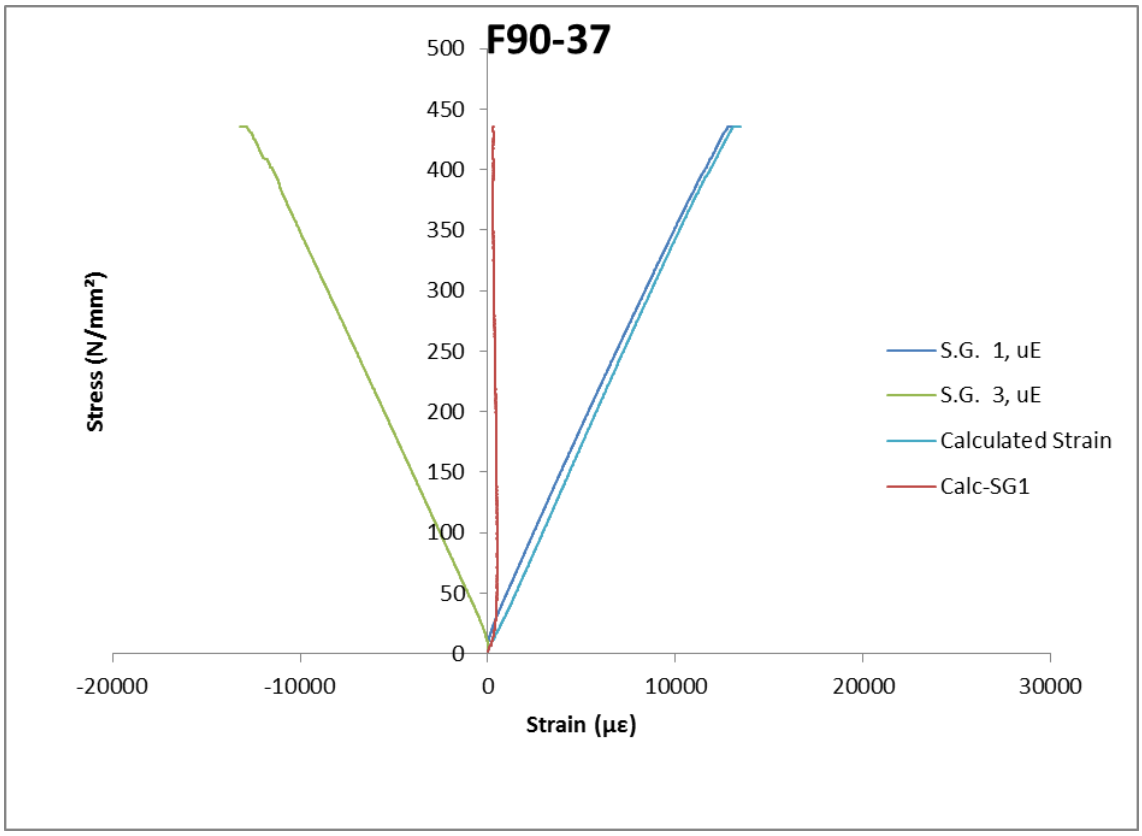

Figure 11-50: Applied Stress v Resulting strain for sample F[90]-37.

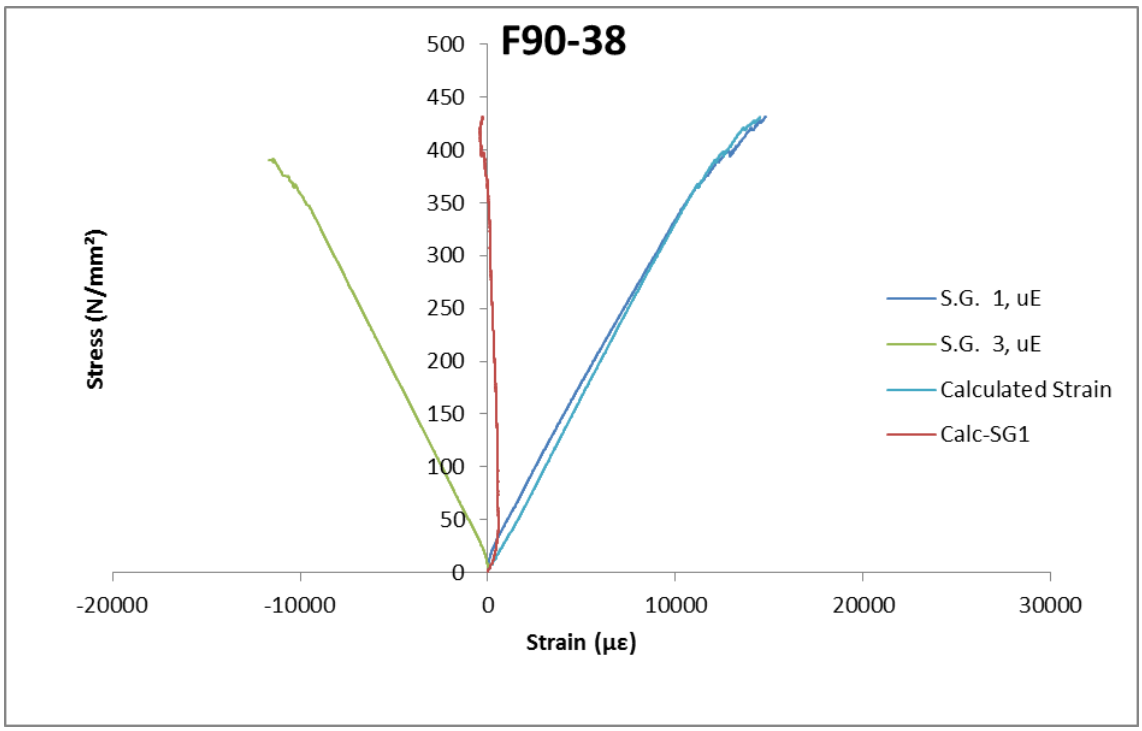

Figure 11-51: Applied Stress v Resulting strain for sample F[90]-38.

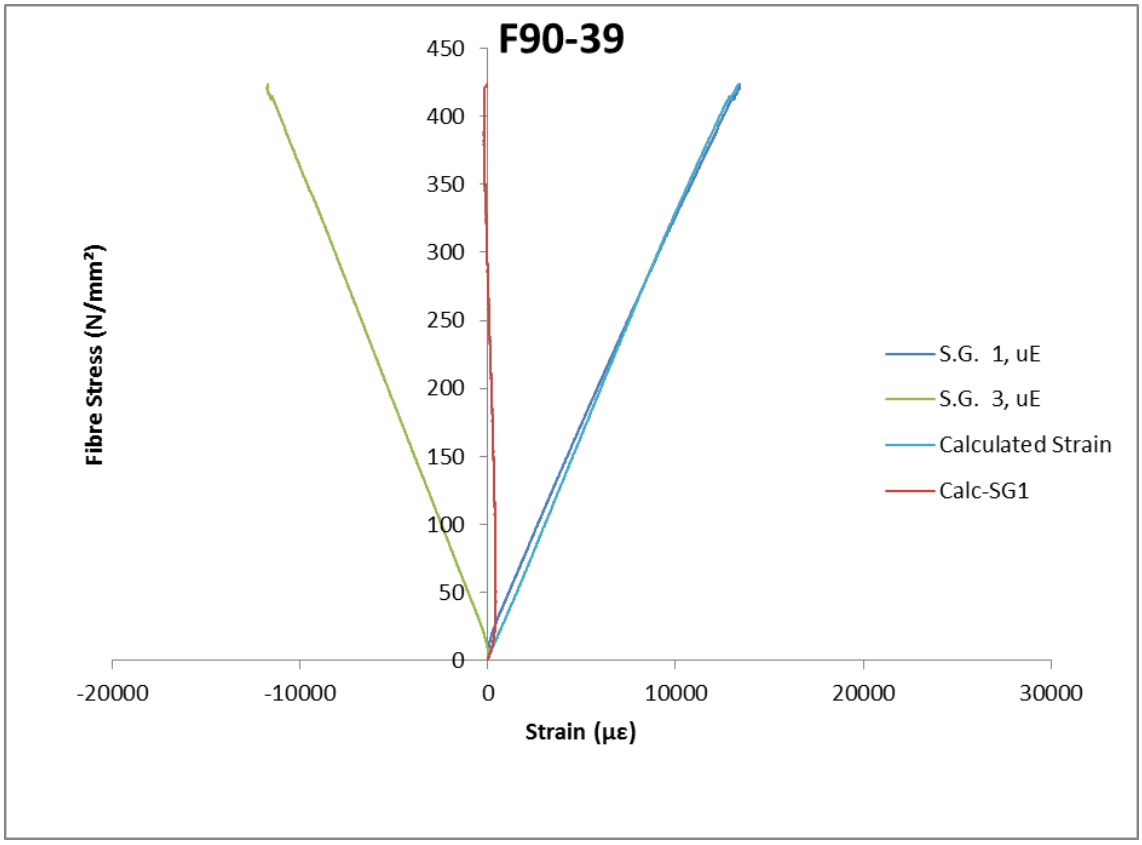

Figure 11-52: Applied Stress v Resulting strain for sample F[90]-39.

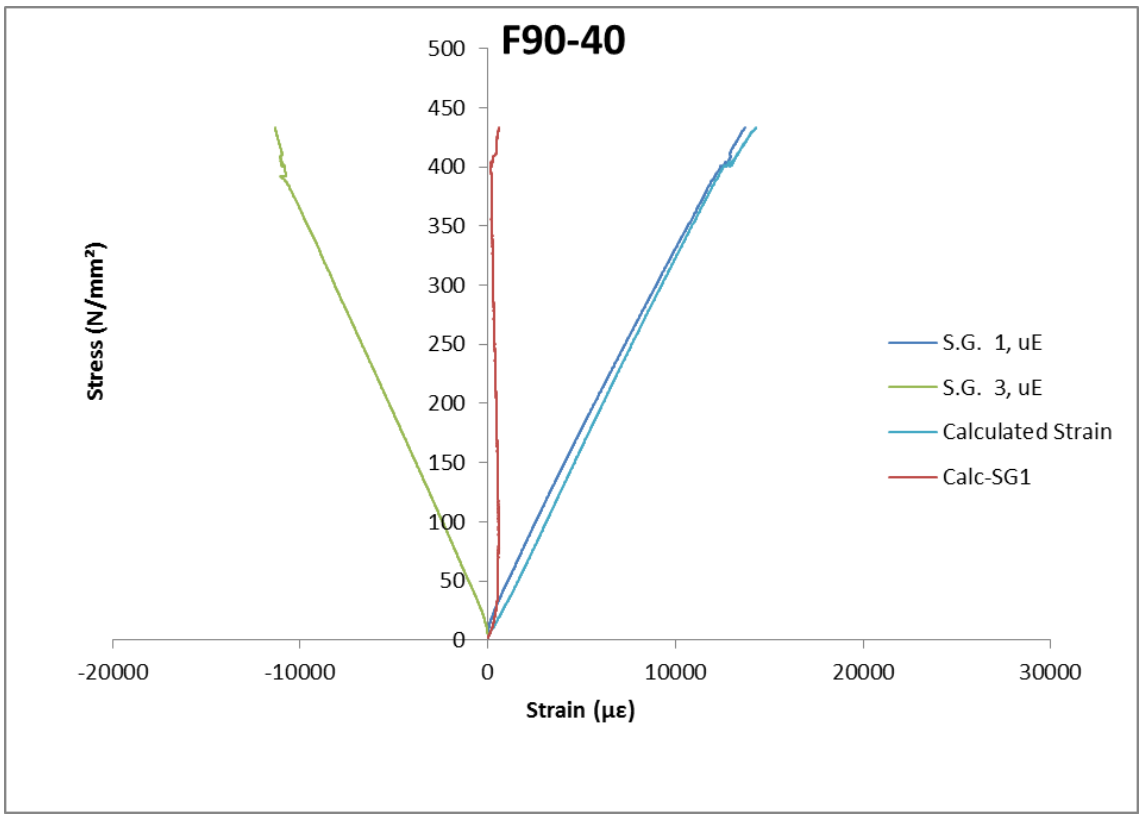

Figure 11-53: Applied Stress v Resulting strain for sample F[90]-40.

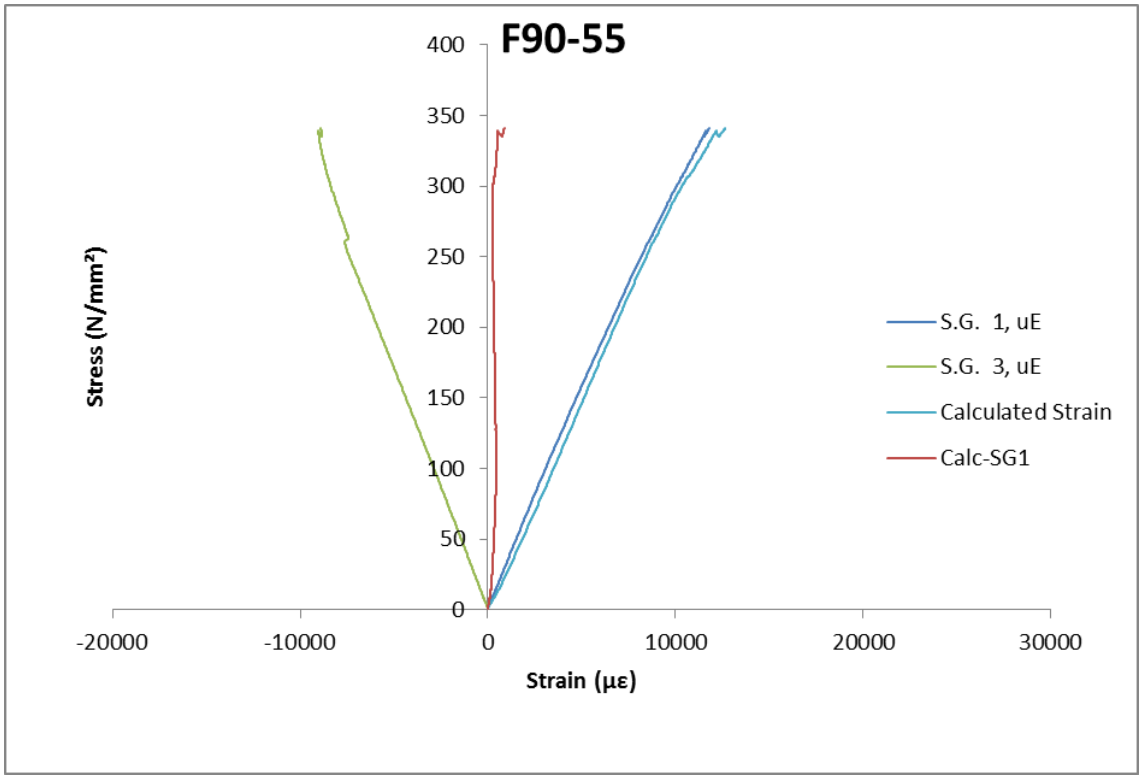

Figure 11-54: Applied Stress v Resulting strain for sample F[90]-55.

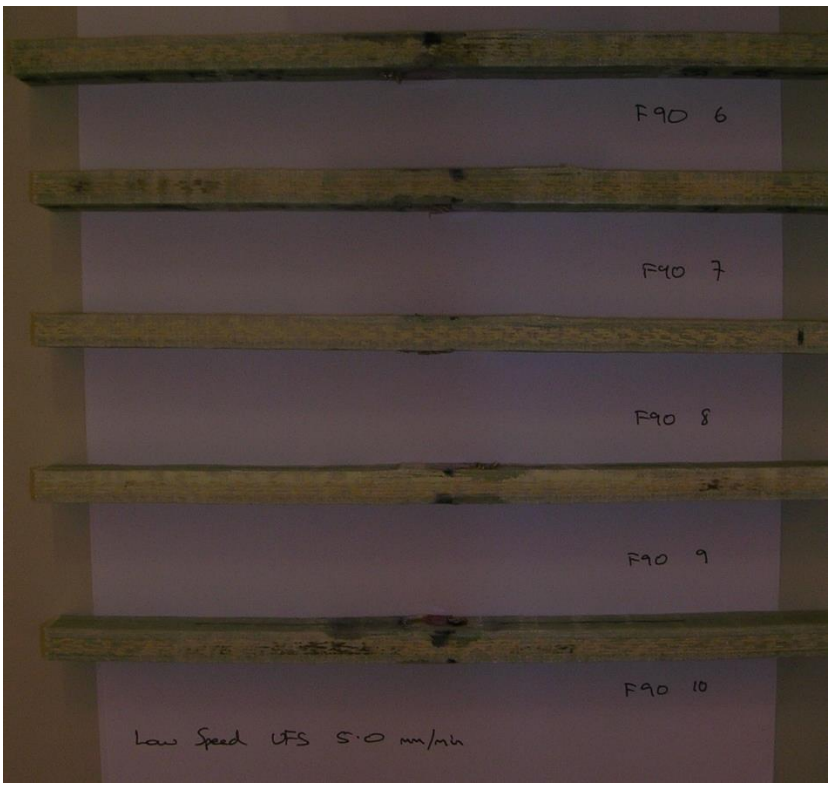

Figure 11-55: [90] Direction UFS Coupons F[90]-06 to 10 tested at a speed of 5mm/min

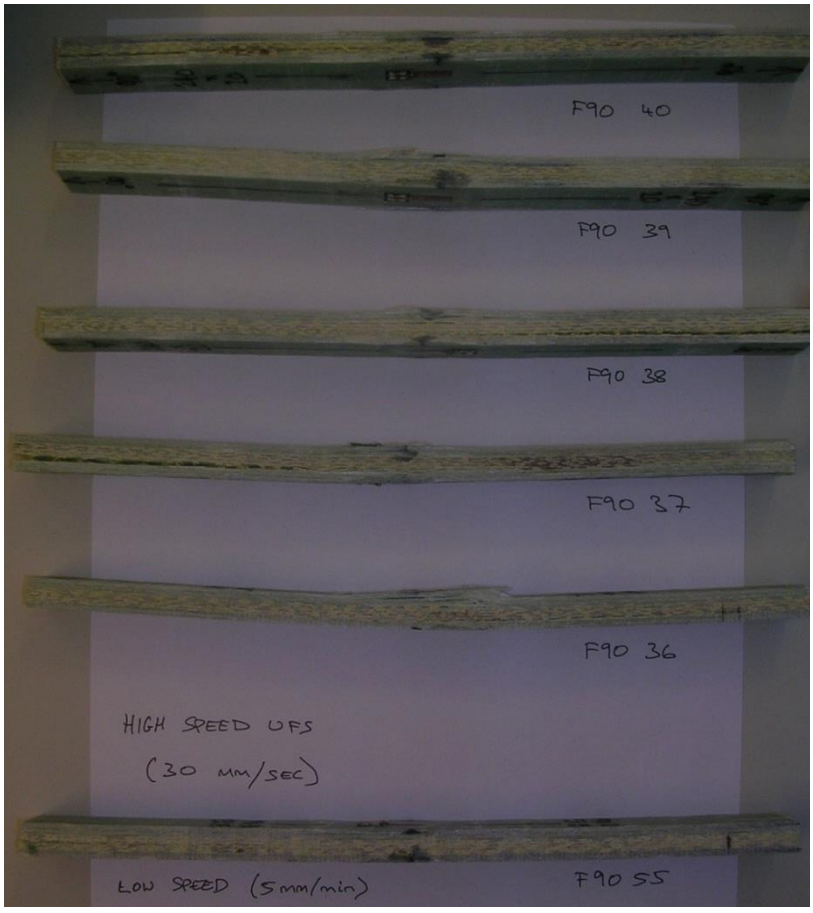

Figure 11-56: [90] Direction UFS Coupons F[90]-36 to 40 tested at a speed of 30mm/sec

11.1.4 Flexural Fatigue Results [0]

11.1.4.1 80% UFS F[0]-16 to F[0]-20

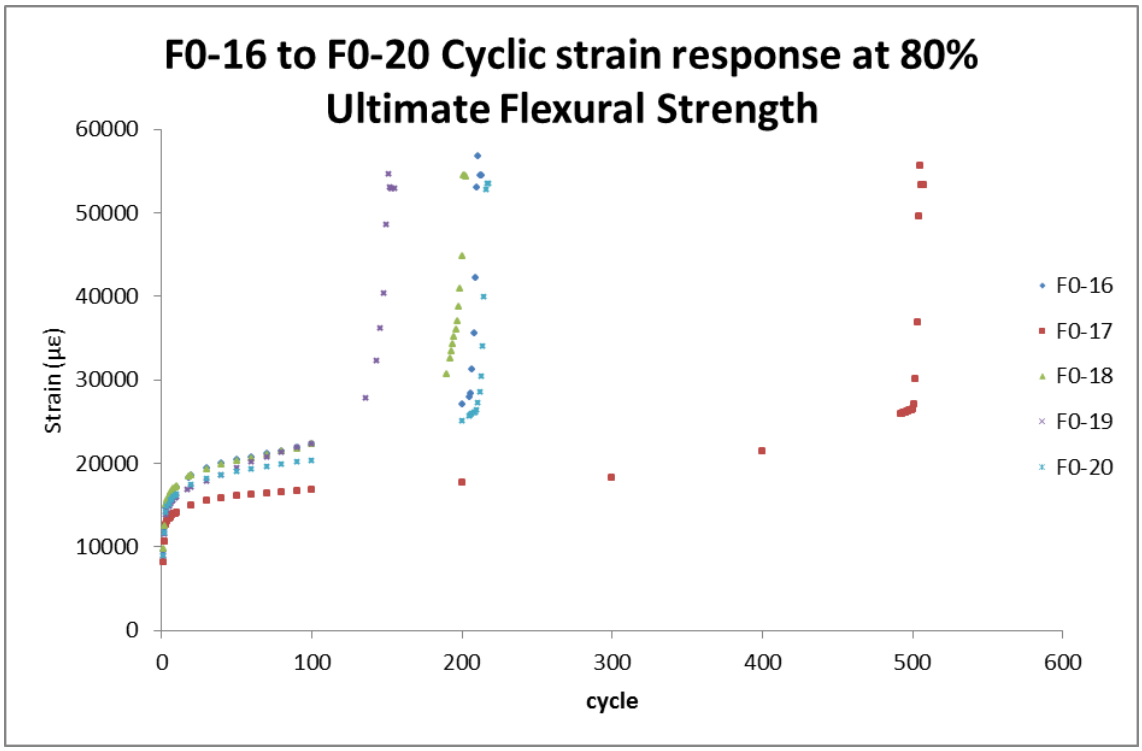

Figure 11-57: Increase in strain response of the coupons F[0] – 16 to 20 with cycle number

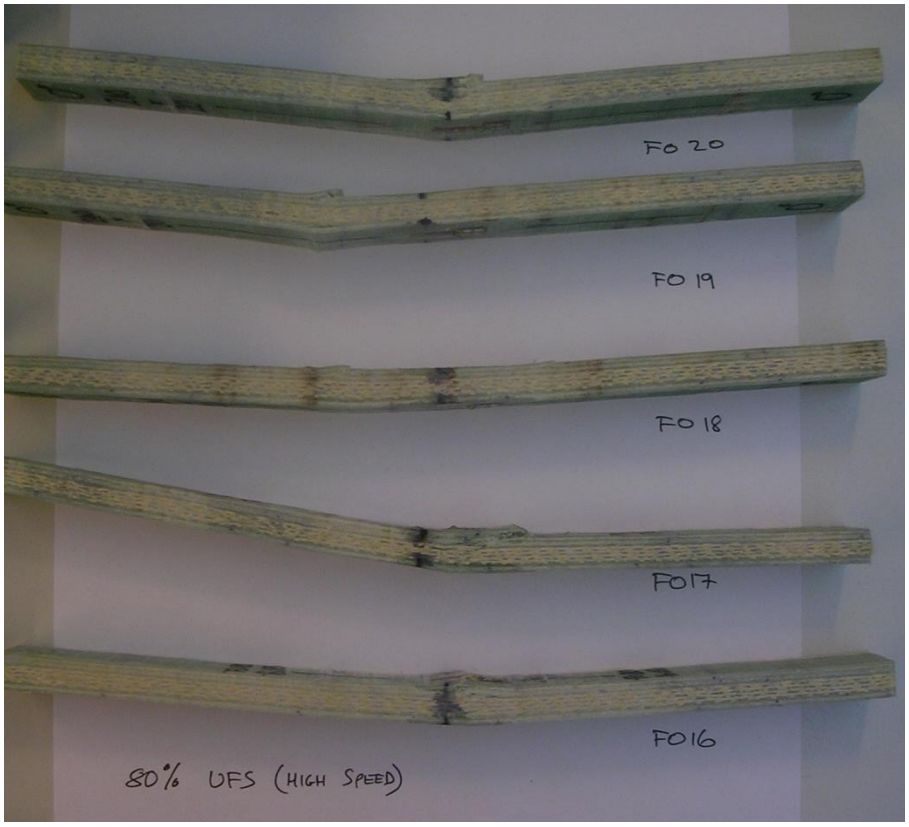

Figure 11-58: Coupons F[0]-16 to F[0]-20 tested at a strain rate of 30mm/min

11.1.4.2 65% UFS F[0]-21 to F[0]-25

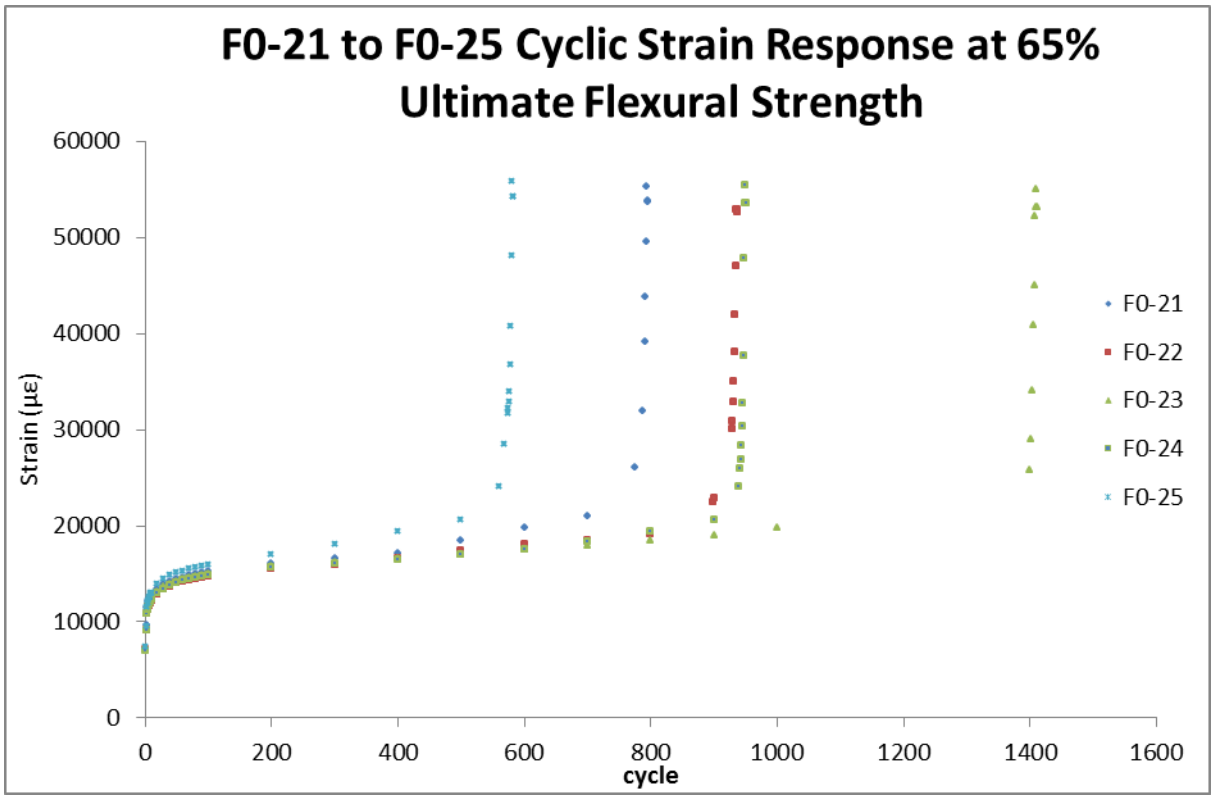

Figure 11-59: Increase in strain response of the coupons F[0] – 16 to 20 with cycle number

Figure 11-60: Coupons F[0]-21 to F[0]-25 tested at a strain rate of 30mm/min

11.1.4.3 55% UFS F[0]-26 to F[0]-29 and F[0]-62

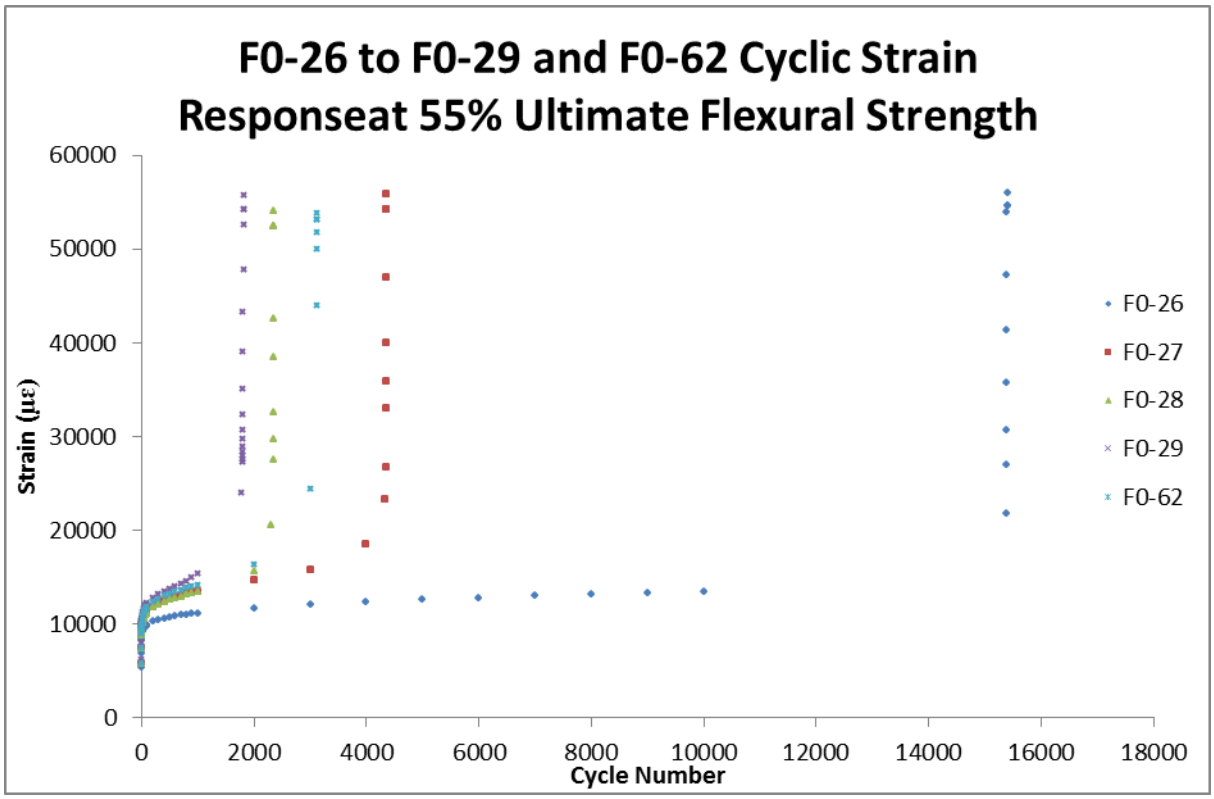

Figure 11-61: Increase in strain response of the coupons F[0] – 26 to 29and F[0]-62 with cycle number

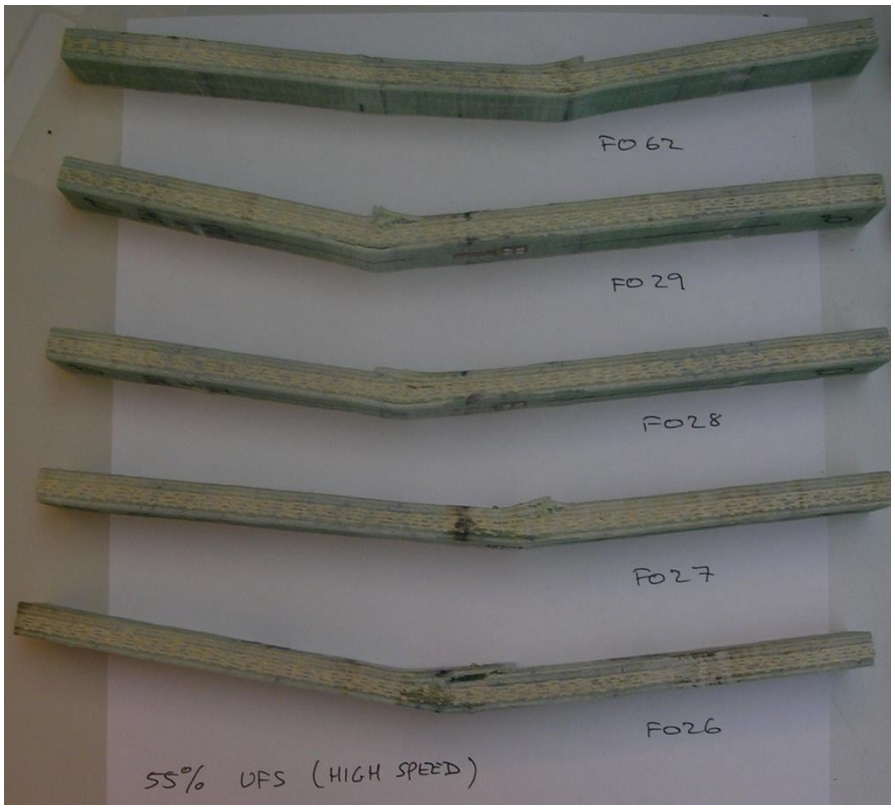

Figure 11-62: Coupons F[0]-26 to F[0]-29 and 62 tested at a strain rate of 30mm/min

11.1.4.4 40% UFS F[0]-32 to F[0]-35 and F[0]-61

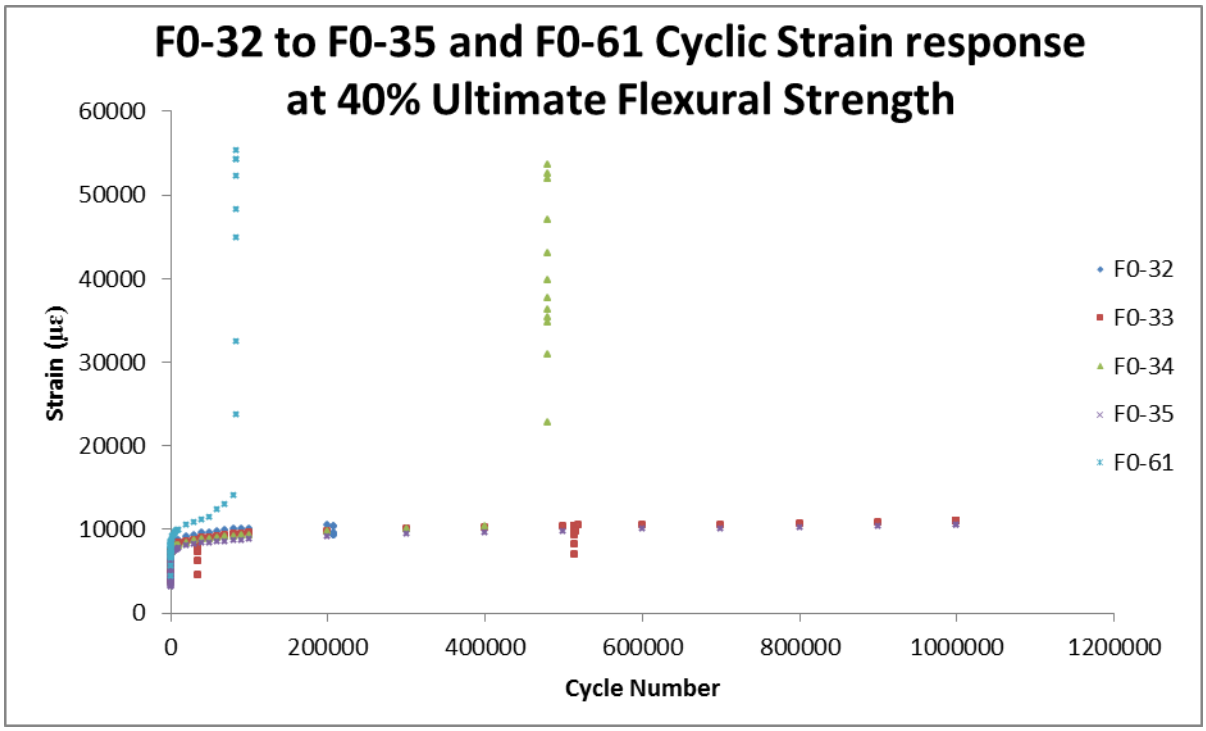

Figure 11-63: Increase in strain response of the coupons F[0] – 23 to 35and F[0]-61 with cycle number.

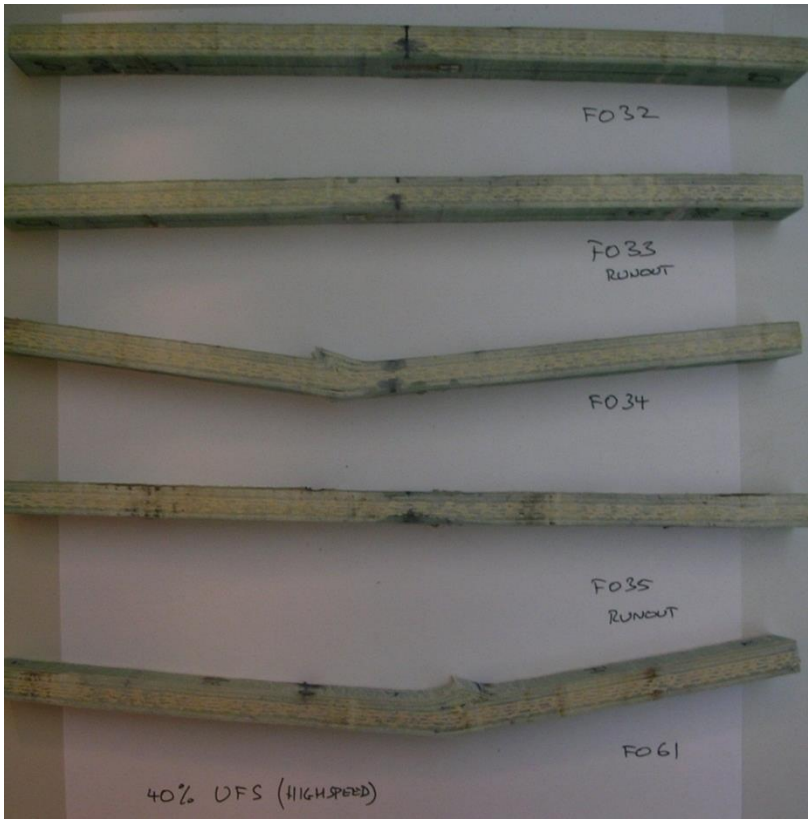

Figure 11-64: Coupons F[0]-32 to F[0]-35 and 61 tested at a strain rate of 30mm/min

11.1.5 Flexural Fatigue Results [90]

11.1.5.1 80% F[90]-41 to F[90]-45

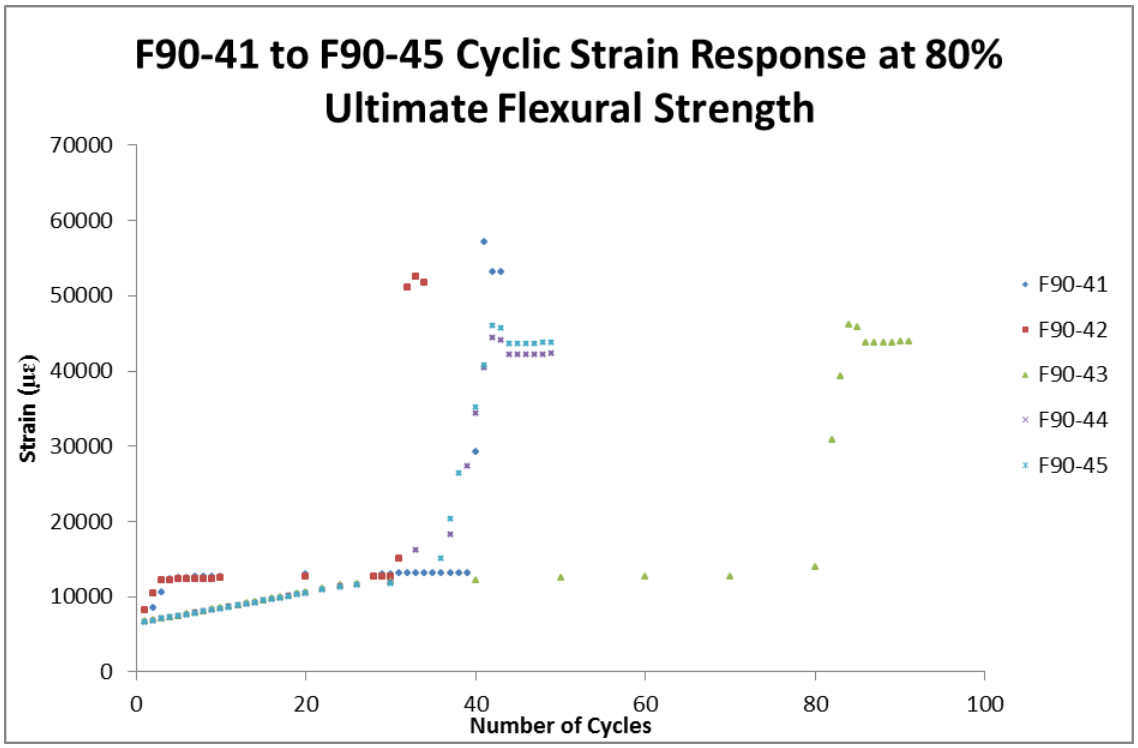

Figure 11-65: Increase in strain response of the coupons F[0] – 41 to 45 with cycle number.

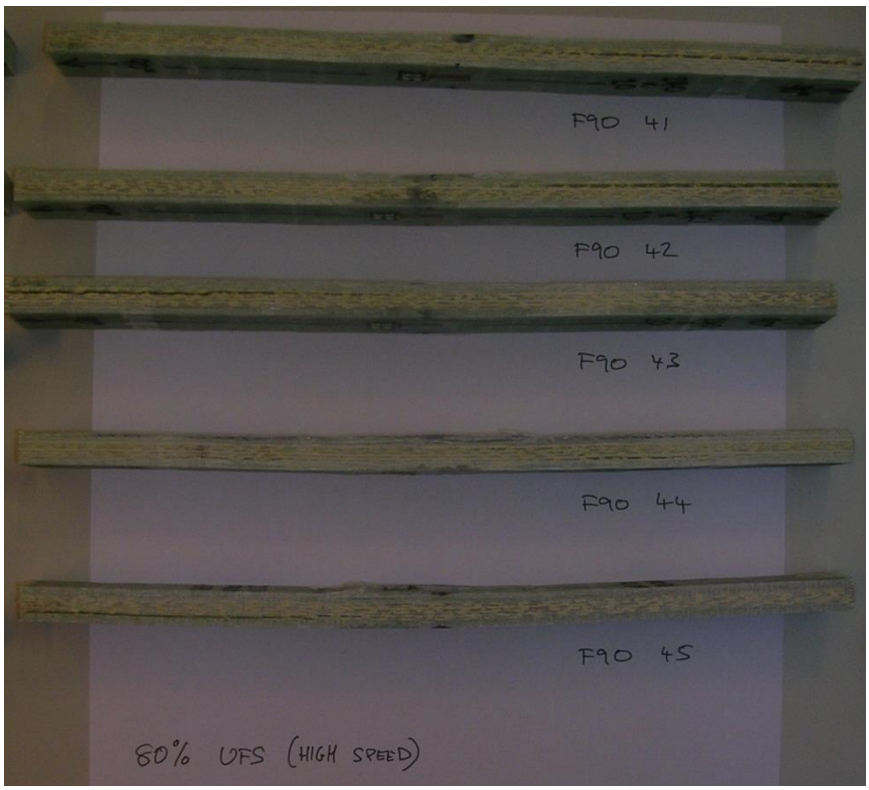

Figure 11-66: Coupons F[0]-41 to F[0]-45 tested at a strain rate of 30mm/min

11.1.5.2 65% F[90]- 46 to F[90] – 50

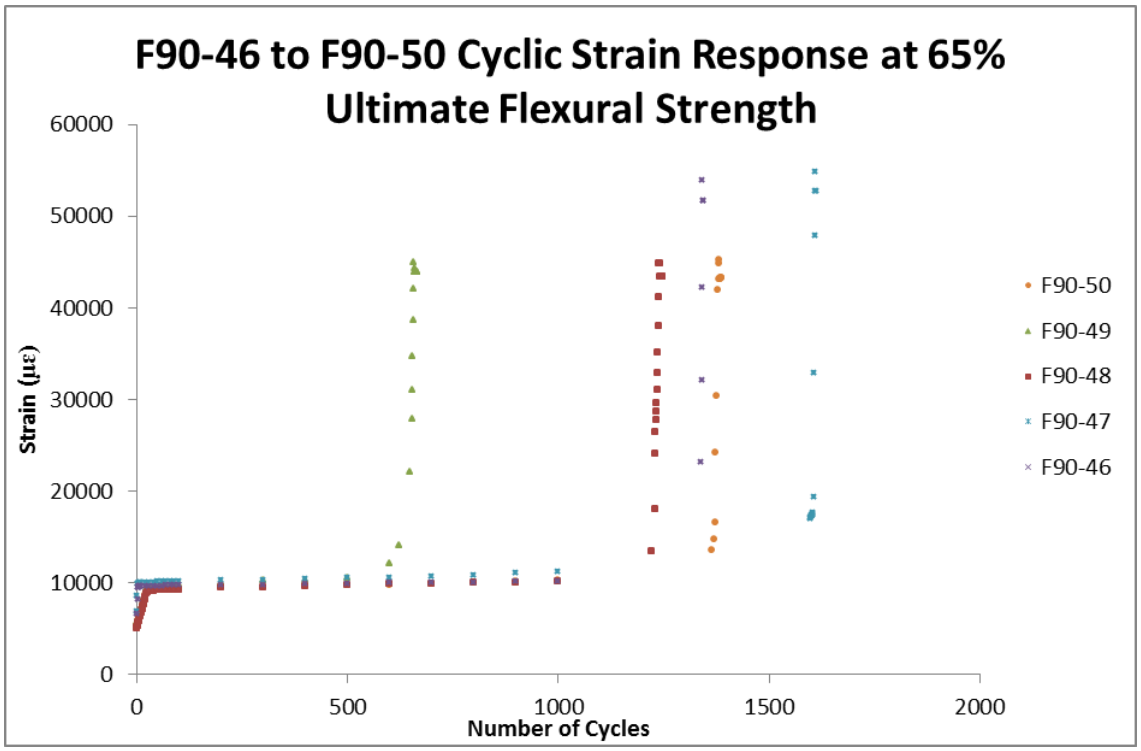

Figure 11-67: Increase in strain response of the coupons F[90] – 46 to 50 with cycle number.

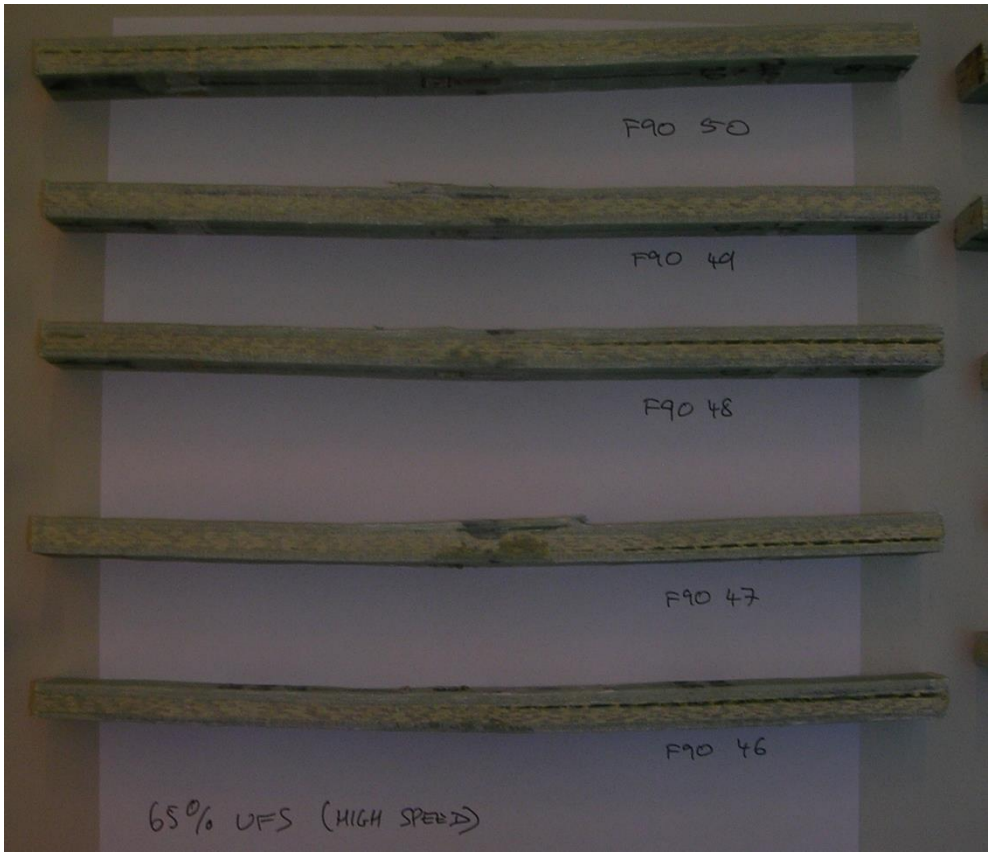

Figure 11-68: Coupons F[90]-46 to F[90]-50 tested at a strain rate of 30mm/min

11.1.5.3 55% F[90] – 51 to F[90] – 54 and F[90]-63

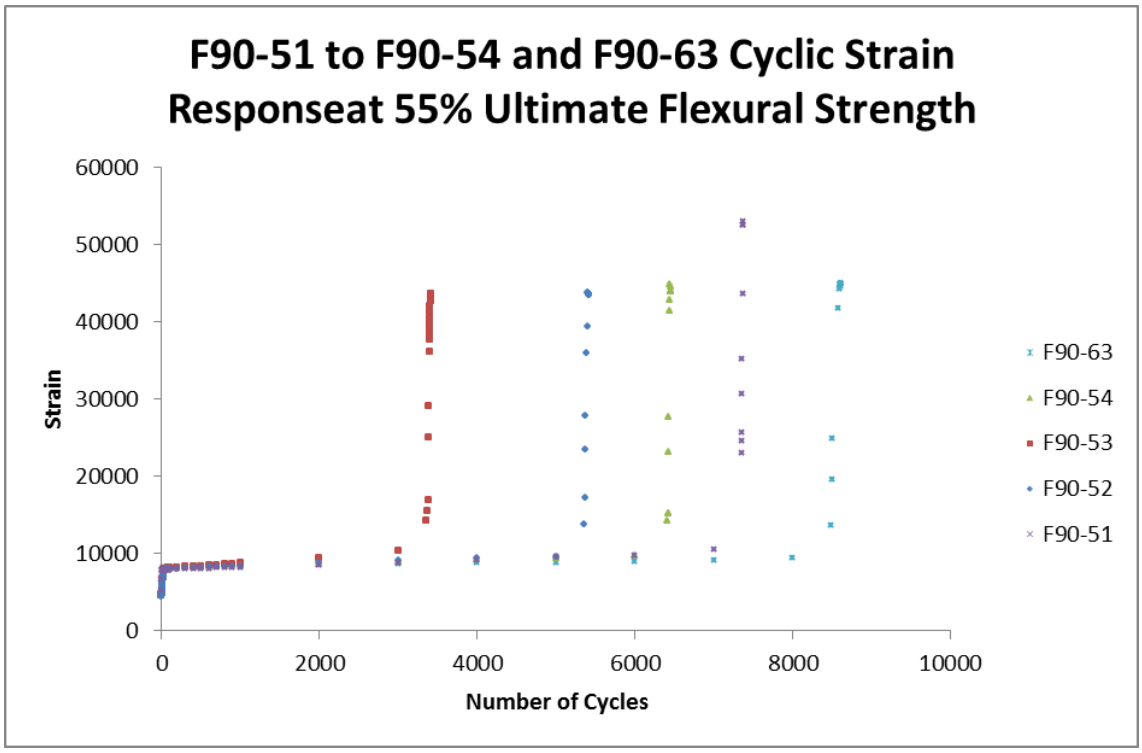

Figure 11-69: Increase in strain response of the coupons F[90] – 51 to 54 and F[90] – 63 with cycle number.

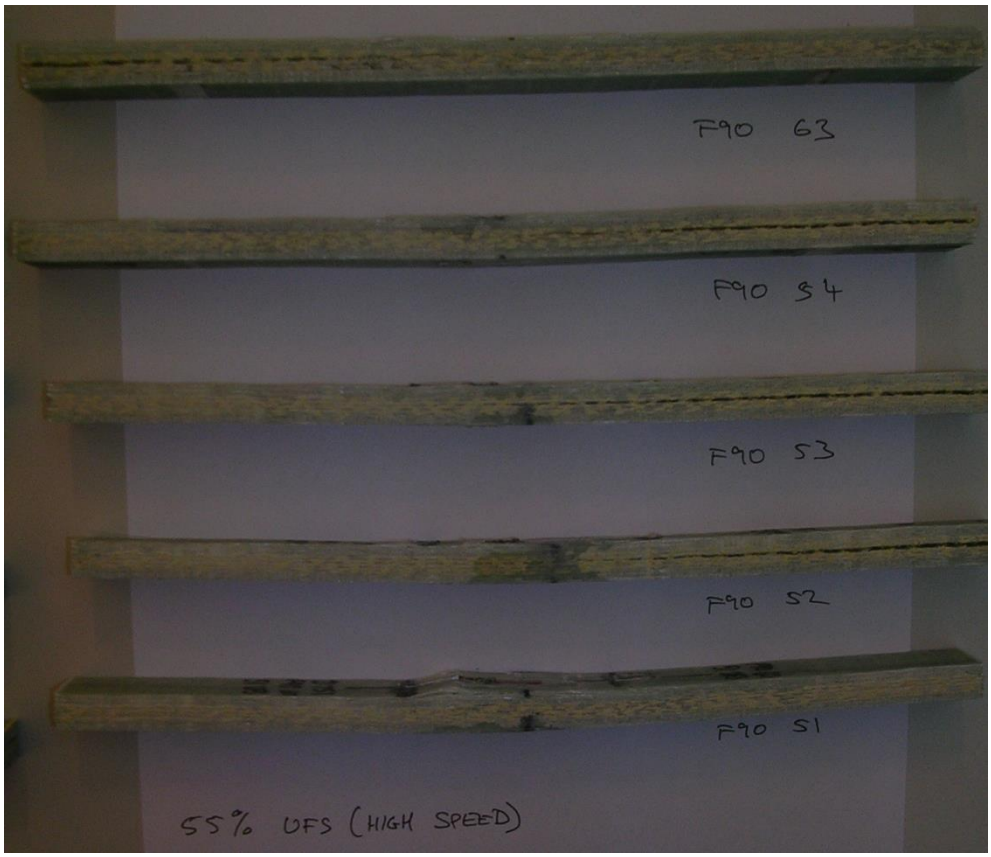

Figure 11-70: Coupons F[90]-51 to F[90]-54 and 63 tested at a strain rate of 30mm/min

11.1.5.4 40% F[90] – 56 to F[90] – 60

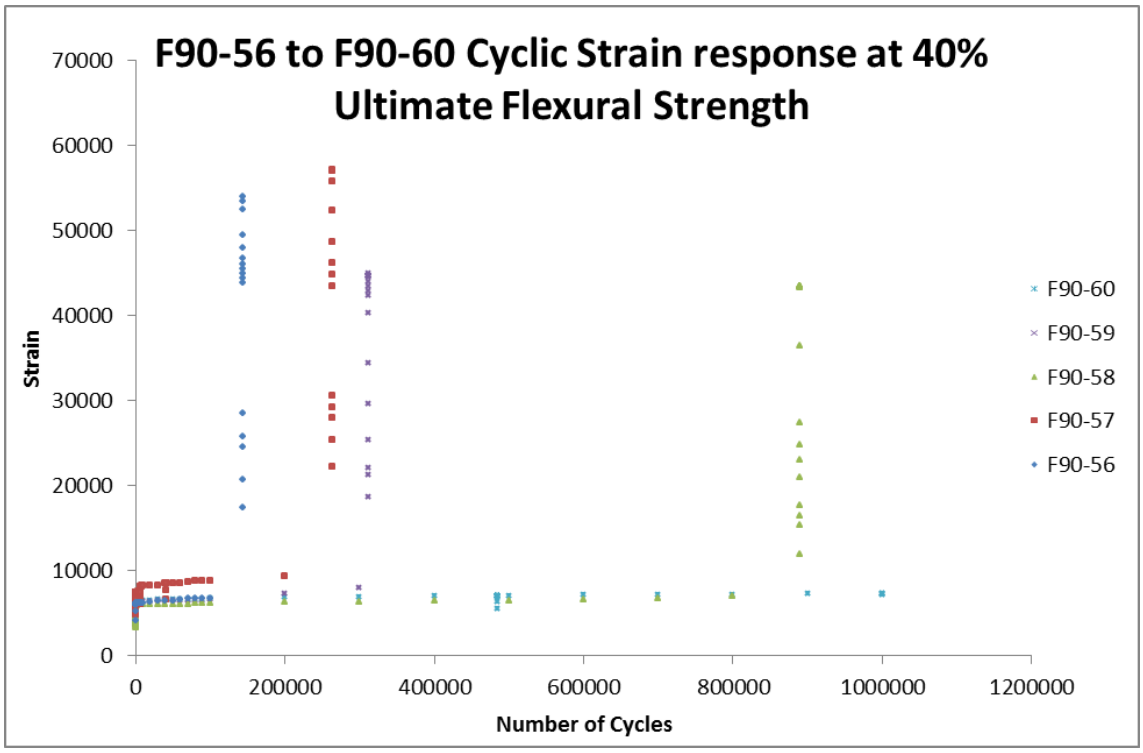

Figure 11-71: Increase in strain response of the coupons F[90] – 51 to 54 and F[90] – 63 with cycle number.

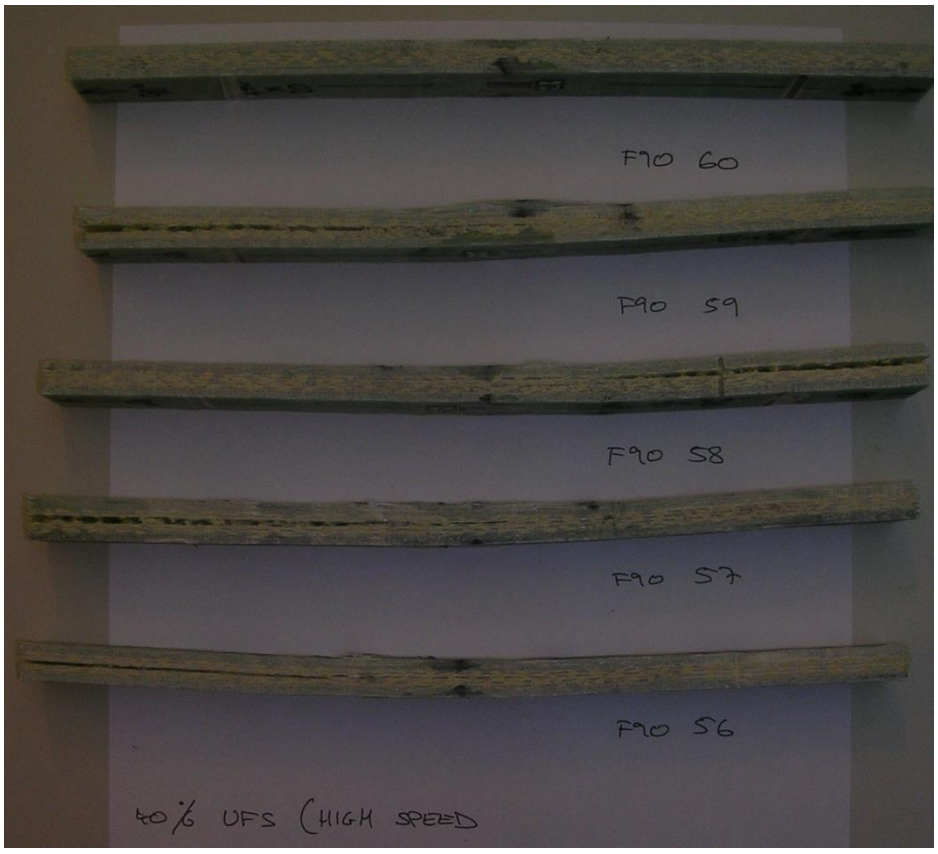

Figure 11-72: Coupons F[90]-51 to F[90]-54 and 63 tested at a strain rate of 30mm/min

11.2 Defining the Operating Environment

11.2.1 Service Durations for ON1221

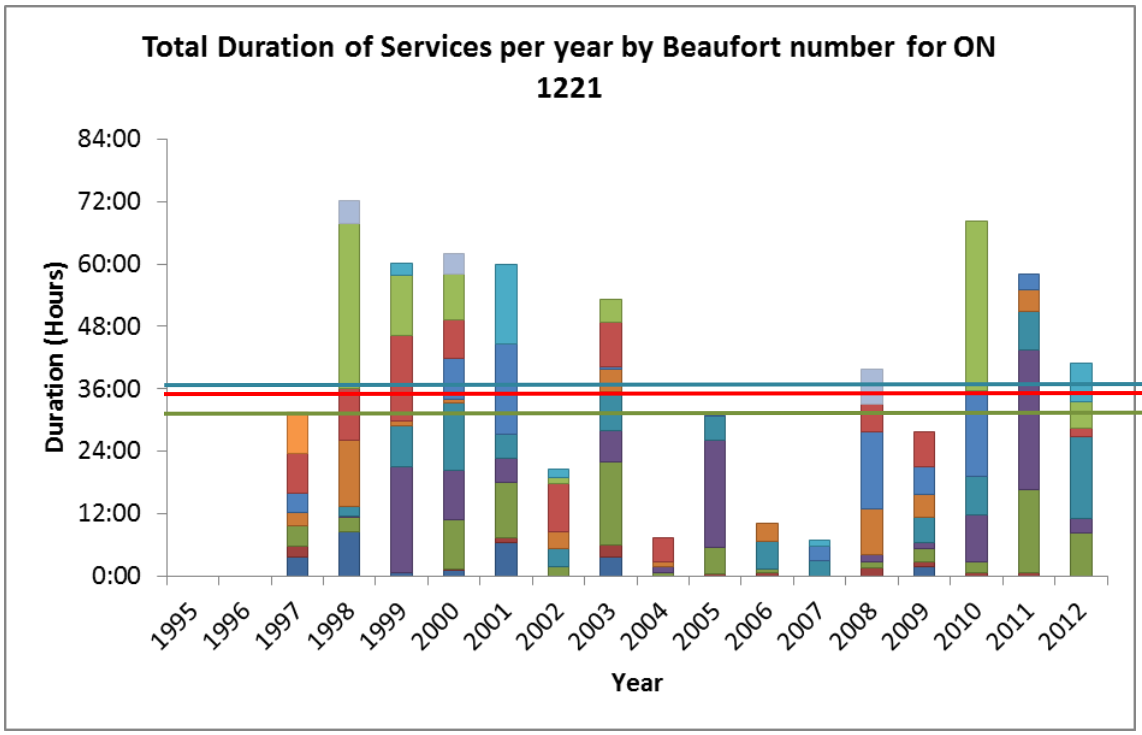

Figure 11-73: General pattern of boat services per year for ON 1221. The average for all Severn class lifeboats calculated from all available service data is shown in blue and that using data from 2005 onwards is shown in green. The red line represents the average for ON 1221.

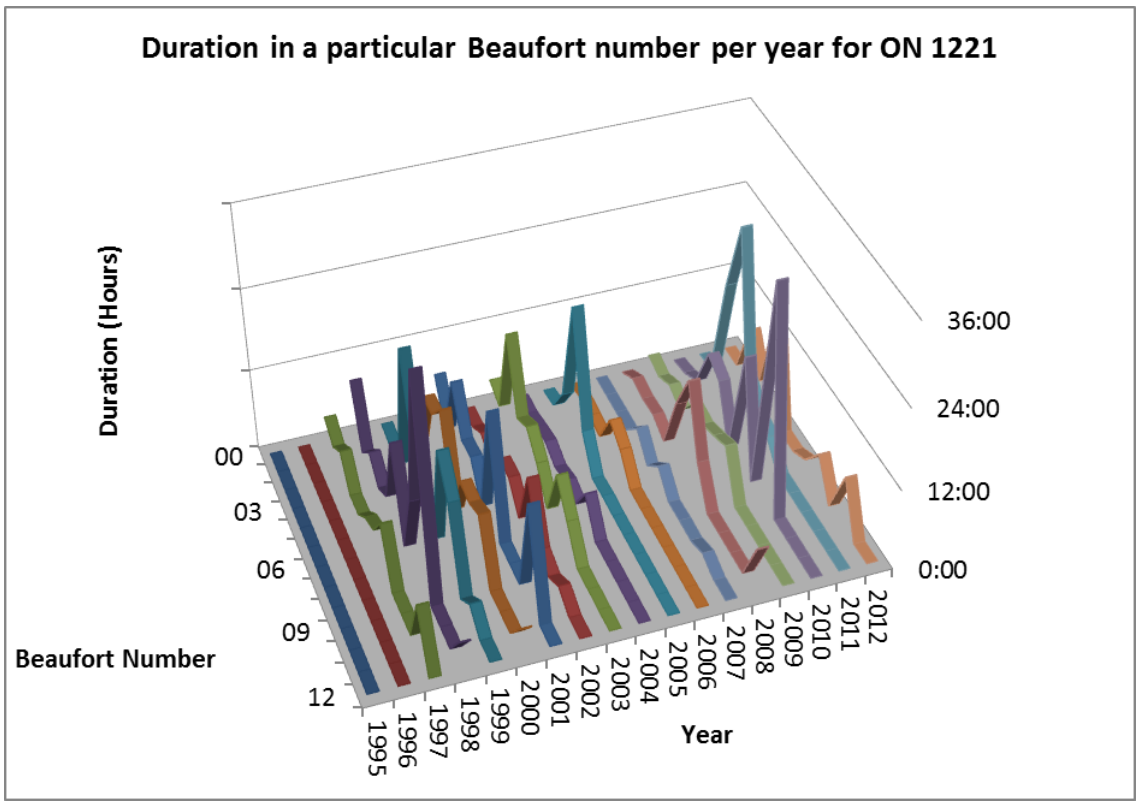

Figure 11-74: The distribution of service durations of ON 1221 for all years in service.

11.2.2 Service Durations for ON1248

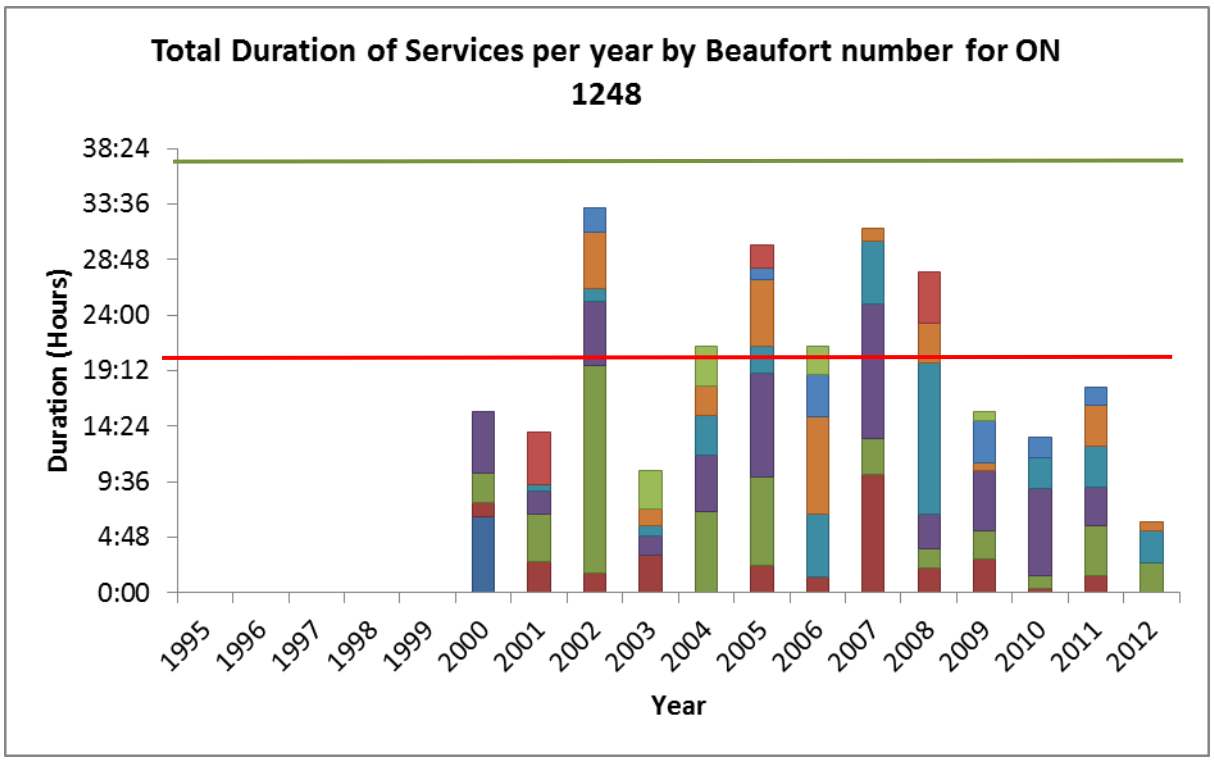

Figure 11-75: General pattern of boat services per year for ON 1248. The average for all Severn class lifeboats calculated from all available service data is shown in blue and that

using data from 2005 onwards is not shown on this graph. The red line represents the average for ON 1248

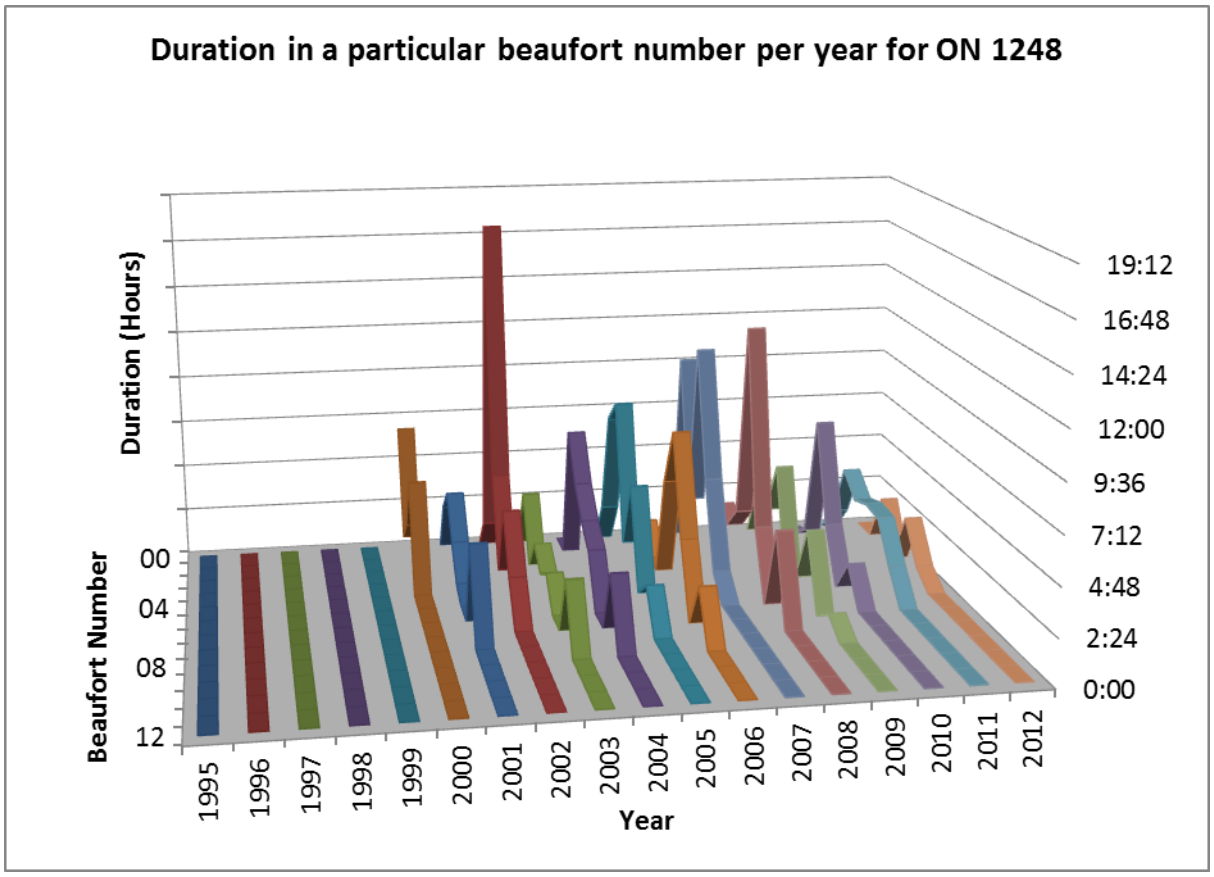

Figure 11-76: The distribution of service durations of ON 1248 for all years in service.

11.3 Data Logging Hardware Summary

Hardware	Purpose	Number
Compact RIO 9074 Real Time Controller	Data flow control and storage	2
C-Series 9036 – Strain Acquisition Module	Strain data acquisition input module	12
CEA 06 250 UR 350 – Strain gauges	Strain data generation	96

Table 11-8: Strain gauge zero values and taken from afloat position in calm weather.

Engine Room			Survivors Space		
Strain gauge	Zero Value (με)	$1+\frac{R_l}{R_g}$	Strain gauge	Zero Value (με)	$1+\frac{R_l}{R_g}$
1	-340.7697014	1.002134172	1	-685.3494452	1.008473958
2	-364.7579068	1.001940033	2	-58.84697193	0.999639221
3	-171.1774385	1.001823639	3	38.75358951	0.999048797
4	-491.2854704	1.004155551	4	-667.6816392	1.004156039
5	334.4486214	1.000931604	5	-73.02294799	1.004784605
6	-385.192153	1.003439782	6	-173.4948237	1.005533339
7	-130.109051	1.001448115	7	-2888.301675	11.96894681
8	95.10013466	0.999694179	8	-239.9177148	1.004922559
9	-6296.695001	0.992868944	9	109.3370567	1.00192032
10	-390.5430567	1.002881598	10	-52854.53839	-0.000214406
11	-264.6009871	1.003709232	11	380.563121	1.005042908
12	-862.3569883	1.004656039	12	59405.56894	0.000214213
13	-410.07381	1.003587416	13	-25.85195773	1.00419233
14	-594.7115196	1.004881371	14	2974.197458	1.002902492
15	-587.9980716	1.005266388	15	-45.6274771	1.004087486
16	-596.9452118	1.002252497	16	-390.5739397	1.006422738
17	-486.6342918	1.004486093	17	214.6833669	1.002289916
18	-354.7097331	1.003293939	18	-108.73936	1.000419326
19	127.4443057	1.001291675	19	307.9807535	1.001393046
20	80.30323536	1.001796544	20	222.6648353	1.004481491

Engine Room			Survivors Space		
Strain gauge	Zero Value (με)	$1+\frac{R_l}{R_g}$	Strain gauge	Zero Value (με)	$1+\frac{R_l}{R_g}$
21	-314.9091588	1.002657097	**21**	160.8242265	1.007106565
22	-352.437487	1.006485636	**22**	462.1752965	1.003638672
23	-269.2473	1.004732652	**23**	447.1868557	-1.101740468
24	-539.8788598	1.004271785	**24**	-133.7407269	1.005786343
25	-202.8427313	1.001372385	**25**	-119.5048625	1.006571393
26	131.8007719	1.002680439	**26**	32.08324655	1.0021043
27	-188.5257546	1.002781304	**27**	-680.1855672	1.005155188
28	187.7597857	1.00191045	**28**	-117.8978623	1.003293374
29	616.0373114	1.002989353	**29**	-501.3552444	1.004536102
30	-79.53557955	1.001895442	**30**	58.81246828	1.00344799
31	-171.0009049	1.006005048	**31**	-813.8150313	1.004511035
32	-19.30667148	0.900040293	**32**	383.0061864	1.003652499
33	-86.20201439	1.002868284	**33**	1118.075971	0.99343167
34	-225.9363581	1.007113432	**34**	-67.92671415	1.003691107
35	-375.9500178	1.003392155	**35**	165.5715809	1.001825384
36	-57.09506726	1.002962161	**36**	-116.9425687	1.00236779
37	-445.2138772	1.002908331	**37**	33.22281254	1.002592847
38	498.3935222	1.001021359	**38**	-279.9683349	1.002885057
39	198.893908	1.000917441	**39**	-281.6568995	1.004308445
40	-79.66531712	1.005595801	**40**	-1257.196228	1.004862409
41	-14.59969713	1.00169293	**41**	-1247.977731	1.003800013
42	-215.069565	1.00161639	**42**	-143.8424838	1.005999599
43	-12.86952159	1.002363417	**43**	-533.1657673	1.004453914
44	-444.372247	1.001958374	**44**	-104.4916202	1.003892872
45	-414.800262	1.002541834	**45**	406.9707956	1.001826685
46	-121.7435216	1.002410146	**46**	-119.658086	1.004061734
47	-222.2962774	1.004393805	**47**	61.33262416	1.000898401
48	-96.60026738	1.001701759	**48**	-121.7355002	1.004950295

Table 11-9: Table showing the channel numbers related to the panels. The engine room and survivors space have the same number of panels with the same strain gauge set up. Panel number 1 in this table is equivalent to 1 and 17 in the schematic in Figure 6-1, 2 equivalent to 2 and 18 and so on.

Panel Number	Strain Gauge Number		
	Longitudinal	Compartment with errors	Transverse
1	6	SS →	2
2	0		5
3	3	← SS	14
4	12	← SS, ER →	8
5	15		11
6	9	← ER	20
7	18		23
8	21		17
9	30		26
10	24		29
11	27		38
12	36	ER →	32
13	39		35
14	33	← SS	44
15	42		47
16	45		41

Appendix 4 contains the software written to control the data loggers.

Appendix 5 contains the post processing software.

Note: To access the data logging software a copy of LabVIEW (Minimum LabVIEW2012) needs to be installed on the machine as well as the FPGA control software.

Appendix 6 contains the rainflow counting outputs for all channels of interest.

Note: The Rainflow analysis was run using a high performance computer cluster to reduce the processing time to a sensible limit.

Appendix 7 contains the spreadsheet used to implement the method in section 7.3.

Note: To successfully use the spreadsheet from Appendix 6, entitled "RF_AMP_P90_Regression_Line.xlsx" will need to be opened as well. And a copy of @RISK needs to be installed on the computer (https://www.palisade.com/risk/).

References

ABS, 2004. Spectral-Based Fatigue Analysis for Vessels (Guide For). American Bureau of shipping, American Bureau of Shipping, ABS Plaza, 16855 Northchase Drive, Houston, USA.

ABS, 2010. Spectral-Based Fatigue Analysis For Floating Production, Storage and Offloading (FPSO) Installations (Guide for). American Bureau of shipping, American Bureau of Shipping, ABS Plaza, 16855 Northchase Drive, Houston, USA.

Agarwal, B.D., Dally, J.W., 1975. PREDICTION OF LOW-CYCLE FATIGUE BEHAVIOUR OF GFRP: AN EXPERIMENTAL APPROACH. Journal of Materials Science 10, 193–199.

Al-Assaf, Y., El Kadi, H., 2001. Fatigue life prediction of unidirectional glass fiber/epoxy composite laminae using neural networks. Composite Structures 53, 65–71.

Allen, R.G., Jones, R.R., 1978. A simplified method for determining structural design limit pressures on high performance marine vehicles, in: AIAA/SNAME Advanced Marine Vehicle Conference.

Aquelet, N., Souli, M., Olovsson, L., 2006. Euler-Lagrange coupling with damping effects: Application to slamming problems. Computer Methods in Applied Mechanics and Engineering 195, 110–132.

Baker, W., McKenzie, I., Jones, R., 2004. Development of life extension strategies for Australian military aircraft, using structural health monitoring of composite repairs and joints. Composite Structures 66, 133–143. doi:10.1016/j.compstruct.2004.04.031

Belgrano, G., 1995. Material Mechanical Properties.

Bishop, R.E.D., Price, W.G., 2005. Hydroelasticity of Ships. Cambridge University Press, Cambridge.

Bisplinghoff, R.L., Doherty, C.S., 1952. Some studies of the impact of vee wedges on a water surface. Journal of the Franklin Institute 253, 547–561. doi:10.1016/0016-0032(52)90674-1

Blech, G., 2000. Aging Aircraft Subsystems Equipment Life Extneiosn within the Tornado Program. Presented at the Aging Engines, Avionics, Subsystems and Helicopters, Research and Technology Organisation (North Atlantic Treaty Organisation), p. 116.

Bond, I.P., 1999. Fatigue life prediction for GRP subjected to variable amplitude loading. Composites - Part A: Applied Science and Manufacturing 30, 961–970.

Bond, I.P., Ansell, M.P., 1998. Fatigue properties of jointed wood composites Part I Statistical analysis, fatigue master curves and constant life diagrams. Journal of Materials Science 33, 2751–2762. doi:10.1023/A:1017565215274

Bond, I.P., Farrow, I.R., 2000. Fatigue life prediction under complex loading for XAS/914 CFRP incorporating a mechanical fastener. International Journal of Fatigue 22, 633–644.

Bottomley, P.J., 1983. Royal National Lifeboat Institution Fast Afloat Boat MKIV (Yacht and Small Craft No. YSCS/620033). Lloyd's Register of Shipping, 71Fenchurch Street, London.

Bretschneider, C.L., 1961. A one dimensional gravity wave spectrum. Ocean Wave Spectra 41–56.

Brodtkorb, P.A., Johannesson, P., Lindgren, G., Rychlik, I., Rydén, J., Sjö, E., 2000. WAFO - a Matlab Toolbox for the Analysis of Random Waves and Loads, in: Proc. 10'th Int. Offshore and Polar Eng. Conf., ISOPE, Seattle, USA. pp. 343–350.

BS 2846-2: 1981, 1981. Statistical determination of data - Part 2: Estimation of the mean confidence interval (Standard), British Standard. BSI.

BS EN ISO 527, P. 4, 1997. Plastics - Determination of tensile properties (Standard No. - Part 4: Test conditions for isotropic and othotropic fibre-reinforced plastic composites), British Standard. British Standards Online.

BS EN ISO 14125, 2011. Fibre Reinforced Plastic Composites - Determination of Flexural Properties (Standard No. 14125:1998+A1:2011), British Standard. BSI.

BS ISO 12110-2, 2012. Metallic materials. Fatigue testing. Variable amplitude fatigue testing. (Standard No. Part 2. Cycle counting and related data reduction methods), British Standard. British Standards Online.

BS ISO 13003, 2003. Fibre-Reinforced Plastics - Determination of fatigue properties under cyclic loading conditions (Standard No. 13003:2003), British Standard. BSI.

Burman, M., Rosén, A., Zenkert, D., 2010. Spectrum Slam Fatigue Loading of Sandwich Materials for Marine Structures, in: ICSS9. Presented at the 9th International Conference on Sandwich Structures, CalTech, Pasadena, USA.

Cavatorta, M.P., 2007. A comparative study of the fatigue and post-fatigue behavior of carbon-glass/epoxy hybrid RTM and hand lay-up composites. Journal of Materials Science 42, 8636–8644.

Chambers, A.R., Earl, J.S., Squires, C.A., Suhot, M.A., 2006. The effect of voids on the flexural fatigue performance of unidirectional carbon fibre composites developed for wind turbine applications. International Journal of Fatigue 28, 1389–1398.

Chen, H.S., Hwang, S.F., 2006. Accelerated fatigue properties of unidirectional carbon/epoxy composite materials. Polymer Composites 27, 138–146.

Chen, H.S., Hwang, S.F., 2009. A fatigue damage model for composite materials. Polymer Composites 30, 301–308.

Clark, S.D., 1997. Long Term Behaviour of FRP Structural Foam Cored Sandwich Beams (Doctor of Philosophy). University of Southampton, Department of Ship Science.

Clark, S.D., Shenoi, R.A., 1998. Fatigue Considerations for FRP sandwich structures of RNLI lifeboats. Trans.Royal Institution of Naval Architect 239–257.

Clark, S.D., Shenoi, R.A., Allen, H.G., 1999. Modelling the fatigue behaviour of sandwich beams under monotonic, 2-step and block-loading regimes. Composites Science and Technology 59, 471–486.

Cross, E.J., Koo, K.Y., Brownjohn, J.M.W., Worden, K., 2013. Long-term monitoring and data analysis of the Tamar Bridge. Mechanical Systems and Signal Processing 35, 16–34. doi:10.1016/j.ymssp.2012.08.026

Daniel, I.M., 2006. Engineering Mechanics of Composite Materials, Second Edition. ed. Oxford University Press, Oxford.

Darbyshire, J., 1955. An investigation of storm waves in the North Atlantic Ocean. Proc. Roy. Soc. London A230, 560–569.

DEFRA, 2012. Our Science [WWW Document]. Centre for Environment, Fisheries & Aquaculture Science. URL http://www.cefas.defra.gov.uk/our-science.aspx (accessed 8.16.12).

Demers, C.E., 1998. Tension–tension axial fatigue of E-glass fiber-reinforced polymeric composites: fatigue life diagram. Construction and Building Materials 12, 303–310. doi:10.1016/S0950-0618(98)00007-5

De Witte, M., 1989. Power plant life estimation and extension: The belgian experience from the users' point of view. International Journal of Pressure Vessels and Piping 39, 41–55. doi:10.1016/0308-0161(89)90037-9

DNV, 2010. Fatigue Assessment of Ship Structures (Classification No. 30.7). Det Norske Veritas, Veritasveien 1, NO-1322 HØVIK, Norway.

El Mahi, A., Bezazi, A., 2009. Describing the flexural behaviour of cross-ply laminates under cyclic fatigue. Applied Composite Materials 16, 33–53.

Enoch, M., Warren, J.P., Valdés Ríos, H., Henríquez Menoyo, E., 2004. The effect of economic restrictions on transport practices in Cuba. Transport Policy 11, 67–76. doi:10.1016/S0967-070X(03)00054-4

Erve, M., Bartholomé, G., 1991. Activities in the field of plant life evaluation, life extension and plant improvement. Nuclear Engineering and Design 128, 103–114. doi:10.1016/0029-5493(91)90254-F

Faltinsen, O.M., 2000. Hydroelastic Slamming. Journal of Marine Science and Technology 5, 49–100.

Fan, L., Luo, M., 2013. Analyzing ship investment behaviour in liner shipping. Maritime Policy & Management 1–23. doi:10.1080/03088839.2013.776183

Farrar, C.R., Worden, K., 2007. An introduction to structural health monitoring. Philosophical Transactions of the Royal Society A: Mathematical, Physical and Engineering Sciences 365, 303–315.

Ferreira, J.A.M., Costa, J.D.M., Reis, P.N.B., Richardson, M.O.W., 1999. Analysis of fatigue and damage in glass-fibre-reinforced polypropylene composite materials. Composites Science and Technology 59, 1461–1467.

Foster, C.L., Monkman, D.C., 2004. Telecom New Zealand future power foundations - Through risk control asset management, in: INTELEC - 26th Annual International Telecommunications Energy Conference, INTELEC 2004, September 19,2004 - September 23,2004, INTELEC, International Telecommunications Energy Conference (Proceedings). Institute of Electrical and Electronics Engineers Inc., Chicago, IL, United states, pp. 561–568.

Fridsma, G., 1971. A systematic study of the rough water performance of planing boats, part ii. Irregular seas. (No. Davidson Laboratory Report 1495). Stevens Institute of Technology.

Garme, K., Rosén, A., Stenius, I., Kuttenkeuler, J., 2012. Rough water performance of lightweight high-speed craft. Proceedings of the Institution of Mechanical Engineers, Part M: Journal of Engineering for the Maritime Environment. doi:10.1177/1475090212460456

Guedes Soares, C., 1986. Assessment of the uncertainty in visual observations of wave height. Ocean Engineering 13, 37–56. doi:10.1016/0029-8018(86)90003-X

Gurit, 2007. ST 94 Single SPRINT.

Gurit, 2008. Ampreg 26 Epoxy Laminating System.

Harman, A., Chaplin, N., Phillps, H., Austen, S., 2011. The Structural and Stability Assessmetn and Subsequent Recovery of a Damaged Lifeboat. Proceedings of The Damaged Ship Conference.

Harper, S.R., Thurston, D.L., 2008. Incorporating environmental impacts in strategic redesign of an engineered system. Journal of Mechanical Design, Transactions of the ASME 130.

Harral, B.B., 1987. The application of a statistical fatigue life prediction method to agricultural equipment. International Journal of Fatigue 9, 115–118. doi:10.1016/0142-1123(87)90053-3

Hasselman, K., Barnett, T.P., Bouws, E., Carlson, H., Cartwright, D.E., Enke, K., Ewing, J.A., Gienapp, H., Hasselmann, D.E., Kruseman, P., Meerburg, A., Miller, P., Olbers, D.J., Richter, K., Sell, W., Walden, H., 1973. Measurements of wind-wave growth and swell decay during the joint North Sea Wave Project (JONSWAP). Ergnzungsheft zur Deutschen Hydrographischen Zeitschrift Reihe 95.

Heller Jr, S.R., Jasper, N.H., 1960. On The Structural Design Of Planing Craft.

Horrocks, P., Mansfield, D., Parker, K., Thomson, J., Atkinson, T., Worsley, J., n.d. Managing Ageing Plant - A Summary Guide. Health and Safety Executive.

Huanchun, C., Shivakumar, K.N., Abali, F., 2008. Application of total fatigue life model to T700 carbon/vinyl ester composite. Composites Part B 39, 36–41.

Hudson, F.D., Hicks, I.A., Cripps, R.M., 1993. Design and development of modern lifeboats. Proceedings of the Institution of Mechanical Engineers, Part A: Journal of Power and Energy 207, 3–22.

Huler, S., 2004. Defining the wind: The Beaufort scale, and how a nineteenth century admiral turned science into poetry. Diane Publishing Co.

James, G., Burley, D., Clements, N., Dyke, P., Searl, J., Wright, J., 2001. Modern Engineering Mathematics, 3rd Edition. ed. Prentice Hall.

Jasper, N.H., 1949. Dynamic Loading of a Motor Torpedo Boat (YP110) During High Speed Operation In Rough Water.

Kassapoglou, C., 2007. Fatigue life prediction of composite structures under constant amplitude loading. Journal of Composite Materials 41, 2737–2754.
Kenney, M.E., 1969. Report on Hull Stress Analysis Trials of 40 Foot R.P. Rescue Launch 40-001. Halmatic LTD, Havant.
Kim, H.C., Ebert, L.J., 1981. Flexural Fatigue Behaviour of Unidirectional Fibreglass Composites. Fibre Science and Technology 14, 3–20.
KP4 Technical Policy - Ageing and Life Extension of Offshore Installations, 2012. . Health & Safety Executive, Offshore Safety Division.
Lankester S.G., 1964. H.M.S. Brave Swordsman Rough Weather Sea Trials (No. 6). Admiralty Experiment Works, Haslar, Gosport, Hampshire.
Mandell, J.F., 2003. DOE-MSU Wind Turbine Blade Composite Material Fatigue Database. Department of Chemical Engineering, Montana State University at Bozman, Montana USA.
Mandell, J.F., 2009. DOE/MSU Composite Material Fatigue Data Base Version 18.1 (No. NM 87185:2004). Sandia National Laboratories, Albuquerque.
Matsubara, G., Ono, H., Tanaka, K., 2006. Mode II fatigue crack growth from delamination in unidirectional tape and satin-woven fabric laminates of high strength GFRP. International Journal of Fatigue 28, 1177–1186.
Miller, P.H., 2001. Fatigue Prediction Verification of Fiberglass Hulls. Marine Technology 38, 278–292.
Miner, M., 1945. Cumulative Damage in Fatigue. Journal of Applied Mechanics 12, A159–A164.
Miyano, Y., Nakada, M., Nishigaki, K., 2006. Prediction of long-term fatigue life of quasi-isotropic CFRP laminates for aircraft use. International Journal of Fatigue 28, 1217–1225.
National Instruments, 2008. Operating Instructions and Specifications NI 9235/9236. 8 Channel, 24-Bit Quarter-Bridge Analog Input.
Neumann, g, 1954. Zur Charakteristik des seeganges. Arch. Meteorol. Geophys. Bioklimatol A7, 352–377.
Nieuwenhuis, P., 2008. From banger to classic – a model for sustainable car consumption? International Journal of Consumer Studies 32, 648–655. doi:10.1111/j.1470-6431.2008.00721.x
O'Brien, T.K., Chawan, A.D., Krueger, R., Paris, I.L., 2002. Transverse tension fatigue life characterization through flexure testing of composite materials. International Journal of Fatigue 24, 127–145.
OKAMURA, H., SAKAI, S., SUSUKI, I., 1979. Cumulative Fatigue Damage Under Random Loads. Fatigue & Fracture of Engineering Materials & Structures 1, 409–419. doi:10.1111/j.1460-2695.1979.tb01328.x
Papakonstantinou, C.G., Balaguru, P.N., 2007. Fatigue behavior of high temperature inorganic matrix composites. Journal of Materials in Civil Engineering 19, 321–328.
Payne, P.R., 1981. The vertical impact of a wedge on a fluid. Ocean Engineering 8, 421–436. doi:10.1016/0029-8018(81)90035-4
Philippidis, T.P., Vassilopoulos, A.P., 2002. Complex stress state effect on fatigue life of GRP laminates. Part I, Experimental. International Journal of Fatigue 24, 813–823.
Picard, H., Verstraten, J., Hakkens, M., Vervaet, R., 2007. Decision model for End of Life management of switchgears, in: 4th Petroleum and Chemical Industry Conference Europe-Electrical and Instrument Applications, PCIC EUROPE, June 13,2007 - June 15,2007, 4th Petroleum and Chemical Industry Conference Europe-Electrical and Instrument Applications, PCIC EUROPE. Inst. of Elec. and Elec. Eng. Computer Society, Paris, France.
Pierson, W., J., Moskowitz, L.A., 1964. Proposed Spectral Form for Fully Developed Wind Seas Based on the Similarity Theory of S. A. Kitaigorodskii. Journal of Geophysical Research 69, 5181–5190.

Post, N.L., Case, S.W., Lesko, J.J., 2008. Modeling the variable amplitude fatigue of composite materials: A review and evaluation of the state of the art for spectrum loading. International Journal of Fatigue 30, 2064–2086.

Prescott, N.J., 1995. Equipment life: can we afford to extend it?, in: Proceedings of the 1995 Annual Reliability and Maintainability Symposium, January 16, 1995 - January 19, 1995, Proceedings of the Annual Reliability and Maintainability Symposium. IEEE, Washington, DC, USA, pp. 529–535.

Qiao, P., Yang, M., 2006. Fatigue life prediction of pultruded E-glass/polyurethane composites. Journal of Composite Materials 40, 815–837.

Rawson, K.., Tupper, E.C., 2001. Basic Ship Theory. Butterworth-Heinemann.

Read, P.J.C.L., Shenoi, R.A., 1995. Review of fatigue damage modelling in the context of marine FRP laminates. Marine Structures 8, 257.

Reinertsen, R., 1996. Residual life of technical systems; diagnosis, prediction and life extension. Reliability Engineering & System Safety 54, 23–34. doi:10.1016/S0951-8320(96)00092-0

Reis, P.N.B., Ferreira, J.A.M., Antunes, F.V., Costa, J.D.M., 2007. Flexural behaviour of hybrid laminated composites. Composites Part A: Applied Science and Manufacturing 38, 1612–1620.

Roberton D.M.V, Shenoi R.A., Boyd S.W., Austen S., 2009. A Plausible Method For Fatigue Life Prediction Of Boats In A Data Scarce Environment, in: Procedings of the 17th International Conference on Composite Materials (ICCM17). p. Paper 14.

Rosén, A., 2004. Loads and Responses for Planing Craft in Waves (PhD). Stockholm University, Stockholm, Sweden.

Rosén, A., 2005. Impact pressure distribution reconstruction from discrete point measurements. International Shipbuilding Progress 52, 91–107.

Rychlik, I., 1987. A new definition of the rainflow cycle counting method. International Journal of Fatigue 9, 119–121. doi:10.1016/0142-1123(87)90054-5

Salvia, M., Fiore, L., Fournier, P., Vincent, L., 1997. Flexural fatigue behavior of UDGFRP experimental approach. International Journal of Fatigue 19, 253–262.

Sangwook, S., Tsai, S.W., 2005. Prediction of fatigue S-N curves of composite laminates by Super Mic-Mac. Composites Part A (Applied Science and Manufacturing) 36, 1381–1388.

Sarkani, S., Michaelov, G., Kihl, D.P., Bonanni, D.L., 2001. Comparative study of nonlinear damage accumulation models in stochastic fatigue of FRP laminates. Journal of structural engineering New York, N.Y. 127, 314–322.

Savitsky, D., 2003. On the subject of high-speed monohulls.

Savitsky, D., Ward Brown P., 1976. Procedures for Hydrodynamic Evaluation of Planing Hulls in Smooth and Rough Water. Marine Technology 13, 381–400.

Seatre, H.J., 1961. On the high wave conditions in the Northern North Atlantic. Inst. Oceanogr. Sci. Report 3.

Shaw, R.M., Pilkington, G.D., 2012. Flexural Fatigue Performance of GRP Material (No. 2012070370). National Physics Laboratory, Teddington.

Shenoi, R., Dulieu-Barton, J., Quinn, S., Blake, J., Boyd, S., 2011. Composite Materials for Marine Applications: Key Challenges for the Future, in: Composite Materials. Springer, pp. 69–89.

Smith, C.S., 1989. Marine Composite Structures. Elsevier.

Sobey, A.J., Blake, J.I.., Shenoi, R.A., 2009. Optimisation approaches to design synthesis of marine composite structures, in: Schifstechnick BD.54 - Ship Technology Research. pp. 24–30.

Socie, D., 1977. Fatigue-life prediction using local stress-strain concepts. Experimental Mechanics 17, 50–56.

Socie, D., Shifflet, G., Burns, H., 1979. A field recording system with applications to fatique analysis. International Journal of Fatigue 1, 103–111. doi:10.1016/0142-1123(79)90015-X

Stacey, A., 2011. KP4: Ageing & Life Extension Inspection Programme - The First Year. Presented at the Offshore Europe, Society of Petroleum Engineers, Aberdeen. doi:10.2118/145518-MS

Stacey, A., Birkinshaw, M., Sharp, J.V., 2008. Life Extension Issues For ageing Offshore Installations, in: OMAE2008. Presented at the 27th International Conference on Offshore Mechanics and Arctic Engineering, Estoril, Portugal.

Stumpf, W.E., 1994. Ageing of materials and methods for the assessment and extension of lifetimes of engineering plant. International Journal of Pressure Vessels and Piping 59, 3–12. doi:10.1016/0308-0161(94)90136-8

Sunder, R., Seetharam, S.A., Bhaskaran, T.A., 1984. Cycle counting for fatigue crack growth analysis. International Journal of Fatigue 6, 147–156. doi:10.1016/0142-1123(84)90032-X

Suzuki, T., Matsuura, T., Sakuma, A., Kodama, H., Takagi, K., Curtis, A., 2006. Recent upgrading and life extension technologies for existing steam turbines. JSME International Journal, Series B: Fluids and Thermal Engineering 49, 198–204.

Talreja, R., 1981. Fatigue of Composite Materials: Damage Mechanisms and Fatigue-Life Diagrams. Proceedings of the Royal Society of London.Series A, Mathematical and Physical Sciences 378, 461–475.

Talreja, R., 2008. Damage and fatigue in composites: a personal account. Composites Science and Technology 68, 2585–2591.

Ten Have, A.A., 1993. WISPER and WISPERX: Summary paper describing their backgrounds, derivation and statistics, in: Proceedings of the 16th Annual Energy - Sources Technology Conference and Exhibition, January 31, 1993 - Febrary 4, 1993, American Society of Mechanical Engineers, Solar Energy Division (Publication) SED. Publ by ASME, Houston, TX, USA, pp. 169–178.

Thirumeni, C., 2005. Rehabilitation and uprating of Ras Abu Fontas MSF desalination units: Process optimisation and life extension. Desalination 182, 67–71.

Timoshenko, S., Woinowsky-Krieger, S., 1987. Theory of Plates and Shells, Second Edition. ed. McGraw-Hill.

Tovo, R., 2002. Cycle distribution and fatigue damage under broad-band random loading. International Journal of Fatigue 24, 1137–1147. doi:10.1016/S0142-1123(02)00032-4

Vassilopoulos, A.P., 2010. Fatigue Life Prediction Of Composites And Composite Structures. Woodhead Publishing Limited.

Von Karman, T., 1929. The Impact on Seaplane Floats During Landing. Aerodynamical Institute of the Technical High School, Aachen.

Wang, S., Soares, G., 2013. Developments in Maritime Transportation and Exploitation of Sea Resources, Proceedings of the 15th International Maritime Assosciation of the Mediterranean Congress. Taylor and Francis Group.

www.matweb.com, n.d. MatWeb Material Property Data [WWW Document]. Matweb. URL http://www.matweb.com/

Yigang, Z., Shijie, Z., Minggao, Y., 1993. A cycle counting method considering load sequence. International Journal of Fatigue 15, 407–411. doi:10.1016/0142-1123(93)90487-B

Young, W.C., Budynas, R.G., 2011. Roark's Formulas For Stress and Strain.